



**N8513850**

---

---

# **ASSESSMENT OF INTEGRATED FLYWHEEL SYSTEM TECHNOLOGY**

**NATIONAL AERONAUTICS AND SPACE  
ADMINISTRATION, HAMPTON, VA. LANGLEY  
RESEARCH CENTER**

**NOV 1984**



*NASA Conference Publication 2346*

# **An Assessment of Integrated Flywheel System Technology**

*Edited by*  
**Claude R. Keckler**  
*Langley Research Center*  
*Hampton, Virginia*

**Robert T. Bechtel**  
*Marshall Space Flight Center*  
*Huntsville, Alabama*

**Nelson J. Groom**  
*Langley Research Center*  
*Hampton, Virginia*

Proceedings of a workshop held at  
NASA Marshall Space Flight Center  
Huntsville, Alabama  
February 7-9, 1984

**NASA**

National Aeronautics  
and Space Administration

Scientific and Technical  
Information Branch

1984

## PREFACE

A 3-day international workshop on integrated flywheel systems technology was held at the Marshall Space Flight Center, Huntsville, Alabama, on February 7-9, 1984. The objectives of this workshop were to determine the current state of the technology in flywheel energy storage systems and ancillary components, to define the technology shortfalls and critical items in light of applications requirements, and to identify and prioritize the technology needs and issues to rectify the denoted shortfalls. This workshop was sponsored by the National Aeronautics and Space Administration and included participants from industrial, academic, and government concerns. A list of attendees is included in this document.

The first day and a half consisted of presentations by various participants on system trades and analyses, flywheel rotor technology, suspension systems technology, power and control electronics, as well as dynamics and attitude control.

These presentations provided an excellent overview of recent and current technology efforts in the U.S. and Europe. The remainder of the workshop schedule was dedicated to working group meetings. Four technology panels were established and chaired by industry experts in each discipline. Workshop participants were requested to attend those working group meetings which they felt would be of greatest interest to them or which would benefit the most from their special knowledge and experience. The working groups were charged with providing answers to the following questions:

- 1) What are the principal component and system technology issues in your particular discipline area relative to the development of large-scale (50-200 kW) integrated flywheel systems for space applications?
- 2) What are the major steps to be taken relative to large-scale integrated flywheel technology development and application to the Space Station?
- 3) Are there any benefits to be derived from or any inherent technical reasons for flight testing as a part of the validation process to demonstrate the viability of an integrated flywheel system?

Results from the working group deliberations were summarized by each chairman and presented to the general audience.

This publication contains a summary of the workshop, which includes a discussion of the major conclusions and recommendations produced by the participants. In addition, copies of the individual papers presented as well as the four working group reports are contained herein.

Use of trademarks or names of manufacturers in this report does not constitute an official endorsement of such products or manufacturers, either expressed or implied, by the National Aeronautics and Space Administration.

PRECEDING PAGE BLANK NOT FILMED

PAGE // INTENTIONALLY BLANK

CONTENTS

PREFACE ..... 111

ATTENDEES ..... vii

INTRODUCTION ..... 1

EXECUTIVE SUMMARY ..... 3

WORKING GROUP SUMMARIES

ROTATING ASSEMBLY WORKING GROUP SUMMARY ..... 7 ✓

ELECTROMECHANICAL/ELECTROMAGNETICS WORKING GROUP SUMMARY ..... 25 ✓

ELECTRICAL/ELECTRONICS WORKING GROUP SUMMARY ..... 29 ✓

DYNAMICS AND CONTROLS WORKING GROUP SUMMARY ..... 39 ✓

PRESENTATIONS

A SUMMARY OF THE 1983 INTEGRATED FLYWHEEL TECHNOLOGY WORKSHOP ..... 49 ✓  
Claude R. Keckler

EUROPEAN DEVELOPMENT EXPERIENCE ON ENERGY STORAGE WHEELS FOR SPACE ..... 65 ✓  
A. A. Robinson

MERITS OF FLYWHEELS FOR SPACECRAFT ENERGY STORAGE ..... 75 ✓  
Sidney Gross

COMPARATIVE ENERGY STORAGE ASSESSMENT ITEM ..... 91 ✓  
Bob Giudici

INERTIAL ENERGY STORAGE FOR SATELLITES ..... 101 ✓  
D. Eisenhaure

PERSPECTIVES ON ENERGY STORAGE WHEELS FOR SPACE STATION APPLICATION ..... 117 ✓  
Ronald E. Oglevie

FLYWHEEL-POWERED X-RAY GENERATOR ..... 129 ✓  
Melvin P. Siedband

WESTINGHOUSE PROGRAMS IN PULSED HOMOPOlar POWER SUPPLIES ..... 141 ✓  
D. C. Litz and E. Mullan

DESCRIPTION OF A LABORATORY MODEL ANNULAR MOMENTUM CONTROL DEVICE (AMCD) ..... 157 ✓  
Nelson J. Groom

GENERIC COMPOSITE FLYWHEEL DESIGNS ..... 169 ✓  
R. S. Steele

PAGE IV INTENTIONALLY BLANK

PRECEDING PAGE BLANK NOT FILMED

SUMMARY RESULTS OF THE DOE FLYWHEEL DEVELOPMENT EFFORT .....	181 ✓
M. Olszewski and J. F. Martin	
FLEXIBLE MATRIX COMPOSITE LAMINATED DISK/RING FLYWHEEL .....	193 ✓
B. P. Gupta and A. J. Hannibal	
GENERAL ELECTRIC COMPOSITE RING-DISK FLYWHEEL: RECENT AND POTENTIAL DEVELOPMENTS .....	209 ✓
Anthony P. Coppa	
THE MULTIPURPOSE COMPOSITE FLYWHEEL .....	233 ✓
B. R. Ginsburg	
FLYWHEEL CONTAINMENT AND SAFETY CONSIDERATIONS .....	243 ✓
Anthony P. Coppa	
MAGNETICALLY SUSPENDED REACTION WHEEL ASSEMBLY .....	265 ✓
George Stocking	
MAGNETIC SUSPENSION OPTIONS FOR SPACECRAFT INERTIA-WHEEL APPLICATIONS .....	281 ✓
J. R. Downer	
OVERVIEW OF MAGNETIC BEARING CONTROL AND LINEARIZATION APPROACHES FOR ANNULAR MAGNETICALLY SUSPENDED DEVICES .....	297 ✓
Nelson J. Groom	
MAGNETICALLY SUSPENDED FLYWHEEL SYSTEM STUDY .....	307 ✓
J. A. Kirk, D. K. Anand, H. E. Evans, and G. E. Rodriguez	
REACTION WHEELS FOR KINETIC ENERGY STORAGE .....	329 ✓
Philip A. Studer	
ADVANCED HIGH-POWER TRANSFER THROUGH ROTARY INTERFACES .....	341 ✓
Pete Jacobson	
HIGH-EFFICIENCY POWER CONVERSION OPTIONS FOR FLYWHEEL ENERGY STORAGE SYSTEMS .....	349 ✓
R. L. Hockney	
DEVELOPMENTS IN SPACE POWER COMPONENTS FOR POWER MANAGEMENT AND DISTRIBUTION .....	369 ✓
David D. Renz	
MOTOR/GENERATOR AND ELECTRONIC CONTROL CONSIDERATIONS FOR ENERGY STORAGE FLYWHEELS .....	389 ✓
Frank Nola	
TORQUE COMMAND STEERING LAW FOR DOUBLE-GIMBALED CONTROL MOMENT GYROS APPLIED TO ROTOR ENERGY STORAGE .....	407 ✓
Hans F. Kennel	
APPENDIX - SYMBOLS AND ABBREVIATIONS .....	423

OMIT TO  
P. 7

ATTENDEES

Dr. W. W. Anderson	NASA
Raymond Beach	NASA
R. T. Bechtel	NASA
R. J. Benhabib	TRW
Baruch Berman	Rockwell International
Joel Bloomer	Boeing Aerospace Co.
L. W. Brantley, Jr.	NASA
H. J. Buchanan	NASA
Paul Burke	Bendix Corporation
W. B. Chubb	NASA
Phil Colgrove	Wright-Patterson AFB
L. J. Cook	NASA
Anthony Coppa	General Electric
Larry Crabtree	NASA
Kent Decker	TRW
James Downer	The Charles Stark Draper Laboratory, Inc.
David B. Eisenhaure	The Charles Stark Draper Laboratory, Inc.
W. K. Fikes	NASA
Bernard R. Ginsberg	Rockwell International
Robert J. Giudici	NASA
Paul T. Golley	NASA
J. R. Graves	NASA
Nelson J. Groom	NASA
Sidney Gross	Boeing Aerospace Co.
Dr. B. P. Gupta	Lord Corporation
Charles Haldeman	MIT-Lincoln Laboratory
A. J. Hannibal	Lord Corporation
Richard Hockney	The Charles Stark Draper Laboratory, Inc.
Henry Hoffman	NASA
H. H. Huie	NASA
Pete Jacobson	Sperry Flight Systems
J. P. Joyce	NASA
K. Jurgensen	NASA
Lloyd Keaffer	NASA
C. R. Keckler	NASA
Robert A. Kennedy	Sperry Flight Systems
Hans F. Kennel	NASA
Richard Keye	NASA
John King	Wyle Laboratories
Dr. James A. Kirk	University of Maryland
Dr. Satish V. Kulkarni	Lawrence Livermore Laboratories
J. R. Lanier	NASA
Don Litz	Westinghouse R & D Center
Col. W. T. McLyman	JPL
J. L. Miller	NASA
D. D. Nixon	NASA
Frank J. Nola	NASA
Dr. G. S. Nurre	NASA
Steve O'Dea	The Charles Stark Draper Laboratory, Inc.
Ronald E. Oglevie	Rockwell International
Dr. Mitchell Olszewski	Oak Ridge National Laboratory
Frank R. Penovich	NASA

Bruce Plyer	Bendix Corp.
Leonard Pursiano	Bendix Corp.
David D. Renz	NASA
Robert R. Rice	NASA
James Rinderle	Carnegie Mellon University
Alan A. Robinson	ESTEC
Gary Rodgers	Sperry Flight Systems
G. E. Rodriguez	NASA
Leo Ruggerio	Bendix Corporation
Arthur D. Schoenfeld	TRW
H. N. Scoffield	NASA
Dr. M. P. Sieband	University of Wisconsin
Dr. Robert Steele	
Jim Stewart	NASA
George Stocking	Sperry Flight Systems
P. A. Studer	NASA
Don Tomlin	NASA
Howard R. Whitman	The Charles Stark Draper Laboratory, Inc.
Bud Wiest	Sperry Flight Systems
William Wilkinson	Johns Hopkins University
J. L. Williams	NASA
Jack Wright	General Electric
Frank Younger	Brobeck and Associates



## INTRODUCTION

The NASA/OAST-sponsored workshop "An Assessment of Integrated Flywheel System Technology" was held at the NASA Marshall Space Flight Center, Huntsville, Alabama, February 7-9, 1984. The purposes of this workshop were to determine the current state of the technology in flywheel energy storage systems and ancillary components, to define the technology shortfalls and critical items in light of applications requirements, and to identify and prioritize the technology needs and issues to rectify the denoted shortfalls. To accomplish these objectives, participants from industrial, academic, and government concerns reported on various tradeoff and system analyses as well as concept and component technology enhancement efforts conducted by each organization. A list of workshop attendees is provided in this document. In addition, working groups comprised of workshop participants and chaired by experts from industry addressed the questions of critical technology needs and issues, applications drivers, and requirements for flight validation. The four working groups, the names and affiliations of the associated chairmen, and the areas of consideration are presented in Table 1. In addition, listings of the participants in each working group are included in the working group summaries in this document.

TABLE 1

Working Groups

ROTATING ASSEMBLY

Dr. Satish V. Kulkarni, LLNL

- Rotor Design and Dynamics
- Material Selection and Analysis
- Structural Modeling
- Containment and Safety
- Integration and Testing

ELECTROMECHANICAL/ELECTROMAGNETICS

David B. Eisenhaure, CSDL

- Suspension
- Motor/Generator
- Sensors and Gimbal Actuators
- Modeling

ELECTRICAL/ELECTRONICS

Arthur D. Schoenfeld, TRW

- Motor/Generator Circuits
- Suspension System Electronics
- Power Transfer Across Rotating Interfaces
- Power Conditioning and Distribution
- Modeling

DYNAMICS AND CONTROLS

Ronald E. Oglevie, RI

- Suspension System Control Laws
- Momentum and Energy Management
- Fault Tolerance/Robustness
- Contingency Criteria After Unit Failure
- Modeling

## EXECUTIVE SUMMARY

An assessment of the state of the technology applicable to integrated flywheel systems was initiated by reviewing the results of a workshop held at the NASA Goddard Space Flight Center in August 1983 on integrated flywheel technology efforts conducted by U.S. government agencies. This was followed by an overview of development work being performed in Europe by various members of the European Space Agency (ESA). Results from ongoing studies in industry and government laboratories were summarized. These dealt with such topics as the merits of flywheel systems for space applications, with emphasis on small satellites and the Space Station; comparisons of these concepts with other storage devices such as batteries and regenerative fuel cells; and laboratory application of various component technologies in the area of rotating assemblies and suspension systems. Data produced by these technology efforts indicated that significant potential benefits could be realized from the application of these developments to a large variety of spacecraft. A review of the recent advances in the area of composite materials as applied to high-speed rotors was presented by a variety of organizations which had participated in recent Department of Energy programs on the application of flywheel technology to terrestrial transportation systems. In addition, some preliminary results from a study of rotor containment issues were discussed.

The use of high-speed flywheels for energy storage in space requires that such systems possess long life characteristics. One method of extending the operational life of these devices is to utilize noncontacting rotor suspension systems such as magnetic bearings. Results from government sponsored and independent research and development efforts in this area were reviewed along with recent advances in magnetic materials and their attendant potential for future applications.

One of the attractive features of flywheel storage devices is their power transfer efficiency. To enhance that characteristic, care must be exercised that all constituent components operate at optimum efficiency themselves. As such, much effort has gone into the development of high-efficiency and high-power electronic devices. In addition, efficient power transfer across rotating interfaces, such as those present in gimballed systems, has been addressed.

Based on previous studies such as the Integrated Power/Attitude Control System (IPACS) studies, strong consideration is being given to the integration of the energy storage/power generation and attitude control functions into one system. In order to accommodate the requirements of these two functions, new momentum and energy management methods must be developed. A potential control law for multiaxis storage and momentum systems was presented and is included in this publication.

Following the individual presentations, the four working groups undertook their deliberations. In these efforts, each group considered the following:

1. What are the principal component and system technology issues in your particular discipline area relating to the development of large-scale (50-200 kW) integrated flywheel systems for space applications?
2. What are the major steps to be taken relative to large-scale integrated flywheel technology development and application to the Space Station?

3. Are there any benefits to be derived from or any inherent technical reasons for flight testing as a part of the validation process to demonstrate the viability of an integrated flywheel system?

A summary of the conclusions and recommendations developed by each working group is presented here. A complete report from each group is presented elsewhere in this document.

## TECHNOLOGY ISSUES

### Rotating Assembly

- Conduct detailed trade studies and system definitions
- Undertake efforts to enhance understanding of time-dependent behavior of composite materials subjected to cyclic stresses and orbital environment conditions
- Screen and support development of new materials to enhance system performance and reliability
- Use DOE facilities and hardware to augment data base on composite material rotors as well as to develop life prediction methodology
- Improve dynamics analysis capabilities for composite material rotors, especially when integrated with magnetic suspension systems
- Address safety management issues as soon as possible
- Undertake a vigorous technology program in this area as soon as possible

### Electromechanical/Electromagnetics

- Immediate study or studies to determine optimal system configuration need to be performed
- Focus program to permit system integration and demonstration by 1987
- Support technology efforts on motor/generators, suspension systems, gimbals, and sensors to take advantage of forecasted and known technological possibilities
- System recommendations
  - . Bus voltage = 200+ volts
  - . Efficiency (round trip)
    - 1987 80 percent required
    - 1992 85 percent required

Electrical/Electronics

- Undertake detailed system studies to define subsystem and component requirements
- Generate high-fidelity analytical models to validate technology approaches and establish performance potentials
- Conduct early laboratory demonstration at the component and system levels

Dynamics and Control

- Technology in the dynamics and control area is considered adequate for flywheel storage system development
- Vigorously pursue flywheel storage technology efforts
- Conduct thorough system trades and analyses to resolve such issues as contingency levels, fault isolation, and robustness
- Highly recommend early laboratory demonstration



N85

3851

INCLAS

N85 13851 D1

ROTATING ASSEMBLY WORKING GROUP SUMMARY

Dr. Satish V. Kulkarni, Lawrence Livermore National Laboratory

Chairman

INTRODUCTION

The output of this working group is represented by this summary report. It follows a format similar to that previously employed in Department of Energy (DOE) programs and shall address the following items (Figure 1):

1. Task goals
2. Rationale
3. Strategy
4. Key pacing issues

The goals associated with the central task need to be identified to provide the necessary focus for the program. The rationale for the program and the strategy for accomplishing the work need to be defined. During the course of the effort several key issues will have to be addressed to insure development success.

The table (Table 1) at the end of this summary identifies the 17 persons who made up this panel and developed these recommendations.

CONCLUSIONS AND RECOMMENDATIONS

The panel addressed the issues associated with such areas as rotor design and dynamics, rotor materials and fabrication, safety, nondestructive testing, and system operational loads and environment. Recommendations arising from the working group deliberations are presented in the following material.

1. Task Goals

The primary objective of this development effort should be (Figure 2) to demonstrate the feasibility of a fail-safe flywheel system comprised of units having a useful energy capacity of 5 kilowatt-hours per unit. This system concept should be expandable to meet power requirements of 50-200 kilowatts. A system energy density of 20 watt-hours/kilogram or more should be achieved, with an operational life requirement of 5-10 years. A key pacing issue (Figure 3) attendant to this program goal is the question of whether the flywheel system should provide attitude control and energy storage simultaneously, or whether it should accommodate energy storage functions only. It is recommended that a system study be conducted to determine the impact of this role combination and to resolve this issue.

6 INTENTIONALLY BLANK

7

## 2. Rationale

Recent studies (Figure 4) conducted by Boeing, NASA, and others have shown the concept of flywheel energy storage to be highly competitive with other more conventional system approaches such as batteries. Three of the major advantages of flywheel systems are longer operational life, higher electrical efficiency, and higher system energy density. The use of composite material flywheels is important for realizing these advantages.

## 3. Strategy

A significant amount of technology is available as a result of programs sponsored by the Department of Energy (DOE), the Department of Transportation (DOT), and the U.S. Army (Figure 5). Every attempt should be made to capitalize on the results of these efforts, especially in the areas of composite materials utilization and flywheel design. Improvements to that data base should be made to optimize the system design and performance capability. In that vein, therefore, a list of published reports on these topics should be generated by personnel at the Lawrence Livermore National Laboratory and at the Oak Ridge National Laboratory, as well as at the other cognizant facilities, and distributed to the participants of this conference.

Having a knowledge of the state of the technology in composite materials, it is then possible to make use of that engineering data base in the definition of candidate rotor designs (Figure 6). One issue which must be pursued at the onset of any flywheel program is to develop an understanding of the time-dependent behavior of composites and, therefore, assess their long-term performance. In parallel with these efforts, there is a need to screen and support the development of new materials for future upgrading of flywheel systems.

In determining a plausible multiyear development program, some critical issues (Figure 7) surfaced. These consisted of questions dealing with matrix and material fiber aspects, as well as engineering design data.

## 4. Fiber Issues

In keeping with a technology ready date of 1987, consideration should be given to designing with existing fibers, since they are well characterized (Figure 8). Characterization of composite materials is a time- and money-consuming task. Therefore, it is possible to utilize such materials as T-300 or Celion-6000 graphite fibers, or even possibly Kevlar-49 or S2 glass. At the same time, efforts should be initiated to obtain data on higher strength fibers such as AS6, IM6, T-700, T-800, or improved Kevlar.

## 5. Matrix Issues

Some data are available in the literature which indicate that matrix materials can withstand temperatures of 3500F with, however, operational capability degradation. Thus, an important step (Figure 9) is to define some test effort on these materials to determine what is the acceptable operational temperature range for the desired performance levels. Other materials which warrant investigation are the flexible resins, such as urethanes, because of their advantages when used in multiring flywheels. Again, there exists some concern on the temperature stability of these materials primarily because of the lack of available data. Some promising candidate materials for use in high-speed rotors are the metal matrices, such as boron/aluminum. These materials



offer some advantages in terms of long-term durability, balance stability, and performance capability at higher temperatures.

#### 6. Engineering Design Data Issues

Additional information is required on these and other materials because the currently available data base is restricted to a terrestrial environment, as opposed to a space environment, where the operational loads and conditions are drastically different (Figure 10). Other areas of concern in the use of composite materials are the effects of radiation on the material properties. In addition, the poor transverse load-carrying capacity of these materials may severely impact some rotor designs and applications. Solutions to the transverse strength question range from "live with it," to "expend a lot of time and money to get a small delta improvement." If the former approach is selected, it is deemed advisable to determine some design values to compensate for the considerable data scatter which exists in the literature regarding transverse strength.

To improve the understanding of the time-dependent behavior of composites, especially in a cyclic load environment, it is recommended that testing of existing DOE rotors be again undertaken. Steps to effect accelerated testing of these devices should also be evaluated. Data obtained from these test programs will be instrumental in the definition of life prediction methodologies.

#### 7. Flywheel Development Issues

The development of the flywheel (Figure 11) must be initiated by a thorough study to define the requirements associated with this device. An answer to such questions as "should the storage device also incorporate the capability of satisfying the control tasks as well as the power system functions?" and "should the energy storage function be the dominating item in the design of the flywheel?" must be provided. Once these and other questions have been satisfactorily addressed, it is then possible to define candidate flywheel concepts. Such definition must emphasize fail-safe designs but must also examine the need and advisability of containment. In addition, an assessment of scalability of the design must also be conducted. The development of the rotor must be performed in concert with the other elements of the storage system and not as an independent item in order to insure the attainment of the desired performance. To effect a timely system development, a two-phase program should be undertaken. Phase I should initiate 2-3 competitive system programs which would result in prototype storage units for thorough laboratory evaluations. The results of these tests would then be used in a final selection of the "optimum" design. Phase II would then produce a final system design, followed by fabrication and evaluation at the system level, which may include flight testing should test results so indicate the need.

#### 8. Rotor Fabrication Issues

One issue (Figure 12) raised by papers presented in the formal session was that an investigation should be conducted which will lead to improvements in filament wound single- or multiple-ring rotor fabrication. In addition, new concepts for attaching the motor/generator and suspension bearing components to the rotor must be developed. These developments are necessary to permit the attainment of the energy density and operational life postulated for this storage concept.

## 9. Testing

In terms of testing and evaluation of rotors, two categories were identified (Figure 13). These consisted of nondestructive inspection and evaluation, and spin testing. Nondestructive inspection will be instrumental in minimizing resources expenditures by allowing for the identification of manufacturing flaws in the rotor prior to the costly spin test program. Furthermore, the establishment of appropriate nondestructive inspection techniques (Figure 14) will facilitate the evaluation of the impact of handling damage or service-induced damage accumulation on system performance. One of the critical items which must be identified to make the nondestructive inspection and evaluation program successful is an accept/reject criteria definition.

## 10. Rotor Dynamics

Rotor failures are frequently preceded by system dynamic instabilities resulting from rotor imbalance. However, not all rotor instabilities lead to failures or are caused by mass imbalances. It is therefore necessary to define methodologies for recognizing the differences and thus improve our understanding of rotor and rotor system dynamics (Figure 15). In the case of the advanced storage systems where magnetic suspensions will be utilized, the impact of the unique characteristics of these suspensions on the rotor systems dynamics must be thoroughly investigated and understood.

## 11. Spin Testing

To reduce the cost burden on the overall development program (Figure 16), an evaluation of the suitability of existing DOE spin test facilities for conducting the test effort associated with this program is required. Should upgrading of these facilities be necessary, then the extent of these modifications and their attendant costs should be defined. In conducting a credible spin-testing effort for these storage devices, it is recommended that a good representation of the cyclic and environmental load spectrum be incorporated into the test setup, along with improved sensing capability for detecting onset of rotor failure based on changes in rotor balance and/or dynamic characteristics.

Safety issues (Figure 17) associated with this storage concept can be addressed during the design task by producing a non-burst or fail-safe design. Such a design would accommodate large safety margins and/or planned failure mechanisms such as the Rocketdyne mechanical fuse. Definition of the approach to be employed in addressing safety management in space applications must be generated.

## 12. Other Issues

Other issues which will have a significant impact on the evolution of this system concept (Figure 18) are the loads to which these devices will be subjected. Among these are the launch loads which are being quoted in the vicinity of 100g and the thermal loads posed by operating temperatures in the range of 850C. It is recommended that some consideration be given to utilizing metallic rotors in the interim period until all the issues raised in the working group deliberations can be resolved.

TABLE 1

ROTATING ASSEMBLY WORKING GROUP

PANEL MEMBERSHIP

<u>NAME</u>	<u>ORGANIZATION</u>
J. A. Kirk	University of Maryland
R. R. Rice	NASA-JSC
F. C. Younger	Brobeck Corporation
J. P. Joyce	NASA-LeRC
B. Wiest	Sperry-Space Systems
P. Burke	Bendix-Guidance Systems
J. Bloomer	Boeing Aerospace Corp.
B. P. Gupta	Lord Corporation
A. J. Hannibal	Lord Corporation
W. W. Anderson	NASA-LaRC
A. A. Robinson	ESA-ESTEC, Netherlands
S. O'Dea	C. S. Draper Laboratory
W. O. Wilkinson	Johns Hopkins U., A-P-L.
A. P. Coppa	G. E.-Space Systems
B. R. Ginsberg	Rockwell Intl., Rocketdyne
S. V. Kulkarni	LLNL
C. Haldeman	MIT Lincoln Laboratories

**PRESENTATION OUTLINE**

- TASK GOALS
- RATIONALE
- STRATEGY
- KEY PACING ISSUES

**. IDENTIFICATION OF TECHNOLOGY TASKS**

Figure 1

**TASK GOALS**

**DEMONSTRATE THE FEASIBILITY OF A FAIL-SAFE FLYWHEEL SYSTEM HAVING  
A USEFUL ENERGY CAPACITY OF ABOUT 5 kW-hr, A SYSTEM ENERGY DENSITY  
OF APPROXIMATELY 20 W-hr/kg, AND A LIFETIME OF 5-10 YEARS.**

Figure 2

TASK GOALS- KEY PACING ISSUE

SHOULD THE SPACE FLYWHEEL SYSTEM PROVIDE AC/ES OR ES ALONE?

- INVESTIGATE THE IMPACT OF A COMBINED AC/ES  
FUNCTION ON THE DESIGN OF AN ES FLYWHEEL  
SYSTEM
- (TRADE-OFF OF A DUAL PURPOSE AC/ES FLYWHEEL  
SYSTEM VS. SINGLE PURPOSE ES OR AC SYSTEM)

Figure 3

### RATIONALE

RECENT ASSESSMENTS (E.G., BOEING, NASA,....) SHOW  
THAT FLYWHEEL ENERGY STORAGE SYSTEMS IN SPACE OFFER  
ADVANTAGES OVER COMPETITIVE SYSTEMS SUCH AS BATTERIES,  
FUEL CELLS,....

- LONGER LIFE
- HIGHER ELECTRICAL EFFICIENCY
- HIGHER SYSTEM ENERGY DENSITY
- COMPOSITE MATERIAL FLYWHEELS ARE  
IMPORTANT FOR REALIZING THESE  
ADVANTAGES

Figure 4

STRATEGY

- UTILIZE EXISTING MATERIALS/FLYWHEEL DESIGN  
TECHNOLOGY DEVELOPED TO DATE  
(DOE, UMTA, U.S. ARMY, ETC.)
- . MAKE IMPROVEMENTS/MODIFICATIONS AS NECESSARY
- MAKE A LIST OF ALL DOE REPORTS AND SEND TO  
PARTICIPANTS

Figure 5

OBJECTIVES FOR MATERIALS TASK

- TO USE ESTABLISHED ENGINEERING DATA BASE ON MATERIALS  
APPLICABLE TO THE CANDIDATE ROTOR DESIGNS
- TO ENHANCE OUR UNDERSTANDING OF THE TIME-DEPENDENT  
BEHAVIOR OF COMPOSITES AND ASSESS THEIR LONG-TERM  
PERFORMANCE
- TO SCREEN AND SUPPORT THE DEVELOPMENT OF NEW MATERIALS FOR  
FUTURE UPGRADING OF FLYWHEELS

Figure 6

CRITICAL ISSUES IN MULTIYEAR PLAN

- MATRIX
  
- FIBER
  
- ENGINEERING DESIGN DATA

Figure 7

ISSUES WITH FIBERS

- FOR THE 1987 TECHNOLOGICAL READINESS DEMONSTRATION, CONSIDER EXISTING FIBERS (T-300, CELION-6000, GRAPHITE, KEVLAR-49, S2-GLASS) WHICH ARE WELL CHARACTERIZED
  
- SIMULTANEOUSLY DEVELOP PRELIMINARY DATA BASE FOR HIGHER STRENGTH FIBERS (AS6, IM6, T-700, T-800 GR, IMPROVED KEVLAR, ETC.)

Figure 8



### ISSUES WITH MATRICES

- ESTABLISH OPERATIONAL TEMPERATURE RANGE FOR THE CURRENTLY USED EPOXIES TO OBTAIN DESIRED PERFORMANCE LEVELS
  
- FLEXIBLE RESINS SHOULD BE INVESTIGATED BECAUSE OF THE ADVANTAGES ASSOCIATED WITH THEIR USE IN FILAMENT WOUND RINGS
  - . ASCERTAIN THEIR SAFE OPERATING TEMPERATURES
  
- INVESTIGATE APPLICABILITY OF METAL MATRIX COMPOSITES (BORON/AL,.....)

Figure 9

### ENGINEERING DATA DESIGN ISSUES

- DESIGN DATA FOR THE EXISTING COMPOSITE MATERIALS HAVE BEEN GENERATED. HOWEVER, ADDITIONAL DATA ARE REQUIRED FOR THE LOADING AND ENVIRONMENT IN SPACE APPLICATIONS
  - . LOAD/THERMAL CYCLING
  - . EFFECT OF RADIATION
  
- WHAT ABOUT POOR TRANSVERSE PROPERTIES OF COMPOSITES?
  - . LIVE WITH THEM?
  - . DETERMINE DESIGN VALUES TO INCLUDE DATA SCATTER?
  
- UTILIZE EXISTING DOE ROTORS TO EVALUATE CYCLIC LIFETIMES
  - . DATA WILL BE USEFUL FOR SPACE FLYWHEEL DESIGN
  
- DEVELOP LIFE PREDICTION METHODOLOGY BY ANALYZING MATERIALS AND SPIN TEST DATA

Figure 10

### ISSUES FOR FLYWHEEL DEVELOPMENT

- DEFINE DESIGN REQUIREMENTS (AC/ES, ES ONLY .....)
  - . ES FUNCTION SHOULD DOMINATE?
  
- DEFINE CANDIDATE FLYWHEEL CONCEPTS
  - . EMPHASIZE FAIL-SAFE DESIGN
  - . ASSESS FEASIBILITY OF SCALE-UP
  
- COMPOSITE ROTOR DEVELOPMENT SHOULD BE PART OF AN OVERALL SYSTEMS PROGRAM AND NOT AN INDEPENDENT ACTIVITY
  
- INITIATE 2-3 COMPETITIVE SYSTEMS PROGRAMS (PHASE I)
  
- NO. OF PROTOTYPES IN PHASE I TO BE DETERMINED BY TEST PROGRAM/RESOURCES (PROOF-OF-CONCEPT, CYCLIC TESTS IN SIMULATED CONDITIONS,.....)
  
- IN PHASE II SELECT ONE OR TWO OF THE DESIGNS FOR THE COMPLETE PROTOTYPE SYSTEM WHICH COULD BE FLIGHT TESTED

Figure 11

### ROTOR FABRICATION ISSUES

- INVESTIGATE IMPROVEMENTS IN FILAMENT WOUND  
(SINGLE/MULTIPLE) RING FABRICATION
- INVESTIGATE CONCEPTS FOR ATTACHING M/G AND  
BEARING COMPONENTS TO FLYWHEEL

Figure 12

### TEST AND EVALUATION OF ROTORS

#### KEY ACTIVITIES

- NONDESTRUCTIVE INSPECTION AND EVALUATION (NDI AND NDE)
- SPIN TESTING

Figure 13

**NONDESTRUCTIVE INSPECTION AND EVALUATION ISSUES**

- **MANUFACTURING DEFECTS, HANDLING DAMAGE, AND SERVICE-INDUCED DAMAGE ACCUMULATION NEED TO BE DETECTED**
  
- **APPROPRIATE NDI TECHNIQUES MUST BE IDENTIFIED**
  
- **ACCEPT/REJECT CRITERIA SHOULD BE DEVELOPED**
  - **METHODOLOGY SHOULD BE DEVELOPED FOR PROOF TESTING OF FLYWHEELS**

**Figure 14**

**ROTOR AND ROTOR SYSTEMS DYNAMICS ISSUES**

- MANY ROTOR FAILURES ARE PRECEDED BY SYSTEM DYNAMIC INSTABILITIES DUE TO IMBALANCE
- OUR UNDERSTANDING OF COMPOSITE ROTOR AND SYSTEMS DYNAMICS IS INADEQUATE
- UNIQUE CHARACTERISTICS OF SUSPENSION SYSTEM SHOULD BE CONSIDERED
- ROTOR DYNAMICS STUDIES TO DATE HAVE BEEN COMPILED AND PRESENTED IN A UNIFIED MANNER

**Figure 15**

### SPIN-TESTING ACTIVITY ISSUES

- UTILIZE EXISTING DOE FACILITIES (APL, Y-12,...) AS FAR AS POSSIBLE
  - DEFINE NEEDS FOR UPGRADING THOSE FACILITIES (FOR HIGHER ENERGY CAPACITY ROTORS AND PERTINENT SUSPENSION SYSTEMS)
  - THE FAILURE MODE OF ROTORS MUST BE CORRECTLY IDENTIFIED
  - EFFECTS OF DIFFERENT SUSPENSION SYSTEMS AND SHIFT IN BALANCE DURING TESTING NEED TO BE INVESTIGATED
  - DYNAMIC INSTABILITIES SHOULD BE DETECTED BEFORE THEY PRECIPITATE FAILURE
  - SPIN TESTING SHOULD BE PERFORMED IN A SIMULATED REAL LIFE LOAD SPECTRUM AND ENVIRONMENT DURING PHASE I
- . WHAT ARE THE FIXED OPERATING COSTS?

Figure 16

#### **SAFETY ISSUES**

- DESIGN ROTOR FOR NON-BURST MODE
  - . INITIAL FAILURE SHOULD BE OF A BENIGN NATURE AND DETECTABLE
- HOW DO WE ADDRESS SAFETY MANAGEMENT IN SPACE APPLICATIONS?

Figure 17

#### **OTHER ISSUES**

- LAUNCH LOADS (APPROXIMATELY 100g)
- SPACE ENVIRONMENT (APPROXIMATELY 85°C)
  - . TOO SEVERE
- USE METALLIC ROTORS IN THE INTERIM (PHASE I)
- MATERIAL COST IS A NON-ISSUE

Figure 18



N85

3852

UNCLAS

N85 13852 D2

ELECTROMECHANICAL/ELECTROMAGNETICS WORKING GROUP SUMMARY  
David B. Eisenhaure, Charles Stark Draper Laboratory, Chairman

INTRODUCTION

There were seven participants in the discussions conducted by this working group. The group deliberations centered on the component and system technology issues associated with the suspension and power conversion systems for the flywheel. The material which follows summarizes the recommendations and conclusions reached by this panel. At the end of this summary a list of the participants in this working group is presented in Table 1.

CONCLUSIONS AND RECOMMENDATIONS

1. Component and System Technology Issues

In view of the material presented during the paper sessions and the expertise of the panel members, it is believed (Figure 1) that adequate technology exists in both the suspension and power conversion areas to render the flywheel energy storage system concept competitive with other conventional approaches. This conclusion is partially predicated on having the Space Station control requirements, as well as the wheel stability characteristics, defined. Definition of these requirements is essential to permit appropriate component designs. For example, although magnetic suspension systems provide the storage device with several advantages, such as long life and higher efficiency, their lower stiffness, when compared with mechanical bearings, may pose a significant design problem to the control system engineer if the vehicle requirements are for high bandwidth control. Therefore, mechanical bearings cannot be ruled out at this point.

Since it is believed that the principal technology exists in these two areas, it is felt that the critical remaining issue is that of integrating the rotor, the suspension system, and the power conversion system into one operational device. To ameliorate this concern, it is recommended that the motor/generator and suspension system be developed as an integrated unit, and that the electronics and control techniques associated with that subsystem be considered an integral element of the subsystem itself.

To aid in the development of these devices, the following recommendations are made regarding efficiencies and operating voltages.

By 1987, it is believed that a storage efficiency of 80 percent should be required. This is a total storage system efficiency and includes standby losses, power conversion losses, motor/generator losses, etc., equivalent to losses normally encountered in other storage approaches such as battery systems. It is recommended, however, that a storage efficiency goal of 90 percent be set for the 1987 time frame. By 1992, it is believed that the storage efficiency requirement should be set at 85 percent with a goal of 92 percent. To insure that full advantage is being taken of the storage efficiency potential of flywheels, it is recommended that a bus voltage of 200+ volts be selected.

The other integration issue is that of combining the functions of attitude control and energy storage into one system. Although this question was not specifically addressed by this panel, it is felt that, based on the studies done by various conference participants, the technology in the power conversion and suspension systems area is adequate to support such an approach. Combining

these functions into one system eliminates some problems associated with cross-coupling which must otherwise be addressed. However, the resolution of this question was left to the system studies recommended in this summary.

## 2. Technology Development

It was recognized that the development of this technology consisted of three major steps and encompassed a complementary mix of analytical efforts and hardware development for validation of design approaches and concept implementations. These major elements included (Figure 2)

1. Immediate studies to determine the optimal system configuration considering gimballed and non-gimballed wheel concepts and incorporating the best 1984 component technology. These studies must also address the impact of rotor configuration on other elements of the system such as motor/generators and magnetic suspension systems in order to permit the selection of the optimal configuration for the demonstration phase.
2. By 1987, focus the development program on integration and demonstration of a complete system including the rotor, suspension, and power conversion subsystems with emphasis on efficiency.
3. In parallel with the integration and demonstration effort, conduct a technology program on motor/generators, suspension systems, gimbals, and sensors to take advantage of known technological advances.

## 3. Flight Testing

Regarding the necessity for flight testing of this technology, the panel concluded that this was not an essential part of the development effort at this time (Figure 3). However, it is recognized that such testing may become essential in the future, depending on the final system configuration and architecture.

TABLE 1

### MEMBERSHIP OF ELECTROMECHANICAL/ELECTROMAGNETICS WORKING GROUP

<u>NAME</u>	<u>ORGANIZATION</u>	<u>PHONE</u>
R. A. Kennedy	Sperry-Flight Systems	(703)892-0100
P. A. Studer	NASA-GSFC	(301)344-5229
L. Pursiano	Bendix-Guidance Systems	(201)393-3007
J. Downer	C. S. Draper Laboratory	(617)258-1458
D. B. Eisenhaure	C. S. Draper Laboratory	(617)258-1421
D. Litz	Westinghouse R&D Center	(412)256-2271
N. J. Groom	NASA-LaRC	(804)865-3350

1. COMPONENT AND SYSTEM TECHNOLOGY ISSUES

1.1 ADEQUATE TECHNOLOGY EXISTS IN BOTH BEARING AND POWER CONVERSION AREAS TO BE COMPETITIVE WITH ALTERNATIVE TECHNOLOGIES IF SPACE STATION CONTROL REQUIREMENTS AND WHEEL STABILITY CHARACTERISTICS ARE DEFINED.

1.2 THE PRINCIPAL CONCERN IS THE INTEGRATION OF THE ROTOR, BEARINGS, AND POWER CONVERSION.

1.3 MOTOR/GENERATOR AND BEARINGS SHOULD BE DEVELOPED AS AN INTEGRATED UNIT TOGETHER WITH THEIR ELECTRONICS AND CONTROLS.

1.4 RECOMMENDED STORAGE EFFICIENCY

1987	80% REQUIRED	90% GOAL
1992	85% REQUIRED	92% GOAL

1.5 RECOMMEND 200+ VOLTS BUS

Figure 1

## 2. MAJOR STEPS

2.1 IMMEDIATE STUDIES TO DETERMINE OPTIMAL OVERALL SYSTEM CONFIGURATION CONSIDERING GIMBALLED AND NON-GIMBALLED APPROACHES INCORPORATING BEST 1984 COMPONENT TECHNOLOGY.

2.2 BY 1987 DEVELOPMENT PROGRAM FOCUSING ON SYSTEM INTEGRATION AND DEMONSTRATION OF COMPLETE SYSTEM INCLUDING ROTOR, BEARING, AND POWER CONVERSION EMPHASIZING HIGH EFFICIENCY.

2.3 TECHNOLOGY PROGRAM ON MOTOR/GENERATORS, SUSPENSIONS, GIMBALS, AND SENSORS AIMED IN SUPPORT OF DEMONSTRATION PROGRAM TO TAKE ADVANTAGE OF KNOWN TECHNOLOGICAL POSSIBILITIES.

Figure 2

## 3. ASSESSMENT OF NEED FOR FLIGHT TESTING

NOT MANDATORY, BUT MAY BE NECESSARY, DEPENDING ON SYSTEM CONFIGURATION.

Figure 3

N85

3853

INCLAS

D3

# N85 13853

## ELECTRICAL/ELECTRONICS WORKING GROUP SUMMARY

Arthur D. Schoenfeld, TRW, Chairman

### INTRODUCTION

This panel considered the electrical/electronics technology area. The major conclusion arising from the discussions held by this group is that there are no foreseeable circuit or component problems (Figure 1) to hinder the implementation of the flywheel energy storage concept. Therefore, the membership of this panel addressed itself to the definition of the major component or technology developments required to permit a technology ready date of 1987. There were 13 participants in these panel discussions. Their names and affiliations are included in Table 1 at the end of this summary.

### CONCLUSIONS AND RECOMMENDATIONS

The committee recommendations deal with the following items: motor/generators, suspension electronics, power transfer, power conditioning and distribution, and modeling. In addition, an introduction to the area of system engineering is also included.

#### 1. System Engineering

Before proceeding with a technology development program, it is essential to define critical requirements and interfaces. A list of design considerations for this area will necessarily be quite long. Therefore, only the more critical aspects will be discussed here (Figure 2). One of these issues is peak power and energy reserves. A paper by Giudici, contained in these proceedings, addressed that topic earlier. In utilizing inertial energy storage systems at a 75 percent depth of discharge, the reserve margin for satisfying peak power demands is limited. Such topics must be addressed in system studies in order to define the peak power and energy reserve margin requirements for the spacecraft under consideration. Some concern has been expressed that too much emphasis is being placed on achieving higher energy density in this concept at the sacrifice of other possibly more important parameters such as life-affecting design factors. Next to life, the characteristic considered of extreme importance, because of its impact on other systems, is system efficiency. The system studies must also define modularity, redundancy, and resupply requirements. Module sizes in the range of 10-30 kilowatts were discussed, but final sizing should result from the specific spacecraft application studies.

As part of the overall system requirements definition, rotor balance and dynamic characteristics must be defined because of their major impact on suspension system stiffness and attitude control system effectiveness.

One of the potentially restrictive characteristics of this energy storage concept is the lack of available power during the deployment phase. Therefore, consideration must be given to a hybrid energy storage approach in which batteries may be used to provide power during deployment and to satisfy short-duration peak power needs.

## 2. Motor/Generator Electronics

The motor/generator electronics, or charge-discharge electronics, must be optimized for efficiency (Figure 3). The cooling of these circuits will become a problem, since dense packaging will be employed, possibly inside the rotor. Therefore, thermal control must be addressed early in the development phase.

Selection of the number of motor/generator poles must be made in concert with the selection of the electronics switching frequency. There is a certain relationship between the output frequency of the generator and the electronics which process and control that power output. Coordination of these selections is essential to insure that they are high enough to provide for high energy density, but not so high as to present a problem to the electronics and result in unacceptable operating efficiencies.

The required and achievable speed/momentum control accuracy of counterrotating MG's must be analyzed and properly specified. This is of special concern if the flywheels are used for storage only rather than integrated with the attitude control system. The specification of momentum control accuracy in counterrotating units, in addition to speed control accuracy, is necessary, since momentum is not a function of only rotational speed.

## 3. Suspension System Electronics

It is concluded that no critical electronics technology issues exist in this area. It is primarily a sensor and feedback control problem (Figure 4), which is covered by a separate working group.

## 4. Power Conditioning and Distribution

The input and output voltage of the inertial storage device should be high voltage dc. Direct current interfaces are easy to define. In addition, dc systems can readily be paralleled in redundant modules. For high-power applications, a value of 200+ volts is felt to be in the appropriate range. In addition to the charge-discharge electronics (Figure 5), there is a need for solar array voltage-limiting or voltage-regulating circuitry. The Space Station will have variable demands placed on its power system by the changing payloads, with the predictable loads being primarily those of the spacecraft housekeeping systems. Therefore, there will be conditions when the withdrawal of energy from the storage units will be considerably smaller than the anticipated average. In such a condition, there will be more energy in the arrays than can be absorbed by the inertia wheels without operating them at speeds above their design limits. Thus, if no control is placed on the array, an overvoltage condition will result which will adversely affect the electronics associated with the energy storage and power distribution systems.

Another protection measure which must be incorporated in the electronics or be an inherent feature of the energy storage system design is a means of surviving the failure of a paralleled energy storage module. Of particular concern is the output of a higher than allowable voltage under such failure conditions.

## 5. Power Transfer Across Rotating Interfaces

A dc rotary power transfer interface is recommended between the solar array and the energy storage system (Figure 6), and it appears that the required technology is well in hand. The rotating wheel energy storage device by itself does not require rotary power transfer interfaces, since the power is collected



ORIGINAL PAGE IS  
OF POOR QUALITY

from the stationary element of the unit. Approaches for effecting power transfer across rotating interfaces, such as presented by gimbals, include slip rings and roll rings. A paper was presented on the roll ring concept at this symposium.

6. Analytical Modeling and Simulation

Since it is unlikely that it will be possible to perform all the desired or even necessary testing, it will be essential to produce well-documented and well-analyzed designs. Therefore, it is recommended that, in parallel with the development of the hardware, modeling and simulation of the energy storage system be addressed (Figure 7). The total electrical power system shall be modeled and analyzed to include the static and dynamic behavior of the motor/generator and its electronics, the magnetic suspension system, the interfacing solar array, and the power distribution and conditioning systems. This modeling must incorporate the proper scaling factors for extrapolation and correlation of scaled-down hardware test results to full-scale storage modules.

The model(s) generated as a part of this effort will be instrumental in developing energy storage system management strategies for normal and abnormal operations. Since a Space-Station-type power system will have independent power buses with significant redundancy requirements, parallel modules are going to be necessary. Therefore, an energy management system is essential.

7. Technology Development Program

To demonstrate technology readiness (Figure 8), it is necessary to establish a data base derived from analytical studies, as well as performance and life testing. The requirements of the system must be defined, and a configuration must be selected as early as possible in order to meet a 1987 technology ready date attendant to the Space Station mission. The high efficiency of the motor/generator and associated electronics and the quality of the power produced by this storage system, as well as its dynamic performance capability, must be demonstrated. The integrated energy storage unit, i.e. the rotor, motor/generator, magnetic suspension, and electronics, must be tested, and its performance as an individual device, as well as an element of paralleled storage modules, must be evaluated. An output of such testing will be the demonstration of the storage system energy balance, redundancy, and failure recovery management capability. An integral part of the system evaluation is life testing to establish the credibility of this concept as a long life storage system capable of essentially unlimited operational cycles.

CONCLUDING REMARKS

It was felt unanimously by the members of this working group that this is a viable technology. It is a promising technology for low Earth orbit energy storage, which should be pursued, regardless of whether it can programmatically satisfy the needs of the early Space Station or whether it will be integrated with the attitude control functions or be used as an energy storage approach only. Integration of these functions into one system is preferred, but the question as to its implementation was left to be resolved by the system studies.

TABLE 1

ELECTRICAL/ELECTRONICS WORKING GROUP

PANEL MEMBERSHIP

<u>NAME</u>	<u>ORGANIZATION</u>	<u>PHONE</u>
A. D. Schoenfeld	TRW	(213)536-1972
F. Nola	NASA-MSFC	(205)453-4255
P. Jacobson	Sperry Space Systems	(602)869-2323
G. Rodgers	Sperry Space Systems	(602)869-2798
R. Hockney	C. S. Draper Lab	(617)258-4051
G. E. Rodriguez	NASA-GSFC	(301)344-6202
W. T. McLyman	JPL	(213)354-6810
J. Wright	GE Ordnance Systems	(413)494-4274
D. Renz	NASA-LaRC	(216)433-4000
B. Berman	Rockwell International	(213)594-2945
K. Juergensen	NASA-MSFC	(205)453-3770
K. Decker	TRW	(213)536-3073
S. Gross	Boeing Aerospace	(206)773-1198

**SUMMARY**

- THERE ARE NO IDENTIFIABLE CIRCUIT OR COMPONENT SHOWSTOPPERS
- 1987 TECHNOLOGY READINESS REQUIRES DEMONSTRATION OF PROGRAM OBJECTIVES BY ANALYSIS AND PROTOTYPE TESTING OF AN INTEGRATED FLYWHEEL SYSTEM CONFIGURATION
- THERE ARE NO INHERENT TECHNICAL REASONS TO DEMONSTRATE VIABILITY THROUGH FLIGHT TESTING

Figure 1

## SYSTEM ENGINEERING

BASED ON SPACE STATION REQUIREMENTS AND TECHNOLOGY TRADE STUDIES, DEFINE FLYWHEEL SYSTEM AND COMPONENTS REQUIREMENTS AND INTERFACES. SOME OF THE MORE CRITICAL DESIGN CONSIDERATIONS ARE

- PEAK POWER AND ENERGY RESERVE MARGINS
- FULL LOAD CHARGE/DISCHARGE EFFICIENCY AND STANDBY LOSSES
- MODULARITY, REDUNDANCY, AND RESUPPLY
- BALANCE AND DYNAMIC STABILITY CHARACTERISTICS
- SUSPENSION STIFFNESS CHARACTERISTICS
- DEPLOYMENT PHASE POWER/ENERGY REQUIREMENTS

Figure 2

### MOTOR/GENERATOR ELECTRONICS

- M-G AND ELECTRONICS OPTIMIZED FOR EFFICIENCY
- PROPER COOLING OF THE ELECTRONIC COMPONENTS MAY REQUIRE HEAT PIPES
- THE SELECTION OF THE NUMBER OF POLES SHALL BE COORDINATED WITH THE SELECTION OF THE ELECTRONICS SWITCHING FREQUENCY
- THE REQUIRED AND ACHIEVABLE SPEED/MOMENTUM CONTROL ACCURACY OF TWO COUNTERROTATING M-G'S SHALL BE ANALYZED AND PROPERLY DEFINED

Figure 3

### SUSPENSION SYSTEM ELECTRONICS

- NO ISSUES. IT IS PRIMARILY A SENSOR AND FEEDBACK CONTROL PROBLEM

Figure 4

#### POWER CONDITIONING AND DISTRIBUTION

- THE INPUT TO AND THE OUTPUT FROM THE INERTIAL ENERGY STORAGE SHALL BE HIGH VOLTAGE DC
- IN ADDITION TO THE ENERGY STORAGE CHARGE AND DISCHARGE ELECTRONICS THERE IS A NEED FOR A SOLAR ARRAY VOLTAGE LIMITER OR VOLTAGE REGULATOR
- THE FAILURE OF A PARALLELED ENERGY STORAGE MODULE SHALL NOT RESULT IN A HIGHER THAN ALLOWABLE OUTPUT VOLTAGE

Figure 5

#### POWER TRANSFER ACROSS ROTATING INTERFACES

- DC ROTATING POWER TRANSFER TECHNOLOGY APPEARS TO BE WELL IN HAND

Figure 6

### ANALYTICAL MODELING AND SIMULATION

- AS PART OF THE INERTIAL ENERGY STORAGE DEVELOPMENT PROGRAM THE STATIC AND DYNAMIC BEHAVIOR OF THE MOTOR/GENERATOR AND ITS ELECTRONICS, THE MAGNETIC SUSPENSION, AND THE ELECTRICAL POWER SYSTEM (CONSISTING OF THE SOLAR ARRAY, ENERGY STORAGE, POWER DISTRIBUTION AND CONDITIONING) SHALL BE MODELED AND ANALYZED
  
- DEFINE PROPER SCALING FACTORS FOR THE EXTRAPOLATION AND CORRELATION OF SCALED-DOWN DEVELOPMENT MODEL TEST RESULTS WITH LARGE-SCALE COMPONENTS AND SYSTEM PERFORMANCE
  
- DEVELOP ENERGY STORAGE SYSTEM MANAGEMENT STRATEGIES FOR NORMAL AND ABNORMAL OPERATION (WHERE THE ENERGY STORAGE SYSTEM WILL CONSIST OF PARALLELED ENERGY STORAGE MODULES CONFIGURED IN MULTIPLE REDUNDANT POWER DISTRIBUTION BUSES)

Figure 7

**MAJOR STEPS TOWARD TECHNOLOGY DEVELOPMENT  
(FOR 1987 TECHNOLOGY READINESS)**

- DEFINE REQUIREMENTS
- DEFINE CANDIDATE CONFIGURATION
- DEMONSTRATE HIGH EFFICIENCY M-G AND ELECTRONICS
- DEMONSTRATE POWER QUALITY (VOLTAGE REGULATION AND RIPPLE) AND DYNAMIC PERFORMANCE
- DEMONSTRATE INTEGRATED M-G AND MAGNETIC SUSPENSION SYSTEM PERFORMANCE OF PARALLELED ENERGY STORAGE MODULES
- DEMONSTRATE ENERGY STORAGE SYSTEM ENERGY BALANCE, REDUNDANCY, AND FAILURE RECOVERY MANAGEMENT
- LIFE TESTING
- COMPILE DATA BASE FOR TECHNOLOGY READINESS DEMONSTRATION

Figure 8



N85

3854

UNCLAS

N85 13854

D4

DYNAMICS AND CONTROLS WORKING GROUP SUMMARY

Ronald E. Oglevie, Rockwell International, Chairman

INTRODUCTION

This working group evaluated the technology status of the dynamics and controls discipline as it applies to energy storage wheel systems. The major conclusion arising from this survey is that no problems were identified for which an adequate solution could not be proposed. In addition to this principal task, the panel undertook to address design issues that influence control. The results of these efforts are presented in this summary report. The membership of the Dynamics and Controls Working Group included 12 persons and is shown in Table 1 at the end of this summary.

CONCLUSIONS AND RECOMMENDATIONS

The group participants addressed the dynamics and controls aspects associated with not only the energy storage system concept and its various constituent parts, but also the controls task attendant to large, manned spacecraft. The conclusions drawn by this panel along with its recommendations for the enhancement of the appropriate technology are presented herein.

1. Working Group Summary and Sample Opinions

The results of the technology evaluation conducted by this group (Figure 1) indicate that there are no problems in the dynamics and controls area for which an adequate solution cannot be presented. It is clear that in the dynamics of high-speed rotating machinery there are potential pitfalls. However, design experience has shown that early recognition of these dynamic pitfalls can reduce them to straightforward engineering problems. Also there were interdisciplinary interactions and Space Station application oriented issues identified which necessitate thorough system level and integration studies (such as integration of thermal control). As with the other working groups, no special benefits could be identified for flight testing this technology at this time as related to the dynamics and controls discipline. It is virtually mandatory that even a flight system be testable in a lg environment. One issue which is recommended for early resolution is that of laboratory verification of energy recovery efficiency.

A sample of the working group opinions on some of the critical issues is indicated in Figure 2. In the area of magnetic suspension control laws, the current techniques are determined to be adequate and can result in the design of a system which is controllable. Available evidence from simulations indicates that the issues associated with momentum and energy management can be handled. Questions to be answered in that area will be addressed shortly. The important issue of fault isolation and robustness must be examined in the course of a thorough systems level engineering study in which an actual fault isolation approach is defined and embodied during the early phases of the system design. Suitable failure detection, isolation, and correction policies must be devised and must encompass potentially unstable failures. It is evident that this is one of the areas in need of a strong systems level design study to support and

complement the component level design efforts. None of these problems were felt to present insurmountable challenges to the designer. It was the consensus of the group that a strong dynamic-modeling, analysis, and simulation effort during the early design phases is the key to avoiding the potential pitfalls in this class of system.

An opinion poll of the working group regarding the need to develop energy storage wheel (ESW) technology and whether attitude control should be integrated with it for the Space Station application is shown at the bottom of Figure 2. The results reflect a strong affirmative consensus on both issues. Regarding the issues of "ball bearings versus magnetic bearings", and "steel versus composite rotor materials", there was considerable diversity of opinion and no consensus was reached.

In order to focus more clearly on the dynamics and control issues, the next two sections have been organized in terms of the system and component level design issues that directly influence them. In this class of equipment, it is imperative that the various design parameters are selected to insure reasonable stability and control.

## 2. System Level Design Issues

Additional issues which the working group deemed to be important in their potential influence on dynamics and control include (Figure 3)

- 1) To what extent should the attitude control function be integrated with the energy storage function?
- 2) How should the system be configured for simultaneous energy and momentum management?
- 3) What are the key physical design parameters requiring system level trades?

With respect to the first item, the question of torque dynamic range must be addressed. The large torques associated with energy management must be compensated by the momentum management system with sufficient precision that relatively small, noise-free attitude control torques can be provided. Also, life-cycle cost, weight, volume, complexity, and technology readiness issues must be addressed.

The impact of energy and momentum management considerations in the definition of the system configuration must be examined to insure that such issues as safety, reliability needs, and fault detection, isolation, and correction are entertained early in the design phase. Once the system issues have been addressed and the operational requirements defined, the storage unit specifications can then be generated. Several trade-offs must be performed to answer the questions of the number of units, their configuration and mounting arrangement, as well as some implementation characteristics such as rotor material and suspension approach for this rotor. Other significant issues are how to maintain thermal control of the ESW rotor and stator, and the compatibility of this approach with the Space Station thermal control system.

## 3. Component Control System Design Issues

Having addressed the system level considerations, we can now focus on the issues associated with the control of an individual energy storage wheel component (Figure 4).

For example, wheel speed control aspects such as resolution, overspeed prevention, and anomaly detection must be examined. The regulation and distribution of the generated power must be specified. If magnetic suspension of the rotor is utilized, then the magnetic actuator control approach for that system must be selected from a variety of candidates such as all-electromagnetic or permanent magnet flux-bias concepts. In addition the impact of that suspension approach and its control scheme on the structural dynamics of the storage unit and the overall system must be evaluated. Magnetic suspension systems also require special provisions during spacecraft launch, and in case of electronic failure, backup bearings. The technique selected for the control of the gimbal(s) will have a direct impact on the controller bandwidth. In addition, limited gimbal travel to simplify power transfer across rotating interfaces will have to be traded off against additional software costs and complexity. A desirable feature, and probably a required one, is the need for this system to be testable in a lg environment. Of course, the system must be designed for long-term operational life, but if failures do occur, then techniques to accommodate such events must be provided in the system design.

An issue of prime importance in any program of this nature is "what is the next major thrust?" This gives rise to the classical engineering compromise (Figure 5): "What level of technology should be pursued versus how long should this program take and how much should it cost?"

#### 4. Major Steps in the Technology Development

Included in this report is a 10-year schedule starting in 1984 and ending in 1994 (Figure 6). The first launch date is shown to be in January 1994. As can be noted from this schedule, the first task is to upgrade the existing IPACS hardware to permit the early demonstration of the energy recovery efficiency of this concept. The system engineering study, previously mentioned, will entertain all the interacting design issues to arrive at an "optimized" system design. Advanced component development is pursued either in an integrated form, or as shown here, in a parallel fashion, in which the rotor and suspension system definitions are conducted simultaneously with the motor/generator and electronics evolutions. Early integrated system testing is a very crucial step in this program, regardless of the development scenario selected for the components. It was felt by the panel membership that this kind of scheduling can result in a technology readiness date of 1987, which is compatible with the Space Station mission. The development schedule for the flight hardware is also depicted here to show that it is possible to overlap these tasks successfully and to indicate that if this kind of success-oriented program can be maintained, sufficient time exists for the Space Station system evolution.

TABLE 1  
DYNAMICS AND CONTROLS WORKING GROUP  
PANEL MEMBERSHIP

<u>NAME</u>	<u>ORGANIZATION</u>	<u>PHONE</u>
H. F. Kennel	NASA-MSFC	(205)453-4718
D. D. Nixon	NASA-MSFC	(205)453-2714
J. L. Williams	NASA-LaRC	(804)865-2486
H. R. Whitman	C.S. Draper Laboratory	(617)258-3374
J. Rinderle	Carnegie-Mellon U.	(412)578-3677
F. R. Penovich	NASA-KSC	(305)867-2036
R. Benhabib	TRW	(213)536-1891
G. Stocking	Sperry-Space Division	(602)869-2033
R. E. Oglevie	Rockwell International	(213)922-0248
H. Hoffman	NASA-GSFC	(301)344-8496
N. J. Groom	NASA-LaRC	(804)865-3350
P. D. Nicaise	NASA-MSFC	(205)453-3668

SUMMARY

- CONTROLS AND DYNAMICS TECHNOLOGY IS ADEQUATE FOR THE DEVELOPMENT OF ESW TECHNOLOGY
  - . MAGNETIC SUSPENSION CONTROL LAWS
  - . MOMENTUM AND ENERGY MANAGEMENT
  - . CONTROL BANDWIDTH CONSIDERATIONS, ETC.
  
- MANY ISSUES DEFINED THAT NEED TO BE INCLUDED IN SYSTEMS LEVEL STUDY DURING TECHNOLOGY DEVELOPMENT PHASE
  
- FLIGHT TESTING NEED?  
NO SPECIAL BENEFITS DEFINED
  
- EARLY LABORATORY VERIFICATION OF ENERGY RECOVERY EFFICIENCY (END-TO-END) IS NEEDED

Figure 1

WORKING GROUP OPINIONS ON EXAMPLE ISSUES

- SUSPENSION SYSTEM CONTROL LAWS?  
CURRENT TECHNIQUES ADEQUATE, DESIGN TO BE CONTROLLABLE
- MOMENTUM AND ENERGY MANAGEMENT?  
NO PROBLEMS
- FAULT ISOLATION/ROBUSTNESS?  
IMPORTANT, BEST APPROACH SHOULD BE DEFINED IN "SYSTEM-LEVEL"  
DESIGN STUDY
- CONTINGENCY CRITERIA AFTER UNIT FAILURE?  
NEED TO DO DYNAMICS AND CONTROL ANALYSIS OF POTENTIAL FAILURE  
MODES, OTHERWISE SAME ANSWER AS ABOVE
- MODELING?  
ENERGY STORAGE UNIT DYNAMICS IMPORTANT, SAME AS ABOVE
- WORKING GROUP OPINIONS BY VOTE:
  - . SHOULD E.S.W. TECHNOLOGY DEVELOPMENT BE PURSUED?  
9 - YES; 0 - NO; 2 - NO OPINION
  - . INTEGRATE ATTITUDE CONTROL WITH ENERGY STORAGE?  
7 - YES; 0 - NC; 4 - NO OPINION

Figure 2

SYSTEM LEVEL DESIGN ISSUES  
(OR "HOW TO DESIGN FOR CONTROLLABILITY")

- EXTENT OF INTEGRATING ACS/EPS?
  - . TORQUE DYNAMIC RANGE COMPATIBILITY
  - . COST, WEIGHT, AND VOLUME SAVINGS?
  - . COMPLEXITY AND READINESS
  
- HOW TO CONFIGURE FOR ENERGY AND MOMENTUM MANAGEMENT?
  - . SPATIAL DISTRIBUTION, CENTRALIZED OR NOT?  
(HOW MANY AND WHERE?)
  - . HOW ACCOMMODATE SAFETY? RELIABILITY NEEDS; FAULT DETECTION,  
ISOLATION, AND CORRECTION? CONTAINMENT VS. OTHERS?
  - . MODULARITY, GROWTH PROVISIONS, TECHNOLOGY UPGRADING
  - . ACCOMMODATION OF STRUCTURAL COMPLIANCE, INTERNAL AND EXTERNAL  
TO UNITS
  
- PHYSICAL CONFIGURATION
  - . NUMBER OF UNITS AND GIMBALS (0, 1, OR 2)?
  - . MOUNTING ARRANGEMENT(S)?
  - . BALL BEARING VS. MAGNETIC?
  - . ROTOR MATERIAL- STEEL VS. COMPOSITE X, Y, OR Z?
  - . THERMAL CONTROL

Figure 3



## COMPONENT CONTROL SYSTEM DESIGN ISSUES

- WHEEL SPEED CONTROL
  - . RESOLUTION
  - . OVERSPEED CONTROL
  - . ANOMALY DETECTION - SENSORS AND SOFTWARE
  
- POWER CONTROL
  - . REGULATION
  - . DISTRIBUTION
  
- MAGNETIC SUSPENSION CONTROL
  - . ELECTROMAGNETIC
  - . PERMANENT MAGNET
  - . STRUCTURAL DYNAMICS
  - . GRACEFUL FAILURE DETECTION
  - . TOUCHDOWN BEARINGS
  - . LAUNCH PROVISIONS
  
- GIMBAL CONTROL
  - . PRECESSION CONTROL
  - . AUXILIARY CONTROL MODES (RUN UP)
  - . NONLINEARITIES (LIMITED GIMBAL FREEDOM)
  
- 1g DEMONSTRATION OF DUAL FUNCTION
  
- DESIGN FOR LONG LIFE
  
- FAILURE ACCOMMODATION TECHNIQUES

Figure 4

**"THE CLASSIC ENGINEERING COMPROMISE"**

**TECHNOLOGY LEVEL**

**VS**

**COST AND SCHEDULE**

**Figure 5**

# MAJOR STEPS IN THE TECHNOLOGY DEVELOPMENT

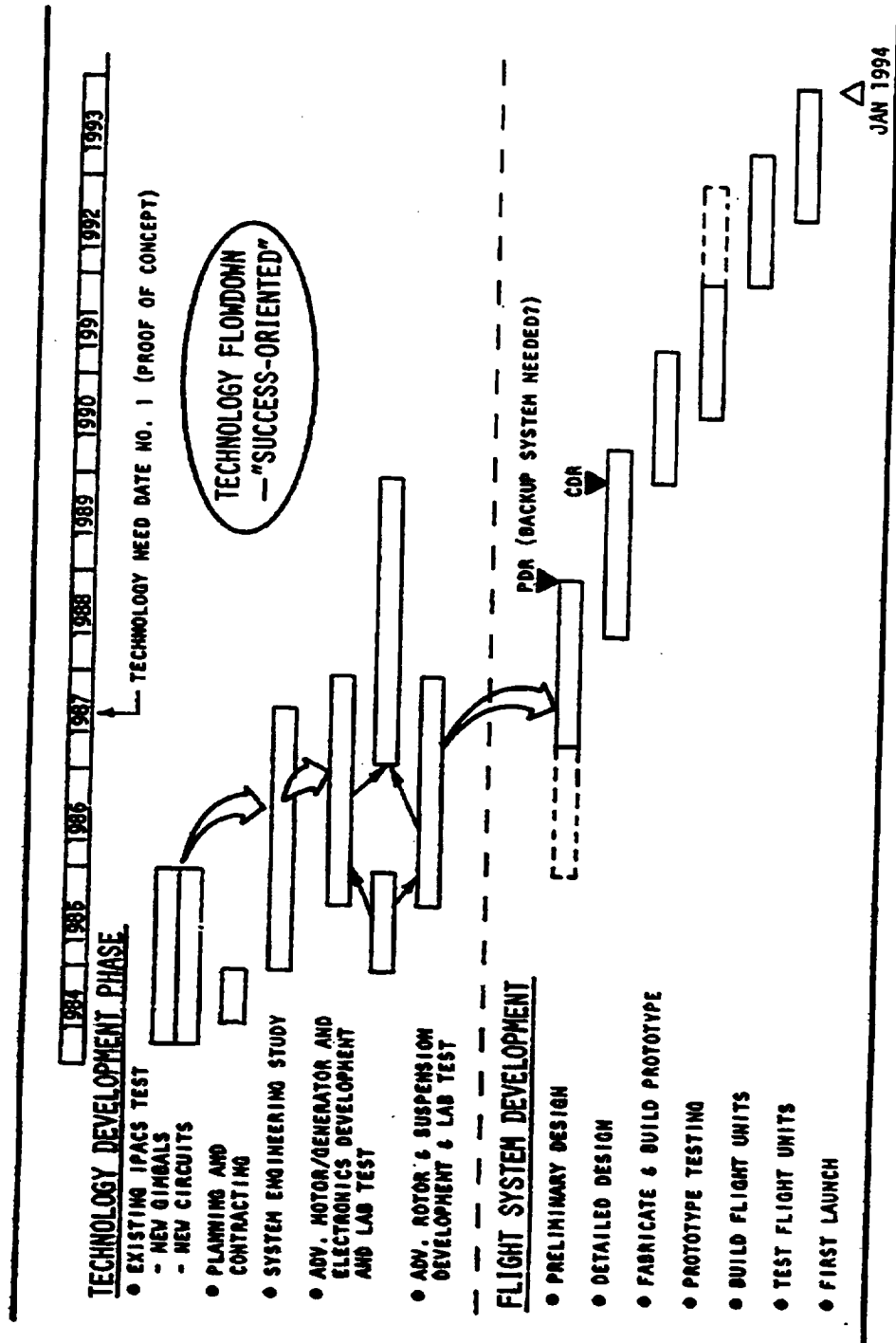


Figure 6

N85

3855

INCIALS

D5

N85 13855

**A SUMMARY OF THE 1983  
INTEGRATED FLYWHEEL TECHNOLOGY WORKSHOP**

Claude R. Keckler  
NASA Langley Research Center  
Hampton, Virginia

## WORKSHOP OBJECTIVES

The use of flywheels to perform the functions of attitude control and/or energy storage on a variety of space missions has been of interest to NASA for several years. Preliminary studies were initiated in the early 1970's and have been carried forward by both government and industrial concerns ever since. Recent interest in this technology, on the part of NASA, resulted in the Integrated Flywheel Technology - 1983 Workshop held at the Goddard Space Flight Center in August 1983. This workshop had four primary objectives, shown in figure 1:

- 1) Determine the potential of flywheels for energy storage system applications as well as for combined energy storage and attitude control concepts.
- 2) Assess the state-of-the-art (SOA) in integrated flywheel technology through a review of government sponsored programs.
- 3) From this assessment, identify those technology areas which are in critical need of development to meet projected space mission requirements.
- 4) And finally, scope a program for the coordinated development of the required technology.

The results of this workshop are contained in NASA CP-2290 (ref. 1) and are summarized in this presentation.

- 0 DETERMINE POTENTIAL OF SYSTEM CONCEPTS
- 0 ASSESS SOA IN INTEGRATED FLYWHEEL SYSTEMS TECHNOLOGY
- 0 IDENTIFY CRITICAL TECHNOLOGY AREAS
- 0 SCOPE PROGRAM FOR COORDINATED ACTIVITY

Figure 1

## PARTICIPATION

A total of 34 participants representing various government programs and interests attended the 1983 Integrated Flywheel Technology Workshop. The high level of interest in this technology within NASA is evident from the number of organizations represented at this conference (fig. 2). Presentations were made by many of the participants covering the disciplines of systems, power, and control. A compilation of those papers is contained in reference 1.

### 0 ORGANIZATIONS

- NASA HEADQUARTERS
- GODDARD SPACE FLIGHT CENTER
- JET PROPULSION LABORATORY
- JOHNSON SPACE CENTER
- LANGLEY RESEARCH CENTER
- LEWIS RESEARCH CENTER
- MARSHALL SPACE FLIGHT CENTER
- DEPARTMENT OF ENERGY

### 0 DISCIPLINES

- SYSTEMS
- POWER
- CONTROL

Figure 2

### INTEGRATED SYSTEM CONCEPT

The system concept discussed during the workshop is depicted in figure 3. As can be seen, solar energy is converted to electricity by solar arrays during the sunlit portion of the orbit. This is used to power the spacecraft's subsystems, as well as to accelerate a rotating flywheel thereby storing energy for future use. During the occulted portion of the orbit, umbra power is obtained by decelerating the rotating wheel and converting the kinetic energy to electricity via a generator attached to the wheel shaft. This approach permits the elimination of the conventional battery storage system. In addition, functional integration with the vehicle's momentum control system can be effected, for example, by mounting these wheels on a set of gimbals.

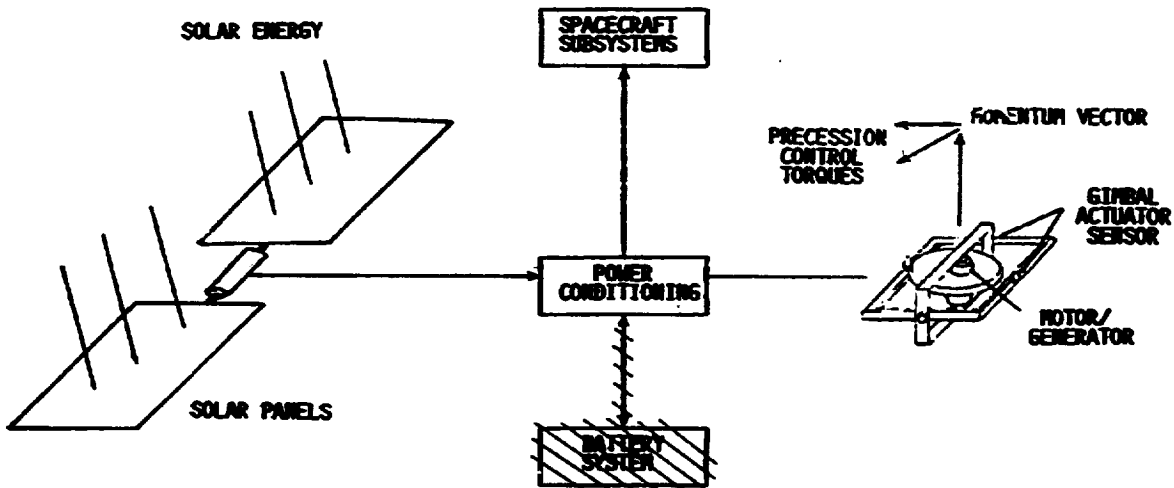


Figure 3



## PRESENTATION TOPICS

The range of topics covered by the various presentations is shown in figure 4. These covered: system sizing and performance study results; information on state-of-the-art and advanced flywheel energy storage system concepts; a description of the DOE program on advanced composite material rotor developments; an overview of technology efforts abroad; data from system trade studies; a summary of advanced technology developments in electronics, rotor suspension and actuators; a definition of a technology program approach and of planned integrated system testing activities. A sample highlight of some of these topics is shown in the figures that follow.

- 0 SYSTEM SIZING TRADES AND PERFORMANCE STUDIES
- 0 ENERGY STORAGE SYSTEM CONCEPTUAL DESIGNS
- 0 FLYWHEEL PROTOTYPE DEVELOPMENTS FOR TERRESTRIAL APPLICATIONS
- 0 OVERVIEW OF EUROPEAN DEVELOPMENTS
- 0 POWER, ENERGY STORAGE, AND ATTITUDE CONTROL TRADE STUDIES
- 0 TECHNOLOGY ADVANCEMENTS IN ELECTRONICS, ROTOR SUSPENSION,  
AND ACTUATORS
- 0 TECHNOLOGY PROGRAM OUTLINE
- 0 INTEGRATED SYSTEM TEST BED ACTIVITIES

Figure 4

### MISSION APPLICATIONS STUDY

One of the system studies, performed in the early 1970's, was to examine the applicability of an integrated power/attitude control system (IPACS) concept over a broad range of mission types. The IPACS utilizes rotating flywheels to perform the dual functions of energy storage/power generation and attitude control. The types of missions examined during this study are listed in the table of figure 5. As can be noted, these selected missions encompassed small near-Earth satellites, geosynchronous satellites, interplanetary missions, and manned space stations. Power requirements ranged from a few hundred watts (180 W) to several kilowatts. Attitude control was specified at between 1 arcsecond and 1 degree. Results from that effort indicated that significant weight, volume, and cost savings could be realized by using the IPACS concept over the proposed conventional approach for all mission classes except the interplanetary flight (ref. 2)

	LAUNCH DATE	MISSION DURATION	MANNING	ORBIT CHARACTERISTICS (KM/HR)	WEIGHT (LB)	POINTING ACCURACY (DEGREES)	POWER LEVEL (WATTS)	REMARKS
NEAR EARTH SATELLITE: EARTH OBSERVATIONS SATELLITE	1978	2 YRS	UNMANNED	SUN SYNCH 1100 (600)	770 (1700)	1.0	727w	EARTH OBSERV. SOLAR ARRAY/BATT
GEOSYNCHRONOUS SATELLITE: TRACKING & DATA RELAY SATELLITE	1977	3 YRS	UNMANNED	0° 35,700 (19,300)	1230 (2717)	0.3	300/180w	COMMUN. SAT. SOLAR ARRAY/BATT
PLANETARY SATELLITE: MARTNER-JUPITER/SATURN	1977	4 YRS	UNMANNED	30° 1.43 x 10 <sup>8</sup> (9.5 A.U.)	680 (1500)	0.05	350w	SCIENTIFIC SAT. ETC
SHUTTLE 30-DAY MISSION: EARTH OBSERVATION & COMMUNICATION TECHNOLOGY	1979	30 DAYS	MANNED	55° 500 (270)	37,500 (215,000)	0.5	3000w	EARTH RESOURCES FUEL CELL
RAM: ADVANCED SOLAR OBSERVATORY	1986	4-6 YRS	UNMANNED OPS. MANNED MAINTEN.	45 TO 55° 500 (270)	12,200 (27,000)	1.66	500w	ASTRONOMY SOLAR ARRAY/BATT
ROBULAR SPACE STATION: NORTH AMERICAN DESIGN	1985	10 YRS	MANNED	55° 500 (270)	\$1,500 (180,000)	0.25	19,000w	GENERAL PURPOSE SOLAR ARRAY/ REGEN F/C

Figure 5

### STATE-OF-THE-ART FLYWHEEL STORAGE UNIT

The encouraging results obtained from the previously mentioned study led to the design and fabrication of a flywheel storage unit. This device, shown in figure 6, is representative of the state of the art in homogeneous material flywheels. This unit is fabricated out of titanium, is suspended on conventional angular contact ball bearings, and is driven by two brushless d.c. motor/generators. Storage capacity of this unit at 35,000 rpm is about 1.5 kW-hrs. This device generates 2.5 kW of power at 52 volts d.c.. A detailed description of this unit can be found in reference 3.

ORIGINAL PAGE IS  
OF POOR QUALITY.

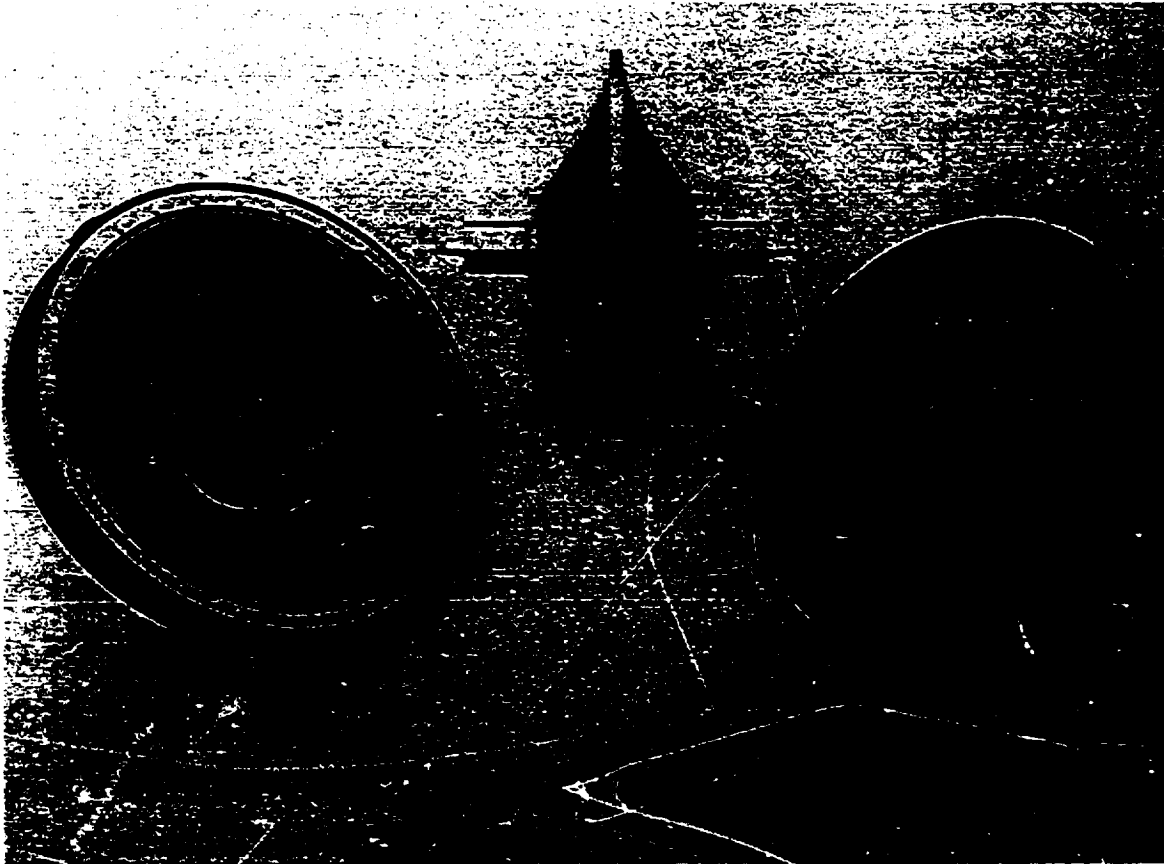


Figure 6

ADVANCED STORAGE UNIT CONCEPT

Capitalizing on significant advances in the state of the technology in composite materials and electromagnetics, several advanced storage system concepts have been postulated. Typical of such concepts is the unit shown in figure 7. This approach utilizes a pair of counter-rotating wheels to minimize the impact on the vehicle control system resulting from momentum variations incurred by the wheels during energy state changes. In addition to striving for higher energy density and safety through the use of composite materials, this concept proposes the use of magnetic bearings for lower system losses and thus higher efficiency and longer operational life. Additional efficiency and operational life gains are anticipated by employing permanent magnet brushless d.c. motor/generators. Details of this concept can be found in references 4-6.

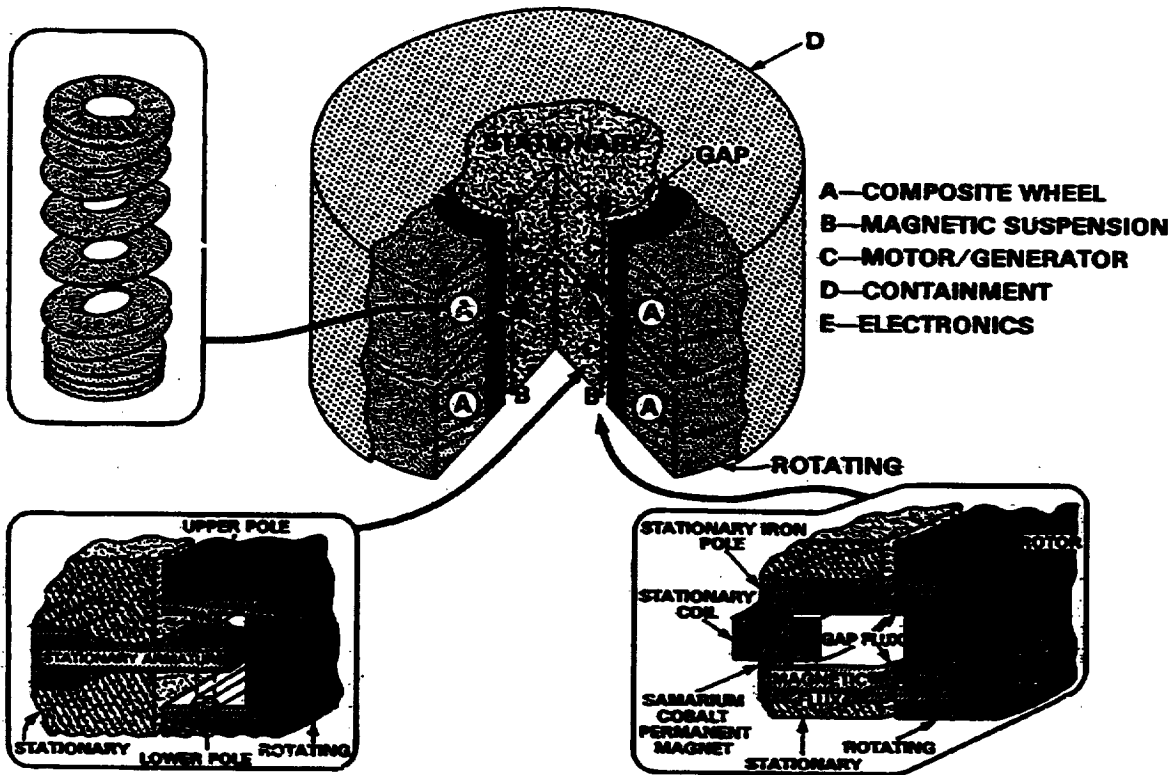


Figure 7

ORIGINAL PAGE IS  
OF POOR QUALITY

## FLYWHEEL MATERIALS

Composite materials applications to flywheels have, until very recently, been concentrated in the Department of Energy. Typical energy densities realized and postulated for flywheels using these materials are shown in figure 8. The benefits offered by composites over isotropic materials are quite evident in this figure. A summary of the DOE program can be found in reference 1, pages 35-46. In addition, advanced flywheels performance projections are given in reference 7.

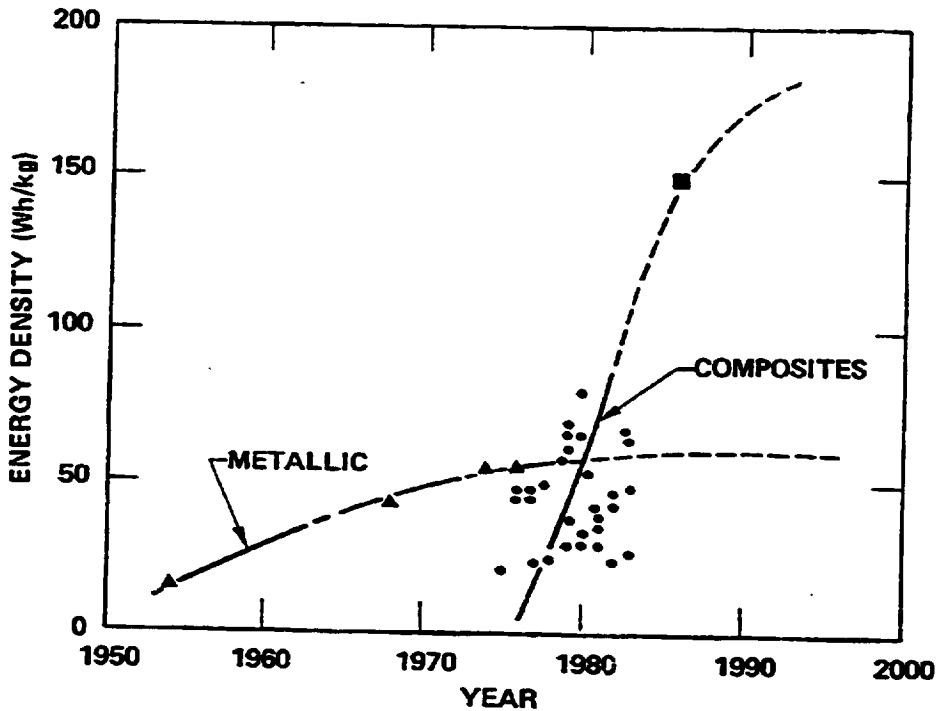


Figure 8

## DOE FLYWHEEL CONCEPTS

In the course of the DOE program, several flywheel designs were generated. A number of these are shown in figure 9. The ten configurations depicted here represent three generic design categories, namely rims, disks, or rim/disk hybrids. Each of these concepts represents a significant advance in the application of composite materials to flywheel use.

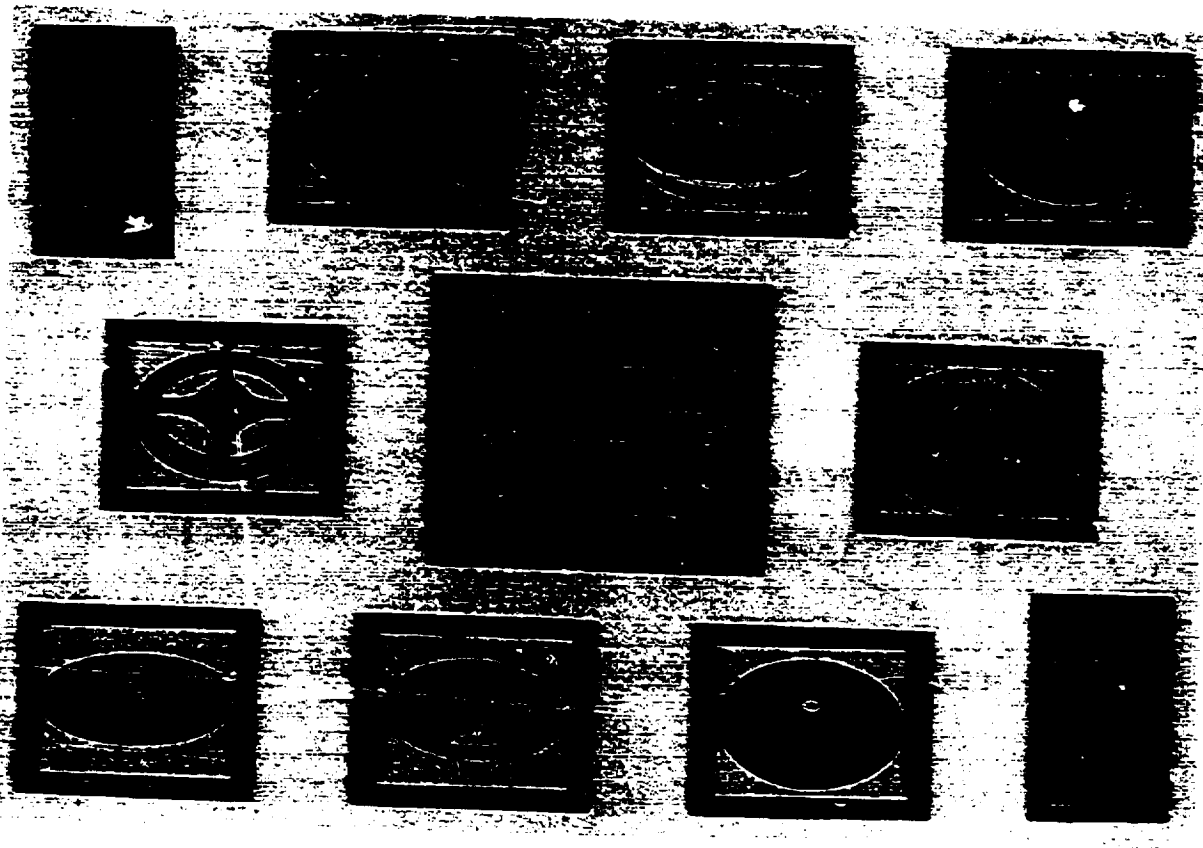


Figure 9

ORIGINAL PAGE IS  
OF POOR QUALITY

## SYSTEMS TRADE STUDIES

A typical example of a large variety of systems trade studies is demonstrated in figure 10. In this study, performed by R. Giudici of MSFC (ref. 1, pages 4<sup>o</sup>-57), the weight to orbit of various energy storage/attitude control system concepts over the life of the intended mission is compared. As can readily be noted, flywheel systems do appear to be very competitive with other postulated concepts.

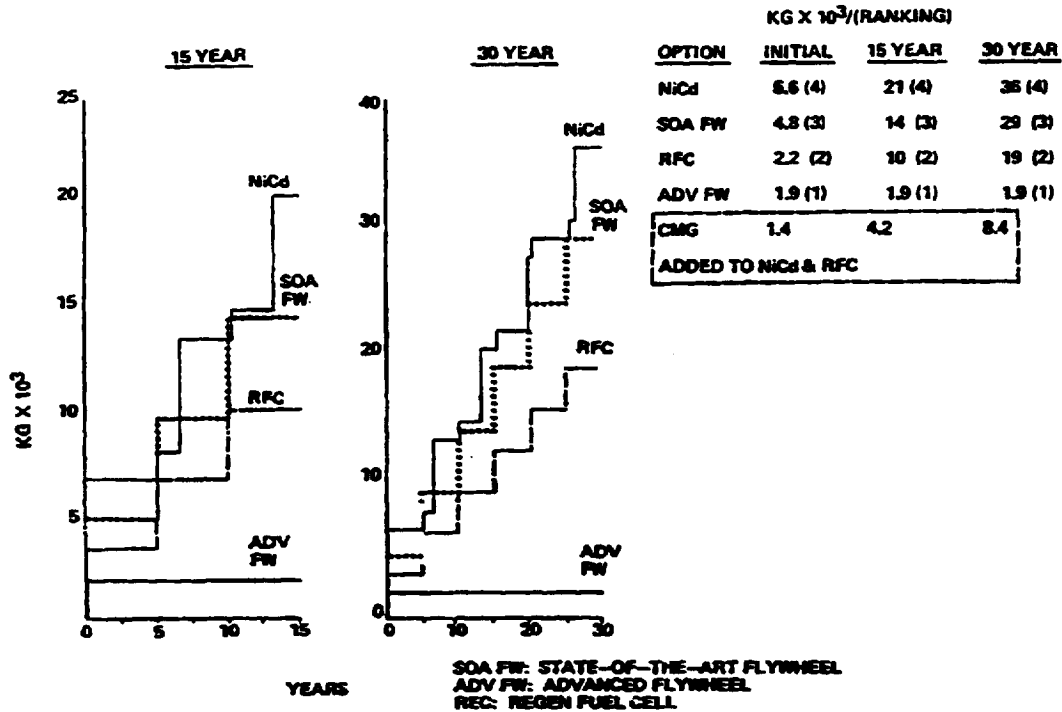


Figure 10

## TECHNOLOGY ADVANCEMENTS

A recurring theme at the 1983 Integrated Flywheel Technology Workshop was the need for technology advanced in the areas of composite materials and their utilization, rotor suspension, and brushless d.c. motor/generators. Some steps have been taken in these areas and are contained in the Langley Research Center Annular Momentum Control Device (AMCD). This 5.5 ft. diameter graphite-epoxy ring is suspended on three magnetic bearing stations located around the rim, and is driven by a rim drive brushless d.c. motor (fig. 11). As can be noted, no contacting elements are used in this unit; therefore, significant efficiency and operational life gains can be achieved. Details of this concept and its applications can be found in references 8 and 9.

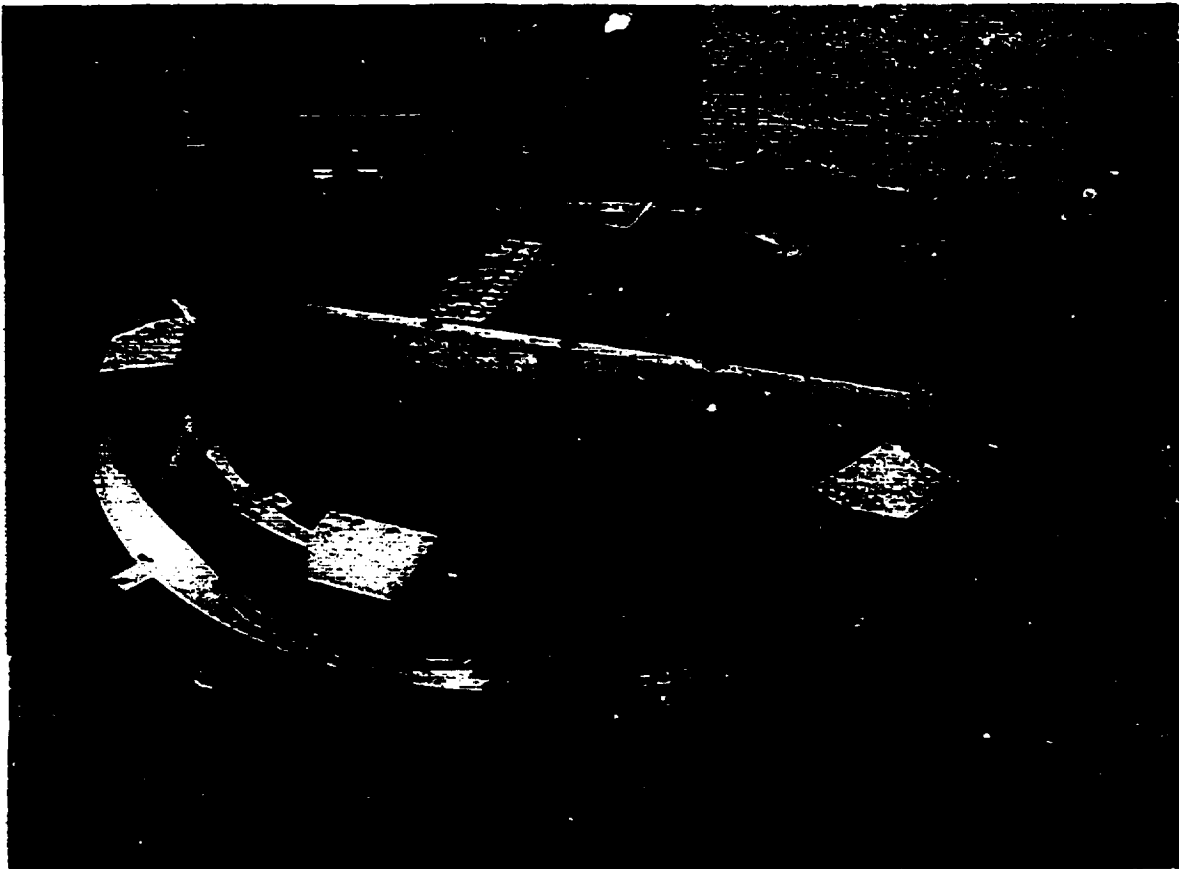


Figure 11

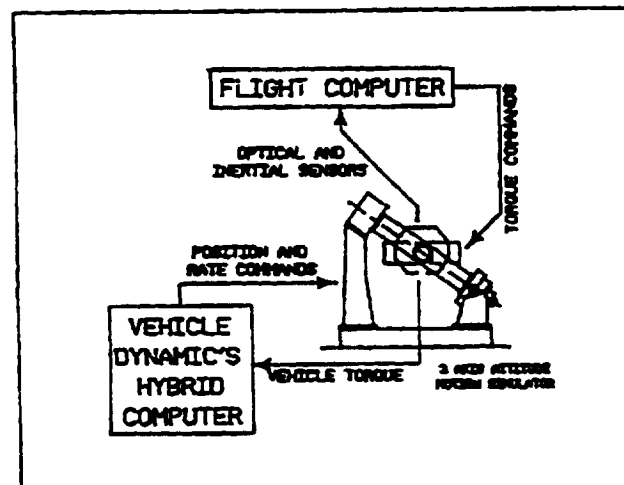
ORIGINAL PAGE IS  
OF POOR QUALITY



## INTEGRATED SYSTEM TESTING

An integral part of the technology evolution process is a thorough ground-based test program which may or may not be complemented by flight experimentation. In the case of the inertial energy storage system concept, testing on an attitude control system test bed, as well as a power system test-bed, simultaneously or separately, is being considered. Such a test-bed activity is described in figure 12.

### SPACE STATION ATTITUDE CONTROL SYSTEM SIMULATOR



#### THE ATTITUDE CONTROL SYSTEM SIMULATOR CONSISTS OF:

- A LARGE 3 DEGREE OF FREEDOM TABLE POWERED BY HYDRAULIC ACTUATORS DESIGNED TO GIVE HIGH BANDWIDTH AND EXTREMELY FINE CONTROL THROUGH LARGE ANGLES
- COMPENSATION FOR EARTH ROTATIONAL RATE
- CONTROL MOMENT GYRO'S
- STAR TRACKER
- RATE GYRO'S
- STAR SIMULATOR AND SOLAR SIMULATOR PROVIDING COLLIMATED LIGHT MIMING THE SPECTRAL CONTENT AND INTENSITY RECEIVED IN EARTH ORBIT

#### THE CONTROL SYSTEM SIMULATOR INCLUDES A 3 DEGREE OF FREEDOM POINTING MOUNT TABLE

- SEVERAL POINTING MIMING POINTING MOUNTS
- POINTING MOUNT CONTROL WILL BE HEAVILY INTERACTIVE WITH SPACE STATION CORE CONTROL AND WITH THE DYNAMICS OF THE STRUCTURE

#### ATTITUDE CONTROL SYSTEM SIMULATION ACTIVITIES

- DEVELOPING A REAL TIME HYBRID SIMULATION OF THE SPACE STATION DYNAMICS AND THE ENVIRONMENT
- EVALUATION OF THE DYNAMIC CHARACTERISTICS OF THE ATTITUDE CONTROL SYSTEM AND THE NEW MOMENTUM MANAGEMENT CONTROL LAW
- EVALUATION OF FAULT ISOLATION AND REDUNDANCY MANAGEMENT TECHNIQUES
- EVALUATION OF MODIFIED AND IMPROVED COMPONENTS SUCH AS GYRO'S AND RATE GYRO'S
- EVALUATION OF THE TRADE BETWEEN FINE BODY POINTING, FINE POINTING MOUNTS, AND FREE FLYERS
- INTEGRATION AND VERIFICATION OF INTERFACES BETWEEN CONTROL COMPONENTS AND SOFTWARE

Figure 12

## TECHNOLOGY ISSUES

In addition to the technical discussions conducted at this workshop, a panel of experts, composed of one representative from each participating NASA field center, addressed the questions of critical technology, system integration, technology program justification and definition. The critical technology issues identified as a result of these efforts are shown in figure 13, and cover such areas as materials, rotor suspension, electromagnetics, electronics, systems integration, and safety.

### 0 MATERIALS

- ANALYSIS CAPABILITY OF MATERIAL PERFORMANCE
- OPTIMUM UTILIZATION OF MATERIAL PROPERTIES
- IMPACT OF ENVIRONMENT ON MATERIAL PROPERTIES

### 0 ROTOR SUSPENSION

- MAGNETIC BEARINGS (DYNAMIC CONTROL AND STABILITY)
- MECHANICAL BEARINGS (LUBRICATION. VIBRATION TRANSMISSION. MAINTENANCE. ON-LINE BALANCING ATTENDANT TO ON-ORBIT BEARING REPLACEMENT. REDUNDANCY)

### 0 POWER GENERATION

- MOTOR/GENERATOR DESIGN AND MATERIALS
- MOTOR/GENERATOR EFFICIENCY
- ELECTRONICS DESIGN AND EFFICIENCY
- POWER/VOLTAGE LEVELS AND BUS REGULATION

### 0 SYSTEMS

- INTEGRATION OF POWER AND CONTROL FUNCTIONS
- IMPACT OF INTEGRATION ON CONTROL LAWS AND ENERGY MANAGEMENT
- CONTINGENCY OPERATION FOLLOWING UNIT FAILURE
- MODULARITY AND/OR SCALABILITY
- SAFETY CONSIDERATIONS
- SYSTEM AND UNIT CHARACTERIZATION
- DATA BASE FOR SYSTEM AND COMPONENTS

Figure 13

## WORKSHOP RECOMMENDATIONS

A major result arising from this workshop was that a general consensus was reached regarding the existence of strong support within the agency for integrated flywheel technology development, and that systems incorporating that technology have strong potential as an alternative energy storage approach for spacecraft applications. As such, the following recommendations (fig. 14) were made:

1) conduct a state of the technology workshop with industry, university, and government participation; 2) undertake a vigorous technology program to address and resolve all the technical issues raised during this conference; and finally, 3) adopt a lead center concept to insure a streamlined and coordinated technology program.

- **CONDUCT STATE OF TECHNOLOGY WORKSHOP (ASAP)**

  - INDUSTRY**

  - UNIVERSITY**

  - GOVERNMENT**

- **UNDERTAKE VIGOROUS TECHNOLOGY PROGRAM**

  - COMPOSITE MATERIALS AND FLYWHEELS**

  - MAGNETIC SUSPENSION**

  - M/G AND ELECTRONICS**

  - SYSTEM INTEGRATION AND OPERATIONS**

  - SYSTEM TRADES AND ANALYSES**

- **ADOPT LEAD CENTER CONCEPT**

  - COORDINATION OF HEADQUARTERS OFFICE GOALS  
AND RESOURCES**

  - CAPITALIZING ON STRENGTHS OF PARTICIPATING  
ORGANIZATIONS**

  - MINIMIZING DUPLICATIONS OF EFFORT AMONG AGENCIES**

Figure 14

#### REFERENCES

1. Keckler, C. R.; Rodriguez, G. E.; and Groom, N. J. (Editors): Integrated Flywheel Technology - 1983. NASA CP-2290, December 1983.
2. Notti, J. E.; Cormack, A.; and Schmill, W. C.: Integrated Power/Attitude Control System (IPACS) Study; Volume I - Feasibility Studies. NASA CR-2383, April 1974.
3. Cormack, A.; and Notti, J. E.: Design Report for the Rotating Assembly for an Integrated Power/Attitude Control System. Rockwell International Report SD74-SA-0100, Sept. 1974. (Available as NASA CR-172317.)
4. Kirk, J. A.; Studer, P. A.; and Evans, H. E.: Mechanical Capacitor. NASA TN D-8185, 1976.
5. Michaelis, T. D.; Schlieben, E. W.; and Scott, R. D.: Design Definition of a Mechanical Capacitor. NASA CR-152613, 1977.
6. Scott, R. D.: Mechanical Capacitor Energy Storage System. NASA CR-170613, 1978.
7. Kulkarni, S. V.: Performance Projections of Fiber-Reinforced Composite Material Flywheels. Lawrence Livermore Laboratory Report UCID-19582, September 1982.
8. Anderson, W. W.; and Groom, N. J.: The Annular Momentum Control Device (AMCD) and Potential Applications. NASA TN D-7866, March 1975.
9. Ball Brothers Research Corporation: Annular Momentum Control Device (AMCD). Volumes I and II. NASA CR-144917, 1976.

N185

3856

ENCLOS

N85 13856

D6

EUROPEAN DEVELOPMENT EXPERIENCE  
ON ENERGY STORAGE WHEELS  
FOR SPACE

A.A. Robinson

ESA Technical Directorate  
ESTEC, Noordwijk, The Netherlands

The main thrust of effort has taken place in two companies, both of which have produced high speed fibre composite rotors suspended by contactless magnetic bearings :

- TELDIX, in Germany
- SNIAS, in France

Numerous other companies and establishments have carried out studies only and/or have engaged in related hardware technology developments of more limited scope.

#### DEVELOPMENTS AT TELDIX

Work at TELDIX on energy wheels began in the early 1970's with the fabrication of hubless (annular) flywheels suspended on fully active (5-axis) magnetic bearings of the electrodynamic kind. This type of bearing is characterized by the absence of ferromagnetic material on its non-rotating part.

The drivers for the choice of annular geometry and active bearings were :

- OPTIMUM UTILISATION OF UNIDIRECTIONAL STRENGTH PROPERTIES OF FIBRE COMPOSITES
- ELIMINATION OF SPOKES AND SPOKE RELATED STRESS PLUS INTERFACE PROBLEMS
- HIGH ENERGY DENSITY POTENTIAL DUE TO INERTIAL CONTRIBUTION OF MOTOR/GENERATOR AND SUSPENSION MAGNETS IN THE RIM
- VERNIER GIMBALLING MOMENTUM ALIGNMENT CAPABILITY
- FAVOURABLE SHAPE AND VOLUME

Two small scale units for feasibility demonstration purposes were completed by 1977. The essential parameters of these models were :

● KINETIC ENERGY	20 Wh	16 Wh
● SPEED	14000 r.p.m.	16000 r.p.m.
● MASS (excl. electronics)	8.5 kg	5 kg
● DIMENSIONS : diameter	292 mm	250 mm
bore	215 mm	140 mm
height	110 mm	80 mm
● POWER CONSUMPTION (0g)	40 W	10 W
● VERNIER GIMBALLING CAPABILITY	0°	± 1.25° (2 axes)
● MAX. PRECESSION RATE	2.5°/s	2.5°/s
● MOTOR/GENERATOR	D.C. BRUSHLESS	
● MAGNETIC SUSPENSION	ELECTRODYNAMIC, 5-AXIS ACTIVE	
● EMERGENCY SUPPORT	SLIDING SURFACES	

The originally expected advantages of the hubless ring concept were generally confirmed. However, a number of fundamental drawbacks inherent to this concept were also shown up :

- MECHANICAL COMPLIANCE OF THE ROTOR AND DILATION WITH SPEED ADVERSELY AFFECT THE MAGNETIC SUSPENSION PERFORMANCE. LARGE O.D./I.D. RATIOS ARE NECESSARY.
- STEEP INCREASE OF SUSPENSION POWER WITH SPEED DUE TO INITIAL AND STRESS INDUCED OUT-OF-ROUNDNESS OF THE ROTOR.
- EMERGENCY SUPPORT AND LAUNCH-LOCK DIFFICULT TO IMPLEMENT AT LARGE RADIUS.
- HIGH BURST ENERGY OF METALLIC PARTS IN THE RIM.
- COMPLEX COMPOSITE/METALLIC RIM DIFFICULT TO MANUFACTURE.
- 5-AXIS BEARING EXHIBITS HIGH SUSPENSION POWER ON GROUND



The above mentioned drawbacks of the hubless ring concept led to its abandonment for energy storage purposes. Subsequent efforts at TELDIX were focussed on conventional (hubbed) wheels with 5-axis electromagnetic suspensions. In all, about six development models with small metallic rotors have been built. Characteristics of the MDR 100-1 model (highest speed version with solid beryllium rotor) are as follows :

- KINETIC ENERGY 23 Wh
- SPEED 16000 r.p.m.
- MASS : wheel 9.2 kg
- electronics 3.4 kg
- DIMENSIONS : diameter 306 mm
- height 180 mm
- POWER CONSUMPTION (0g) 13 W
- VERNIER GIMBALLING CAPABILITY  $\pm 0.6^\circ$  (2 axes)
- MAX. PRECESSION RATE  $2.5^\circ/s$
- MOTOR/GENERATOR D.C. BRUSHLESS
- MAGNETIC SUSPENSION ELECTROMAGNETIC, 5-AXIS ACTIVE
- EMERGENCY SUPPORT BALL BEARINGS

#### DEVELOPMENTS AT SNIAS

SNIAS have also been engaged for more than a decade on development of energy storage wheels and systems. Initial work took place in the framework of a COMSAT technological research contract which resulted in a prototype wheel with the following characteristics :

- KINETIC ENERGY 35 Wh
- SPEED 24000 r.p.m.
- MASS (excl. electronics) 11 kg
- DIMENSIONS : diameter 350 mm
- height 250 mm
- POWER CONSUMPTION 28 W
- MOTOR/GENERATOR D.C. BRUSHLESS
- MAGNETIC SUSPENSION ELECTROMAGNETIC, 1-AXIS
- EMERGENCY SUPPORT BALL BEARINGS
- ROTOR GRAPHITE FIBRE
- CYCLOPROFILE CONSTRUCTION

In 1978 SNIAS was awarded a follow-up contract the objective of which was to demonstrate a complete flywheel based energy storage system.

The development aims were :

- SYSTEM CAPACITY 2 - 3 kWh (at 75% D.O.D.)
- FLYWHEEL CAPACITY 500 Wh (4 per system)
- FLYWHEEL ENERGY DENSITY 20 Wh/kg (usable)
- FLYWHEEL DIAMETER 500 mm
- FLYWHEEL SPEED 30 000 r.p.m.

These targets proved unachievable with the original CYCLOPROFILE rotor concept due to poor manufacturing reproducibility.

The next development step was a rotor with high strength graphite fibre rim and light glass fibre spokes. Matching of rim and spoke elongations was assured by small metallic masses incorporated in the spokes at their outermost extremities. This design was fully integrated with the magnetic bearing support but subsequent testing showed the balance integrity of the rotor itself to be inadequate at speeds exceeding 17000 r.p.m.

Recent development effort has been focussed on a modified form of rotor consisting of a high modulus graphite fibre rim supported by a thin metallic alloy disc. In tests on a high speed burst test facility this rotor has consistently achieved speeds of 30 000 r.p.m. (peripheral speed 785 m/s) without balance shift or stress rupture problems.

At time of writing, this latest form of rotor is undergoing further evaluation and detailed design finalisation before being integrated with the existing magnetic bearing support. It is perhaps a little early to be too optimistic but current performance expectations for a fully assembled wheel if no new major problems arise are :

- USABLE ENERGY CAPACITY 500 Wh
- SPEED 30 000 r.p.m.
- DIMENSIONS : diameter 500 mm  
height 200 mm
- MASS 25 kg
- USABLE ENERGY DENSITY 20 Wh/kg
- POWER CONSUMPTION 15 W

Present indications are that the above indicated performances may even be exceeded. However, allowing a safety margin to cover materials degradation under cyclic stress, and eventual inclusion of containment mass, the indicated energy density figure should be regarded as a realistically achievable maximum for the immediate future.

COMPARATIVE STUDY OF WHEELS VS. BATTERIES

In 1977, ESA placed a study contract with the French company MATRA to assess the overall mass, volume and cost implications of flywheels vs. batteries in typical mission scenarios.

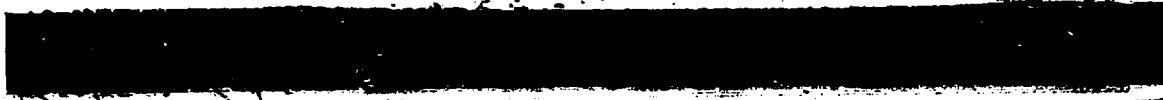
The study was based on three hypothetical mission models as outlined below :

<u>MISSION</u>	<u>EOS</u>	<u>LCS</u>	<u>TVBS</u>
Orbit	Sunsynchronous 600 - 1000 km	Geostationary	Geostationary
Eclipse Duration	0.58 hours	1.2 hours max. 2 x 42 days per year	1.2 hours max. 2 x 42 days per year
On-Board Power Demand	500 W average	1500 W continuous	5000 W continuous
Eclipse Energy Requirements	300 Wh	1800 Wh	6000 Wh (24 hour TV service capability)
Spacecraft Mass	600 - 1000 kg	830 kg (BOL)	950 kg (BOL)
Attitude Control Requirements (3σ)	Pitch 0.05° Roll 0.05° Yaw 0.1°	Pitch 0.075° Roll 0.075° Yaw 0.35°	Pitch 0.1° Roll 0.1° Yaw 0.5°
Lifetime	5 years	7 years	7 years

EOS Earth Observation Satellite

LCS Large Communication Satellite

TVBS Television Broadcast Satellite



The flywheel inputs to the study were based on projected performance parameters supplied by SNIAS and TELDIX for passive and active magnetic bearing wheels respectively.

Comparative data for Ni-Cd, Ni-H<sub>2</sub>, and Ag-H<sub>2</sub> electrochemical batteries was obtained from a leading battery manufacturer.

The essential quantitative conclusions of this study are summarised in the following table :

MISSION	TOTAL MASS, VOLUME, COST OF ACS + PSS SUBSYSTEMS WITH E.S.W.s				TOTAL MASS, VOLUME, COST OF ACS + PSS SUBSYSTEMS WITH BATTERIES				OVERALL MASS, VOLUME, COST IMPLICATIONS OF E.S.W.'s W.R.T. BATTERIES				
	MASS (kg)	VOLUME (LTR)	COST <sup>a</sup> (MAU)		MASS (kg)	VOLUME (LTR)	COST <sup>a</sup> (MAU)		MASS SAVING		VOLUME SAVING (l)	COST PENALTY OF E.S.W.'s W.R.T.	
			Dev't	Flight Eqpts			(kg)	% of S/C MASS at B.O.L.	Dev't	Flight Eqpts			
EOS	115	90	3.5	2.0	131	145	2.6	1.6	16	2.02	55	0.9	0.4
LCS	206	124	3.5	2.2	211	196	2.3	1.2	5	0.62	72	1.2	1.0
TVBS	471	589	6.2	5.8	549	498	2.6	2.2	78	8.22	-91	3.6	3.6

<sup>a</sup> Note : Costs indicated are approximate only, based on June 1977 labour rates. Only costs of equipment not common to ESW and battery systems are considered.

The main finding is that the mass saving achieved by the use of wheels in place of Ni-H<sub>2</sub> or Ag-H<sub>2</sub> batteries is rather small as a percentage of overall spacecraft mass. The rather larger mass saving established for the TVBS mission (8.2%) is not realistic as it would be impossible to fit a power/attitude control subsystem weighing 471 kg into a spacecraft of only 950 kg at BOL.

Because of the lack of reliable data, the study was not able to assess the relative merits of wheels vs. batteries with respect to charge/discharge cycle life. Today, the substantially greater cyclic life potential of wheels (of particular importance in low orbit spacecraft), is seen as one of the main drivers for continued research and development effort.



## CONCLUSION

European industry has acquired a considerable expertise in the study and fabrication of energy storage wheels and magnetic suspension systems for space. Sufficient energy density performance for space viability is on the threshold of being achieved on fully representative hardware. Stress cycle testing to demonstrate life capability as well as the development of burst containment structures remains to be done and is the next logical step.

REFERENCE

1. Nguyen, H. N.; and Mariau, F.: Study of System Implications of High Speed Flywheels as Energy Storage Devices on Satellites. ESA-CR(P)-1168, vols. I and II, 1978.

N85

3857

UNCLAS

N85 13857

D7

MERITS OF FLYWHEELS FOR SPACECRAFT ENERGY STORAGE

Sidney Gross  
Boeing Aerospace Company  
Seattle, Washington

PAGE 74 INTENTIONALLY BLANK

PRECEDING PAGE BLANK NOT FILMED



## MERITS OF FLYWHEELS FOR SPACECRAFT ENERGY STORAGE

Sidney Gross  
Boeing Aerospace Company  
Seattle, Washington 98124

### SUMMARY

Flywheel energy storage systems have a very good potential for use in spacecraft. This system can be superior to alkaline secondary batteries and regenerable fuel cells in most of the areas that are important in spacecraft applications. Of special importance, relative to batteries, are lighter weight, longer cycle and operating life, and high efficiency which minimizes solar array size and the amount of orbital makeup fuel required. In addition, flywheel systems have a long shelf life, give a precise state of charge indication, have modest thermal control needs, are capable of multiple discharges per orbit, have simple ground handling needs, and have characteristics which would be useful for military applications.

The major disadvantages of flywheel energy storage systems are that power is not available during the launch phase without special provisions; and in-flight failure of units may force shutdown of good counter-rotating units, amplifying the effects of failure and limiting power distribution system options. Additional disadvantages are: no inherent emergency power capability unless specifically designed for, and a high level of complexity compared with batteries. In net balance, the potential advantages of the flywheel energy storage system far outweigh the disadvantages.

### INTRODUCTION

Energy storage systems for spacecraft in the past have used nickel-cadmium and nickel-hydrogen batteries for rechargeable systems, or hydrogen-oxygen fuel cells for relatively short duration missions, such as Apollo or Shuttle. Regenerable fuel cells have also been evaluated and found to have good potential for space stations (Ref. 1). Though flywheel systems have been suggested for spacecraft for many years (Refs. 2 to 4), only recently have they been given serious consideration for spacecraft (Ref. 5).

In the flywheel energy storage concept, energy is stored in the form of rotational kinetic energy using a spinning wheel. Energy is extracted from the flywheel using an attached electrical generator; energy is provided to the flywheel by a motor, which operates during sunlight using solar array power. The motor and the generator may or may not be the same device. Either magnetic bearings or mechanical bearings may be considered for flywheel systems.

### EFFICIENCY CONSIDERATIONS

Energy storage efficiency is a key factor in the optimization of spacecraft energy storage systems, and also in the choice between one system and another. The problems of large sized solar arrays are well out of proportion to the modest weight involved, and an efficient energy storage system reduces the size of the solar array. This is shown parametrically in Figure 1. For high-power spacecraft with large solar arrays, significant quantities of propulsion fuel must be resupplied regularly to offset the effects of solar array drag and maintain the spacecraft within the selected orbit. Inefficient energy storage systems require greater solar area and hence more propulsion fuel. This is shown in Figure 2 for a typical space station design using either hydrazine or hydrogen-oxygen propellants. This penalty can be considerable over the life of the spacecraft.

The calculated efficiency of the flywheel energy storage system is shown in Table 1. For the intermediate design objective, the overall efficiency is 81.1 percent; for the advanced design objective, the overall efficiency is 92.8 percent. Motor/generator efficiency is the major contributor to losses in both cases. Electrochemical systems, by comparison, are on the order of 55 to 65 percent efficient.

#### **UTILIZATION OF EXCESS SUNRISE POWER**

Spacecraft solar arrays become cold during occultation. Upon emergence into the sunlight, there is a higher voltage output; hence a high power output. This increased power condition lasts for about 20 minutes, depending on the time to reach steady sunlit temperature, which is determined mostly by the unit thermal mass of the solar array. Typical solar array performance in low earth orbit is shown in Figure 3. The incremental power due to the low temperature transient is seen to be an increase in solar array output of approximately seven percent. This potential for extra power usually is not used. In a shunt regulated power system, the excess voltage is not used; in the less common series regulated system with pulse-width modulated control, part of the excess power is sometimes used for battery charging, but this can compromise the batteries, which are charge-rate sensitive. Flywheels, within limits, are not charge-rate sensitive and thus can make use of this additional power.

#### **VOLTAGE RANGE EFFECTS**

An inherent characteristic of secondary batteries is a relatively wide bus voltage spread due to the large difference between charge and discharge voltage. A regenerative fuel cell system will have about half the voltage spread of a Ni-H<sub>2</sub> battery. A flywheel generator, on the other hand, will control voltages very closely, within approximately two percent. This makes the design of internal power supplies lighter and more efficient. An estimate of the typical improvement in efficiency of these loads is shown in Figure 4. It is seen that most of the loads could be reduced 0.8 percent using the tighter voltage regulation obtainable with a motor/generator. Non-essential loads, such as payloads, could probably take advantage of the potential saving. However, loads essential to the operation of the spacecraft probably would have to be designed to meet the expected wide voltage range of the launch power source and the emergency batteries and therefore could not take advantage of this.

#### **WEIGHT COMPARISON**

Flywheel energy storage system weights are shown in Figure 5. It is seen that both the intermediate and advanced design flywheels are lighter than any of the battery systems when comparisons are made at the design depth-of-discharge, for the flywheel can cycle repetitively at deeper depths-of-discharge than can batteries. This can be a valid comparison only if the reserve capacity of the battery systems is not depended upon for emergency power. The flywheel system is not practical for depths-of-discharge much greater than 75%, and the upper practical limit for battery systems for occasional discharges is approximately 85% depth-of-discharge for nickel-hydrogen, and 75% for nickel-cadmium batteries. A weight comparison for these design values is given in Figure 6, applicable for comparison of emergency power capability. Even for this condition the flywheel system is lightest.

The amount of emergency power required has an important bearing on the weight comparison of flywheels versus batteries. If the emergency requirement is small enough to be handled by the reserve capacity of batteries, then the power system trade essentially is between batteries at about 75 to 85 percent depth-of-discharge, and a flywheel system at approximately 75 percent depth-of-discharge. On the other

hand, if the emergency requirement is very large, then it must be supplied independently by a primary battery system; the power system trade then focuses on the main load, being essentially between batteries at 25-35 percent depth-of-discharge, and a flywheel system at approximately 75 percent depth-of-discharge.

Accessory equipment associated with the batteries and flywheels gives a further weight advantage to the flywheel system. There are significant differences in thermal control penalties, namely: (1) flywheel system efficiency is greater than for batteries, resulting in less heat to be dissipated (for overall flywheel and battery system efficiencies of 80 percent and 65 percent, respectively, the flywheel thermal load is 57 percent of the battery thermal load); (2) flywheel system heat is removed at a higher temperature (typically about 30°C) than with batteries (typically about 10°C); (3) the heat load is more uniform with time for the flywheel system than for batteries. One thermal advantage batteries have over the flywheel system is a much greater transient heat storage capability.

Another important item is the fact that the flywheel system does not need a separate charge controller, as do batteries, for this function is accommodated in the motor/generator electronic controls. Still another difference stems from the fact that the voltage regulation of the flywheel system is very fine and essentially provides a regulated bus; this can be reflected in higher overall spacecraft power efficiency and lower weight power supplies for the user equipment. Of particular importance is the smaller solar array size resulting from the high efficiency obtainable with the flywheel system; this gives important systems advantages in addition to the weight saving.

Typical weight comparisons have been made at the spacecraft level between flywheel, regenerative fuel cells, and battery systems (Table 2). The power system load for this comparison is arbitrarily set at 50 kW for both sunlight and occultation. It is seen that the flywheel energy storage system is lighter than batteries. The higher efficiency of the flywheel system accounts for an important part of the weight saving. Flywheel equipment weight increases significantly if it is designed for emergency power capability equivalent to that of batteries; nevertheless, total weight remains lightest for the flywheel system even when designed to such a requirement. Lower propellant resupply over a period of many years can be a major advantage for the flywheel system.

#### **LIFE AND RELIABILITY**

Life and reliability of nickel-cadmium batteries are important concerns for all spacecraft applications, including the space station. Nickel-hydrogen batteries have the potential for improved life and reliability, and efforts are now being expended to develop that potential. For either system, however, it is expected that periodic battery replacement will be necessary to meet the space station lifetime requirements.

Flywheel systems have the capability for much longer lifetimes than do battery systems; when developed, the flywheel system should be able to operate without replacement during the life of a space station, which is in the range of 10 to 30 years. Flywheel system lifetime probably is limited by the associated electronics, which can be designed to be replaceable.

In assessing the life and reliability of the flywheel motor/generator system, those items considered to be key to long life and reliability are: (1) fatigue and long term creep of the flywheel rotor; (2) bearings; (3) motor control electronics; (4) cooling system; (5) forced shutdown of counter-rotating units.

Suitable derating factors can be applied to allow for fatigue over the design life. Figure 7 gives the fatigue behavior of a typical carbon-fiber composite and shows the very high resistance of these composites to fatigue. It is likely that some of the degradation seen is due to the epoxy matrix, which is believed not to be optimum for cyclic loading applications. These data suggest that a derating factor for 15 years should be approximately 0.942, excluding design margin. It may be noted that the fatigue effects on other materials sometimes used for flywheels, such as glass or Kevlar, are much more severe than for carbon-fiber materials. Creep can be important in causing wheel unbalance, but little information is available on this.

Magnetic bearings offer the most promise for long life spacecraft applications. These need involve no mechanical contact between the rotating equipment and the stationary elements. Degradation of the permanent magnet elements in the bearings is believed to be minor over 15 years. Thus, the electronics required for the magnetic bearing control may be the critical long life item for the bearings. With suitable electronics redundancy, very long life should be achievable for bearing control and for operation of the motor/generator.

Flywheel systems have an advantage over batteries with respect to temperature control. The components of flywheel systems tolerate higher temperatures (about 350°C) and accept much wider temperature control (estimated about +350°C) than do batteries, which require low temperature (50°C) and close control (+50°C). Though it is easier to meet the temperature control needs of flywheels, once a satisfactory thermal design has been made for either batteries or flywheels, good reliability is expected for both systems.

With a system not integrated with attitude control, counter-rotating flywheels are appropriate to prevent interference with the spacecraft momentum management system. In order to prevent angular momentum unbalance, failure of a flywheel unit would appear to require that a second equipollent unit, rotating in the opposite direction, will also have to be shut down. This doubling effect is an important limitation of flywheel systems. Spin direction reversal can limit the number of good units which are forced to be shut down, however.

#### **SHELF LIFE CONSIDERATIONS**

Batteries begin their degradation at the time of electrolyte addition during manufacture. To minimize shelf life problems, an attempt is often made to schedule manufacture completion as close as possible to the launch date. Nevertheless, for a variety of reasons, battery service may not begin until several years after manufacture. Therefore, shelf life often is an important factor in the use of energy storage systems. Flywheel systems, in contrast to batteries, have nearly indefinite shelf life.

#### **PEAK POWER CONSIDERATIONS**

A major difference between batteries and the flywheel systems is that system voltage with battery systems drops during power peaks and also reduces with time as batteries degrade, whereas output voltage is always regulated for the flywheel motor/generator system. Thus, flywheel system performance at high power is always constant and predictable.

Designing for peak power is a necessary requirement for all space power systems. Nickel-cadmium and nickel-hydrogen batteries have an inherent good capability for

(4)

high peak power and generally can meet peak requirements easily if voltage limits are not too restrictive. The flywheel system can be designed also for very high peak power and can in fact be expressly designed for special applications to convert all its kinetic energy into electricity in a fraction of a second, using a special generator. Even for moderately high peak power, however, the motor/generator must be increased in rating to meet the specific requirements.

An important capability of flywheel energy storage systems is the ability for multiple discharges per orbit, augmenting the solar array for high power loads during the sunlit portion of the orbit as well as satisfying the usual occultation load. For applications where the load is highly variable, this makes it expedient to reduce solar array area, allowing the array to be sized close to the average power rather than sized to peak power. This would put a demand on the energy storage system which batteries are not well equipped to cope with, partly due to the increased number of cycles, but primarily from the higher charge rates needed with multiple discharges and charges. The most strenuous needs for multiple charges and discharges per orbit are expected to be military applications.

#### **EMERGENCY POWER CONSIDERATIONS**

A flywheel energy storage system can be inferior to a battery or regenerable fuel cell system with regard to emergency power unless specifically designed with capability for emergencies. A flywheel system typically would be designed for 75 percent depth of discharge, obtained by operating over a speed range of full speed to half speed. Withdrawal of most of the remaining 25 percent capacity is impracticable because of the much increased speed range needed, which would impact overall efficiency. Batteries, on the other hand, would typically be discharged in the 25-35 percent range and in an emergency could be discharged up to about 85 percent. Regenerable fuel cells can obtain very long emergency capability by increasing the inventory of hydrogen and oxygen without an increase in the other hardware.

For a manned space station, valid arguments can be made that the emergency power system should be a system separate from the main system. This could be necessary to isolate a failure and provide a level of emergency power well above what could be provided from the undischarged reserve in the secondary batteries. Should this rationale prevail for the space station, then the reserve power limitations of a flywheel energy storage system would be a minor factor.

#### **LAUNCH-PHASE POWER**

Batteries have the capability to provide electrical power during the launch phase, and frequently power is turned over to the batteries several minutes before launch for additional system verification. Flywheels cannot be operated during the high vibration environment of launch unless a suitable bearing can be developed for operation during the high vibration environment of launch. An alternative approach would be a separate battery provided for the launch phase.

#### **RECONDITIONING**

Reconditioning is proven to be a worthwhile and even necessary procedure for nickel-cadmium batteries, especially in synchronous orbit. Flywheel systems do not require reconditioning discharges.

#### **STATE-OF-CHARGE**

No practical method has been developed to determine the capacity of a nickel-cadmium battery in advance of a full discharge. Nickel-hydrogen batteries reveal their ampere-hour capacity by the cell hydrogen pressure, though there is a gradual

change in end of charge pressure with time which must be accounted for. Even if the ampere-hour capacity were known, discharge voltage for both battery systems cannot always be well predicted; hence there is uncertainty on the watt-hours available. The flywheel system is superior to both battery types, for after an initial calibration discharge, voltage and energy can be accurately predicted for a full range of operating conditions; except for secondary changes, this calibration should remain constant over the operating life of the system. Thus, the flywheel system offers excellent energy storage predictability, unmatched by any battery system.

#### **EVALUATION OF ENERGY STORAGE METHODS**

A simplified comparison between batteries, regenerative fuel cells, and flywheels is shown in Table 3. Distinctions are made between energy storage characteristics that are very important and those that are useful but only moderately important. Division into these two categories is a personal judgement, and it could be argued, for example, that the weight penalty for providing emergency power is not very important since this should be a separate power source.

It is seen from Table 3 that the flywheel system is best in most of the important categories. Its capability for emergency power is limited unless specifically designed for, and it may present limitations in providing power during the launch phase. Possible forced shutdown of good counter-rotating units when a unit fails is a disadvantage of flywheel systems, amplifying the effects of failure and limiting the power distribution system options. Nevertheless, the strong points of the flywheel system are so important, such as life, weight and efficiency, that the flywheel energy storage system should command more attention for spacecraft energy storage systems.

#### **ACKNOWLEDGEMENT**

The paper is based on a study performed by the Boeing Aerospace Company, for the Johnson Space Center, Contract NAS9-16151, Mod 75. Keith Van Tassel was the technical monitor. The final report, "Study of Flywheel Energy Storage For Space Stations", was released February 1984 as D180-27951-1.

#### **REFERENCES**

1. S. Gross, "Analysis of Regenerative Fuel Cells", D180-27160-1, Dec. 20, 1982, Contract NAS9-16151, NASA CR-171783.
2. W. W. Anderson and C. R. Keckler, "An Integrated Power/Attitude Control System For Space Vehicle Application", Fifth IFAC Symposium on Automatic Control in Space, Genoa, June 5-9, 1975.
3. J. E. Notti, A. Cormack III, and W. C. Schmill, "Integrated Power/Attitude Control System (IPACS) Study, NASA CR-2383, April 1974, Vol. I and II.
4. A. Cormack III, J. E. Notti, Jr., and M. I. Ruiz, "Design and Test of a Flywheel Energy Storage Unit for Spacecraft Application", Tenth IECEC, p. 1275, Aug. 1975.
5. G. E. Rodriguez, P. A. Studer, and D. A. Baer, "Assessment of Flywheel Energy Storage For Spacecraft Power Systems", NASA TM 85061, May 1983.

Table 1. Energy Storage Efficiency With Flywheels

	EFFICIENCY	
	INTERMEDIATE DESIGN OBJECTIVE	ADVANCED DESIGN OBJECTIVE
LOSSES FROM CYCLIC STRESS	100%	100%
MOTOR EFFICIENCY	99.5%	99.5%
GENERATOR EFFICIENCY	91.0%	99.5%
SOLAR ARRAY CHARGE AREA EFF.	100%	100%
HEAT PIPE POWER	100%	100%
MAGNETIC BEARING POWER	99.61%	99.72%
OVERALL EFFICIENCY	81.1%	92.8%

Table 2. Weights for Energy Storage Systems -- 50 KW Continuously

	BATTERIES			REGENERATIVE FUEL CELLS		FLYWHEELS	
	NiCd (28% DOD)	NiH <sub>2</sub> (28% DOD)	NiH <sub>2</sub> (30% DOD)	WEIGHT OPTIMIZED	EFFICIENCY OPTIMIZED	INTERMEDIATE DESIGN OBJECTIVE	ADVANCED DESIGN OBJECTIVE
SOLAR ARRAY WEIGHT	3,246	3,401	3,246	3,817	3,246	2,789	2,839
(SOLAR ARRAY POWER)	(108.1 KW)	(111.2 KW)	(108.1 KW)	(124.8 KW)	(108.1 KW)	(81.5 KW)	(86.3 KW)
RADIATOR	880	1,047	980	521	386	316	121
FUEL CELLS <sup>①</sup>	—	—	—	880	1,830	—	—
ELECTROLYSIS CELLS <sup>①</sup>	—	—	—	386	636	—	—
BATTERIES <sup>①</sup>	8,788	6,788	6,782	—	—	—	—
PROPELLANTS <sup>②</sup> (H <sub>2</sub> -O <sub>2</sub> ANNUAL REQMT)	3,281	3,438	3,281	3,880	3,281	2,829	2,688
COLD PLATES	886	638	744	—	—	18	18
HEAT EXCHANGERS	—	—	—	50	40	—	—
TANKS	—	—	—	282	240	—	—
FLYWHEEL SYSTEM	—	—	—	—	—	1,781 <sup>③</sup>	1,273 <sup>③</sup>
						4,931 <sup>④</sup>	3,564 <sup>④</sup>
TOTAL, LBS	17,220	14,321	14,892	9,736	9,488	7,723 <sup>③</sup>	6,719 <sup>③</sup>
						30,883 <sup>④</sup>	8,010 <sup>④</sup>

- ① ASSUMES 8-YEAR BASIC LIFE
- ② ALTITUDE MAINTENANCE TO COUNTERACT SOLAR ARRAY DRAG ONLY
- ③ DESIGNED FOR LEO LOADS ONLY
- ④ DESIGNED FOR SAME EMERGENCY CAPABILITY AS BATTERIES -- CAPACITY = 2.8 TIMES OCCULTATION LOAD

Table 3. Evaluation of Energy Storage Methods

	CHARACTERISTICS	Ni-Cd	Ni-H <sub>2</sub>	H <sub>2</sub> -O <sub>2</sub> REGEN FUEL CELLS	FLYWHEEL
VERY IMPORTANT ITEMS	WEIGHT, ORBITAL LOAD				BEST
	WEIGHT, EMERGENCY LOAD			BEST	BEST
	LIFE				BEST
	HIGH VOLTAGE CAPABILITY				BEST
	PARALLEL DISCHARGE CAPABILITY				BEST
	EFFICIENCY				BEST
	DISTRIBUTION CONSIDERING FAILURES	BEST	BEST		
MODERATELY IMPORTANT ITEMS	SHELF LIFE				BEST
	PEAK POWER	BEST	BEST		
	MULTIPLE DISCHARGES PER ORBIT				BEST
	SAFETY				
	PRELAUNCH TESTING	BEST	BEST		
	THERMAL REQUIREMENTS				BEST
	STATE-OF-CHARGE				BEST
	UTILIZATION OF EXCESS SUNRISE PWR				BEST
	POWER DURING LAUNCH PHASE	BEST	BEST		



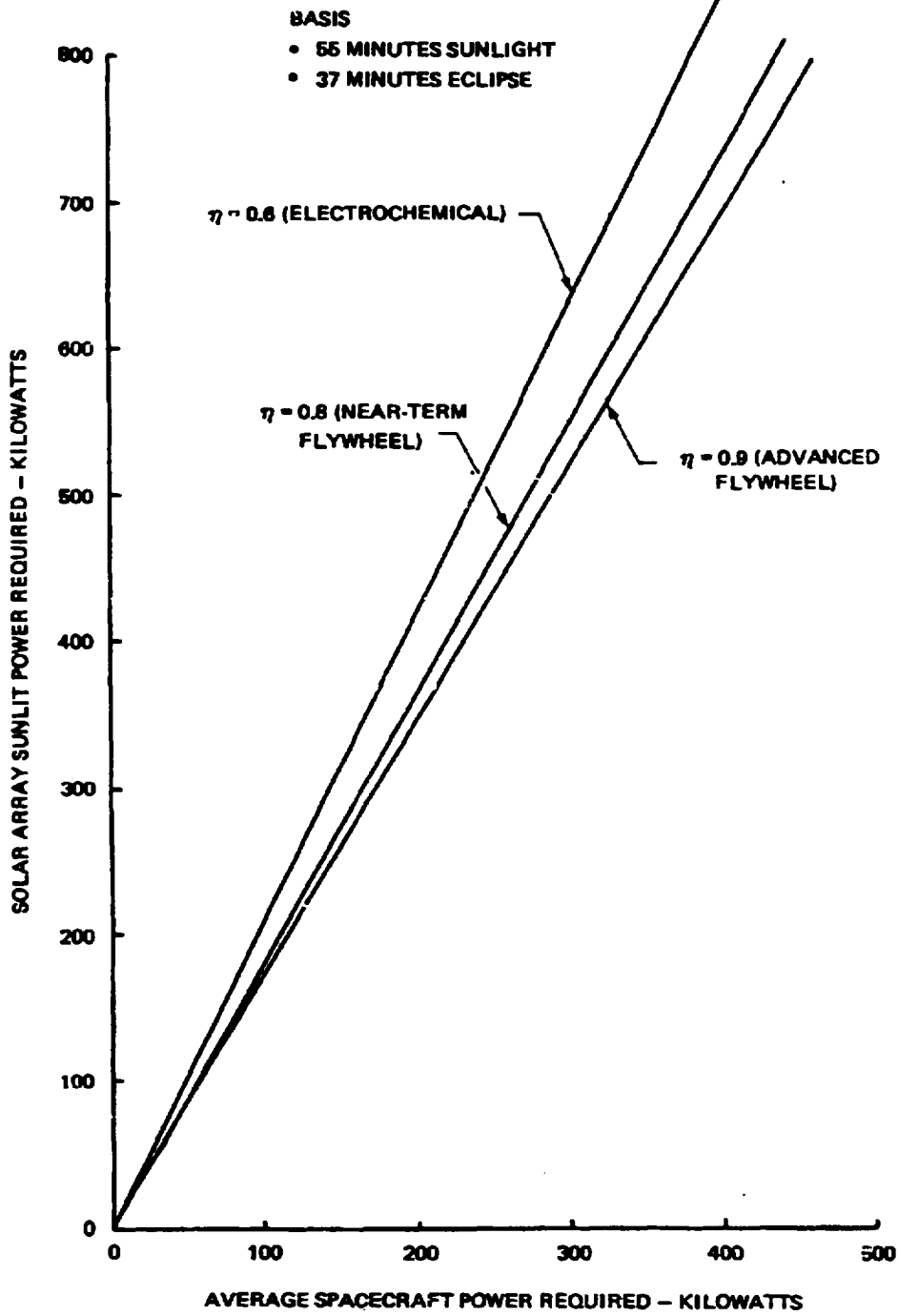


Figure 1. High Efficiency Energy Storage Systems Result in Smaller Solar Arrays

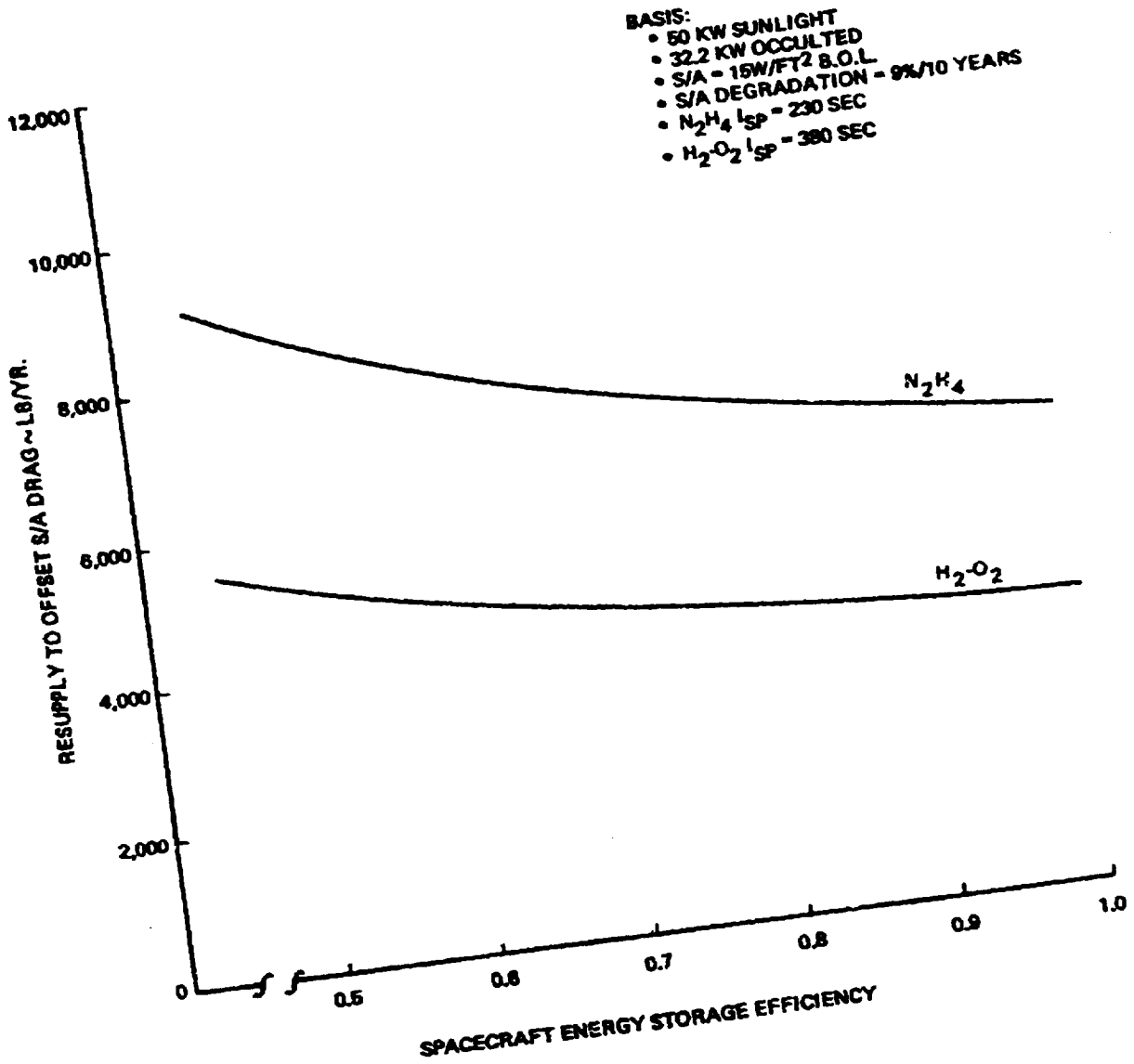


Figure 2. Propulsion Resupply Due to Solar Array Drag

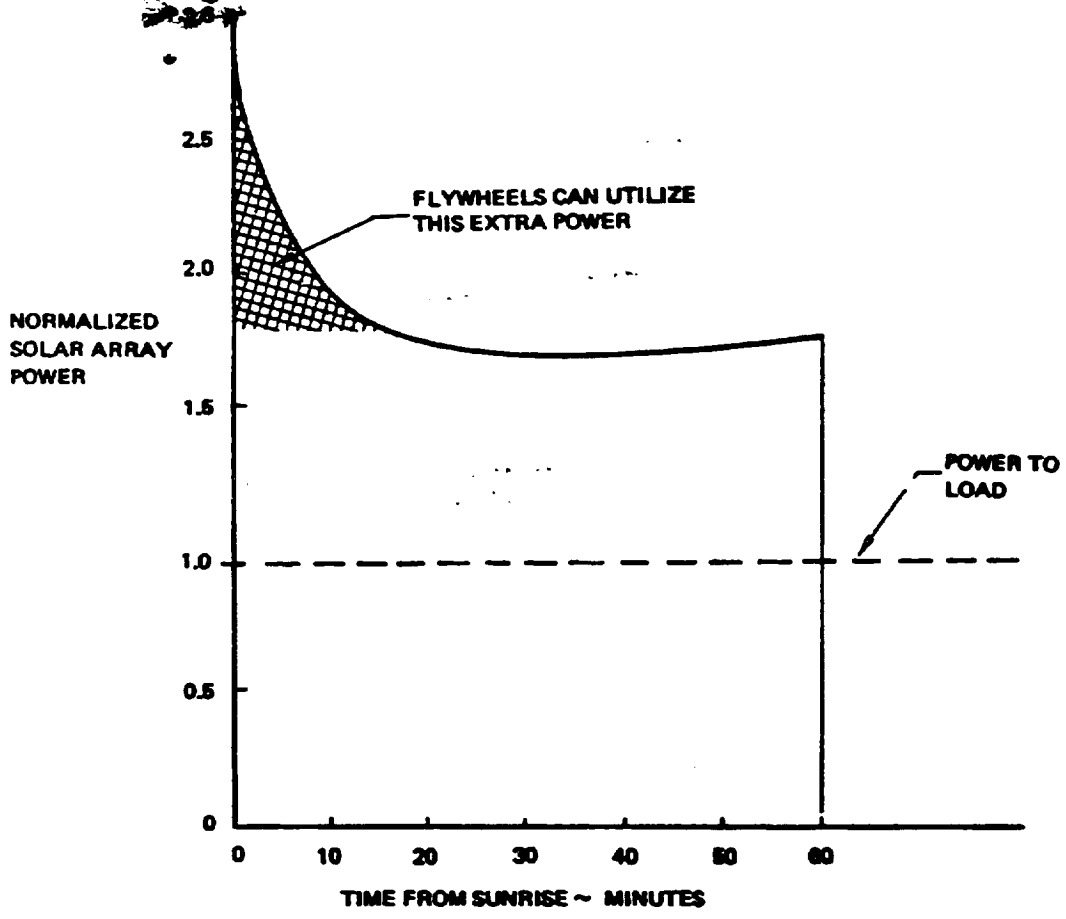


Figure 3. Typical Sun-Oriented Solar Array Performance in Low Earth Orbit

C-2

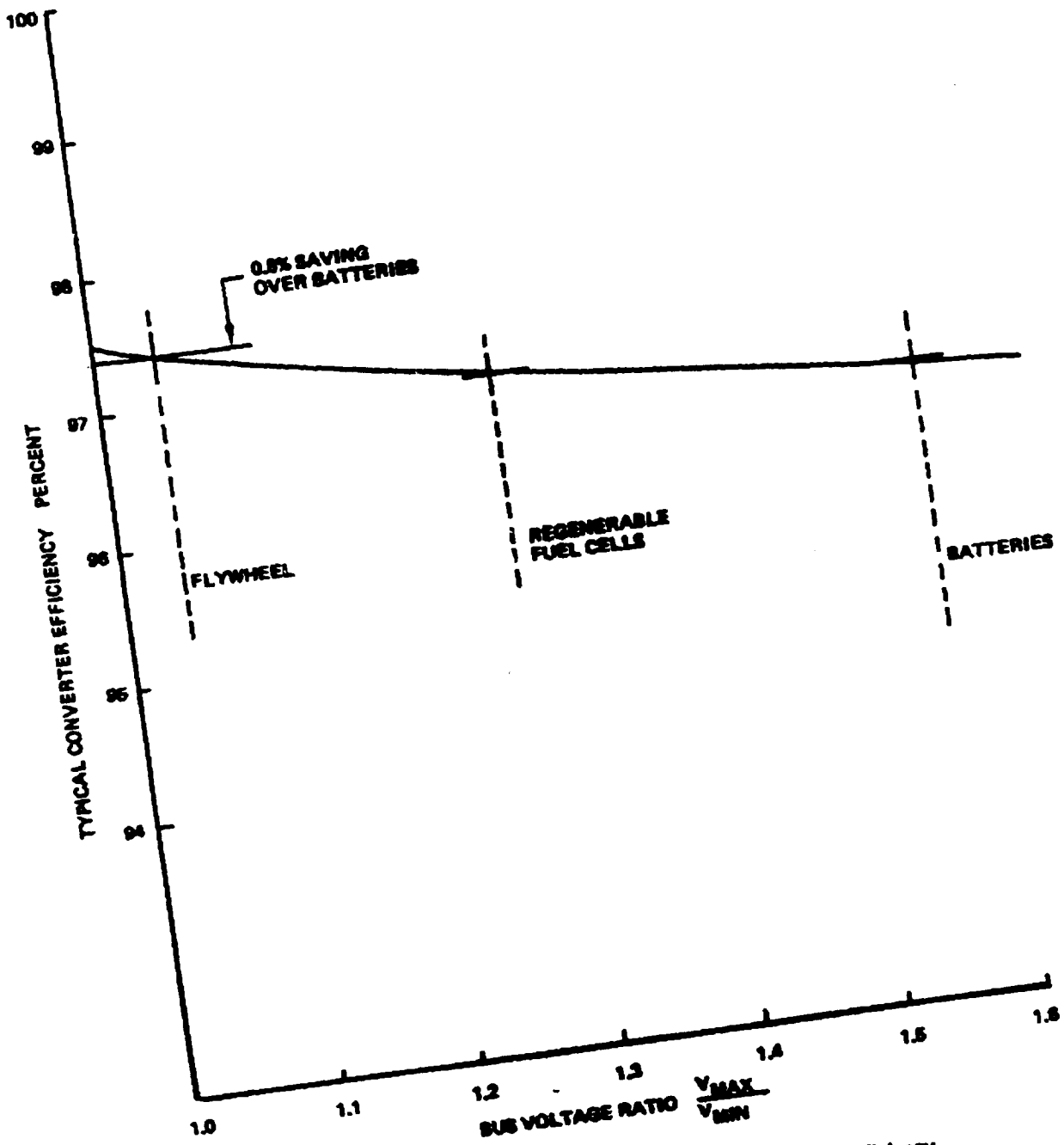


Figure 4. Effect of Bus Volt Regulation on Power System Efficiency

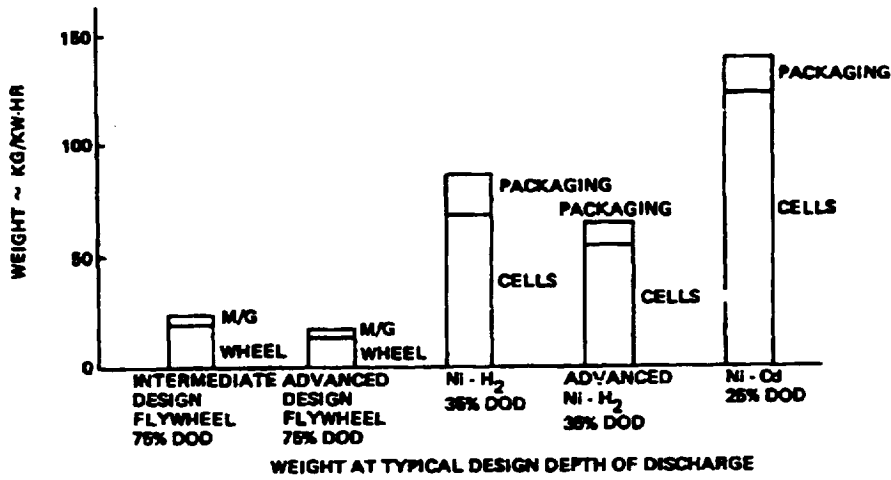


Figure 5. Comparative Weights of Energy Storage Devices

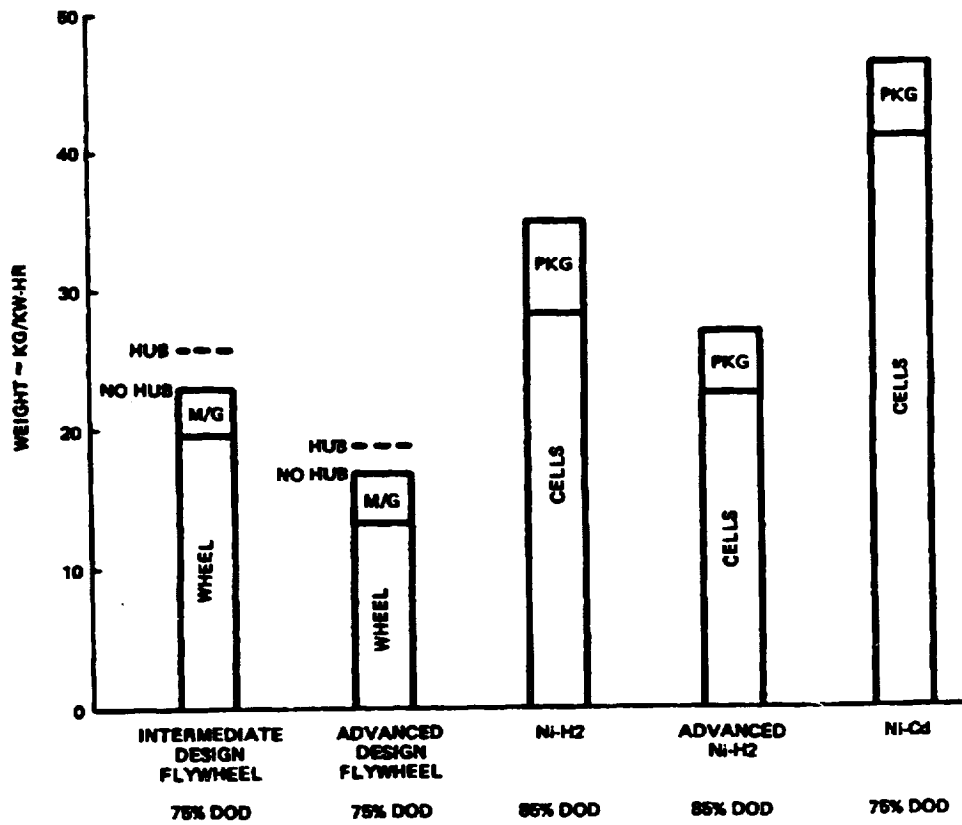


Figure 6. Comparative Weights of Energy Storage Devices Sized for Emergency Condition

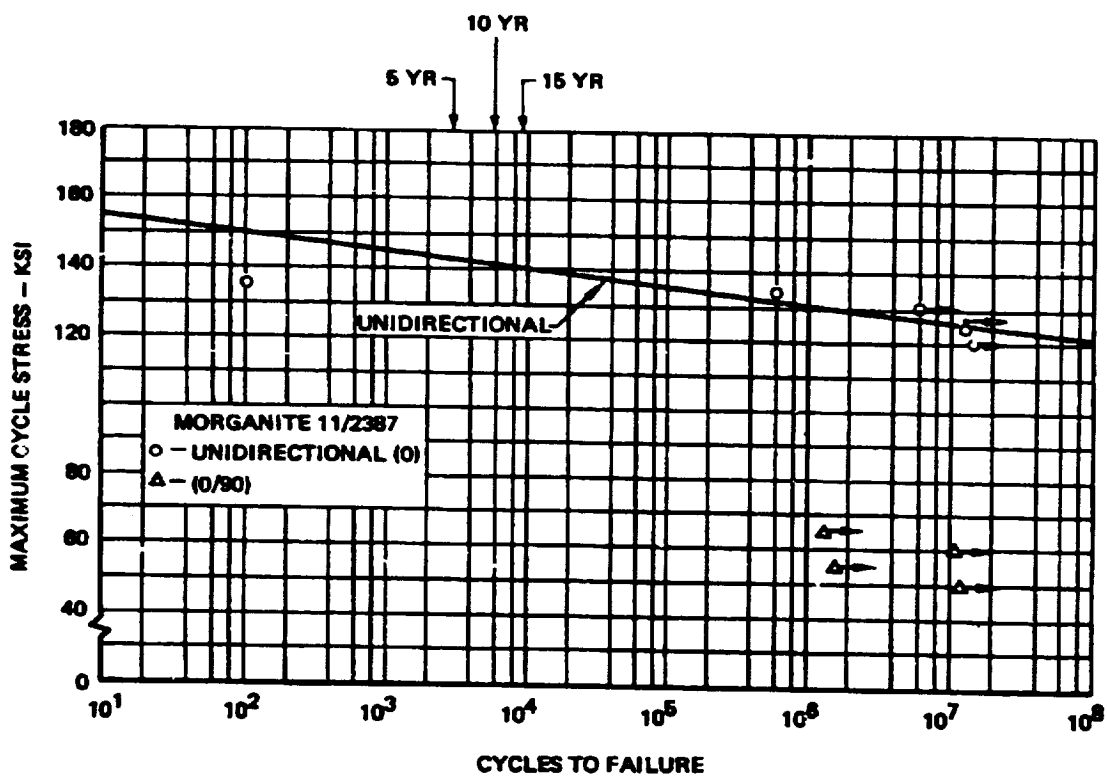


Figure 7. Constant Amplitude Unidirectional Fatigue Properties of Typical High-Strength Graphite/Epoxy Composite

N85

3858

UNCLAS

D-8

N85 13858

COMPARATIVE ENERGY STORAGE ASSESSMENT ITEM

Bob Giudici  
Marshall Space Flight Center  
Huntsville, Alabama

PRECEDING PAGE BLANK NOT FILMED



## INTRODUCTION

Inertial energy storage, or flywheels, emerged as a promising alternative to electrochemical storage methods with the concept of Integrated Power and Attitude Control (IPAC). Energy stored in the flywheel during sunlight portions of the orbit was used to supply spacecraft power during Earth occultation. The flywheel was mounted on double gimbals similar to a control moment gyro (CMG) to permit three-axis control of the spacecraft throughout the orbit. Thus, a single device performed the functions of both power and attitude control. The potential merit of an IPAC concept had been foreseen in the early 1970's and the necessary system application studies and technology demonstrations have since been completed.<sup>(1,2)</sup> This analysis, a Space Station application study, rediscovered IPAC and found the approach to have lower initial and resupply weight and lower initial and resupply cost than either battery/CMG or regenerative fuel cell/CMG systems. The highly favorable results of this study and companion in-house studies led MSFC to consider IPACS as a strong candidate for the initial Space Station. Technology developments subsequent to the earlier work make flywheels even more attractive for growth Space Stations and free-flying science platforms. These developments include composite rotor material, magnetic suspension and improved charge/discharge electronics. This study found order-of-magnitude advantages over conventional or advanced electrochemical/CMG systems when potential performance improvements were considered.

## REFERENCE SPACE STATION

Space Station Concept Definition studies considered a wide range of approaches, including Space Stations and man-tended Space Platforms having power requirements ranging from 20 kW to 140 kW. Orbital altitude and inclination were also variables. The set of requirements assumed for the purpose of this discussion are tabulated in Table 1.

TABLE 1 - MISSION ASSUMPTIONS

Power Source: Photovoltaic, 100 W/m <sup>2</sup> and 50 W/kg
Power Level During Sunlight: 75 kW Nominal
Power Level During Occultation: 75 kW Nominal
Peak Power: 1.5 x Nominal
Minimum Power: Nominal/1.5
Altitude: 463 km
Inclination: 28°
Mission Duration: 15 years
Technology Readiness: 1987

Based on studies performed for a range of mission requirements, study results were considered to be applicable for the spectrum of Space Station concepts.

## TRADE STUDIES

Preliminary trade studies were performed comparing Integrated Power and Attitude Control (IPAC) with equivalent independent electrochemical power and control moment gyro (CMG) control approaches. Technologies considered to have adequate status for an initial Space Station were: (1) nickel-cadmium batteries (NiCd batteries), (2) regenerative fuel cells (RFC), (3) Skylab class CMG's, and (4) state-of-the-art IPAC using metal wheels and ball bearing suspension (SOA-IPAC). An advanced IPAC (ADV-IPAC) employing composite rotor material and magnetic suspension was included in the comparisons to illustrate a possible range of performance and cost of inertial systems. The candidates were compared on the basis of initial weight and cost and on the basis of resupply weight and cost for a 15-year mission.

## CRITERIA

The differentiating criteria applied to the candidate energy storage options were: (1) integration potential with other subsystems, (2) initial weight and cost, (3) resupply requirements and (4) system efficiency.

The potential for integration with other subsystems was implicit in the IPAC option but more complex for the RFC option. A RFC could be oversized to provide hydrogen and oxygen to the propulsion subsystem and to the Environmental Control/Life Support (ECLS) subsystem. However, the determination of possible cost and weight savings was beyond the scope of this study. There is no integration potential for NiCd batteries.

Resupply cost was based on a 15-year mission because longer missions, such as 30 years, placed unrealistic emphasis on this cost element. Cost discounting was considered to be a more technical method of accounting for resupply cost; however, the option to discount resupply cost by considering a 15-year mission life was adopted for simplicity. The effect was approximately the same as discounting a 30-year resupply cost at an 8 percent rate.

The solar array size required to deliver 75 kW to the user bus is an accurate measure of the charge/discharge efficiency of the energy storage system. Cost penalties relative to a solar array required by flywheel systems were assessed against RFC's and batteries and included: (1) solar array design and development (D&D), (2) solar array recurring, (3) launch, and (4) propellants to compensate for solar array drag.

A possible psychological factor among some electrical power system engineers against the use of rotating machinery may have hindered the acceptance of flywheels in previous studies even though attitude control designers had flown three large CMG's on Skylab and were planning an ever larger system for the Space Station. The principle of rotating machinery would therefore appear to be acceptable despite several design differences; namely, (1) higher rotating speed (8000 RPM for CMG's and 20,000 to 40,000 RPM for flywheels) and (2) rotor configurations.

The significance of the IPAC concept and/or the performance advantages promised by composite rotor material and magnetic suspension is illustrated by the following energy storage trade study results.

ENERGY STORAGE/MOMENTUM EXCHANGE WEIGHT

Weight-to-orbit for a 15-year mission is depicted in bar chart format in Figure 1. The candidates were first compared on the basis of energy storage only (i.e., as they would normally be compared in electrical power subsystem trade studies). Next, the comparison was made for the combined weight of electrical power and attitude control for the purpose of investigating the possible merit of integrating power and attitude control (the IPAC concept). When results appeared favorable to the IPAC concept, special features of flywheel systems were investigated. The effect of high system efficiency is shown in the third representation.

The lifetime of the RFC option was assumed to be either 5 or 7.5 years. The weight differential between one resupply (5-year life) and two (7.5-year life) is indicated in Table 2. Weights and lifetimes for the set of energy storage options investigated are tabulated in Table 2.

TABLE 2 - WEIGHT/LIFETIME SUMMARY

OPTION	INITIAL kg	YEARS
NiCd	8400	7.5
SOA-FW	4600	5
RFC	2600*	5 or 7.5)
ADV-FW	1800	15

\* Tanks not replaced (311 kg)

The "Power Only" comparison (fig. 1) was considered to favor the selection of RFC's. They offered a significant weight reduction over conventional NiCd batteries and were competitive with the initial weight of advanced flywheels. The absence of resupply weight from the advanced flywheel might easily be overlooked by Space Station study teams that typically place primary emphasis on initial weight. Placing the emphasis on technology development and the flight experience with fuel cells would also favor adoption of RFC's. Selection of regenerative fuel cells might readily be prophesied if this scenario proved correct.

The introduction of the IPAC concept greatly enhanced inertial energy storage options. The effect is illustrated by the second representation in Figure 1 where the mass of CMG's required for attitude control was added to the mass of the electrochemical options. The comparison now strongly favored the advanced IPAC option via the combined effects of high performance, long life and integration of power with attitude control. The Space Station was assumed to require six CMG's based on previous in-house studies. Total CMG weight was 1400 kg and lifetime was 5 years.

State-of-the-art IPAC systems were also shown to be competitive with electrochemical options. Weights were significantly lower than conventional battery systems and competitive with regenerative fuel cell systems. The comparison with regenerative fuel cells was therefore pursued in more detail.

Flywheel systems were found to exhibit a high effective power system efficiency because the controller used for charge/discharge control had the inherent capability to provide regulated voltage to the system without further power processing. An accounting of system efficiency was made by comparing the solar array size required by each of the energy storage options. Solar array weight and the difference in stationkeeping propellants resulting from array sizes relative to the array required by inertial systems are tabulated in Table 3.

TABLE 3 - ENERGY STORAGE SYSTEM PENALITIES TO SOLAR ARRAY DESIGN  
RELATIVE TO 160 kW ARRAY FOR INERTIAL SYSTEMS

ITEM	NiCd BATTERIES	RFC
Power Delta	+ 21 kW	+ 31 kW
Weight	+ 420 kg	+ 620 kg
15-Year Drag	+ 2400 kg	+3600 kg

The third representation shown by Figure 1 includes the addition of initial solar array weight and resupply propellants to compensate for solar array drag. The weight of the state-of-the-art IPAC option was slightly lower than that of the RFC/CMG option.

Heat rejection requirements were considered subjectively to benefit flywheel options. Electrochemical systems generated heat primarily during discharge whereas flywheel heat rejection was relatively constant. Determination of possible differentiating criteria, including thermal storage capacitors or relative radiator sizes, and the complexity of relating such factors into equivalent CER's for thermal control systems were beyond the scope of this study.

Results of the weight analysis gave the indication that the SOA-IPAC concept was competitive with regenerative fuel cell/CMG systems, and therefore a preliminary cost analysis was initiated.

#### ENERGY STORAGE/MOMENTUM EXCHANGE COST

Cost estimating relationships (CER's) for NiCd batteries, regenerative fuel cells, and control moment gyros (CMG's) were based on current projections obtained from the Space Station definition activity. Complexity factors relative to CMG's were used to estimate the cost of inertial systems. Cost estimates used for the comparison are tabulated in Table 4.

TABLE 4 - COST SUMMARY (\$ X 10<sup>6</sup>)

ITEM	NiCd	RFC	SOA-IPAC	ADV-IPAC	CMG
D&D	3	30-150	30	45	24
FH	49.5	50	39	44	14
Launch	11.8	3.7	6.5	2.5	2.0
Resupply Flts	1	1 or 2	2	0	2

Results of the cost analysis are shown by the bar charts in Figure 2 and follow the same format that was adopted for the comparison of weight (i.e., power only, power + CMG's and power + CMG's + solar array deltas).

The "Power Only" comparison was considered to favor conventional NiCd batteries by virtue of the very low D&D cost. The disadvantage of weight was largely discounted because launch cost was a small part of total. Many studies ignore the launch weight of particular subsystems and base launch cost solely on utility module volume.

The potential advantage of advanced IPAC systems was indicated only when resupply cost for a 15-year mission was added to the battery option. The low technology status of advanced flywheels and the typical discounting of resupply costs would make NiCd batteries a likely selection for the initial Space Station.

As was the case for the weight comparison, consideration of the IPAC concept greatly altered the relationships. The initial cost of both IPAC options was lower than either of the electrochemical options. Surprisingly, the SOA-IPAC system had the lowest initial cost.

Consideration of relative system efficiencies further benefited the inertial storage options but not to the extent shown in the weight comparison. Solar array cost deltas are tabulated in Table 5.

TABLE 5 - SOLAR ARRAYS RELATIVE TO 160 KW ARRAY  
FOR INERTIAL SYSTEMS

ITEM	NiCd BATTERIES	RFC
Power Delta	+ 21 kW	+ 31 kW
D&D	+ 1.0	+ 1.4
FH	+ 6.0	+ 8.8
Launch	+ 1.3	+ 2.0
Total Initial	+ \$ 8.3 M	+ \$ 12.2 M
15-Year Drag	+ \$ 3.3 M	+ \$ 5.0 M

The objective of the cost analysis was to explore the close weight comparison between RFC's and SOA-IPAC options. Results strongly favored SOA-IPAC. Further, the SOA-IPAC option had lower initial and lower 15-year mission costs than either electrochemical/CMG option, and projected technology improvements offered the technology transparency desired for growth Space Stations.

## CONCLUSIONS

The weight comparison found SOA-IPAC competitive with RFC/CMG systems. Both of these systems were much lighter than conventional NiCd battery/CMG systems.

Results from the cost analysis strongly favored SOA-IPAC over RFC/CMG systems and also showed lower costs than NiCd/CMG systems. Thus, SOA-IPAC would appear to be an attractive approach for the initial Space Station and possible technology improvements would further the appeal for the initial and/or growth Space Station.

## REFERENCES

- (1) Notti, J. E.; Cormack, A. III; and Schmill, W. C.: Integrated Power/Attitude Control System (IPACS) Study, Volume I - Feasibility Studies. NASA CR-2283, April 1974.
- (2) Will, R. W.; Keckler, C. R.; Jacobs, K. L.; Description and Simulation of an Integrated Power and Attitude Control System Concept for Space-Vehicle Application. NASA TN D-7459, April 1974.

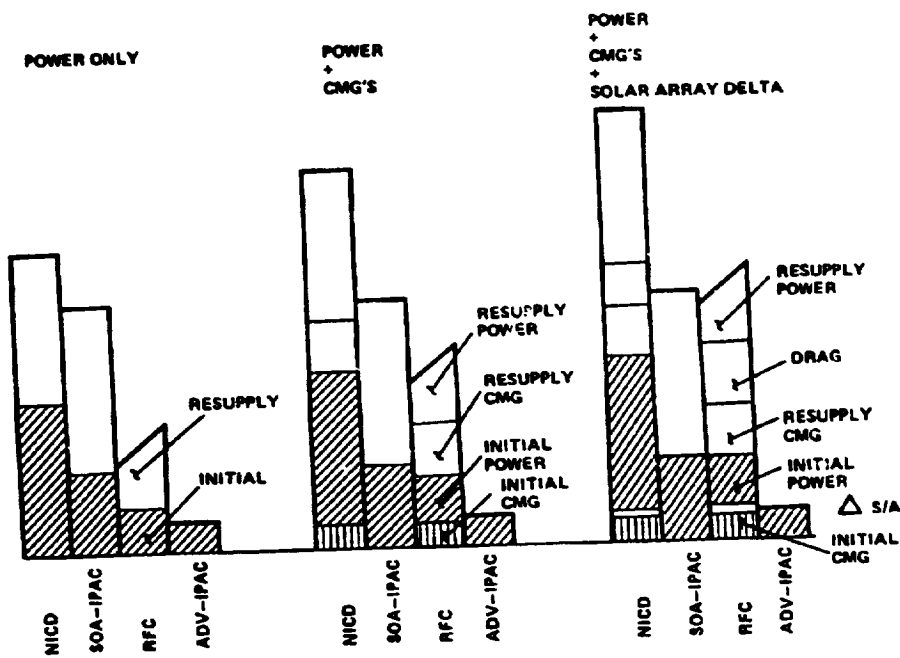


Figure 1.- Weight comparison.

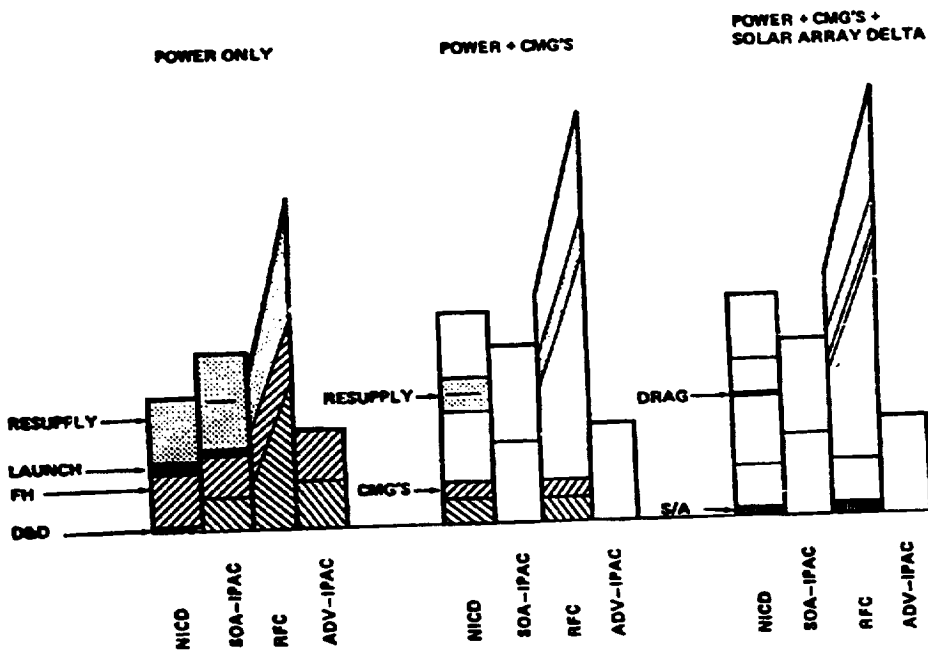


Figure 2.- Cost comparison.





N85

3859

UNCLAS



D-9

N85 13859

**INERTIAL ENERGY STORAGE FOR SATELLITES**

**D. Eisenhaure  
The Charles Stark Draper Laboratory, Inc.  
Cambridge, Massachusetts**

PRECEDING PAGE BLANK NOT FILMED

## ABSTRACT

The Charles Stark Draper Laboratory is developing a new system that performs satellite attitude control, attitude reference, and energy storage utilizing inertia wheels. The baseline approach consists of two counter-rotating flywheels suspended in specially designed magnetic bearings, spin-axis motor/generators, and a control system. The control system regulates the magnetic bearings and spin-axis motor/generators and interacts with other satellite subsystems (photovoltaic array, star trackers, sun sensors, magnetic torquers, etc.) to perform the three functions.

Existing satellites utilize separate subsystems to perform attitude control, provide attitude reference, and store energy. These functions are currently performed using reaction or momentum wheels, gyros, batteries, and devices that provide an absolute reference (sun sensors and star trackers). A Combined Attitude, Reference, and Energy Storage (CARES) system based on high energy density inertial energy storage wheels (flywheels) has potential advantages over existing technologies. Even when used only for energy storage, this system offers the potential for substantial improvements in life, energy efficiency, and weight over existing battery technologies. Utilizing this same device for both attitude control and attitude reference would result in significant additional savings in overall satellite weight and complexity.

## SATELLITE INERTIAL ENERGY STORAGE

- **POTENTIAL FOR COMBINING ATTITUDE, REFERENCE, AND ENERGY STORAGE SYSTEMS**
- **FUNCTIONAL PRIORITY**
  - 1) **ENERGY STORAGE (REPLACES BATTERIES)**
  - 2) **ATTITUDE CONTROL**
  - 3) **ATTITUDE REFERENCE**
- **APPROACH**

**CONFIGURE A BASELINE SYSTEM BASED ON THE REQUIREMENTS OF:**

- 1) **SMALL SATELLITE APPLICATION**
- 2) **TYPICAL SPACE STATION**

The small satellite system studied to date is sized to meet the requirements of the Solar Max Mission (SMM) configuration of the Multimission Modular Spacecraft (MMS) satellite. The components which would be replaced with the CARES system include the batteries, IRU, reaction wheels, and some functions of the power regulation unit. With minor modifications, the baseline system could be used to provide a subset of the CARES functions. In particular, the system could be configured to provide energy storage and attitude control, energy storage alone, or attitude reference alone.

### **SMM MISSION SPECS**

#### **POWER SYSTEM**

**BATTERIES: THREE 20-Ah Ni-Cd**  
**WEIGHT: 158 lb**  
**DOD: 2-yr MISSION 40%**  
**CAPACITY: 806 Wh (2-yr MISSION)**  
**POWER: 1200 W**

#### **ATTITUDE CONTROL SYSTEM**

**4 REACTION WHEELS**  
**MAX TORQUE PER WHEEL: 0.15 N·m**  
**MAX H PER WHEEL: 20 N·m·s**  
**SLEW RATE: 5 min arc/30 s**

**MAG TORQUERS: 0.0035 -0.007 N·m**

#### **ATTITUDE REFERENCE SYSTEM**

**3 TWO-DEGREE-OF-FREEDOM GYROS**  
**ACCURACY: 100 ppm DEVIATION**  
**<1/2% ABSOLUTE**  
**POWER CONSUMPTION: 7 W/AXIS**

#### **COMPONENTS REPLACED WITH CARES SYSTEM**

**BATTERIES**

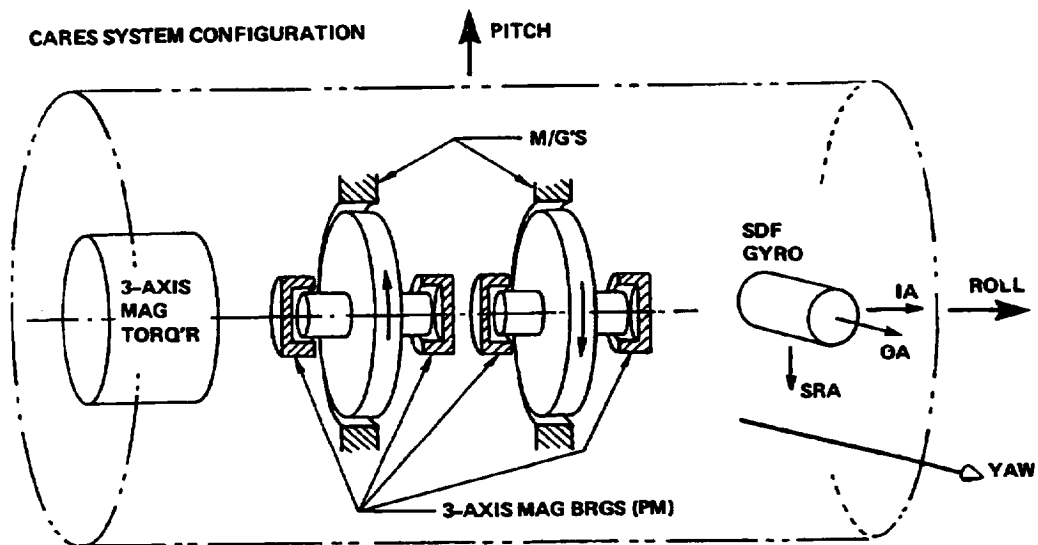
**POWER REGULATOR**

**REACTION WHEELS**

**ATTITUDE CONTROL  
ELECTRONICS**

**IRU**

The mechanical configuration of the baseline system is shown below. During periods of sunlight, motors accelerate the flywheels, thus storing the excess energy from the photovoltaic array (PVA) as kinetic energy. During periods of eclipse, these motors function as generators and provide power for satellite systems. The CARES system provides attitude control about the roll, pitch, and yaw axes. Control about the roll axis is obtained by differentially torquing the motor/generators. Control about the pitch and yaw axes is obtained by tilting the flywheels within the magnetic bearings at a controlled rate. Two axes, therefore, are controlled by utilizing the wheels as control moment gyros while the third axis is controlled by utilizing the wheels as reaction wheels. Attitude rate information about the pitch and yaw axes can be computed from bearing torque and gap information. Attitude rate information about the roll axis is provided with a gyro or other external sensor. In alternative configurations, three axes of rate information could be provided and all gyros could be eliminated.

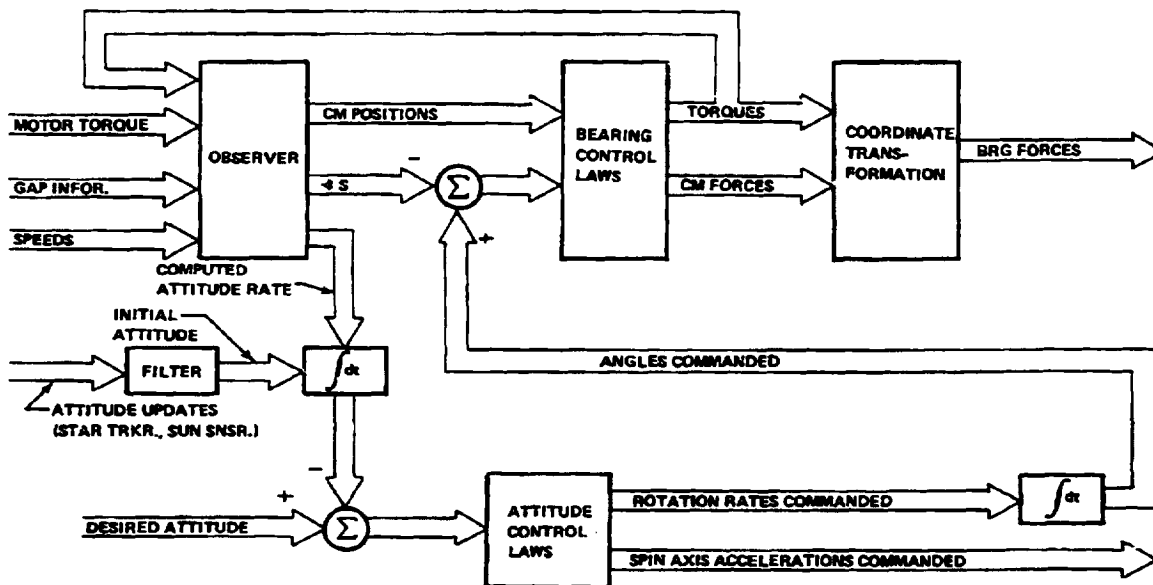




ORIGINAL PAGE IS  
OF POOR QUALITY

The magnetic suspension produces net torques about the pitch and yaw axes of the satellite in response to either commanded attitude changes of the satellite or external disturbances. For example, consider a commanded rotation of the satellite about its pitch axis. The control system would initially command a rate of tilt (with respect to the satellite) of the flywheels about the yaw axis. In order to affect this tilt rate, the magnetic suspensions exert torques about the pitch axis of the satellite. The satellite will continue to accelerate about the pitch axis until one or both of the flywheels have reached their maximum allowed angle of tilt. At this point, the inclinations of the flywheels remain fixed, and the satellite continues to rotate about its pitch axis at a constant rate. While the satellite is rotating about its pitch axis, the control system automatically supplies equal and opposite torques to each wheel. These torques cause the wheels to precess at the satellite rate but yield no net torque on the satellite. When the satellite nears completion of the desired motion, the control system commands an oppositely directed rate of tilting of the flywheel spin axes. This removes the satellite angular momentum and brings the attitude of the satellite to its desired value.

#### CARES SYSTEMS CONTROL CONFIGURATION



The magnetic suspension functions as a bearing, torquer, and inertial rate sensor. Because of its multiple uses, the suspension must have negligible cross-axis coupling, gain that is independent of rotor position, and stable torque characteristics. These are all characteristics in which magnetic bearings have traditionally had deficiencies. The baseline system utilizes an "ironless" 3-axis magnetic suspension concept employing high energy product samarium cobalt permanent magnets. This suspension has the potential for overcoming many of the deficiencies in existing magnetic bearings.

**CANDIDATE ROTOR MATERIALS—75% DOD**

	WHEEL SPEED (r/min)	RADIUS (in.)	WEIGHT (lb)	VOLUME (in. <sup>3</sup> )	Wh/lb	Wh/lb @ BURST
STEEL VASCO MAX 300	25,292	5.6	80	280	6.7	12.2 (21.2 demonstrated)
TITANIUM Ti 6Al-4V	26,320	6.2	61	378	8.85	9.6
<b>BORON/ALUMINUM</b>	<b>40,760</b>	<b>5.71</b>	<b>29.3</b>	<b>298</b>	<b>18.31</b>	<b>26 BASELINE</b>
BORON/EPOXY	38,400	6.19	28	380	19.1	38.2
GRAPHITE/EPOXY	35,250	6.41	31.6	421	16.7	32.4 (28.4 demonstrated)

**FACTORS AFFECTING MAGNETIC BEARING DESIGN**

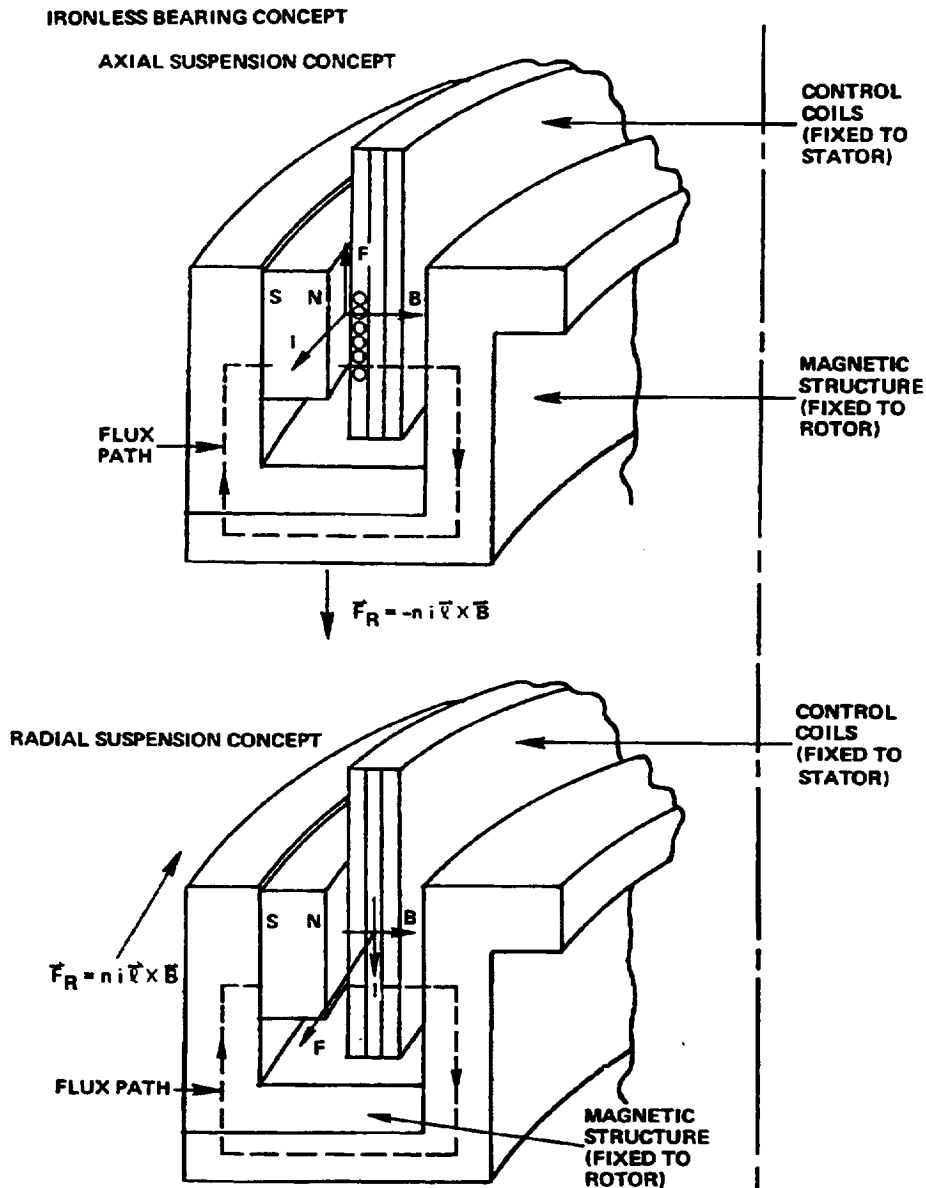
- WHEEL ANGULAR MOMENTUM
- REQUIRED SLEW RATES OF SATELLITE
- REQUIRED SATELLITE TORQUE
- WHEEL IMBALANCE
- WHEEL SPEED
- STRUCTURAL COMPLIANCES AND INTERACTIONS

**FUNCTIONS PERFORMED**

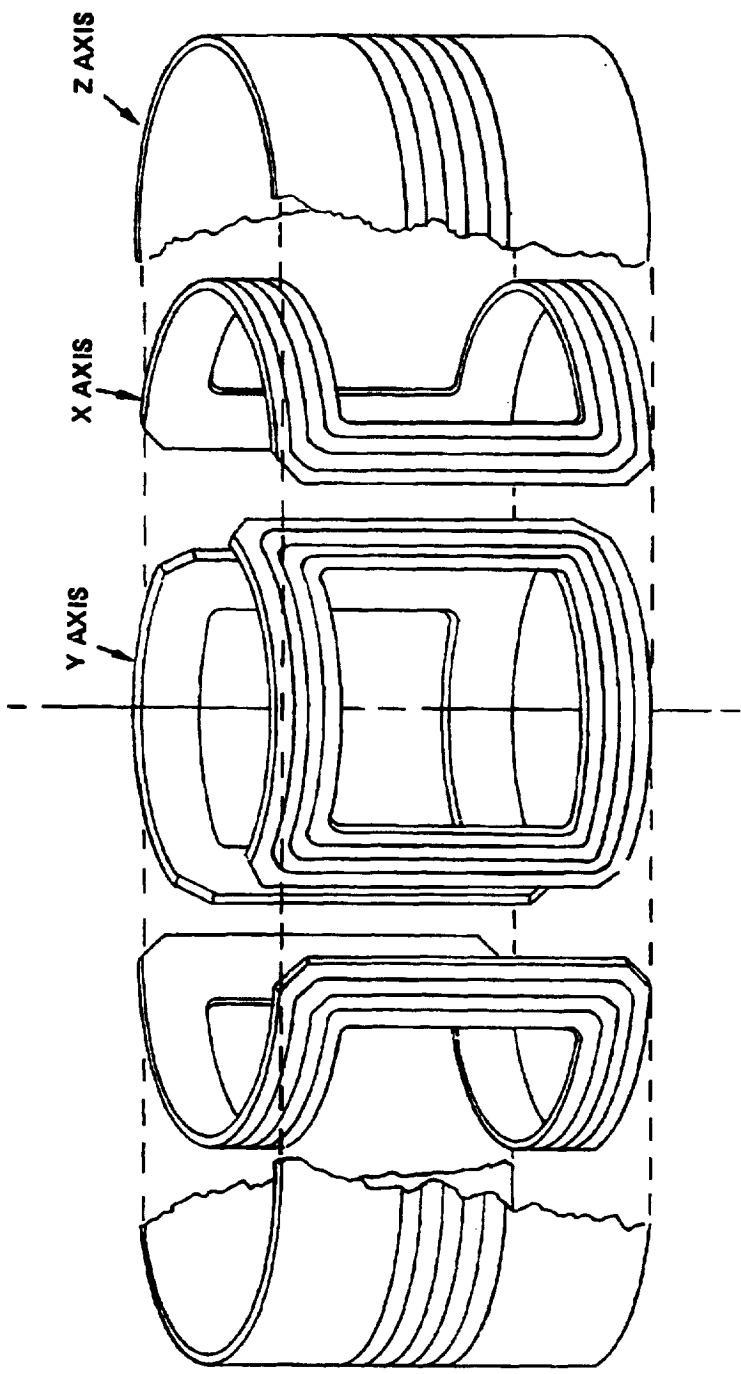
- BEARING
- TORQUER
- RATE SENSOR



Forces are exerted on the flywheel due to the interaction of rotating permanent magnets and stationary control coils. The figure shows the configuration required to produce these forces. The windings of the control coil structure are shown assembled and in exploded form. Rotor position is determined by a 3-axis capacitive position sensor. Flywheel motion is detected by the change in capacitance of several electrical paths between the flywheel and housing.



CONTROL COILS  
DETAILED



A flywheel energy storage system for a satellite might consist of a photovoltaic array (PVA), a peak power tracker (PPT), and a pair each of regulators, motor/generators (M/G), and flywheels as shown. The two motors would require two control loops -- one a differential loop for roll axis stabilization, the other a common mode loop such that the bus voltage is maintained.

## **FUNCTIONS PERFORMED BY POWER DISTRIBUTION SYSTEM**

- **BUS VOLTAGE REGULATION**
- **SPIN-AXIS ATTITUDE CONTROL**
- **PEAK POWER TRACKING**

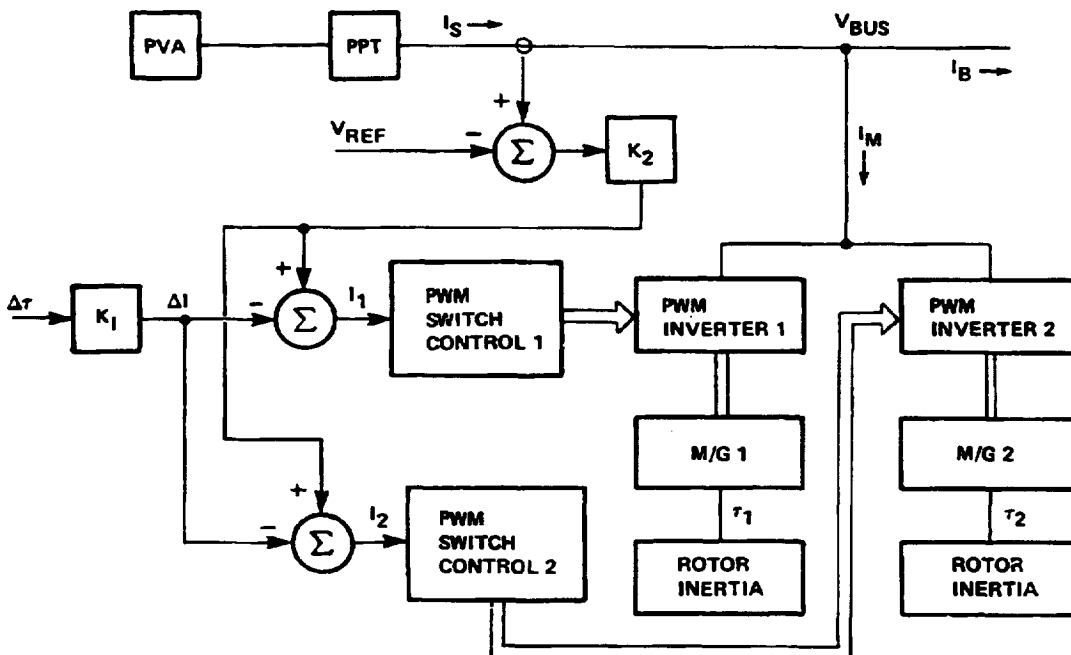
## **POWER HANDLING COMPONENTS**

- **SOLAR ARRAY**
- **PEAK POWER TRACKER**
- **PWM dc/ac MOTOR DRIVES (2)**
- **IRONLESS PM MOTOR/GENERATORS (2)**

A power distribution system for satellites typically provides the functions of peak power tracking of the PV array and voltage regulation of the satellite's power bus(es). In the CARES system, the power distribution system components are also used for roll axis attitude control.

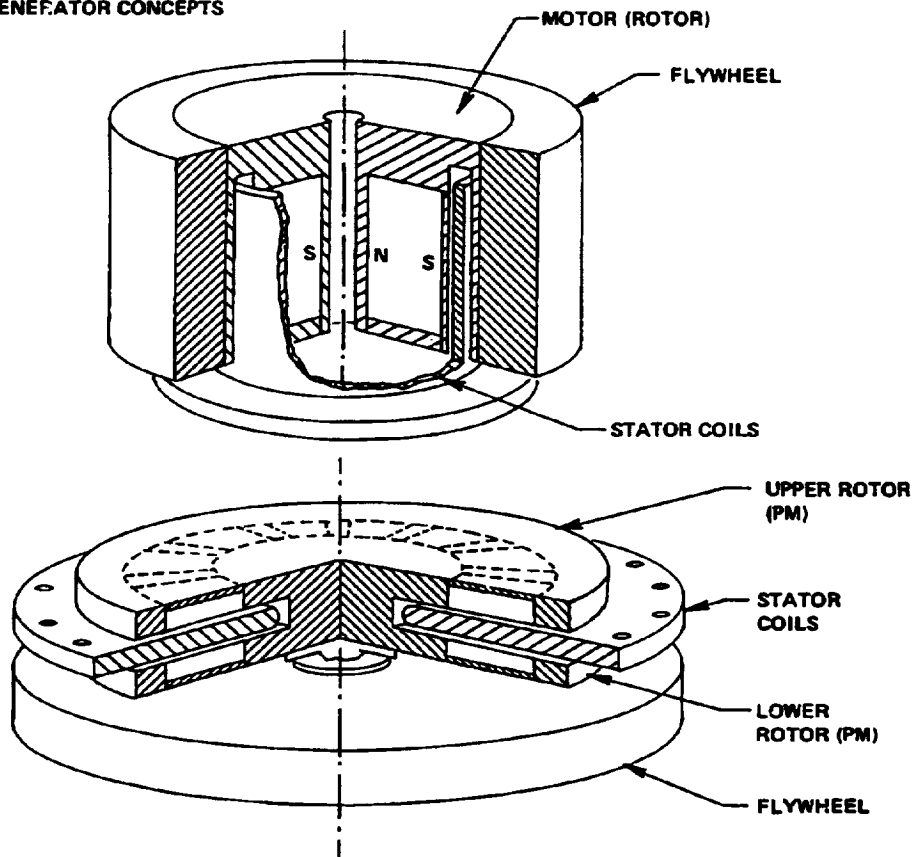
The roll axis of the satellite is stabilized by feeding back an error signal proportional to the difference between the desired roll axis torque and the actual applied torque ( $\Delta\tau$ ). The M/G control system performs the function of torque regulation about a desired set point. To decouple the functions of attitude control and energy storage (provide a subset of the CARES functions), the torque set point is made equal to zero. Note that the regulators and meters consist of pulse width modulated (PWM) inverters and permanent magnet (PM) motor/generators.

### SPIN AXIS CONTROL LOOP



The system can be implemented using a variety of configurations. Minimization of interactions between the drives and the suspension, however, suggests the use of ironless PM motor/generators such as those shown. The PM configuration requires the feedback of rotor position to the PWM in a minor loop. The PWM configuration should be implemented with output current used as the control variable, since this control variable is convenient for both the attitude control system ( $I \propto \tau$ ) and bus voltage control loops.

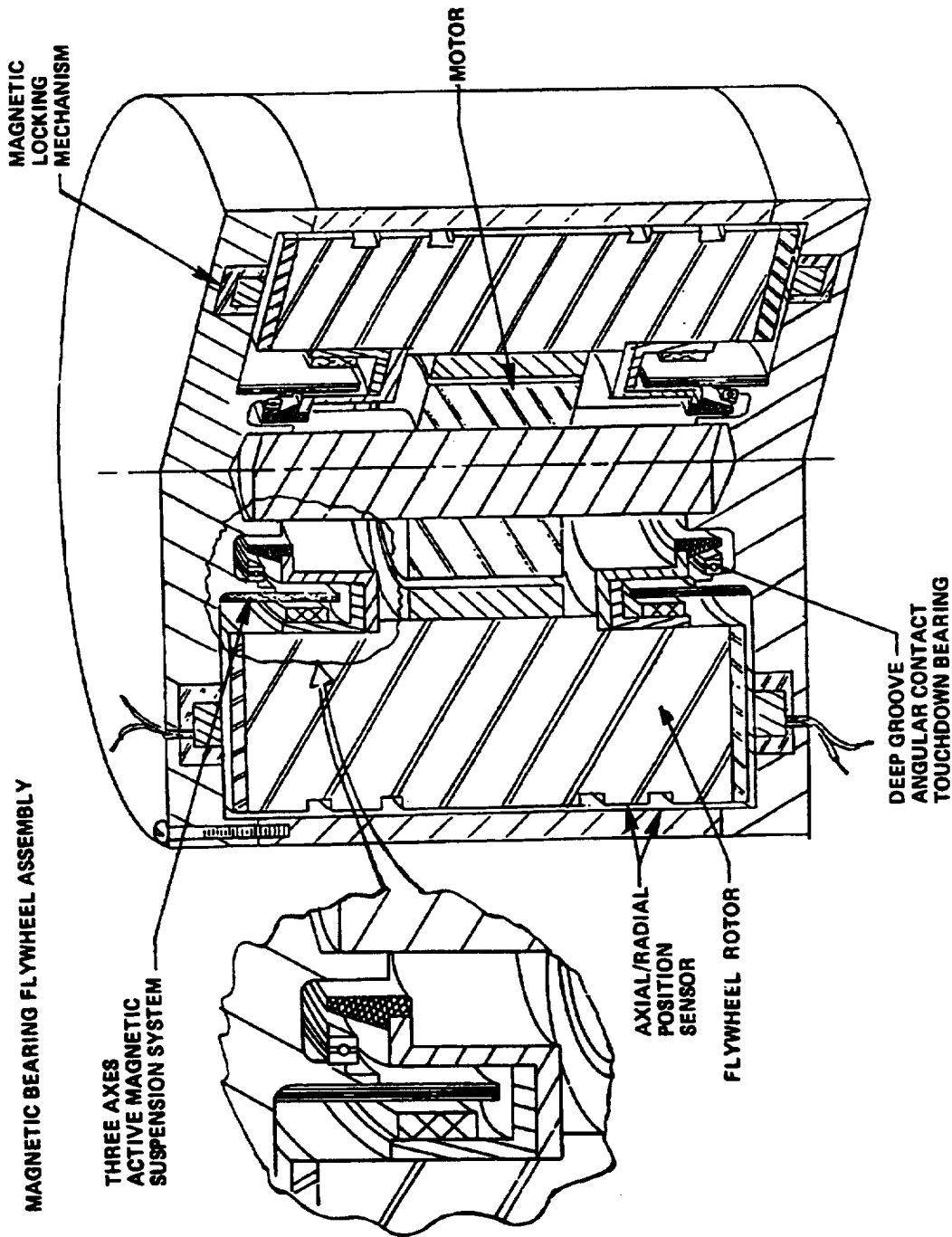
**IRONLESS MOTOR/GENERATOR CONCEPTS**



There are several advantages of the CARES approach over conventional approaches. First, storage weight and volume are greatly reduced; second, storage life is substantially extended; third, and perhaps most important, the extremely high potential efficiencies can have substantial impact on satellite PV arrays and radiators.

SYSTEM COMPARISON

FLYWHEEL SYSTEM 75% DOD		FLYWHEEL SYSTEM 50% DOD		CONVENTIONAL 2 YEAR		CONVENTIONAL 5 YEAR	
ROTORS (2)	58.6 lb	ROTORS (2)	88 lb	BATTERIES	158 lb	BATTERIES	252 lb
MOTOR/GEN	10 lb	MOTOR/GEN (2)	10 lb	IRU	37.2 lb	IRU	37.2 lb
MAG BEARINGS	13.3 lb	MAG BEARINGS	20 lb	REACTION WHEELS (4)	79.2 lb	REACTION WHEELS	79.2 lb
GYRO (1)	3 lb	GYRO (1)	3 lb				
STRUCTURE	17 lb	STRUCTURE	23 lb				
	101.9 lb		144 lb		274 lb		368.4 lb
	1192 in. <sup>3</sup>		1792 in. <sup>3</sup>		4282 in. <sup>3</sup>		6140 in. <sup>3</sup>



## CONCLUSION

Over the last ten years, the government has funded the design and development of a large number of composite flywheel rotors. This research, which received early support from NSF-RAND, has recently been funded almost exclusively by DOE and its predecessor, ERDA. This program has resulted in the development and test of many composite rotor systems. In addition to the DOE developed systems, a number of promising composite systems exist, which DOE ruled out for consideration based on either high cost or unavailability. These systems include metal matrices such as boron/aluminum or silicon carbide/aluminum, together with more conventional composites such as boron/epoxy.

In recent years, a number of organizations, including CSDL, MIT, Cambion, Sperry, Aerospatiale, and Teldix have built and demonstrated magnetic bearings. These developments were enhanced or even made feasible by advances in permanent magnetic materials, improved magnetic iron, and new semiconductor concepts.

Advances in recent years in magnetics (e.g., samarium cobalt magnets) and power semiconductors (e.g., MOSFET's) have made possible very efficient, high-power-density power conversion systems. These new conversion systems allow for the design of flywheel systems which are expected to have significantly higher storage efficiencies than batteries or other storage technologies.

The above advances in component technology allow CARES systems to be designed for space applications ranging from small satellites to large space stations. Utilizing a CARES system will result in significant savings in overall spacecraft weight and complexity over more conventional approaches.

- **SIGNIFICANT WEIGHT AND VOLUME REDUCTIONS ACHIEVED THROUGH THE USE OF ENERGY STORAGE FLYWHEELS**
- **ADDITIONAL SAVINGS DUE TO CONSOLIDATION OF CRITICAL FUNCTIONS**
  - **ENERGY STORAGE**
  - **ATTITUDE CONTROL**
  - **ATTITUDE REFERENCE**
- **KEY COMPONENT TECHNOLOGIES HAVE BEEN DEMONSTRATED**
  - **ROTOR**
  - **MAGNETIC SUSPENSION**
  - **MOTOR/GENERATOR**
  - **POWER CONVERSION**



## BIBLIOGRAPHY

- D. Eisenhaure, B. Johnson, T. Bliamptis, and E. St. George: Development of a Dual-Field Heteropolar Power Converter. Final Report to NASA Lewis Research Center, DOE/NASA/0817-1, NASA CR-165168, CSDL Report R-1489, Aug. 1981.
- D. Eisenhaure, B. Johnson, and R. Drescher: The Influence of Material Properties on Flywheel Optimization Criteria. Final Report to LLNL, CSDL Report R-1477, June 1981.
- D. Eisenhaure and J. Downer: Aerodynamic Heating and Windage Loss Characteristics of Flywheel Rotors. Final Report to Lawrence Livermore National Laboratory, CSDL Report R-1472, June 1981.
- D. Eisenhaure, J. Downer, and R. Hockney: Factors Affecting the Control of a Magnetically Suspended Flywheel. 1980 Flywheel Technology Symposium, Rep. No. CONF-801022, Dep. Energy, 1980.
- D. Eisenhaure, W. Stanton, E. St. George, and T. Bliamptis: Utilization of Field-Modulated Machines for Flywheel Applications. 1980 Flywheel Technology Symposium, Rep. No. CONF-801022, Dep. Energy, 1980.
- D. Eisenhaure, W. Stanton, R. Hockney, and T. Bliamptis: MOSFET-Based Power Converters for High-Speed Flywheels. 1980 Flywheel Technology Symposium, Rep. No. CONF-801022, Dep. Energy, 1980.
- D. Eisenhaure, G. Oberbeck, S. O'Dea, and W. Stanton: Final Report on Research Toward Improved Flywheel Suspension and Energy Conversion Systems. NSF Final Report, CSDL Report R-1108, Nov. 1977.

N85

3860

UNCLAS

D-10

N85 13860

PERSPECTIVES ON ENERGY STORAGE WHEELS  
FOR SPACE STATION APPLICATION

Ronald E. Oglevie  
Rockwell International  
Shuttle Integration &  
Satellite Systems Division  
Downey, California

## OVERVIEW

The purpose of this paper is to address several of the issues of the workshop from the perspective of a potential Space Station developer and energy wheel user. Systems' considerations are emphasized rather than component technology. The issues of concern are: What is the potential of energy storage wheel (ESW) concepts? What is the current status of the technology base? Does justification exist for advanced technology development? How should such a technology program be defined? .... etc.

Fig. 1 illustrates the logic flow of the presentation. The study concludes that energy storage in wheels is an attractive concept for immediate technology development and future Space Station application.

- THE IPACS LEGACY
- TECHNOLOGY ADVANCE IN LAST DECADE
- HOW DO ESWs STACK UP FOR SPACE STATION?
  - A SYSTEMS POINT OF VIEW
- TECHNOLOGY ISSUES
- CONCLUSIONS & RECOMMENDATIONS

Figure 1

## SUMMARY OF IPACS FEASIBILITY WORK (1970)

The Integrated Power and Attitude Control System (IPACS) work was performed by the NASA Langley Research Center and its contractor, Rockwell International (see refs. 1, 2, and 3). This effort provides a valuable legacy of information for several reasons. In terms of scope, it is the most comprehensive treatment of the application of ESW's to spacecraft at this time despite being approximately 10 years old. It treats systems as well as component-level issues on a rational and consistent basis.

A brief summary of the work and the related conclusions are given in Fig. 2. A much more comprehensive summary is given in ref. 1. In general, the major conclusions of the study are still valid today.

- DESIGN CONCEPTS DEVELOPED FOR A VARIETY OF SPACE APPLICATIONS
    - (MODULAR SPACE STATION, TDRS, EARTH OBSERVATION SPACECRAFT, RESEARCH & APPLICATIONS MODULE, MJS PLANETARY SPACECRAFT, & EXTENDED-DURATION ORBITER)
  - COST & WEIGHT ADVANTAGES FOR MOST MISSIONS
  - TYPICAL ENERGY DENSITIES APPROXIMATELY TWICE THAT OF NiCd BATTERIES
  - ADVANTAGES INCREASE WITH NUMBER OF CHARGE/DISCHARGE CYCLES
  - READILY ADAPTABLE TO GIMBALED & NONGIMBALED APPLICATIONS
  - SUBSTANTIAL PERFORMANCE IMPROVEMENT SHOWN WITH CONSERVATIVE TECHNOLOGY ADVANCES
  - DYNAMIC SIMULATION OF SIMULTANEOUS ENERGY MANAGEMENT & ATTITUDE CONTROL, NO SIGNIFICANT PERFORMANCE OR DYNAMIC INTERACTION PROBLEMS
  - DETAILED DESIGN APPROACH ESTABLISHED
  - ROTATING ASSEMBLY EMPLOYING TITANIUM ROTOR DEVELOPED & SUCCESSFULLY TESTED
  - MODIFIED CONSTANT STRESS ROTOR SHAPE UTILIZED
- TECHNICAL FEASIBILITY, PERFORMANCE & COST ADVANTAGES ESTABLISHED
  - MOST APPLICABLE TO SPACECRAFT WITH LARGER ENERGY & MOMENTUM STORAGE REQUIREMENTS & LONG LIFE

Figure 2

IPACS DESIGN CONCEPT  
(EARLY 1970's TECHNOLOGY)

Fig. 3 illustrates the IPACS design concept considered to be state-of-the-art technology in the early 1970's. The laboratory test model employed a high-strength-to-weight titanium alloy rotor and ball bearings with thin-film lubrication for low losses. The rotor design was a modified constant stress shape. Other parameters include:

- Component weight: 173 lb
- Rated angular momentum: 1075 ft-lb-sec
- Rated power delivery: 2.5 kW
- Rated energy storage: 1.1 kWh
- Operating speed range: 17,500 to 35,000 rpm

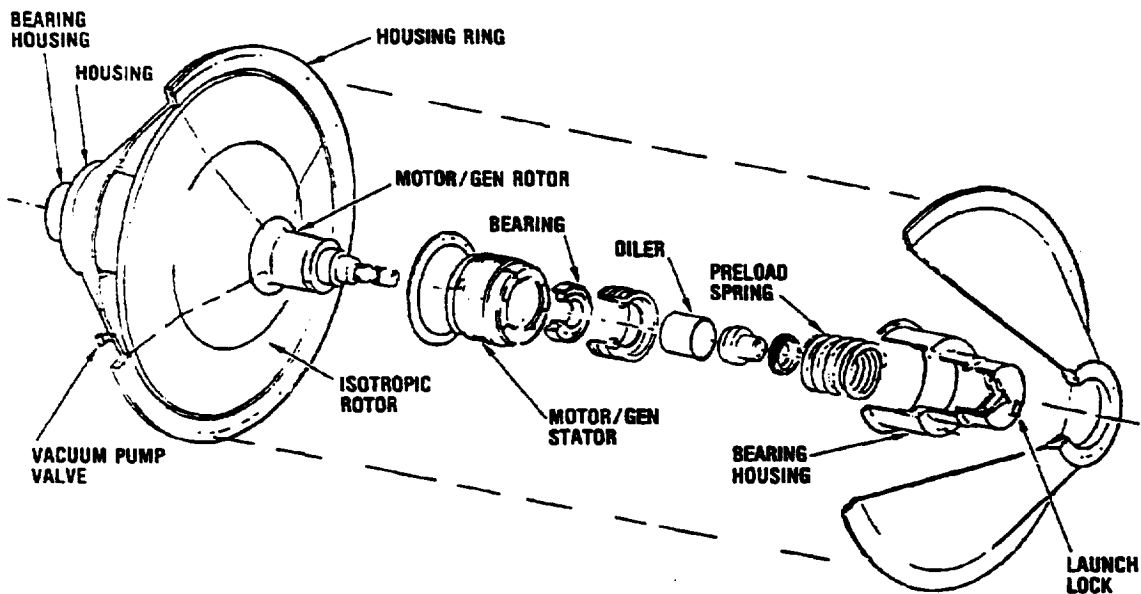


Figure 3

TECHNOLOGY ADVANCES SUPPORTING SPACE APPLICATIONS OF ESW's  
(LAST DECADE)

During the last decade, appreciable advances have occurred in the three basic technology areas which form the constituent parts of an advanced ESW System (Fig. 4). Improvements in permanent magnets, design of the magnetic elements, and advancements in power processing and control circuitry have given rise to improved energy recovery efficiencies. These have gone from the 60% range to a potential value over 90% under certain ideal conditions. Ref. 4 presents favorable test data approaching this range.

The magnetic bearing technology has seen many more laboratory and operational system developments and tests. Although the specific magnetic bearing design concept most appropriate to ESW application may not have been selected yet, the general technology is sufficient for incorporation in ESW space applications. The potential merits of very low friction, controlled rotor dynamics, and a maintenance-free, long-life rotor system are sufficient to suggest leap-frogging past the use of ball-bearing technology along with the attendant lifetime and maintenance concerns. The magnetic bearings are the crucial element in achieving a 20-year lifetime without rotor servicing and maintenance. The long-life potential of ESW's may well prove to be their single biggest cost advantage relative to regenerative fuel cell and battery systems which require much more frequent changeout (order of five years) and even more frequent servicing.

The composite rotor technology is the key to achieving higher energy densities, and the recent DOE energy wheel development testing program (see ref. 5) provides a valuable legacy in this area. If historical precedent has meaning, the advances in composite system stress-bearing properties are increasing at a rate that exceeds the energy density improvements seen in secondary battery systems over the last 15 years. Extrapolation suggests that future improvement in composite rotor energy density will advance faster than that of batteries.

There are many agencies and firms beyond those named in figure 4 who have provided strong contributions to the ESW technology base, and the author apologizes for these omissions.

It is concluded that the three basic technology building blocks in figure 4 are adequately developed to support the ESW technology advancement. The next most important technology program step is to define how best to integrate these three areas into a highly efficient ESW System and provide laboratory verification of the performance. Improvements in the three technology areas should also be supported since further advances seem quite feasible.

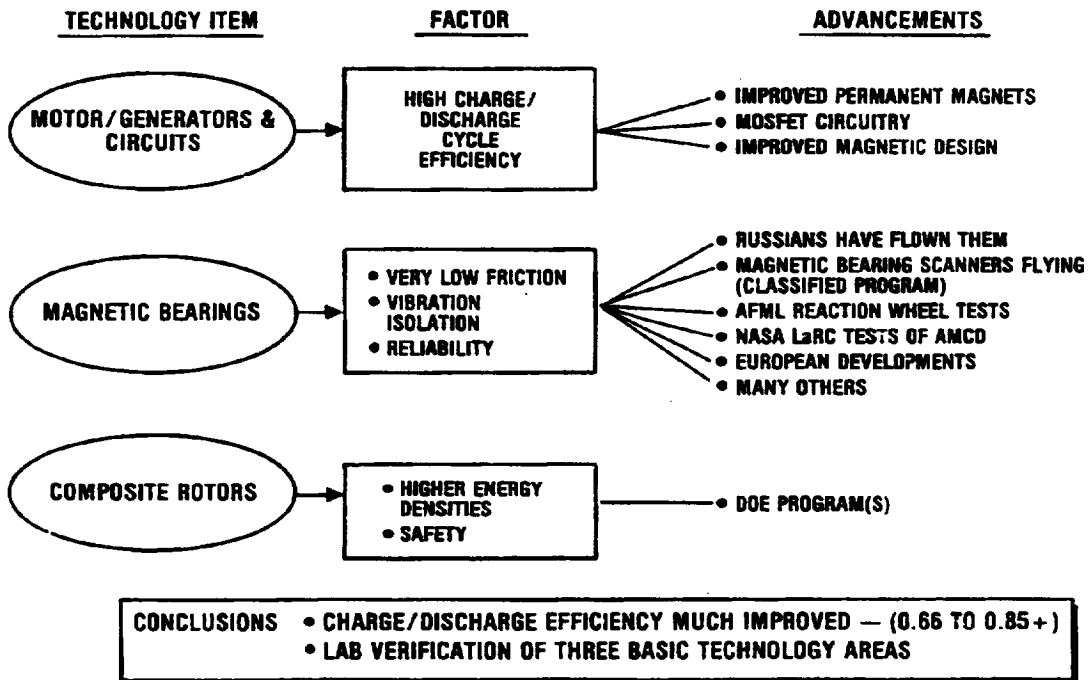


Figure 4



**ELECTRICAL POWER SYSTEM MASS FOR VARIOUS  
STORAGE COMPONENT EFFICIENCIES & ENERGY DENSITIES**

The curves and data points shown in Fig. 5 present estimates of the electrical power system (EPS) mass for several parameter variations and for three potential energy storage component types. The data show a distinct advantage for the ESW System. Of course, it is recognized that relatively few test data exist for this type of system, and its predicted performance is more uncertain.

In addition to EPS mass, the storage component energy recovery efficiency has a significant impact on other subsystems, such as the extra thermal control system capacity needed to reject the heat dissipated in the storage element, and propellant required to overcome the drag due to solar array size increases. The ESW System has a clear-cut advantage in these two areas. Of course, the most notable mass saving is in the attitude control system. The control moment gyro mass savings, by integrating the attitude control function with the ESW System, is in excess of 1.8 megagrams for a typical Space Station.

Over the 20-year Space Station life cycle, relatively large mass savings also accrue for the ESW System due to its potential 20-year life. The competing systems typically require changeout at much more frequent intervals as previously noted.

It is concluded that appreciable system mass savings beyond the energy storage element itself can result from its higher energy recovery efficiency. Although formal costing has not been done, these results tend to indicate a possible cost saving.

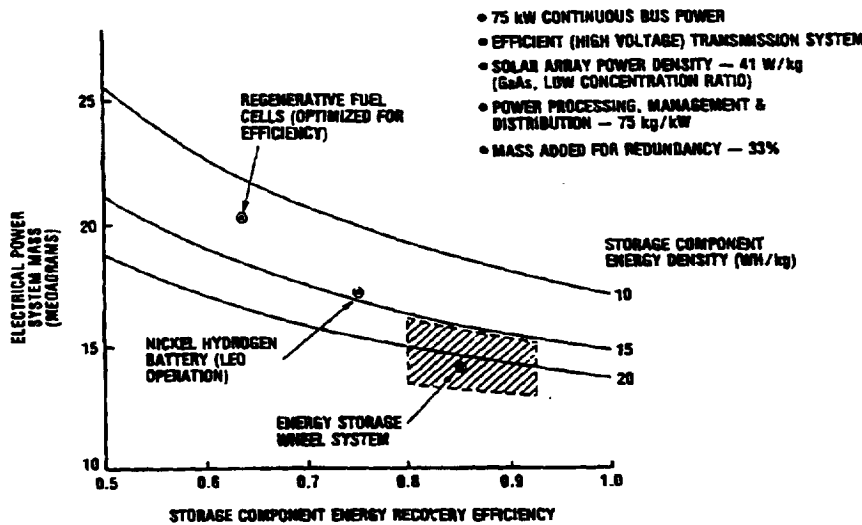


Figure 5

### MOMENTUM BUILDUP FROM VARIOUS SOURCES

Fig. 6 provides data for typical sizing of Space Station control moment gyros (CMG's) and for a variety of conditions and situations. Normal CMG sizing of about 20,000 ft-lb-sec (approximately 4000 lb weight) is possible. This is achieved by flying in constrained (low disturbance torque) orientations and by performing the infrequent operations requiring large angular momentum with reaction control thrusters. Use of the Integrated Power and Attitude Control System (IPACS) approach can save most of this CMG weight and cost. In addition, the ESW's produce an excess of angular momentum which will enable more robust operation than is possible with CMG's. Ref. 6 presents additional data and rationale as to why the CMG sizing can become much larger in the absence of prudent attitude constraints, payload operations, and momentum management techniques.

ITEM	BASIS	MOMENTUM BUILDUP* (ft-lb-sec)	
		WITH ORBITER	WITHOUT ORBITER
<b>GRAV GRAD TORQUE:</b>			
• LVLH ATTITUDE	PRINCIPAL AXES $\pm 10^\circ$ FROM LVLH	8,470	2,250
• LVLH ATTITUDE	BODY AXES ALIGNED TO LVLH	200,000	12,000
• LVLH ATTITUDE	WORST CASE PRINCIPAL AXES ORIENTATION	243,000	64,500
• INERTIAL ATTITUDE	PRINCIPAL AXIS $\pm 10^\circ$ FROM POP	18,800	5,120
<b>AERODYNAMIC TORQUE</b>	90-day ORBIT DECAY, CP-CG = 10 ft	—	10,700
<b>DYNAMIC PAYLOAD OPERATIONS</b>	LARGE PAYLOAD MOVED WITHIN 1 ORBIT PERIOD	2,000	2,000
<b>ATTITUDE MANEUVERING</b>	MINIMUM SLEW RATE = $40^\circ/\text{min}$ ( $90^\circ$ IN QUARTER ORBIT)	64,900	22,600
<b>CREW DISTURBANCE</b>	200 lb PUSH-OFF IN WORST LOCATION	6,000	4,000
<b>DOCKING DISTURBANCE</b>	CLOSURE VELOCITY = 0.5 ft/sec	81,110	—

\*MOMENTUM STORAGE CAPACITY REQUIRED IF CONTROLLED WITH MOMENTUM STORAGE DEVICES, SECULAR COMPONENTS BASED ON BUILDUP OVER ONE ORBIT

Figure 6

## SOME ENERGY STORAGE WHEEL (ESW) SYSTEM DESIGN ISSUES

Fig. 7 presents a series of design issues related to the Space Station application and should be given consideration in ESW technology development programs. Many of the earlier design concepts from previous studies and other ESW applications may no longer be appropriate due to the unique requirements of Space Station and due to the availability of new design concepts. A methodical search for the best design approaches and rigorous engineering is necessary to avoid time-consuming and costly correction of design problems. It is concluded that the cost-effective development of the ESW technology and systems presents an achievable design challenge.

### SYSTEM LEVEL

- ENERGY STORAGE ONLY vs INTEGRATED WITH ATTITUDE CONTROL?
- BEST WHEEL ARRAY CONFIGURATION?
  - GIMBALED vs NONGIMBALED?
  - COUNTER-ROTATING PAIRS vs SKEWED ARRAYS, etc.?
- REDUNDANCY & RELIABILITY?
- THERMAL CONTROL?
- ACCOMMODATION OF STATION GROWTH?  
& TECHNOLOGY UPGRADING

### ELEMENT LEVEL

- BEARINGS — BALL vs MAGNETIC?
- MAGNETIC BEARING DESIGN APPROACH?
- BEST ROTOR SHAPE?, HOOP vs HUB, etc.?
- MOTOR/GENERATOR TYPE & DESIGN?
- CIRCUITRY?
- COMPOSITE ROTOR DESIGN?
- SAFETY APPROACH?

**DESIGN OF ESW SYSTEMS FOR SPACE STATION REPRESENTS A FORMIDABLE, BUT ACHIEVABLE, DESIGN CHALLENGE**

Figure 7

## CONCLUSIONS AND RECOMMENDATIONS

Many supporting conclusions are drawn in the text, and the major ones are summarized in Fig. 8. The ESW concept is found to be a very attractive option for Space Station (as it was a decade ago). The prompt initiation of a well-conceived technology development program, including laboratory testing, is necessary in order to meet a technology readiness need date that is consistent with the Space Station development goals established by the President. The destiny of such a technology development program may well rest on the action of this workshop.

- **THE THREE BASIC TECHNOLOGY BUILDING BLOCKS (MOTOR/GENERATOR/ CIRCUITRY, COMPOSITE ROTORS, & MAGNETIC BEARINGS) ARE ADEQUATELY DEVELOPED TO PROCEED WITH ESW TECHNOLOGY DEVELOPMENT**
  
- **THE MOST IMMEDIATE TECHNOLOGY NEED IS DEFINING HOW TO INTEGRATE THESE BUILDING BLOCKS INTO A WELL ENGINEERED ESW SYSTEM & VALIDATING ITS PERFORMANCE. LABORATORY PERFORMANCE VERIFICATION IS MANDATORY**
  
- **ADVANCES IN THE THREE BASIC TECHNOLOGY AREAS ARE DESIRABLE & WILL FURTHER ENHANCE THE APPLICABILITY OF THE CONCEPT**
  
- **DEVELOPMENT OF THE ESW TECHNOLOGY & SYSTEMS FOR SPACE STATION PRESENTS AN ACHIEVABLE, ENGINEERING CHALLENGE**

Figure 8

#### REFERENCES

1. Keckler, C. R.; Rodriguez, G. E.; and Groom, Nelson J. Integrated Flywheel Technology—1983. NASA CP-2290, 1983, p. 5.
2. Notti, J. E.; Cormack, A., III; Schmill, W. C.; and Klein, W. J.: Integrated Power/Attitude Control System (IPACS) Study, Vol. I—Feasibility Studies, and Vol. II—Conceptual Designs. NASA CR-2383, April 1974.
3. Notti, J. E.; and Cormack, A., III: Design and Testing of an Energy Flywheel for an Integrated Power/Attitude Control System (IPACS). AIAA Paper 75-1107, August 1975.
4. Jarvinen, Philip D.: Advanced Flywheel Storage System. DOE/ET 20279-157, presented at Mechanical, Magnetic, and Underground Energy Storage Contractors Review, 1981.
5. Kulkarni, Satish V.: Flywheel Rotor and Containment Technology Development Program of the U.S. Department of Energy. Presented at the Third International Conference on Composite Materials, 1980.
6. Oglevie, R. E.: Space Station Attitude Control—Challenges and Options. AAS Paper 83-06; presented at the AAS Annual Rocky Mountain Guidance and Control Conference, Feb. 5-7, 1983.

N85

3861

UNCLAS

D-11

N85 13861

FLYWHEEL-POWERED X-RAY GENERATOR

Melvin P. Siegband  
Department of Medical Physics  
University of Wisconsin  
Madison, Wisconsin

## ABSTRACT

In order to have stop-action image quality of radiographs, high instantaneous power levels are required. When medical x-ray systems are installed in hospitals, three-phase power lines can provide power levels in excess of 100 kWp to meet this need. Mobile x-ray systems or systems for field use are limited by their power sources. Presently available power sources for these applications include: ninety volt nickel-cadmium batteries capable of 120 amperes, 220 vac power lines capable of pulse currents of 100 amperes, capacitor discharge systems using a 1.0  $\mu\text{F}$  capacitor charged up to 100 KV or the use of a large electrolytic capacitor of 0.3 F charged to 330 V and discharged through a regulator-inverter circuit. In each case, instantaneous power is usually limited to 10 kWp or has some other energy restriction. In the case of the 1.0  $\mu\text{F}$  system, the restriction is due to the drop of x-ray tube anode voltage during the x-ray exposure. The single phase 220 vac power line generates a non-constant voltage at the anode which is about 60% effective in producing x-rays as the more constant voltage of a three phase rectifier or of a filtered inverter. Electrolytic capacitors have other technical problems of rate limitations, fall-off during the output cycle, large size and internal heating. The use of a small flywheel appears to be a practical alternative to these power sources for mobile x-ray system applications. A 5 kg flywheel has been constructed which runs at 10 krpm and stores 30 kJ while requiring less than 500 W to bring the system up to speed. The wheel is coupled to an aircraft alternator and can yield pulsed power levels over 50 kWp. The aircraft alternator has the advantage of high frequency output which has also permitted the design of smaller high voltage transformers. A series of optical sensors detecting shaft position function as an electronic commutator so that the alternator may operate as a motor to bring the wheel up to operating speed. The system permits the generation of extremely powerful x-rays from a variety of low power sources such as household power outlets, automobile batteries or sources of poorly regulated electrical power such as those found in third world countries.



## INTRODUCTION

One of the main problems in the design of mobile x-ray generators is that of obtaining the very high power levels to allow high exposure rates and short exposure times. Power lines for use by mobile systems are often limited in output or have varying line resistance so that constant output voltage cannot be assured. Storage battery power sources are also resistance limited: practical constraints of size and weight limit instantaneous power levels to about 10 kWp. The battery power is converted to high frequency alternating voltage and fed to a step-up transformer, rectified and fed to the x-ray tube. Newer systems are improved over older systems by using even larger batteries and weigh over 350 kg. They are difficult to move to the patient site except by means of motor-assisted drives (a further drain on the batteries). Real improvements may come with some new developments in the design of storage batteries. The use of a very large electrolytic capacitor feeding a commutating regulator and high frequency inverter has promise of providing the power needed but is presently limited by peak current ratings of the capacitor, internal heating of the capacitor, size and other circuit limitations to power levels of about 10 kWp. Using high voltage capacitors for storage of the actual tube anode voltage and gating the tube anode current by tube grid control have a rather severe and subtle limitation. Such circuits operate in a way similar to an electronic flash used for photography. In the flash, energy discharged through the flash tube is converted to light for as long as the gas remains ionized. In the x-ray tube, the x-ray photon energy distribution is related to the instantaneous anode voltage. As the capacitor discharges, the voltage falls and the x-ray beam energy also falls. Lower beam energies are less penetrating, cause less film darkening and produce undesirable radiation effects on the patient.

Operation of these types of mobile x-ray generators is still marginal when high power levels and proper beam energy distribution are required for stop-motion images at low exposure levels to the patient. The 90 volt battery-powered machines at 10 kWp will draw about 140 amp, if we assume 80% efficiency. These batteries are quite heavy. Single phase line-powered systems operating at 100 kVp and 200 mA will draw more than 100 amps from a 220 vac power line. Operation from the common 115 vac line is obviously precluded by the 2 kW limit of such lines. Even though the input power to the x-ray tube is about 20 kWp, the waveform of the anode voltage reduces the actual x-ray output to almost the same level as that produced by constant potential power of 10 kWp. Power lines rated at peak current levels of 100 amps and 220 vac can be wired in hospitals and factories but are not usually found in the field. Small and portable 60 Hz power generators are usually rated at peak power levels of 5 kW or less. The capacitor discharge machine using a 1.0  $\mu\text{F}$  capacitor (actually 2.0  $\mu\text{F}$  capacitors in series, one at the anode and one at the cathode of the x-ray tube) will drop 1 kV for each 1 mA discharged at the capacitor. The capacitor can be charged at a low rate, well within the capability of the small power generator. Film darkening as a result of passage of x-ray photons through the patient is proportional to the 5th power of anode voltage. To compare the effective mAs of the capacitor discharge circuit to that of a constant potential generator, the voltage waveform of the linear discharge to the 5th power can be integrated from 100 kVp to 0 kVp:

$$\begin{aligned} \text{Eff. mA/s} &= 100 \int_0^1 (1-v)^5 dv \\ &= 17 \text{ mA/s} \end{aligned}$$

This can be interpreted as meaning that the total effective x-ray energy of a 1.0  $\mu\text{F}$  system discharged to 0 kVp is less than 17 mAs of the energy produced by a constant potential machine. This low total energy is not sufficient for many diagnostic procedures. The capacitor discharge machine is limited to the radiography of the chest or the extremities and cannot take high-quality pictures of the abdomen or the head. Battery-powered or line-powered machines can take pictures of any body part but the power rating may require that the exposure time be increased and some image motion blur may occur. The use of very large electrolytic capacitors coupled to switching regulators and high-frequency inverters is a recent development. The switching regulators compensate for the falling voltage of the capacitor as charge is withdrawn to feed the inverter. Internal series resistance and effective inductance of the storage capacitor as well as size are limitations to this approach.

The study at the University of Wisconsin has shown that power levels in the 30 kWp range and above are achievable using a flywheel alternator system. While the use of a common shaft with the motor-alternator has not been successful, a simple spline (quill) coupling and separate suspension and bearings for the wheel assembly have resulted in a simple low-loss design of very high peak power capability.

#### FLYWHEEL ENERGY STORAGE

In the flywheel energy storage system the alternator is operated as a motor to bring the flywheel up to speed. The circuits are then switched back to the alternator mode and power is taken from the flywheel to drive the alternator with the field current of the alternator controlled to produce a particular constant potential at the anode of the x-ray tube despite changes of wheel angular velocity, tube current or other factors. The power ratio between alternator and motor modes can exceed 100. Figure 1 is a block diagram and shows the relationships between the major components of the system.

A standard 115 vac power source rated at about 1 kW provides power to the motor drive, to the various control circuits and to the rotor and filament circuits of the x-ray tube. The motor drive circuit is shown in Figure 2. The 115 vac is fed to a transformer and an SCR bridge to provide a voltage controlled to between 15 and 55 vdc which is then fed to a six step driver circuit. The switching control for the six step driver is obtained from three optical sensors (retro-reflective LED-transistors, sensing shaft position - a special form of a shaft position encoder.) The output of the three sensors is fed to a 32x8 ROM where the other two inputs are determined by a simple tachometer circuit.

Thus, the output of the ROM consists of the six step drive signals with four modes of phase shift as a function of shaft speed. Final speed control is done by controlling the power supply voltage by means of the SCR's.

Relays disconnect the motor-alternator from the drive circuit and connect it to the high tension transformer. The field excitation is used to control the output of the alternator during the exposure to set the voltage at the x-ray tube. Feed-forward control maintains this voltage at the pre-set value over the changes of rotor speed and the effects of the changes of excitation due to field reactance and other factors.

The flywheel is a 5 Kg heat treated steel alloy 25 cm diameter disc spline coupled to a Bendix 28B262-35-B aircraft alternator. A second model is also under test using a Bendix 28B135-126-A aircraft alternator. These lightweight alternators are each rated at 20 kW with ram air cooling and are capable of short pulse loads in excess of 50 kWp. The run-up time is three minutes with a maximum line power requirement of 750 W. This will bring the wheel to 10 krpm which corresponds to about 30 kJ of stored energy. Controlled output of over 25 kWp has been achieved.

#### MECHANICAL CONSIDERATIONS

The design of the system requires that the total energy be limited to that obtainable from the power line for a short period of time - less than three minutes. It must yield short bursts of power of less than one second duration. The mechanical coupling must be reasonably efficient for both motor and alternator modes. The power ratio between alternator and motor modes is quite high. Reasonable efficiency in the alternator mode results in unacceptable losses in the motor mode. For that reason, various gear and belt drives could not be used. The use of a differential gear arrangement to drive counter-rotating wheels was also discarded for that same reason. Mounting of the wheel directly on the alternator shaft resulted in a configuration that had resonant frequencies below the maximum operating frequencies (Hz vs rps) so that a separate wheel mounting with a spline coupling to the alternator shaft was used. The complete assembly can be considered as a series of coupled cylinders: the flywheel, the rotor, the shaft and the bearings. For such systems, the rotational energy  $E$  at angular velocity  $\omega$  is:

$$E = 1/2 \sum_i I_i \omega^2$$

where  $I_i$  is the moment of the  $i$ th component. For a cylinder,  $I_i$  is given by:

$$I_i = 1/2 M_i R_i^2$$

where  $M_i$  is the mass and  $R_i$  is the radius of the  $i$ th component.

When power P is taken from the system, the reactive torque T(t) can be found from:

$$P(t) = dE/dt = -\sum_i I_i \omega \, d\omega/dt = -T(t)\omega(t)$$

Increased  $\omega$  will result in reduced reactive torque. The rate of change of torque during the x-ray exposure will be reduced with an increase of the initial stored energy. There are several practical limitations to increasing  $\omega$ . These include rises in the material stresses, bearing stresses, the effects of imbalances and losses due to series reactance and other effects in the alternator.

The flywheel can be considered as a homogeneous disc of outer radius a and inner radius b. The maximum tangential stress,  $\sigma_{tmax}$  and the maximum radial stress  $\sigma_{rmax}$  are estimated:

$$\sigma_{tmax} = 1/4 \rho \omega^2 ((3 + \nu)a^2 + (1 - \nu)b^2)$$

$$\sigma_{rmax} = ((3 + \nu)/8) (\rho \omega^2 (a - b)^2)$$

where  $\rho$  is the material density,  $\omega$  is the angular velocity and  $\nu$  the Poisson ratio. For the 4340 steel plate used,

$$\rho = 7.8 \times 10^3 \text{ kg/m}^3 \text{ and } \nu = 0.25 \text{ to } 0.30$$

These estimates ignore localized effects due to machining and mounting. A safety factor of five times these estimates is reasonable and prudent. For the heat treated 4340 or similar steels, yield strengths of over 860 MN/m<sup>2</sup> are attainable with elongation sufficient for braking action of the wheel against a close-tolerance housing in the event of a material failure.

The use of conventional, high quality, grease lubricated bearings limits operation to about 18 m/s for steel caged bearings and to 24 m/s for phenolic caged bearings. Because of the need for a shaft diameter of sufficient stiffness and strength, a practical angular velocity is limited by the bearings to about 15 krpm.

The requirements for stored energy, the limit of angular velocity and the safety factors chosen for steel are sufficient to define the dimensions of an annular disc flywheel (Fig.3). However, a dynamic system must consider vibrational modes as well. These include those due to rotor imbalance, obliquity of the disc, bearing mounting and shaft deflection. Vibrational modes include whirling and torsional and frame displacements of the system support. In this design, a separately supported flywheel was chosen over a single long shaft design because the short and stiff shaft would have a higher resonant frequency and better vibrational characteristics. The wheel was designed to store 30 kJ at 10 krpm with a maximum stress of of 140 MN/m<sup>2</sup>. When dynamically balanced to within  $2.8 \times 10^{-3}$  N-m, no resonant states (eigenvalues) are observed during operation.

## ALTERNATOR CHARACTERISTICS

The mechanical characteristics of the wheel are within the range of operation of aircraft alternators. Such alternators are operated at between 8 and 12 krpm and certain models produce power at a continuous output rating of 20 kW with short time ratings of 50 kW. The power output frequency in the 400 Hz range permits the design of high voltage transformers smaller than are used in conventional 60 Hz x-ray systems. To design the control necessary to produce constant power during the high power transient operation, the alternator has been modelled as a salient pole machine of one pole pair. Transient operation requires that some form of anticipation or feed-forward control be used to overcome the inherent delays of the control windings (field reactance) in order to maintain constant output during the x-ray pulse.

## MOTOR OPERATION

The alternator is operated as a motor by sensing wheel position and developing a six step drive. A tachometer circuit shifts the electrical lead angle as a function of speed and a start-up circuit limits starting current. The derivation of the six step drive (Fig. 4) and the phase shift is done by means of a 32 x 8 ROM fed by the position sensors and the 2 bit output of the tachometer circuit. The same circuit that limits the starting current also limits the operating current when a signal from the tachometer indicates that maximum operating speed has been reached.

## ALTERNATOR CONTROL

The control of the alternator field is a feed-forward system of open loop control based on shaft speed and x-ray tube kVp and mA. It was found that the inductance of the rotor field was the main cause of the very slow response time (close to the short circuit response time of the alternator). For the short pulses of power required of the system, the exponential response characteristic can be compensated for by means of a step increase in the exciter current just prior to the actual application of the load. The system exposure timer and control circuits must accomplish several tasks: transfer operation of the alternator from the motor mode to generator mode, apply power to the rotating anode of the x-ray tube in anticipation of the x-ray exposure, boost the filament power of the x-ray tube to that required to produce the selected anode current, set the exciter current and wait until the operator signals the start of the exposure. When the actual exposure is required in this "ready" condition, the circuit applies the required step input to the exciter current, waits 50 ms and closes the power contactor to make the exposure for the selected pulse duration. The application of the step input assures that the output pulse will be constant during the x-ray exposure (Fig. 5).

## CONCLUSION

The flywheel powered x-ray system has been constructed as described above. The total weight of the flywheel power source and control circuits is under 40 kg, far less than for comparable battery sources of lower power capability. The system has provided over 20 kWp of controlled power with levels of over 40 kWp expected as work continues. The simple approach of using the high speed, low torque wheel, the six step drive and the feed forward control appears to yield a practical solution to the problem of providing high power x-ray pulses of short duration for excellent stop-motion radiography.

## ACKNOWLEDGMENTS

The work was supported by Contract DAMD 17-82-C-2050 with the US Army Medical Research and Development Command, Ft. Dietrick, MD. The important contributions of the Project Associate, Dr. Donald Showers, and of graduate students David Trumble and Joseph Kidder were main factors in the success of this work.

## BIBLIOGRAPHY

1. Melvin P. Siedband, Donald K. Showers, Flywheel Energy Storage for X-Ray Machines (to be published in Medical Physics).
2. Melvin P. Siedband in Proceedings of the Symposium on Optimization of Chest Radiography (HHS Publication (FDA) 80-8124) 1980.
3. Raymond Roark, Warren Young, Formulas for Stress and Strain, 5th ed. (McGraw-Hill, N.Y.) p. 567.
4. Ed Flugge, Handbook of Engineering Mechanics (McGraw-Hill, N.Y.) 1962.
5. New Departure Hyatt Roller Bearing Catalog RC-7, Sandusky, Ohio.
6. John Hannatt, R. C. Stephens, Examples in Mechanical Vibrations (Edward Arnold Ltd., London) 1956.
7. J. B. Wilcox, Dynamic Balancing of Rotating Machinery (Pitman & Sons Ltd., London) 1967.
8. R. H. Park, "Two Reaction Theory of Synchronous Machines- Analysis, Part I", AIEE Trans. Vol. 48, pp 716-727, 1929.
9. R. H. Park, "Two Reaction Theory of Synchronous Machines II" AIEE Trans. Vol. 52, pp 352-355, 1933.
10. D. W. Novotny, "Equivalent Circuit Steady State Analysis of Inverter Driven Electric Machines", Engrg. Exp. Station Report ECE-80-19, University of Wisconsin- Madison, 1980.

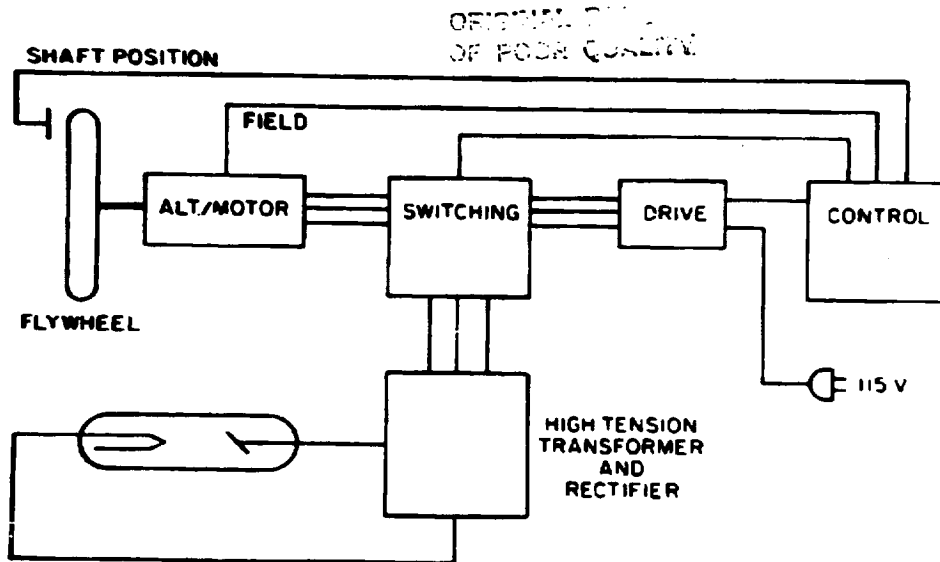


Figure 1. Block Diagram of the Flywheel-Powered X-Ray Generator.

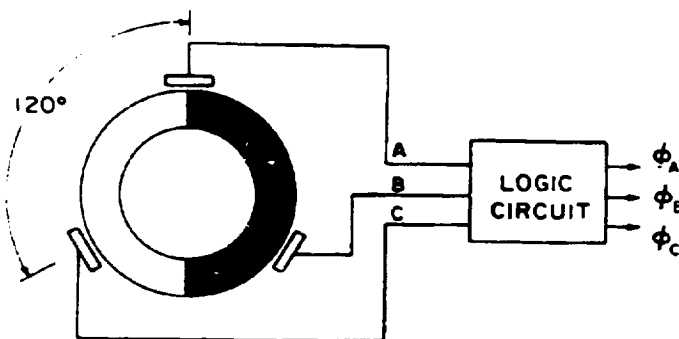


Figure 2. Diagram of Optical Commutator. In actual use, one black-white pair is used for each pole pair of the alternator-motor. Only three reflective sensors are used.

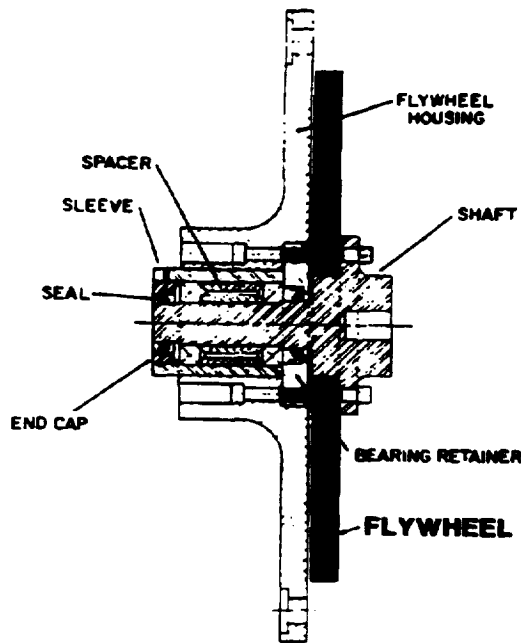


Figure 3. The Flywheel Assembly. To keep the resonance frequencies above the operating frequency, the wheel is mounted independently of the motor-alternator and is quill-coupled.

SIX STEP DRIVE SEQUENCE

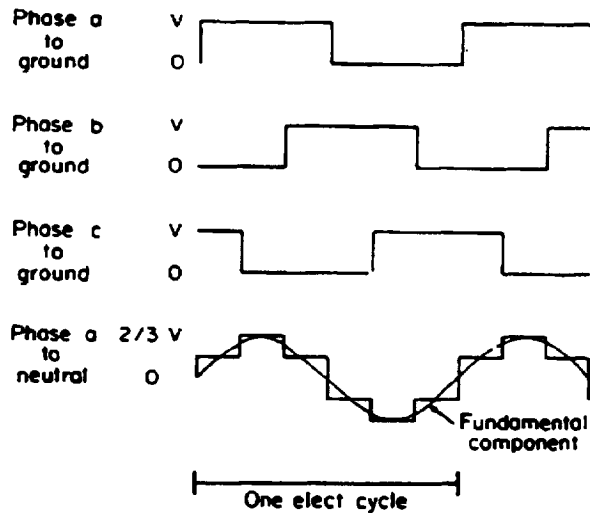


Figure 4. Six Step Drive. Because the alternator is Y-Connected, each drive signal adds within the motor. The three-phase drive is obtained by this summation.



ORIGINAL COPY  
OF POOR QUALITY

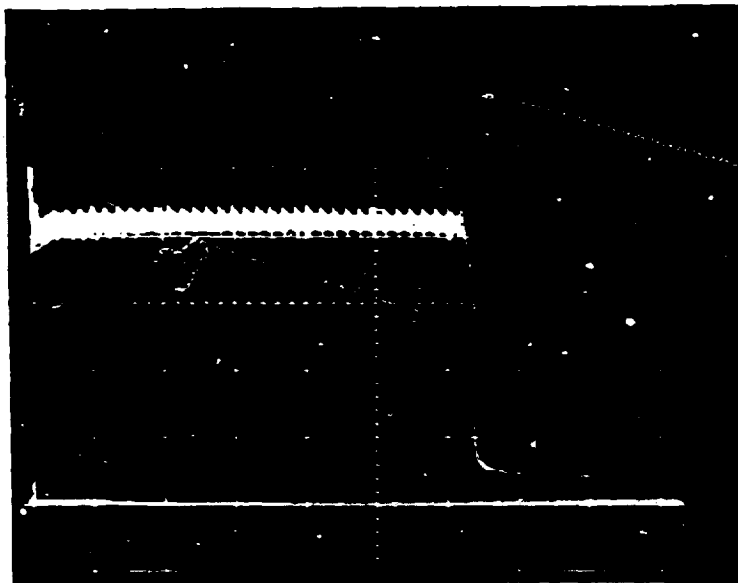
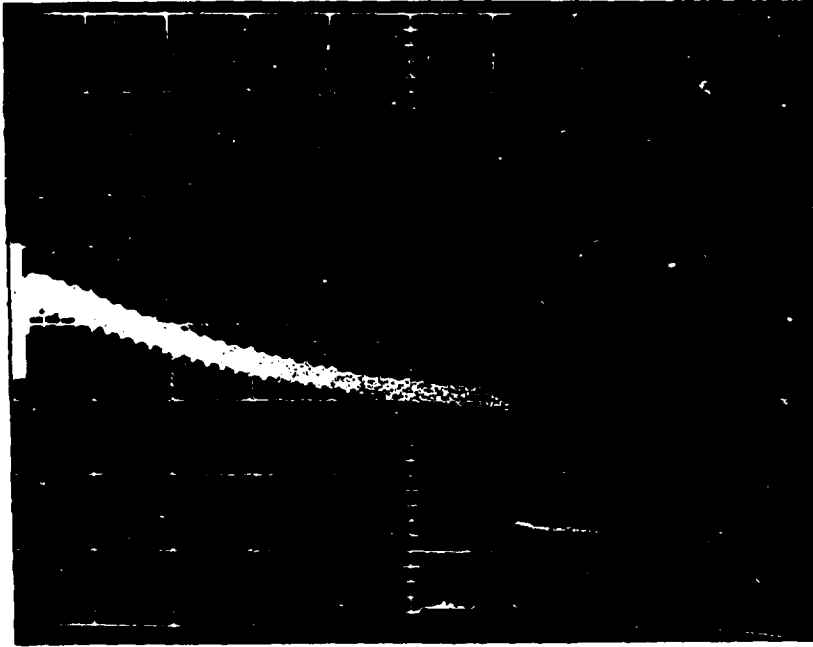


Figure 5. X-Ray Tube Anode Waveforms. Scale: 20 kVp/cm and 10 ms/cm. Tube current is 100 mA. The transient recovery time of the alternator is almost 0.25 sec., too long for x-ray applications. The use of feed-forward control corrects the output sag due to the short output pulse.

N85

3862

UNCLAS

N85 13862

D-12

Westinghouse Programs

in

Pulsed Homopolar Power Supplies

D. C. Litz  
E. Mullan  
Westinghouse R&D Center  
Pittsburgh, PA

RECORDING PAGE BLANK NOT FILMED

### Disc Type Homopolar Machine

The disc type homopolar machine shown in Figure 1 is the simplest form of an electrical machine. The machine consists of a disc rotating in an axial field provided by an electric coil positioned at the disc outside diameter. If brushes are placed on the disc OD and ID a voltage will be generated if a prime mover is provided for the disc for continuous power generation. The machine is a simple turn configuration and therefore generates a very low voltage. This low voltage requires a large current for reasonable machine horsepower. The development of these machines has been limited because of the massive current collection systems required to transfer the current from the rotor to the stator. Advances in high current density current collectors and the need for high power density power supplies have resulted in increased interest in homopolar machines. In pulsed applications, the disc is accelerated to speed, thus acting as an energy storage flywheel. If the leads are connected to a load the mechanical energy stored in the disc will be converted to electrical power and delivered to the load as the disc decelerates. Since the voltage is generated in the same element that stores the energy, there are no transient torques as would be encountered in flywheel-generator combinations. The deceleration force on the energy storage disc introduces shear stresses in the disc during the energy conversion phase. For normal configurations these shear stresses are usually very low as compared with shaft shear stresses in a flywheel-generator combination.

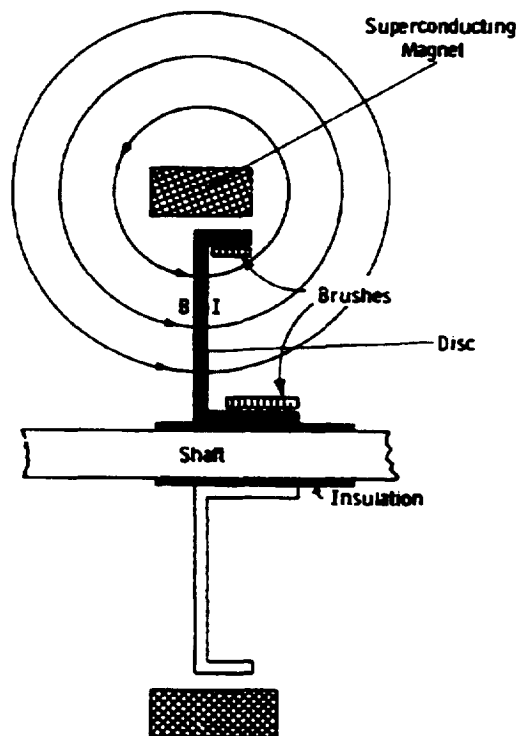


Figure 1

ORIGINAL  
OF POOR QUALITY

Drum Type Homopolar Machine

An alternate form of this concept is a drum machine shown in Figure 2. A drum or cylinder rotates in a radial magnetic field produced by two opposed solenoid coils. If brushes are placed on the cylinder surface as shown power will be generated as was the case with the disc machine. The drum machine can also act as an inertia storage device.

ORIGINAL DESIGN  
OF FOUR COILS

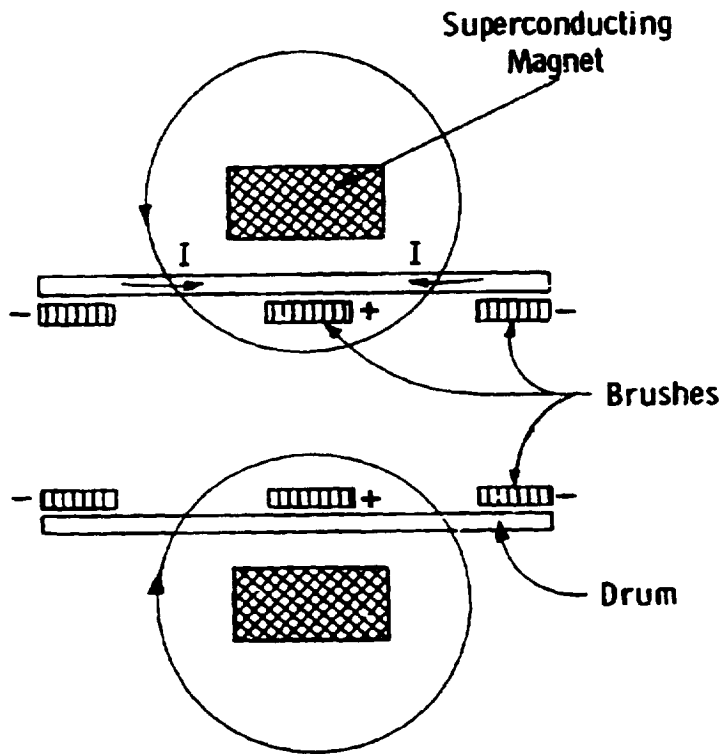


Figure 2

### Pulsed Homopolar Characteristics

Homopolar machines are inherently low voltage, high current machines. When used as a pulsed power supply, they behave as a large mechanical capacitor with an extremely low internal inductance and resistance. The integral flywheel generator concept provides a high power density pulsed power supply. From a mechanical standpoint the machine is inexpensive, simple and rugged with uncomplicated dynamic components. The only area requiring a higher level of technology is the current collection system. These characteristics are summarized in Figure 3.

### Pulsed Homopolar Characterist.cs

- Mechanical Capacitor

$$C = \frac{2E}{v^2}$$

C = Capacitance  
E = Energy stored  
V = Generated voltage

- Voltage Generated

$$V = \beta v l$$

$\beta$  = Flux density  
v = Tip speed  
l = Machine active length

- Low resistance and inductance
- Rugged design
- Simple
- Current collection dominates the design

Figure 3

### Westinghouse Homopolar Machine Experience

Westinghouse experience with homopolar machines started in 1929 with most of the work being done in the 1970's and 80's as shown in Figure 4. These included steady state DC power supplies, current collection test machines and pulsed power sources. The development of these machines required establishing expertise in support technologies including: current collection, both solid brush and liquid metal, rotor stability, AC losses, system integration, innovative cooling concepts and machine design.

1929 Homopolar Welding Power Supply  
1972 Liquid Metal Homopolar  
1974 Homopolar Energy Transfer System  
1978 Machine Environment Brush Tester  
1982 Rail Gun Homopolar Generator  
1983 Artillery Rail Gun Homopolar Generator  
1983 Space Borne Homopolar Generator

Figure 4

Westinghouse Welding Power Supply

In 1929 Westinghouse shipped a homopolar generator, shown in Figure 5, to Youngstown Sheet and Tube as a power supply for welding seamed tubing. This unit was capable of producing up to 100,000 amps at a terminal voltage of 10 volts. The machine is a modified drum design with axial bars imbedded in a ferromagnetic rotor core. The excitation was provided by a copper field coil operating at room temperature. The generator was dominated by current collection since the technology of that era dictated brush current densities of about 60-100 amps/in<sup>2</sup>. This machine operated until the late 1970's when the pipe mill was retired.

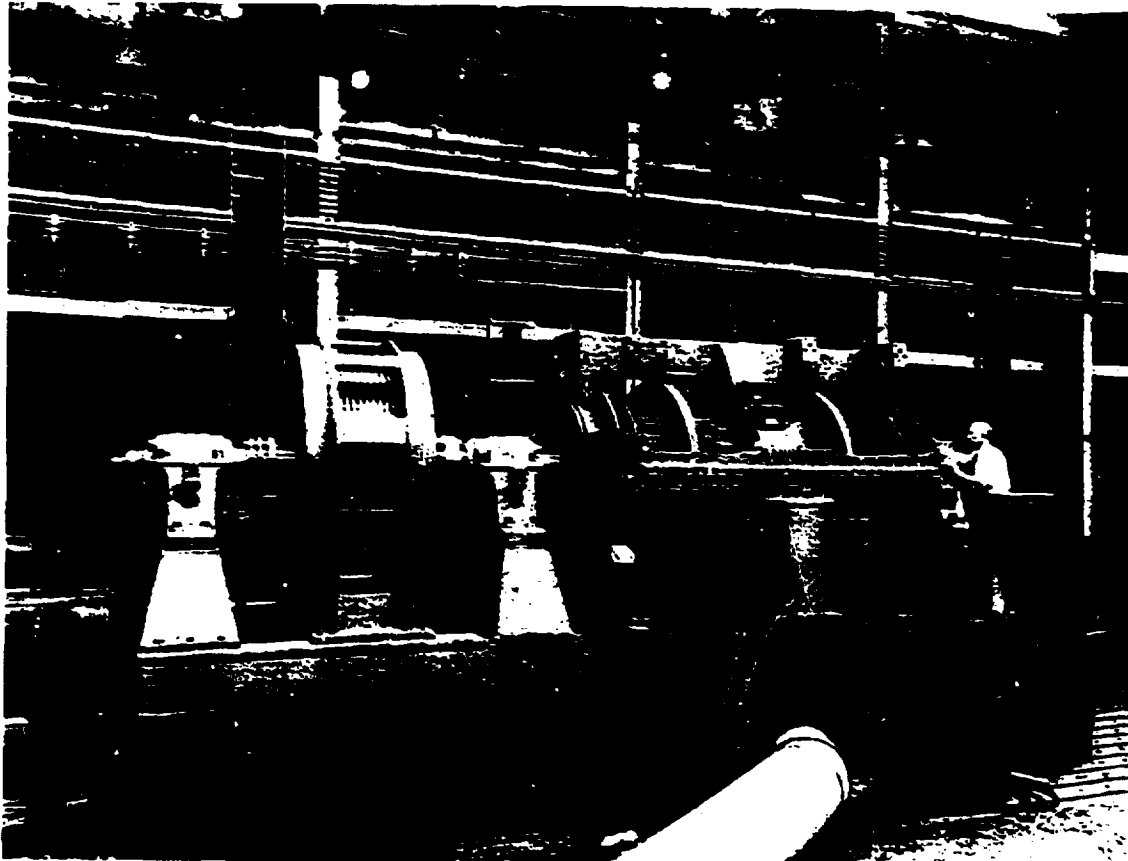


Figure 5

ORIGINAL PHOTOGRAPH  
OF POOR QUALITY



### Liquid Metal Homopolar Generator

CRITICAL  
OF POWER CONSUMPTION

In the early 1970's interest in homopolar machines as ship's propulsion motors and generators increased. The major disadvantage of the machine was its low power density due to the low current density of available current collection systems. One current collection system, using liquid metal instead of solid brushes, showed a potential for current collection current densities as high as 25,000 amps/in<sup>2</sup>. A program<sup>1)</sup> was undertaken at the Westinghouse R&D Center to investigate homopolars with liquid metal current collectors. As a result of this program a 3000 HP machine shown in Figure 6 was designed, built and tested. The machine which used NaK in the current collection system produced 100,000 amps at 20 volts DC. The study also evaluated gallium indium. The liquid metal was maintained in the current collection zone by viscous and centrifugal forces due to the rotation of the rotor. The behavior of liquid metal current collectors is very complex. Westinghouse, as part of this study performed an experimental program to develop the operating characteristics of the collector. Analytical and experimental work was completed on magneto hydrodynamics, liquid metal wetting, environmental control, viscous losses and current carrying capabilities. The results of this program, coupled with advances in solid brush current collection, showed the advantages of high current density liquid metal collectors were offset by their complex operating requirements and auxiliary support systems.

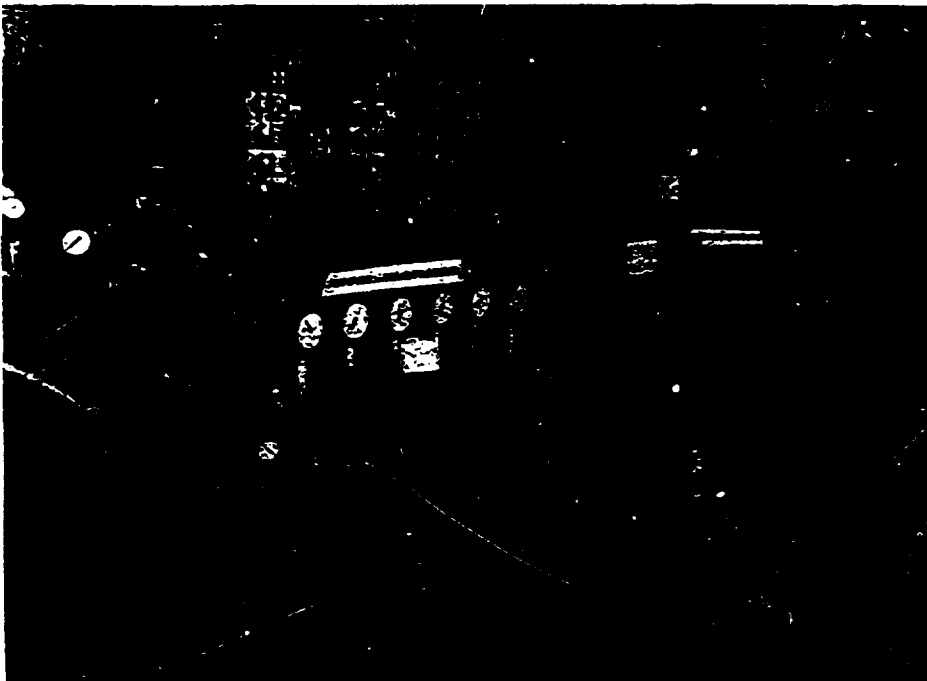


Figure 6

### Homopolar Energy Transfer System (HETS)

The emergence of fusion reactors as a viable power supply triggered interest in homopolar machines as pulsed energy sources. The pulsed energy source design objective was to deliver to, accept from and store energy at high efficiency for the fusion reactor. Westinghouse performed a study<sup>2)</sup> to develop an engineering design for a homopolar machine to perform this function. A conceptual design, shown in Figure 7, was developed as part of this study. The machine delivered 1.3 GJ of energy in 30 millisecc, using eight counter-rotating energy storage rotors. The peak current was 12.25 megamps at a peak terminal voltage of 11 kilovolts. The machine has 13 meters of rotor active length with a 2-meter-diameter rotor spinning at a tip speed of 277 m/sec. The machine used a superconducting field excitation coil with a maximum field of 8 tesla. An iron flux return path was provided to limit stray fields. The machine overall diameter was 7 meters, the overall length was 20.5 meters and the energy transfer efficiency was 95%.

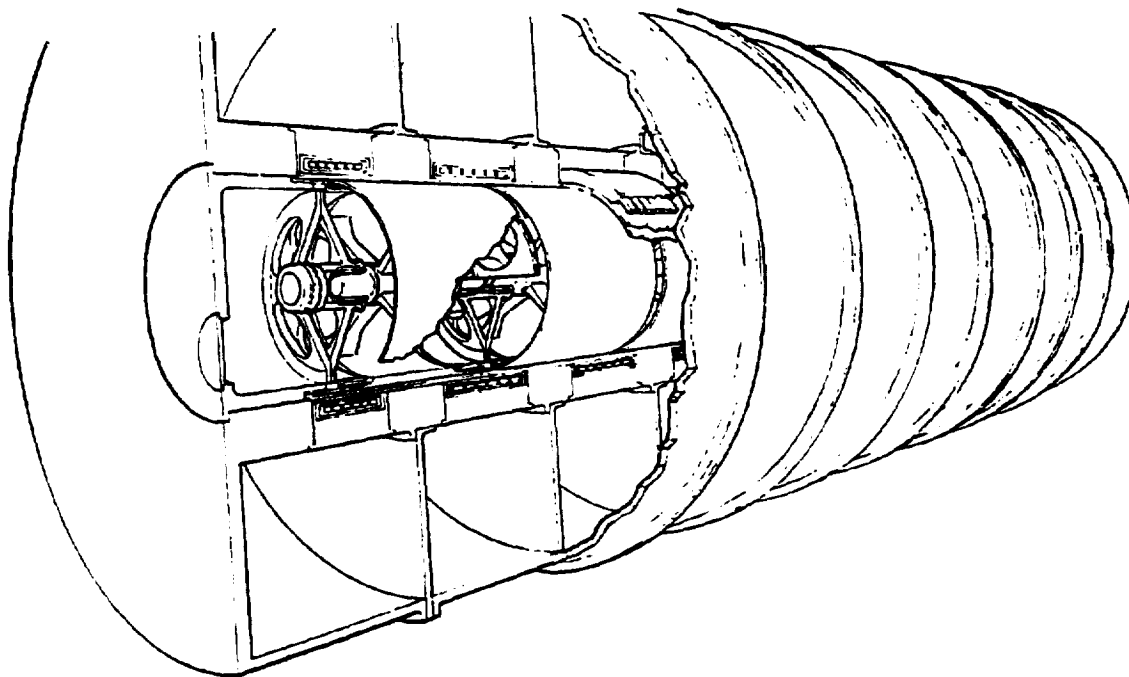


Figure 7

OF POOR QUALITY.

HETS Engineering Demonstration Model

ORNL  
OF POWER GENERATION

The development of the HETS concept required the design of a demonstration unit to evaluate machine performance characteristics and to test the current collection system in the machine environment. Westinghouse developed an engineering design for such a prototype. This machine, shown in Figure 8, was designed to evaluate all machine technologies used in the large 1.3 GJ homopolar generator. The machine is a drive homopolar with two counter-rotating rotors, each storing 5 MJ. The rotor drums rotating it at a tip speed of 277 m/sec were fabricated from high strength aluminum and supported from a central shaft with constant strength discs. The machine incorporated the current collection system used in the larger machine. Field excitation was provided by a Niobium-Tin ( $Nb_3Sn$ ) superconducting field winding. Counter-rotating design was used to eliminate the large torque reaction on the machine base.



Figure 8

### Homopolar Pulsed Current Collection Testing

The implementation of the HETS concept required the development of a current collection system that would operate at a high current density and tip speed with low losses in a high (6 T) magnetic field. These design requirements are far beyond the state of the art for current collection systems that had been developed. Achievement of these design objectives requires a new concept in solid brush system design. The design adopted was a segmented brush with a pneumatic actuator. A prototype current collection system was designed, built and tested on the test rig shown in Figure 9. The test rig used two brush box modes on a 14-inch-diameter wheel rotating with a tip speed of up to 277 m/sec. A pulsed power supply provided an electric current that flowed into one brush to the rotor and into the other brush to complete the circuit. An air actuator system was provided to lower the brush onto the rotor. The current collection system was tested with a brush current density of 12000 amps/in<sup>2</sup> at a tip speed of 277 m/sec with a discharge time of up to 80 millisecc. This exceeded the design requirement for the HETS application.

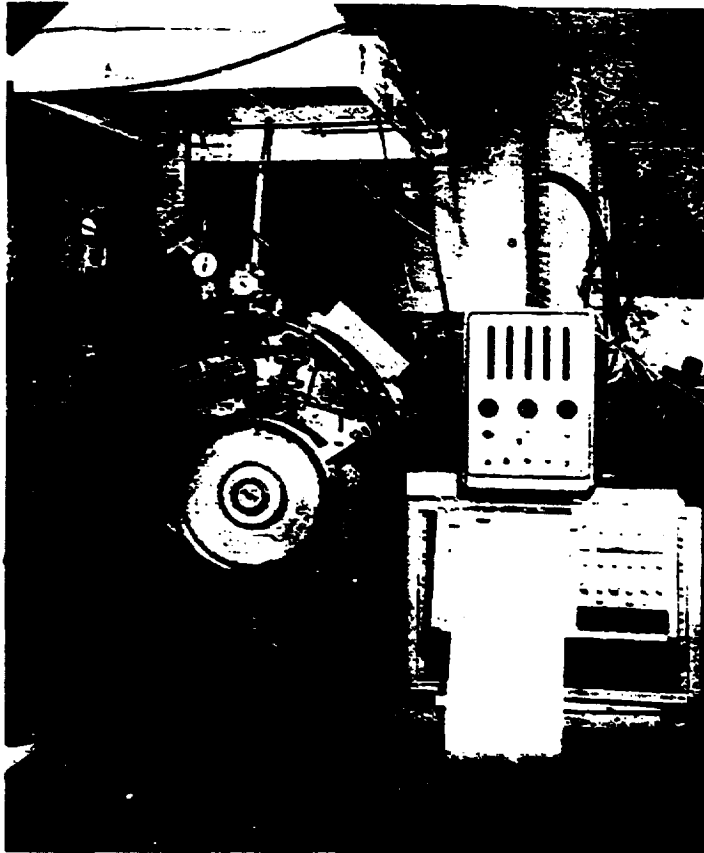


Figure 9

(4)

ORNL  
Prototype Homopolar Pulsed Power Supply OF POCW (CONT'D)

The testing required to qualify the HETS current collection system required development of a power supply to deliver energy to the test rig. The power supply consisted of a homopolar generator and pulse shaping inductor shown in Figure 10. In addition to its primary function as a power source, the homopolar generator also acted as a test rig to study the stability of parallel brushes on a common slip ring. Current sharing of high current density multiple parallel brushes had not been studied to date. The machine produced 20,000 amperes at .8 volts and was driven by a variable speed DC machine. Each brush system had 23 parallel brushes operating at a current density of 10000 amps/in<sup>2</sup>. In order to limit the rotor losses, a unique water cooling system was provided for the rotor. The machine was successfully operated in conjunction with the test rig demonstrating that high current density multiple brushes can operate stably during pulse loading duty cycles.



Figure 10

(4)

Naval Research Laboratory Self-Excited Homopolar

A novel new approach in pulsed homopolar machines was developed at NRL.<sup>3)</sup> This machine shown in Figure 11 uses a series wound approach in that the armature and field coil are connected in series, thus eliminating the need for a separate excitation coil. The machine's constant stress counter-rotating rotor is accelerated to speed and the starting circuit is connected to introduce a starting current in the armature-field circuit shown in Figure 11. During acceleration the circuit breaker is closed. The starting circuit produces a low magnetic field that generates an EMF in the series connected rotors. This results in a current buildup in the circuit through the circuit breaker. When the desired current is reached, the circuit breaker is opened and the current is commutated into the load. Westinghouse participated in this program by providing a new concept current collection system using fiber brushes. These brushes were developed at the R&D Center for high current density during pulse loads.

Westinghouse is also evaluating the self-excited homopolar concept as a lightweight alternative to iron cored machines.

LAYOUT AND ELECTRICAL CIRCUIT OF NRL 10 MJ HOMOPOLAR MACHINE

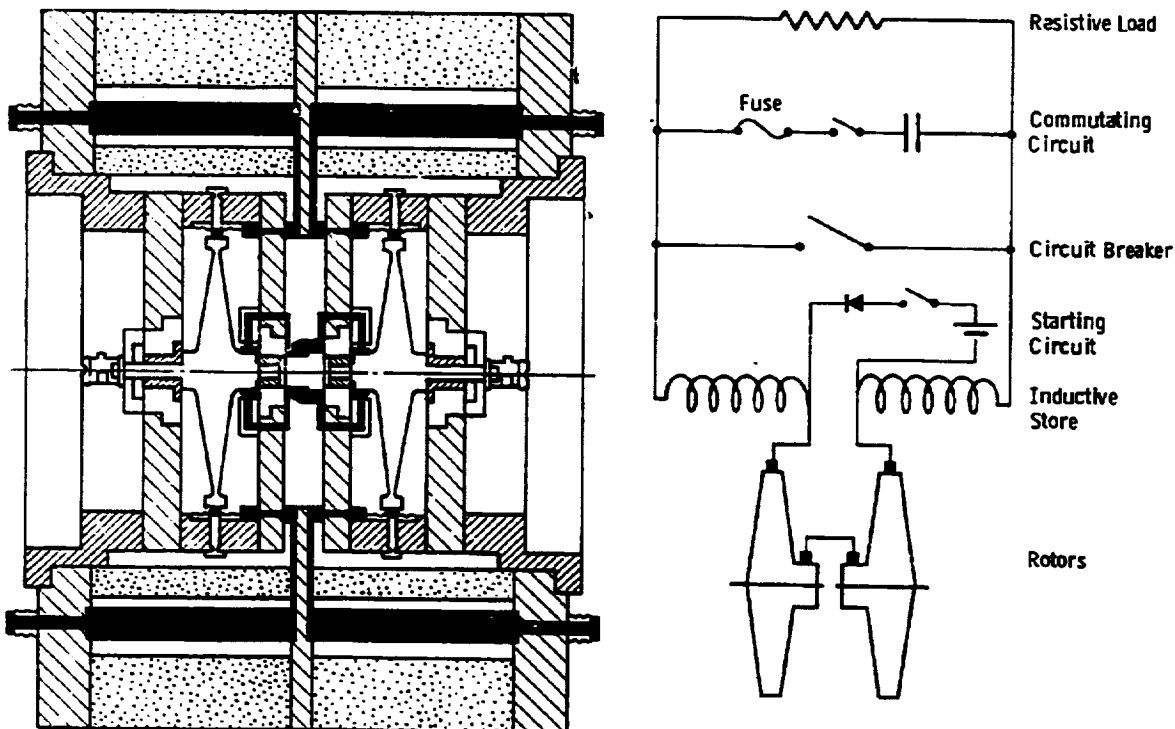


Figure 11

OF PCOR

### Electromagnetic Launcher Homopolar Supply

Westinghouse has designed, built and tested an Electromagnetic Launcher (EML)<sup>4)</sup> for the U.S. Army that uses a pulsed homopolar<sup>5)</sup> as the primary power supply. This machine, shown in Figure 12, is designed to deliver 17.5 MJ of energy to the system in 120 millisecc with a peak current of 2.16 megamps and peak voltage of 108 volts. The current collection system for the machine is a modified HETS design that operated at a brush current density of 13000 amps/in<sup>2</sup> and on a rotor surface moving at 225 m/sec. The machine rotor is 24.5 inches in diameter and 24 inches long, while the overall machine is 48 inches in diameter and 37 inches long. The machine was tested as a part of the overall EML system at the R&D Center. The system has subsequently been installed at a U.S. Army Laboratory at Picatinny Arsenal where it is being used for laboratory experiments on EML programs.

ORIGINALLY  
OF POOR QUALITY



Figure 12

### Westinghouse Pulsed HPG Programs

Westinghouse has studied several applications for homopolar machines. These applications all required short bursts of energy in the several to ten's of megajoule range. In single discharge machines the rotor must be sized to deliver the energy required at the voltage and machine capacitance to provide the pulse shape necessary. The prime movers for this application are small since the time required to accelerate the rotor to speed is arbitrary. The homopolar machines for this application are simple and straightforward, with the machine losses being absorbed by temperature rises in the machine parts. At present these systems are primarily research tools to study the technology of pulsed power systems in specific experiments. As these power supplies move from the laboratory to the field, the duty cycle becomes more stringent which is reflected in the machine design. The repetitive discharge is a repeat of the single discharge with several seconds between pulses. In recent studies at Westinghouse, these systems require a large prime mover such as a gas turbine, since the average power required is larger. The homopolar machine also is more complex since the disposition of losses is more important. For a short number of cycles, the losses can be absorbed in the machine mass by contracting the losses. As the number of cycles increases, cooling systems within the machine are required to maintain machine temperatures within acceptable limits. The extended rapid discharge duty cycle remains the most challenging to the designer. In this system it is not practical to store the mission total energy in the rotating mass of the system. In this application the power is furnished by a  $H_2$  turbine with the machine rotor supplying sufficient stored energy to stabilize the voltage between bursts. The homopolar machine for this application requires strict control of losses and exotic cooling systems to survive. The characteristics of these applications are shown in Figure 13.

### Inertia Storage System Studies

1. Single Discharge
  - Accelerate rotor to speed
  - Discharge into load
  - Extended reconfiguration (minute to hours)
2. Repetitive Discharge
  - Accelerate rotor to speed
  - Discharge into load
  - Reconfigure and re-accelerate (several seconds)
  - Discharge
3. Extended Rapid Discharge
  - Accelerate rotor to speed
  - Series of discharges (milliseconds between cycles)

Figure 13



### Summary

Westinghouse has been associated with homopolar machines since 1929 with the major effort occurring in the early 1970's to the present. The effort has enabled Westinghouse to develop expertise in the technology required for the design, fabrication and testing of such machines. This includes (Figure 14) electrical design, electromagnetic analysis, current collection, mechanical design, advanced cooling, stress analysis, transient rotor performance, bearing analysis and seal technology. Westinghouse is using this capability to explore the use of homopolar machines as pulsed power supplies for future systems in both military and commercial applications.

### Westinghouse Homopolar Technology

- Electrical Design
- Electromagnetic Analysis
- Current Collection
- Mechanical Design
- Advanced Cooling
- Stress Analysis
- Transient Rotor Performance
- Bearing Analysis
- Seal Technology

Figure 14

### References

1. Design and Development of a Segmented Magnet Homopolar Torque Converter, Final Report; Department of Defense, Advanced Research Projects Agency, Contract No. DAHC 15-72-C-0229, September 1976.
2. Conceptual Engineering Design of a One GJ Fast Discharging Homopolar for the Reference Theta Pinch Reactor, EPRI ER-246, August 1976.
3. Robson, A. E., et al., (1976): An Inductive Energy Storage System Based on a Self-Excited Homopolar Generator, 6th Symposium on Engineering Problems in Fusion Research, IEEE Pub. No. 75 CH 1097-5-NPS (1976), p. 298.
4. Deis, D. W. and McNab, I. R.: A Laboratory Demonstration Electromagnetic Launcher, IEEE, Transaction on Magnetics, Vol. 18, No. 1.
5. Proceedings of the 1983 International Current Collection Conference. David Taylor Naval Research Facility, October 18-20, 1983.

N85

3863

UNCLAS

N85 13863

D-13

DESCRIPTION OF A LABORATORY MODEL  
ANNULAR MOMENTUM CONTROL DEVICE (AMCD)

Nelson J. Groom  
Langley Research Center  
Hampton, VA 23665

## AMCD BACKGROUND

The basic concept of the Annular Momentum Control Device (AMCD) is that of a rotating annular rim suspended by noncontacting magnetic bearings and driven by a noncontacting electromagnetic spin motor. A brief discussion of the AMCD concept, applications, and advantages (as a momentum storage device) was presented at the first OAST Integrated Flywheel Technology Workshop (Ref. 1). A more detailed discussion of the AMCD concept is presented in Reference 2. The purpose of this paper is to highlight some of the design requirements for AMCD's in general and describe how these requirements were met in the implementation of a laboratory test model AMCD. An AMCD background summary is presented in Figure 1.

### □ CONCEPT

- Magnetically suspended rotating rim powered by a noncontacting electromagnetic spin motor.

### □ APPLICATIONS

- Attitude Control
  - Spin assembly for conventional momentum storage devices such as CMG's, reaction wheels, etc.
  - New, large radius, large momentum applications made possible by unique geometry.
- Energy Storage
  - Rim shape allows full utilization of the filament strengths of composite materials by allowing a unidirectional layup.
- Combined Attitude Control/Energy Storage
  - Tradeoff between optimum H/M and energy density rim design.

Figure 1

## LABORATORY MODEL AMCD PARAMETERS

Figure 2 presents a summary of the laboratory test model AMCD hardware characteristics. It should be pointed out that the laboratory model was not sized to meet the requirements of a particular mission but was sized to fit an existing torque measuring fixture.

- MOMENTUM
  - 3000 ft-lb-sec
- RIM DIAMETER
  - 5.5 ft.
- RIM WEIGHT
  - 50 lb.
- RIM SPEED
  - 3000 RPM

Figure 2

### LABORATORY TEST MODEL AMCD

Figure 3 is a photograph of the laboratory model AMCD. Using this figure, and subsequent figures, a description of the model will be given and related to general design requirements in three different areas. These areas are rotating assembly, electromechanical/electromagnetic, and dynamics and control. The following discussion will, of necessity, be brief. For a general discussion of AMCD spin assembly hardware considerations, see Reference 2 and for a detailed description of the AMCD laboratory test model, as originally delivered, see Reference 3.

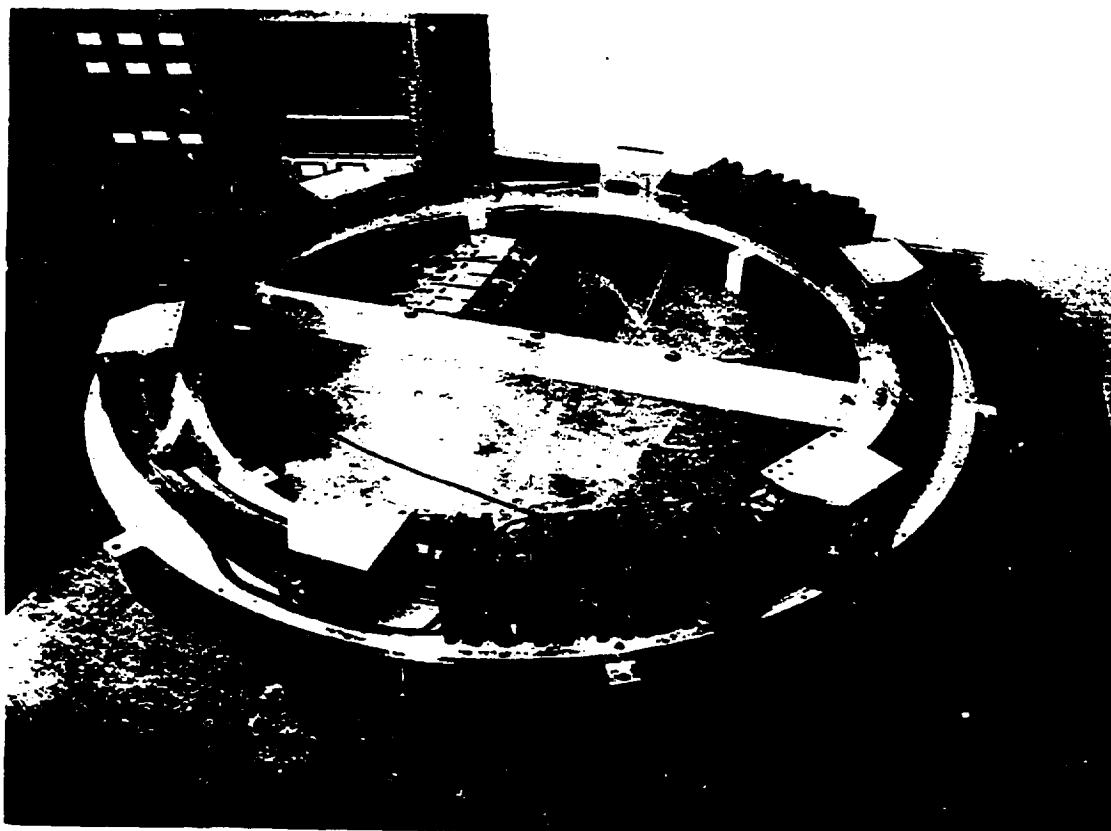


Figure 3

ORIGIN  
OF POOR QUALITY

## ROTATING ASSEMBLY (RIM)

The basic requirements for an AMCD rim (Fig. 4) are that it have high structural strength, good magnetic suspension characteristics, and good motor characteristics. Since these are conflicting requirements, at present the only solution appears to be an integrated structure. In the AMCD laboratory model (See Fig. 3), the basic rim structure consists of a high strength graphite-epoxy composite material with unidirectional layup. In order to provide a magnetic circuit for the magnetic suspension, a low loss ferrite material is embedded in the rim. For the motor requirements, there are 72 equally spaced samarium cobalt permanent magnets embedded in the outer part of the rim that act as motor poles.

### □ RIM MATERIAL REQUIREMENTS

- High structural strength.
- Good magnetic suspension characteristics
  - Low reluctance
  - Low eddy current and hysteresis losses
- Good motor characteristics
  - Good conductor (if induction motor)
  - Discontinuous ferromagnetic or permanent magnet (if commutated or other motor design).

### □ AMCD LABORATORY MODEL DESIGN

- Basic structure of graphite epoxy with unidirectional layup.
- Low loss ferrite material embedded in rim (magnetic suspension).
- Samarium Cobalt permanent magnets embedded in rim (motor poles).

Figure 4



## ELECTROMECHANICAL/ELECTROMAGNETIC (MAGNETIC SUSPENSION)

The basic requirements for an AMCD magnetic suspension system (Fig. 5) are segmented bearings, active control of the momentum vector (axial direction), and linear actuator characteristics over the suspension operating range. In the AMCD laboratory model (Fig. 3), the rim is suspended by three equally spaced suspension stations. Magnetic bearing elements located in the suspension stations interact with the previously mentioned ferrite material, embedded in the rim, to produce axial and radial suspension forces. The suspension system is active in both axes. The control approach used for the magnetic bearing elements was permanent magnet flux biasing which provides linear force characteristics over a small region about a fixed operating point. This approach is discussed in more detail in Reference 4.

### □ MAGNETIC SUSPENSION REQUIREMENTS

- Segmented bearings to minimize weight (minimum of three stations)
- Active in axial axis to provide control of momentum vector
- Linear over control range

### □ AMCD LABORATORY MODEL DESIGN

- Three suspension stations
- Active in axial and radial axes
- Permanent magnet flux bias

Figure 5

## ELECTROMECHANICAL/ELECTROMAGNETIC (MOTOR)

Basic requirements for an AMCD drive motor (Fig. 6) are segmented stator elements, relatively large gaps to allow rim motion, and minimum interaction with the magnetic suspension. Interaction with the magnetic suspension can take the form of magnetic interaction or, for high torque capacity motors, side forces that interfere with the magnetic suspension. In the case of the laboratory model AMCD (Fig. 3) the spin motor forces are much lower than suspension forces so the concern was magnetic interaction. The laboratory model AMCD motor is basically a large permanent magnet brushless d.c. spin motor. The motor consists of stator elements, located in the suspension stations, that push and pull against 72 samarium cobalt permanent magnets, embedded in the rim near the outer edge, to produce spin torques. The stator-element drive electronics are commutated by signals from a Hall effect device which senses the position of the magnets.

### □ MOTOR REQUIREMENTS

- Segmented stator elements
- Relatively large gaps
- Minimum interaction with magnetic suspension

### □ AMCD LABORATORY MODEL DESIGN

- Segmented stator elements (located in suspension stations)
- Brushless d.c. spin motor with permanent magnet poles in rim
- Motor poles separated from suspension elements maximum amount allowed by size constraints

Figure 6

### SUSPENSION STATION CROSS-SECTION

In order to provide a better view of the elements previously discussed, a cross-sectional drawing of a suspension station is presented in Figure 7. This drawing shows the magnetic bearing elements, motor stator elements, and rim, with ferrite and permanent magnet inserts, in more detail. The magnetic-bearing gaps with the rim centered are 0.1 inch.

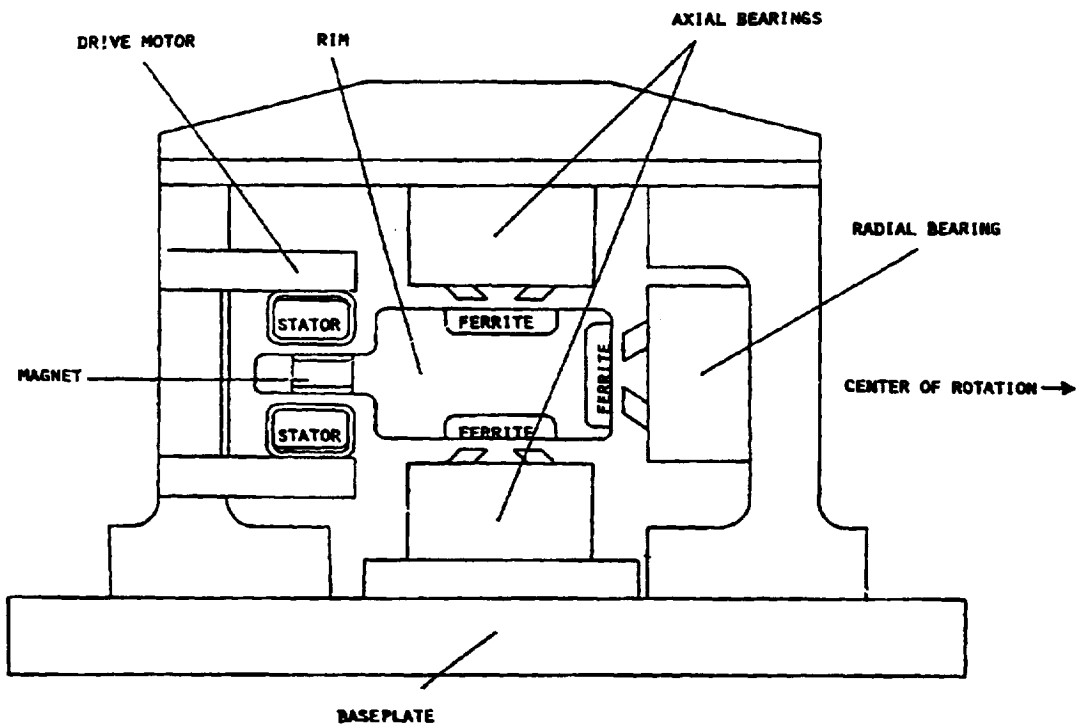


Figure 7

## DYNAMICS AND CONTROL (MAGNETIC SUSPENSION)

The basic requirement for an AMCD magnetic suspension system (Fig. 8) is to provide 5 degree-of-freedom control of a rotating rim whose motion is coupled through a momentum vector that changes magnitude as the rim is spun up. In the laboratory model AMCD, the magnetic suspension system provides active positioning control of the rim in both the axial and radial directions. The original axial control approach was to use independent control loops for each suspension station. At zero rim spin speed (zero momentum), for three magnetic bearing suspension stations spaced equidistantly around the rim and for theoretical rim inertia distribution, it can be shown (Ref. 5) that axial motions of the rim in each of the bearing stations are uncoupled. Consequently, at zero momentum the axial magnetic bearing control system can be represented as three identical independent systems; and a single design, using a simplified suspended mass model, can be performed. In the radial system, all three stations are coupled since the radial actuators can only produce a unidirectional force.

### □ MAGNETIC SUSPENSION REQUIREMENTS

- Basic Requirement: 5 degree-of-freedom control of rotating rim with motion coupled through momentum vector that changes magnitude as rim is spun up.

### □ AMCD LABORATORY MODEL DESIGN

- Separate axial and radial control systems.
- Single station, single input single-output control approach used for axial system
  - Because of geometry (thin rim, three suspension stations) rim motion in each suspension station uncoupled at zero speed.
- Three station coupled radial control system
  - Unidirectional magnetic actuators at each station.
- Rigid body dynamics assumed.

Figure 8

## AREAS REQUIRING FURTHER DEVELOPMENT

Tests conducted with the laboratory model AMCD have identified two general areas requiring further development (Fig. 9). These areas are magnetic suspension and magnetic suspension control system. A discussion of preliminary test results is presented in Reference 6. Reference 7 discusses an alternate magnetic bearing control approach which was implemented for the laboratory model, and Reference 5 presents a linear analysis and nonlinear simulation of the original magnetic suspension and magnetic suspension control approach.

### □ ELECTROMECHANICAL/ELECTROMAGNETIC

#### • Magnetic Suspension

- Permanent magnet flux-biasing presented problems from control system standpoint (bandwidth required to stabilize bearings too high).
- Zero bias-flux magnetic bearings investigated as alternate approach but proved to be very sensitive to calibration and alignment accuracy.
- Other approaches currently being investigated include flux feedback and force feedback.

### □ DYNAMICS AND CONTROL

#### • Magnetic Suspension Control System

- Initial approach using classical single-input single-output control theory and single station control will be replaced by multi-input multi-output control approaches.
- Combination of rim parameters and overall control requirements may result in requirement of flexible body control of rim.

Figure 9

#### REFERENCES

- (1) Groom, Nelson J.: Annular Momentum Control Device (AMCD). Integrated Flywheel Technology 1983. NASA CP-2290, 1983, pp. 123-132.
- (2) Anderson, Willard W.; and Groom, Nelson J.: The Annular Momentum Control Device (AMCD) and Potential Applications. NASA TN D-7866, March 1975.
- (3) Ball Brothers Research Corporation: Annular Momentum Control Device (AMCD). Volumes I and II. NASA CR-144917, 1976.
- (4) Anderson, Willard W.; Groom, Nelson J.; and Woolley, Charles T.: The Annular Suspension and Pointing System. Journal of Guidance and Control, Vol. 2, No. 5, September-October 1979, pp. 367-373.
- (5) Groom, Nelson J.; Woolley, Charles T.; and Joshi, Suresh M.: Analysis and Simulation of a Magnetic Bearing Suspension System for a Laboratory Test Model Annular Momentum Control Device (AMCD). NASA TP-1799, March 1981.
- (6) Groom, Nelson J.; and Terray, David E.: Evaluation of a Laboratory Test Model Annular Momentum Control Device. NASA TP-1142, March 1978.
- (7) Groom, Nelson J.; and Waldeck, Gary C.: Magnetic Suspension System for a Laboratory Model Annular Momentum Control Device. A Collection of Technical Papers--AIAA Guidance and Control Conference, August 6-8, 1979, pp. 423-428. (Available as AIAA Paper 79-1755).

N85

3864

UNCLAS

N85 13864

D-14

GENERIC COMPOSITE FLYWHEEL DESIGNS

R. S. Steele\*  
Greenville, South Carolina

\*Private flywheel consultant.



Fiber reinforced composites belong to a new class of materials. They allow such flexibility that free thinking individuals are encouraged to "let themselves go" with their design. The most efficient flywheel may no longer have the classic "Stodola" taper and indeed, may not even be round. Since selection of an optimum design can be the subject of a sizeable study [refs. 1 and 2], I thought that it might be instructive to review some of the flywheel designs that have been developed and comment on what NASA might learn from this experience.

Although choice of material, mounts and service requirements often dictates the final design choice for a particular application, I have chosen to classify these composite flywheels within a geometric framework. The breakdown given in figure 1 is probably not exhaustive but will suffice for today's discussion.

**NON-ROUND ROTORS**

- Bar
- Brush

**ROUND ROTORS**

Solid Disk

Flat disk (pseudo-isotropic)

Alpha-ply layup

Without rim

With rim

Molded (sheet molding compound)

Plywood

Tapered disk (constant stress)

Stodola

Modified Stodola

Pierced Disk (rims)

Woven

Radial stringers

Helical weave

Thin Circ Wound

Rollers

Levitated

Thick Circ Wound

Single material (residual stress)

Single step winding

Multi-step winding

Multi-material rims

Circular

Sub-circular

Figure 1.- Classification of generic rotor designs.

Let me start with a few comments regarding non-round rotors (fig. 2). They are generally simple to construct, and in the case of the fan-brush type [ref. 3] possess a relatively benign failure mode. A major problem is their low volume efficiency. They do not fully occupy the volume in which they spin.

The bar type tends to split at the tips and take on a fan-brush character. The splitting is the result of low transverse strength in the composite. As we will see, this is usually the limiting characteristic of composites.

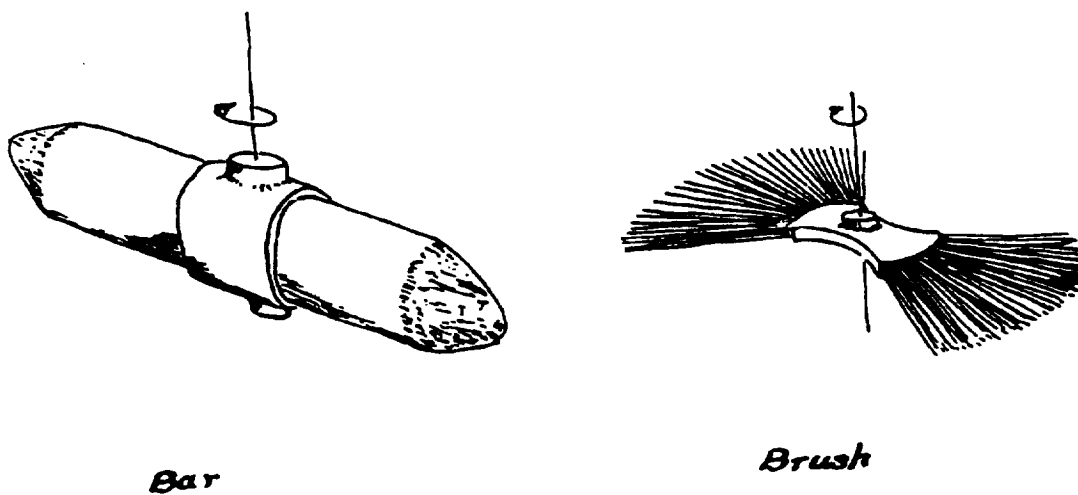


Figure 2.- Non-round rotors.

Before discussing the various perturbations of circular flywheels, we should look at a simple stress analysis of a circular disk [ref. 4]. (See fig. 3.) This analysis shows that a constant thickness disk with a small central hole can have a greater hoop stress at its center than if it did not have the hole. On the other hand, the maximum radial stress will be lower.

Now consider the two types of construction used. The first has a fiber orientation that macroscopically simulates the character of an isotropic material (metal). These were called pseudo-isotropic in the DOE program. They lean to the solid disk designs because even though their overall composite strength is lower than the unidirectional fiber composite, they can survive the high radial stresses.

The other is characterized by a highly structured (usually orthogonal) fiber orientation that places the strength of the fiber in the direction of the major principal stress component. This allows the composite structure to survive a very high major principal stress so long as the minor principal stress does not exceed the transverse strength of the composite.

The favorite structured orientation is a hoop wound cylinder which naturally possesses a central hole. The limiting factors have been either the low strength transverse to the fibers or items independent of the rim. The larger the diameter of the hole, the lower the transverse stress. Thus the designer is faced with balancing his desire for a thick, high energy rim with the maximum transverse stress his material can stand.

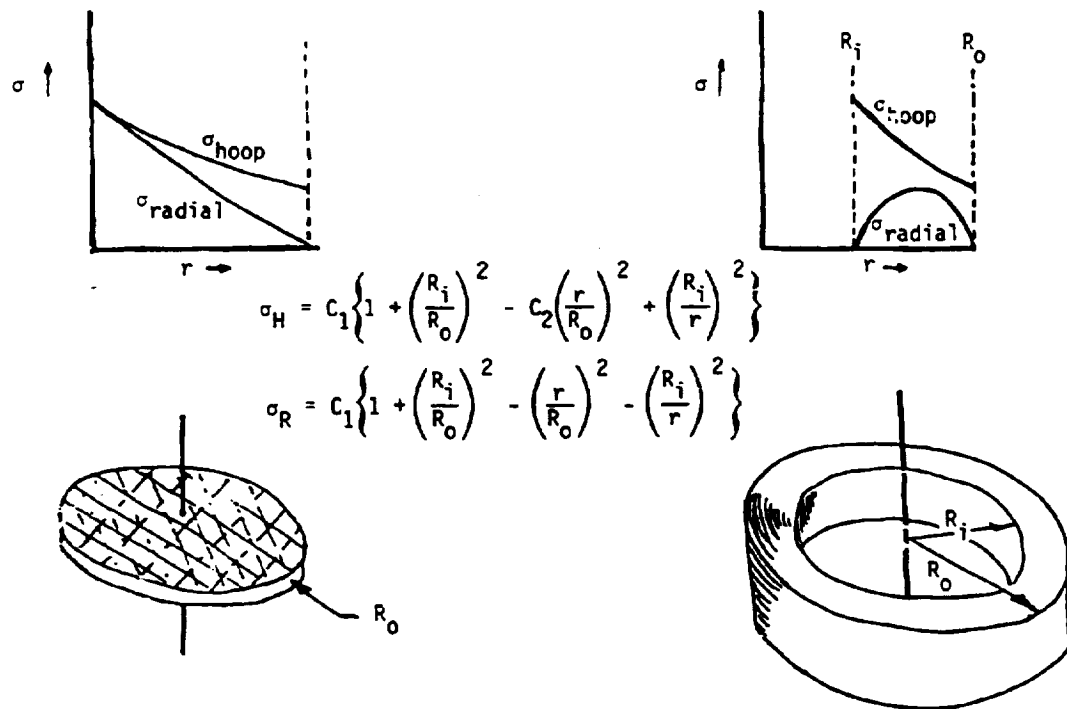


Figure 3.- Stress analysis of spinning circular disk.

Let me review some of our experience with actual rotors. I will rely upon my own experience with the Department of Energy's Mechanical Energy program as test director at the Oak Ridge Y-12 Plant's Flywheel Evaluation Laboratory.

Pseudo-isotropic flywheels demonstrated lower energy densities but also had relatively low fabrication cost. They also demonstrated a higher level of durability than their competition. One type was built using an alpha-ply [ref. 5] layup in which sheets of unidirectional fibers in an epoxy matrix were stacked at various angles until the desired thickness was reached. Circular disks were machined from the cured plates and, in some cases, tapered to simulate the constant stress shape [ref. 6] used in high performance metal flywheels.

A pseudo-isotropic flywheel (fig. 4) survived our only 10,000 cycle fatigue test. The graphite version of the modified Stodola flywheel achieved close to 1000 m/s tip speed, giving it the top speed in our record book.

Two problems persisted [ref. 7]. An elastomeric interface is required between the the metallic arbor mount and the composite surface. Unless the metallic arbor and the disk mass centers both lie on the spin axis (a very remote possibility), the distance between them will vary with speed. This adds complexity to the suspension system. The fatigue stresses at the bonded interface are also found to be detrimental to the life of the rotor.

The other problem is the severe failure modes. The constant thickness disks usually failed at the drive shaft interface. This allowed the entire disk to roll around inside our containment, setting up severe vibratory stresses in the containment for several seconds. A "lightweight" containment vessel would not stand the failure. The tapered disk performed such that it disintegrated in an explosion that sent chunks of graphite composite into our containment ring. What we must learn is that the pseudo-isotropic rotor can produce the full range of failure problems, thus making containment development difficult and expensive.

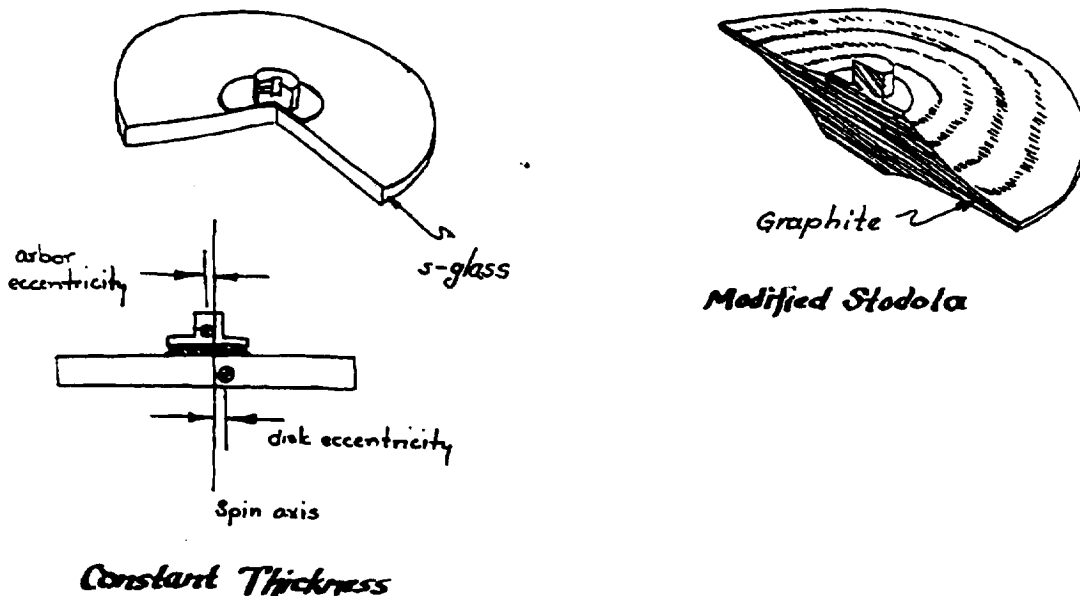


Figure 4.- Pseudo-isotropic disk.

A second method of accomplishing isotropy was demonstrated by the molded, chopped fiberglass rotors [ref. 8]. They required a hoop wound support ring to achieve the highest energy density. A similar arbor attachment was used and the same balance problems were encountered. The failure mode was consistent [ref. 9]. The hoop supports usually burst, leaving the disk no longer able to support itself. The entire rotor broke into small fibrous wads of mass, fairly uniformly distributed in the chamber.

Finally, a very inexpensive flywheel was proposed and built from hexagonal, birch plywood [ref. 10]. (See fig. 5.) Successful testing was reported with respectable energy densities for the cost involved.

However, since NASA will place more importance upon performance than cost, it is unlikely that a solid disk from any composite will be chosen for space applications.

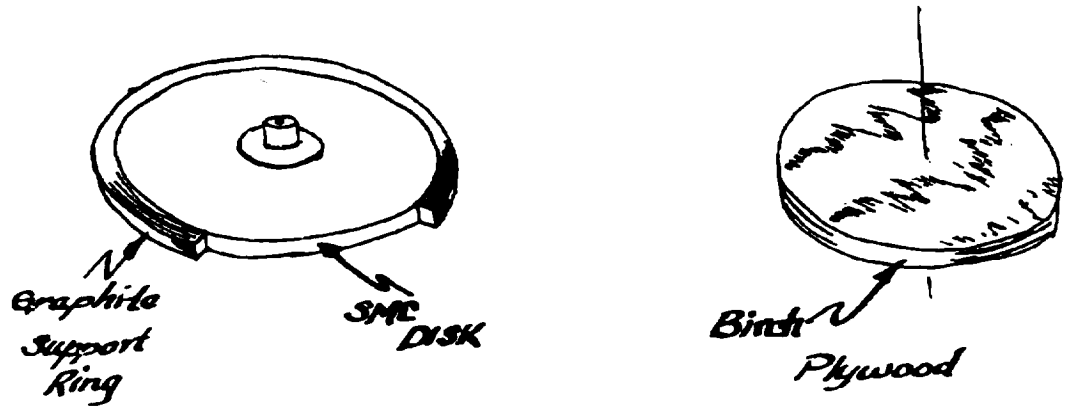


Figure 5.- Lower cost pseudo-isotropic disk.

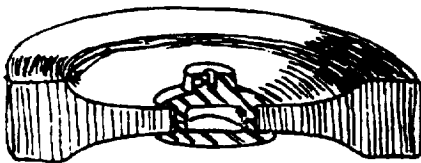
If you are going to use a composite flywheel, it will be a disk with a hole. Should it have a big hole or a little hole? I know of at least one composite flywheel that was circumferentially wound around a 25-mm spindle with an outer diameter of about 1 m. When tested, it failed at a very low speed due to transverse cracking. (See fig. 3.) The smaller the hole relative to the overall diameter, the greater the transverse stress. Thus the limiting material factor in thick, orthogonal composite rings is the transverse composite strength.

You have two problems: how to make the rim as thick as possible so it will be volume efficient and how to attach it to the outside world.

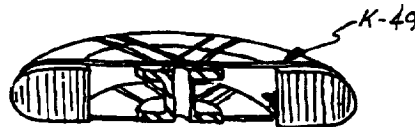
Several attempts have been made to wind a residual stress state into the flywheel so that the inner circumference is in compression at rest. This allows a thicker rim at a given speed.

I am familiar with two flywheels that use this technique. In the one pictured in figure 6(a), carbon fibers were used in a polysulfone matrix [ref. 11] that was cured during winding. The design speed was not achieved because the transverse strength of the composite with this matrix was lower than the designer had expected. The one in figure 6(b) used 14 wind-cure steps to produce the rim. The band-wrap [ref. 12] technique was used to attach the rim to a central shaft. Pre-stressing did result in an improvement upon an earlier non-pre-stressed wheel. However, the ultimate speed was limited by the band-wraps.

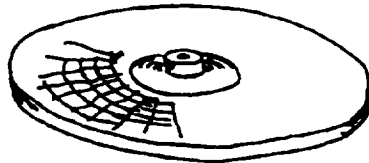
Another method to increase the thickness of a rim is to place radial reinforcements in the rotor [ref. 13]. (See fig. 6(c).) These rotors were fairly successful but suffered interface problems with the drive shaft.



(a) Continuous winding with residual stress.



(b) Step winding with residual stress.



(c) Radial stringers or bidirectional weave.

Figure 6.- Thick rims.

Another successful and less expensive method is to wind the rim from several materials. An inner material with a lower modulus/density ratio will grow radially, with speed, into the higher modulus/density rings [ref. 14]. This creates compressive radial stresses at the interface between the layers. To my knowledge, no one has yet been able to create a hoop failure in such a flywheel. Failures in the attachment system always come first.

Attaching a rim to the outside world is not simple. The primary problem is to accommodate the radial growth of the rim without having such a "soft" system that the flywheel would have resonant frequencies in the operating range.

The most successful design with the rim/shaft interface in tension used rotational catenary spokes [ref. 15]. (See fig. 7(a).) These were carefully designed to grow with the rim.

The other successful approach used compressive spokes and a sub-circular rim [ref. 16]. (See fig. 7(b).) This required a rim made of multiple, concentric, thin rings held together at rest by a small interference fit. The spokes remained in compression until the rim grew circular. The rim failures that have occurred in this type resulted from overheating and fatigue. The outer layers are most susceptible, and if the rest of the rim can be supported by the shaft and spoke system, the containment problems are minimized. The designer of the flywheel shown in figure 7(c) needed a very rugged flywheel [ref. 17] for his intended application and used aluminum plates in the center of the rim with 16 slip-pins to accommodate the differential radial growth. Unfortunately, the tolerance on the slip-pins was insufficient to maintain adequate balance. We were unable to confirm its 4 kWh potential energy storage capability.

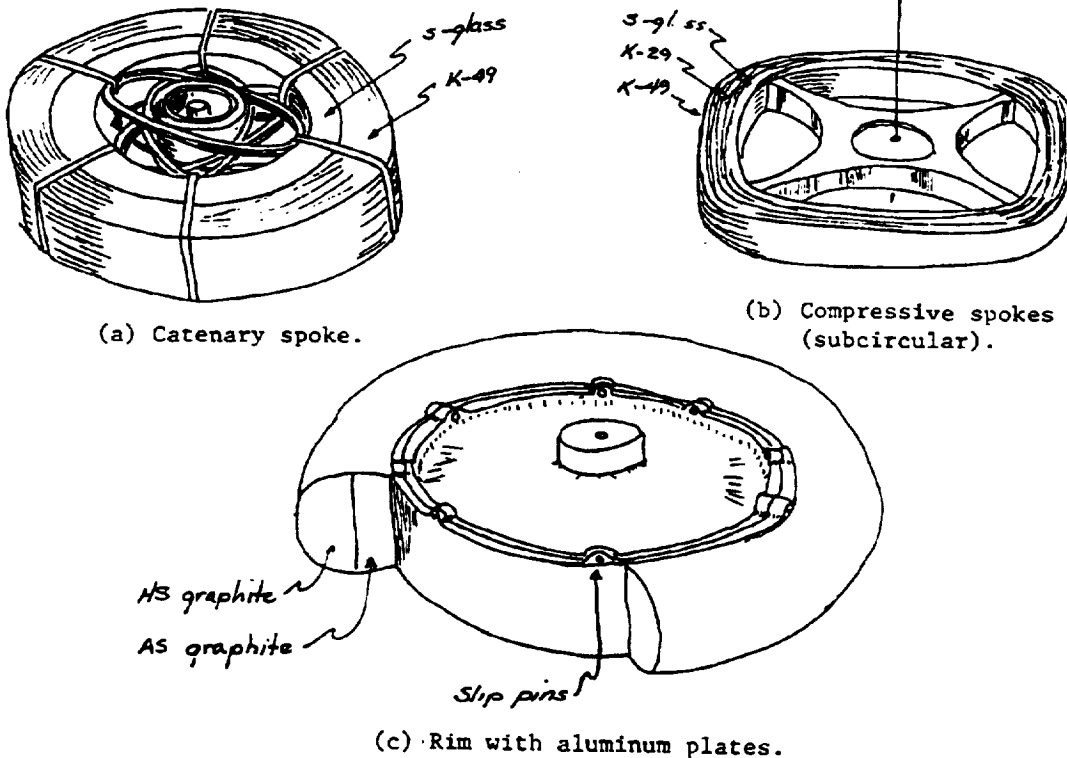


Figure 7.- Multi-material rims.

Finally we come to the rim without a central shaft. I know of two basic designs. The first is a thin ring supported on rollers. Power I/O was through a rack and pinion system on its inside surface. The proposed rim was 1 meter thick, 2 meters tall, and 1 kilometer in diameter. The composite material was steel reinforced concrete. That rim was never built.

The other is also a thin ring but is magnetically levitated and functions as the rotor of a motor/generator. The test results I have seen regarding this design involve control and power studies. I know of no test results concerning the life or performance characteristics of these rotor designs. It strikes me, though, that since a 1-meter-diameter rotor will have about 5 mm radial growth at operating speed (2% graphite operating with a 50% knockdown factor), the electrical coupling could be severely degraded at maximum speed. An inefficient coupling may lead to high temperatures at the highly stressed inner surface of the rotor and thus reduce life.

Only testing under these specific conditions will provide the confidence needed in the lifetime for one of these units.

A rim type rotor can be built that will have an energy density suitable to NASA's requirements. The levitated rim type appears structurally attractive if the electronic coupling doesn't suffer too much from radial growth.

I am concerned that two areas might be neglected. The containment problems are not trivial. A composite flywheel does not simply break up into fluff. It loses a lot of energy as it stops. If it attempts to stop too suddenly, you have a containment problem. For instance, a rim contained in a small cavity will tend to jam suddenly, creating a tremendous torque [refs. 18, 19, and 20]. The severity of the problem is known to vary with materials, but the test results needed for accurate design optimization do not exist.

Neither does good data exist for my other concern, which is the effect of long term exposure to sustained high stress in vacuum. Composite properties, and in particular matrix properties, will change with time. Very little data exists to estimate what the material characteristics will be after one to five years of operation.

I have touched on many different topics that have been addressed in the development of composite flywheels. My final words are to encourage NASA to approach composite flywheels cautiously and with a healthy respect for the energies involved (fig. 8).

\* Containment Development will NOT be Trivial

- . Remember total energy involved
- . Look for fast stops

\* Long Term Effects Need Assessment

- . Sustained stress
- . Continuous vacuum
- . Radiation

Figure 8.- Concerns needing study.



## REFERENCES

1. Flanagan, R.C.; Wong, J.M.; Munro, M.B.: Fibre Composite Rotor Selection and Design. IECEC 82: Proceedings of the Seventeenth Intersociety Energy Conference. Vol. 4. IEEE, NY, 1982, pp. 1961-1966.
2. Johnson, D.E.; Gorman, J.J.: Maximum Energy Densities for Composite Flywheels. 1980 Flywheel Technology Symposium. (Rep. No. CONF-801022, Dept. Energy, 1980.
3. Lampe, D.: Superflywheels. Popular Mechanics, vol. 142, Nov. 1974.
4. Timoshenko, S.: Strength of Materials, Part II, Advanced Theory and Problems, Third Ed., Robert E. Krieger Publ. Co., 1956.
5. Nimmer, R.P.: Laminated, Composite Flywheel Failure Analysis. 1980 Flywheel Technology Symposium. Rep. No. CONF-801022, Dept. Energy, 1980.
6. Barlow, T.M.; Crothers, W.T.; Chiao, T.T.; Frank, D.N.; King, D.M.; Kulkarni, S.V.: Mechanical Energy Storage Technology Project: Annual Report for CY-1980, Lawrence Livermore National Laboratory, Livermore, UCRL-50056-80, 1981.
7. Steele, R.S.; Babelay, E.F.: Rotor Testing in FY 1981. Proceedings of the Mechanical, Magnetic and Underground Energy Storage 1981 Annual Contractors' Review. Rep. No. CONF-810833, Dept. Energy, 1981.
8. Kay, J.F.: Low-Cost Compression Molded Fiber Reinforced Flywheels. Proceedings of Mechanical, Magnetic and Underground Energy Storage 1980 Annual Contractors' Review, Rep. No. CONF-81128, Dept. Energy, 1981.
9. Olszewski, M.: Mechanical Energy Storage Technology Program FY-1982, Technical Progress Report. Rep. No. ONRL/TM8765, Oak Ridge National Laboratory, Oak Ridge, TN, May 1982.
10. Rabenhorst, D.W.: Applicability of Wood Technology to Kinetic Energy Storage. Johns Hopkins University, Applied Physics Laboratory, APL/JHU Digest, Vol. 11, No. 5. May/June 1972.
11. Barlow, T.M.; Crothers, W.T.; Chiao, T.T.; Frank, D.N.; King, D.M.; and Kulkarni, S.V.: Mechanical Energy Storage Technology Project. Annual Report, 1980. Rep. No. UCRL-50056-80, Lawrence Livermore National Laboratory, May 1981.
12. Knight, C.E.; Kelly, J.J.; Huddleston, R.L.; Pollard, R.E.: Development of the "Bandwrap" Flywheel. 1977 Flywheel Technology Symposium Proceedings, Rep. No. CONF-771053, Dept. Energy, 1977.
13. Sapowith, A.D.; Handy, W.E.: Circular Weave Flywheel Materials Evaluation. Proceedings of the Mechanical, Magnetic and Underground Energy Storage 1981 Annual Contractors' Review, Rep. No. CONF-810833, Dept. Energy, 1981.

14. Foral, R.F.: On the Performance of Hoop Wound Composite Flywheel Rotors. Proceedings of the Mechanical, Magnetic and Underground Energy Storage 1981 Annual Contractors' Review, Rep. No. CONF-810833, Dept. Energy, 1981.
15. Younger, F.R.: Tension-Balanced Spokes for Fiber-Composite Flywheel Rims 1977 Flywheel Technology Symposium Proceedings, Rep. No. CONF-771053, Dept. Energy, 1977.
16. Towgood, D.A.: An Advanced Vehicular Flywheel System for the ERDA Electric Powered Passenger Vehicle. 1977 Flywheel Technology Symposium Proceedings, Rep. No. CONF-771053, Dept. Energy, 1977.
17. RPE-10 Composite Flywheel Final Report, Rockwell International, Rocketdyne Division, Canoga Park, Calif., RI/RD79-334, October 1979.
18. Steele, R.S., Jr.; Babelay, E.F., Jr.; Sutton, B.F.: Oak Ridge Flywheel Evaluation Laboratory Annual Report (October 1, 1979 - September 30, 1980). Rep. No. Y-2233, Oak Ridge Y-12 Plant, Oak Ridge, TN, 1981.
19. Coppa, A.P.: Flywheel Housing Design-Concept Development. Proceedings of the Mechanical, Magnetic and Underground Energy Storage 1981 Annual Contractors' Review, Rep. No. CONF-810833, Dept. Energy, 1981.
20. Sapowith, A.D.; Handy, W.E.: Composite Flywheel Burst Containment. Proceedings of the Mechanical, Magnetic and Underground Energy Storage 1981 Annual Contractors' Review, Rep. No. CONF-810833, Dept. Energy, 1981.

N85

3865

UNCLAS

D15

N85 13865

SUMMARY RESULTS OF THE DOE FLYWHEEL  
DEVELOPMENT EFFORT

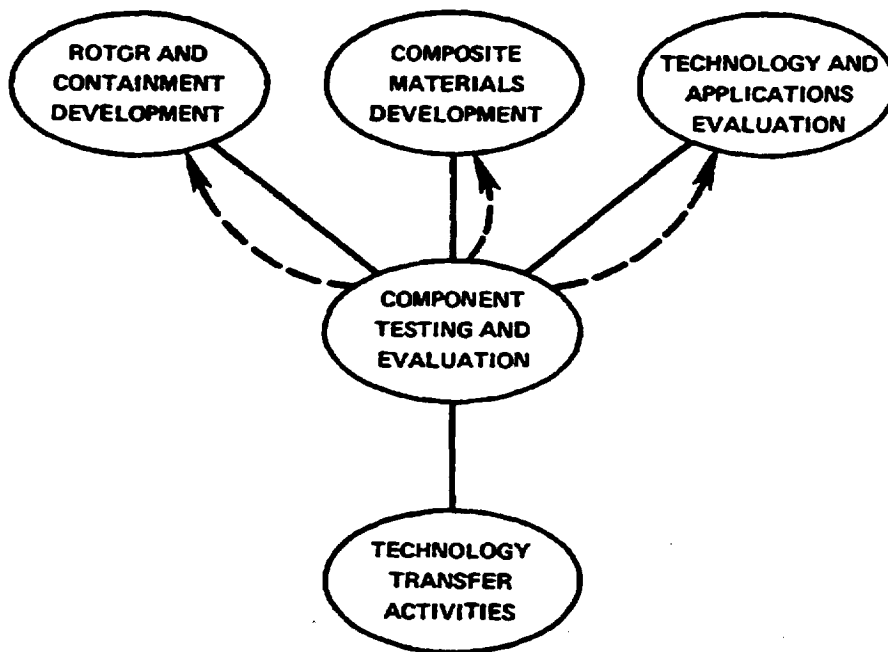
M. Olszewski  
J. F. Martin  
Oak Ridge National Laboratory  
Oak Ridge, Tennessee

PRECEDING PAGE BLANK NOT FILMED

C-3

The technology and applications evaluation task focuses on defining performance and cost requirements for flywheels in the various areas of application. To date the DOE program has focused on automotive applications. The composite materials effort entails the testing of new commercial composites to determine their engineering properties. The rotor and containment development work uses data from these program elements to design and fabricate flywheels. The flywheels are then tested at the Oak Ridge Flywheel Evaluation Laboratory and their performance is evaluated to indicate possible areas for improvement. Once a rotor has been fully developed it is transferred to the private sector.

### THE FIVE COMPONENTS OF FLYWHEEL DEVELOPMENT EFFORT ARE INTERACTIVE



The Oak Ridge National Laboratory is the lead center for the DOE flywheel effort. This includes program management functions as well as technical development in the area of testing. Fabricated rotors are supplied by the private sector. This is done to ease technology transfer once developmental activities have been completed.

## THE MEST PROGRAM HAS INVOLVED PUBLIC AND PRIVATE SECTOR PARTICIPATION

- ORNL
  - MANAGES AND DIRECTS PROGRAM
  - TESTING OF FLYWHEELS IN OAK RIDGE FLYWHEEL EVALUATION LABORATORY (ORFEL)
  - DEVELOPMENT OF ADVANCED TESTING TECHNIQUES TO OBTAIN MORE COMPLETE DATA FROM TESTS
  - DEVELOPMENT OF NONDESTRUCTIVE INSPECTION TO PREDICT INCIPENT FAILURE
- LLNL
  - ROTOR TEST DATA ANALYSIS EFFORTS
  - ENGINEERING DATA FOR NEW COMPOSITES
- PRIVATE SECTOR PARTICIPANTS SUPPLIED ROTORS
  - GENERAL ELECTRIC
  - GARRETT AIRESEARCH
  - AVCO
  - BROBECK
  - OWENS CORNING/LORD KINEMATICS

Three rotors were chosen for second generation testing activities. The disk/ring design uses an SMC  $\alpha$ -ply layup disk with a wound graphite/epoxy ring. The subcircular rim wheel is composed of a 9 or 15 ring rim using a Kevlar/epoxy material with a graphite spoke system. The bidirectional weave wheel uses a fabric of Kevlar fibers in a helically wound configuration. After layup, the fabric is impregnated with resin.

## ROTOR AND CONTAINMENT DEVELOPMENT ACTIVITIES INCLUDE

- DESIGN SPECIFICATIONS FOR ROTORS
  - PRESENT ROTOR DESIGNS SELECTED FOR EVALUATION INCLUDE
    - HYBRID DISK/RING
    - SUBCIRCULAR RIM
    - BIDIRECTIONAL WEAVE
- DESIGN DATA FOR ROTOR/HUB ELASTOMERIC BOND
- COST ANALYSIS

The MEST Program was focused on automotive applications. Consistent with this application, flywheel development centered on rotors with a total stored energy of  $< 1$  kWh with values near 0.25 kWh being quite adequate for the application. Size constraints imposed by the automobile required a maximum diameter of about 0.6 m. The test facility was capable of supplying a maximum input power level of 3 kw to accelerate the flywheel.

## PERFORMANCE PARAMETERS WERE SPECIFIED BY VARIOUS ASPECTS OF THE PROGRAM

- AUTOMOTIVE APPLICATION EMPHASIS
  - TOTAL STORED ENERGY  $< 1$  kWh
  - ROTOR SIZE OF ABOUT 0.6 m (2 ft)
- TESTING PROGRAM
  - INPUT POWER 3 kW MAXIMUM
- ENERGY DENSITY AT ULTIMATE SPEED OF 88 Wh/kg



The first generation wheels concentrated on rim and disk type designs. A variety of composite materials were used and the performance of the wheels varied greatly. This initial phase of testing concentrated on obtaining energy density data at the maximum wheel speed. The maximum speed is defined as that speed where a limiting failure mechanism is first observed. This includes material failures (e.g., cracks or fragments slung off the wheel), unacceptable imbalance, or radial runout in excess of 20 mils. The highest energy density obtained was 79.5 Wh/kg using a rim design.

### FIRST GENERATION ROTORS SHOWED A WIDE VARIATION IN PERFORMANCE

<u>MANUFACTURER</u>	<u>WHEEL TYPE</u>	<u>MATERIAL</u>	<u>ENERGY DENSITY AT MAXIMUM SPEED (Wh/kg)</u>	<u>ENERGY STORED (kWh)</u>
ORNL	OVERWRAP	K49	49.3	0.56
BROBECK	RIM	SG/K49	63.7	0.71
GARRETT/ AIRESEARCH	RIM	K49/K29/SG	79.5	1.23
ROCKETDYNE	OVERWRAP RIM	G	39.6	2.13
APL-METGLASS	RIM	M	24.4	0.04
HERCULES	DISK (CONTOURED PIERCED)	G	37.4	0.85
AVCO	DISK (PIERCED)	SG	44.0	0.40
LLNL	DISK (TAPERED)	G	62.6	0.31
LLNL	DISK (FLAT)	SG	67.1	0.16
GE	DISK (SOLID)	SG/G	55.1	0.28
OWENS/LORD	DISK	SMG/G	27.8	0.36
		SMC/G	36.6	0.40
		SMC/G	25.0	0.28
		SMC	17.5	0.17

SG = S GLASS; K49 = KEVLAR 49; K29 = KEVLAR 29; G = GRAPHITE; M = METGLASS;  
SMC = S-GLASS SHEET MOLDING COMPOUND

During FY 1983 the advanced design wheels were tested. The disk and disk/ring designs successfully completed 10,000 cycle fatigue tests. Subsequent ultimate speed tests indicated energy densities higher than that achieved by similar wheels that had not been fatigued. The sub-circular rim design wheel did not successfully complete the cyclic fatigue test, failing at 2585 cycles. In addition, energy storage densities at ultimate speed were 26% below design specifications. The bidirectional weave design showed a very low energy storage density. This very low value may be attributable to poor resin impregnation during fabrication.

## ADVANCED ROTORS HAVE UNDERGONE CYCLIC FATIGUE AND ULTIMATE SPEED TESTS

	FLYWHEEL DESIGN			
	DISK	DISK/RIM	SUBCIRCULAR RIM	BIDIRECTIONAL WEAVE
MATERIAL	SMC	SMC/G	K49	K49
COMPLETED 10,000 CYCLE TEST	YES	YES	NO <sup>1</sup>	
ULTIMATE ENERGY DENSITY (Wh/kg)	48.6 <sup>2</sup>	63.5 <sup>2</sup>	65.7	37.3
TOTAL STORED ENERGY (Wh)	517	644	622	416
SPEED AT FAILURE (rpm)	40,638	47,058	30,012	27,575

<sup>1</sup> ROTOR FAILED AT 2586 CYCLES

<sup>2</sup> ROTOR HAD PREVIOUSLY COMPLETED CYCLIC TEST

With cost constraints loosened (as opposed to automotive applications), a 2% strain graphite fiber becomes a very attractive candidate for space flywheel systems. Its ultimate tensile strength of 700 ksi or greater would make possible much higher energy densities. Use of this fiber with a flexible resin would permit the fabrication and operation of a thick rim design having an ID/OD ratio of 0.5 or less. This design could yield energy storage densities of 150 Wh/kg or greater.

## **ADVANCED FIBERS COULD SIGNIFICANTLY INCREASE STORAGE DENSITIES**

- **THE 2% STRAIN GRAPHITE FIBER DEVELOPED BY HERCULES PROMISES TO GIVE A 700 ksi ULTIMATE TENSILE STRENGTH**
- **IT HAS NOT BEEN INVESTIGATED FOR TERRESTRIAL APPLICATIONS BECAUSE AT \$30/lb IT IS TOO COSTLY**
- **FOR SPACE APPLICATIONS, WHERE WEIGHT OR VOLUME IS A PREMIUM, THE MATERIAL-RELATED STORAGE COST IS NOT UNREASONABLE**
- **WE ESTIMATE THAT THE USE OF THE 2% STRAIN GRAPHITE IN A THICK RIM DESIGN COULD RESULT IN AN ENERGY DENSITY OF 150 Wh/kg AT ULTIMATE SPEED**

Spin testing of flywheels is a very important component of the DOE program. The testing program is designed to confirm failure modes of the flywheel as well as determine how a material performs in a specific design.

## **SPIN TESTING IS A CRITICAL COMPONENT OF FLYWHEEL DEVELOPMENT**

- **CONFIRM MATERIAL PERFORMANCE AS USED IN A SPECIFIC DESIGN**
- **CONFIRM FAILURE MODE**
- **GENERATE DATA CONCERNING EFFECTS OF CYCLING ON WHEEL**
  - **FATIGUE**
  - **RELAXATION**
- **LOOK FOR CRITICAL RESONANCES IN DESIGN**

The Oak Ridge Flywheel Evaluation Laboratory represents the state of the art for spin testing flywheels. High speed balancing before the test insures that material limits will be reached during the test. Radial runouts of the arbor, hub, and wheel are monitored continuously during the test and can be used to indicate if something is going wrong with the flywheel during the test. Other parameters measured during the test include flywheel temperature, axial runout, and vacuum.

**THE ORFEL FACILITY OFFERS UNIQUE INSTRUMENTATION  
AND DATA ANALYSIS CAPABILITIES NOT  
AVAILABLE IN OTHER FACILITIES**

- **BEFORE TEST ACTIVITIES INCLUDE**
  - HIGH SPEED (UP TO 30,000 rpm) BALANCING
  - COMPUTATION OF WHIRL FREQUENCIES
  - DETERMINATION OF FORCE RESONANCE FREQUENCY
  
- **DURING THE TEST THE FOLLOWING PARAMETERS ARE MONITORED**
  - FLYWHEEL TEMPERATURE VIA PYROMETRY
  - RADIAL RUNOUT OF ARBOR, HUB AND WHEEL
  - AXIAL RUNOUT TO DETERMINE TILT OF WHEEL
  - VACUUM
  
- **CRITICAL PARAMETERS SUCH AS WHIRL AND FORCED RESONANCE ARE ALSO ANALYZED DURING THE TEST USING AN ON-LINE COMPUTER AND FREQUENCY SPECTRUM ANALYZER**

It would be useful if a technique was available to predict incipient failure of the flywheel while in service. To this end ORNL has begun investigations concerning non-contact strain measurement and nondestructive inspection. These techniques show promise but have not been developed to the point where they are a useful diagnostic tool.

## PRELIMINARY INVESTIGATIONS HAVE BEEN MADE FOR OTHER MEASUREMENT TECHNIQUES

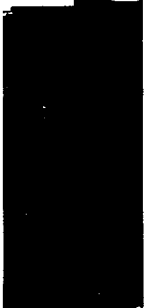
- NON-CONTACT STRAIN MEASUREMENT
  - USES CHANGE IN DIFFRACTION ANGLE OF A LASER-ILLUMINATED DIFFRACTION GRATING, BONDED TO FLYWHEEL AS INDICATOR OF STRAIN
  - COMMERCIAL GRATINGS (14,000 LINE/INCH) YIELDED RESOLUTIONS NOT ADEQUATE FOR THE LOW STRAIN (~ 0.7%) MATERIALS USED
  - RESOLUTION MAY BE ADEQUATE FOR 2% STRAIN MATERIAL
- NDI
  - ULTRASONIC DETECTION OF MICROCRACKING IN THE MATRIX
  - PRELIMINARY RESULTS SHOWED FREQUENCY ATTENUATION INCREASES MONOTONICALLY WITH STRAIN HISTORY
  - NOT YET ABLE TO USE TECHNIQUE TO PREDICT INCIPIENT FAILURE



N85

3866

UNCLAS



N85 13866

D16

FLEXIBLE MATRIX COMPOSITE LAMINATED DISK/RING FLYWHEEL

B. P. Gupta and A. J. Hannibal  
Lord Corporation  
Erie, Pennsylvania

PRECEDING PAGE BLANK NOT FILMED



#### ABSTRACT

An energy storage flywheel consisting of a quasi-isotropic composite disk overwrapped by a circumferentially wound ring made of carbon fiber and an elastomeric matrix is proposed. Through analysis it has been demonstrated that with an elastomeric matrix to relieve the radial stresses, a laminated disk/ring flywheel can be designed to store at least 80.3 Wh/kg or about 68% more than previous disk/ring designs. At the same time the simple construction is preserved.

## I. INTRODUCTION

Nearly a dozen different rotor concepts have been developed over the past ten years under the auspices of the Department of Energy. (DOE). All these designs were fabricated and underwent destructive testing. From analytical studies and experimental results which included energy density at burst, identification of failure modes, dynamic stability, requirements for containment and system cost, two designs were chosen for continued development. They were Garrett-Air Research's Multi-Ring Rim Rotor and General Electric's Laminated Disk/Ring Hybrid Rotor.

Garrett's multi-ring design stored 79.4 Wh/kg at burst, the highest energy density per unit weight of any flywheel studied in the DOE's Energy Storage Program. However, in a 10,000 cycle test at a maximum energy density of roughly one-half the ultimate value, the multi-ring design failed catastrophically after 2,586 cycles [Ref. 1]. The General Electric Disk/Ring Rotor stored 52.1 Wh/kg and 68 Wh/kg in two separate tests after having successfully completed 10,000 cycles at a maximum energy density of 22.5 Wh/kg. The failure mode was circumferential rupture induced by resin failure in the radial direction.

Other factors that demonstrate the high performance of the hybrid design are its energy density per unit volume, which is roughly three times that of the multi-ring design, and the controlled manner in which it fails.

In this paper the laminated disk/ring concept is modified by replacing the epoxy matrix in the ring with a urethane elastomer. It is demonstrated analytically that the circumferential rupture mode of failure is eliminated and the energy density increased by roughly 68% when using a high strain fiber. There are several other benefits derived from this substitution. First, the ring can be made very thick, reducing the manufacturing complexity required for multi-ring configurations. Also, the disk might be eliminated altogether in lieu of a small hub, possibly metal. Second, the maximum tensile stress occurs near the outside of the ring rather than at the interface like the carbon/epoxy ring. Third, the problem of ring/disk separation is eliminated.

The laminated disk/ring concept with a high performance fiber/elastomeric ring offers the potential for the highest energy density achieved with any flywheel concept to date while maintaining simplicity in construction. (See Figure 1.)

## II. ANALYSIS AND DESIGN OF DISK/RING FLYWHEELS

Three disk/ring flywheels having different ring materials were evaluated analytically. The properties of the laminated glass/epoxy disk material, which is common to all three flywheels, were taken from Reference 2 and are recorded in Table 1. S-glass, carbon and high strain carbon (1.75% elongation) were considered as candidate fibers for the ring. S-glass fibers were rejected on the basis of disk/ring separation and will not be discussed in this paper. The matrix materials were epoxy and a relatively soft urethane elastomer having a Young's modulus of 13.8 MPa. The mechanical properties of the carbon/epoxy ring were also taken from Reference 2 and are recorded in Table 2. Some of the properties of the carbon/urethane rings were calculated using the method described in Reference 3 and others were estimated based on previous experimental measurements.

The analytical method was based on the equations developed in Reference 4. They provide the stresses relating to the four major considerations when designing a disk/ring flywheel. They are: (1) maximum stress in the disk; (2) maximum radial stress in the ring; (3) maximum circumferential stress in the ring; and (4) disk/ring separation.

Table 3 records the optimum flywheel configurations considered in this study. Configuration No. 1 has a carbon/epoxy ring with a radius ratio,  $a/b$ , of 0.85. Below this value the disk/ring separates as indicated by the low value of interface pressure. Failure occurs in the disk at an energy density of 47.74 Wh/kg. Configurations No. 2 and No. 3 have a radius ratio of 0.6. Lower values are possible without the fear of disk/ring separation, but the energy densities are not increased. Configuration No. 2 fails through longitudinal fiber breakage at an energy density of 58.96 Wh/kg, 23.5% greater than Configuration No. 1. Configuration No. 3, however, with its high strain capability, increases the stored energy density at burst to 80.3 Wh/kg or 68% greater than Configuration No. 1. Its failure could be either radial ring failure or circumferential ring failure.

TABLE 1 -  
PROPERTIES OF S2-GLASS/EPOXY DISK

PROPERTIES	VALUE
Elastic Modulus, $E_d$	20.0 GPa (2.9 x 10 <sup>6</sup> psi)
Poissons Ratio, $\nu_d$	0.3
Density, $\gamma_d$	1.805 g/cm <sup>3</sup> (0.065 lb/in. <sup>3</sup> )
Ultimate Strength, $\sigma_{ud}$	386 MPa (56,000 psi)

In Figure 2 the maximum normalized stress factor (SD) in the disk is observed to be nearly the same for all three configurations over the entire range of  $a/b$ . For thicker annular rings, which are possible with configurations No. 2. and No. 3, the stress in the disk is reduced and therefore becomes less of a concern.

The maximum tangential stress factor (SLT) for the ring is also presented in Figure 2. Below a radius ratio of about 0.77 the carbon/urethane configurations (No. 2 and No. 3) pay a penalty in higher tangential stress. SLT for the carbon/epoxy configuration (No. 1) minimizes at 0.56 while configurations No. 2 and No. 3 minimize at an SLT of 0.858. This difference is fairly constant for all  $a/b$  ratios less than 0.56.

The higher tangential stress factors for the carbon/urethane configurations are more than offset by the advantage gained in the radial stress factor (SLR) of the ring as illustrated in Figure 3. Clearly for all radius ratios below 0.85 the carbon/urethane configurations have a dramatic advantage over a carbon/epoxy ring. For a radius ratio below about 0.8, SLR is constant for configurations No. 2 and No. 3, allowing a ring of arbitrary annular thickness without an increase in radial stress. This is clearly not the case for configuration No. 1.

In Figure 4 the interface pressure (PL) versus radius ratio is presented. A negative value of PL indicates disk/ring separation. For configuration No. 1 separation would exist for all values of radius ratios below 0.85, although this value can be lowered somewhat by applying a precompression during assembly. Configurations No. 2 and No. 3, on the other hand, show no sign of separation at any radius ratio.

Figures 5 through 8 present the stresses along the radius of the flywheels. The interface of the disk and the ring is indicated by a vertical line. The maximum circumferential stress in the ring is at the interface in configuration No. 1, but near the outside of the ring for configuration No. 3. If failure should occur in the circumferential direction in configuration No. 3, a more benign failure mode would be expected. The compressive radial stress at the interface shown in Figure 8 for configuration No. 3 indicates the absence of separation.

TABLE 2 - PROPERTIES OF RING MATERIALS  
( $V_f = 60\%$ )

Flywheel Configuration No.	1	2	3
Composite Material	Carbon/Epoxy	Carbon/Urethane	High Strain Carbon/Urethane
Density, $\gamma_h$ g/cm <sup>3</sup> (lb/in. <sup>3</sup> )	1.509 (0.0545)	1.467 (0.053)	1.467 (0.053)
Poisson's Ratio, $\nu_h$	0.33	0.39	0.39
Tangential Modulus, $E_\theta$ GPa (psi)	126.2 (18.3 x 10 <sup>6</sup> )	126.2 (18.3 x 10 <sup>6</sup> )	126.2 (18.3 x 10 <sup>6</sup> )
Radial Modulus, $E_r$ GPa (psi)	9.59 (1.39 x 10 <sup>6</sup> )	0.38 (54,800)	0.38 (54,800)
Tangential Strength, $\sigma_{\theta 0}$ MPa (psi)	1124.1 (163,000)	1124.1 (163,000)	1575.2 (228,400)
Radial Strength, $\sigma_{r0}$ MPa (psi)	12.4 (1,800)	12.4 (1,800)	12.4 (1,800)
Ratio, $M = E_\theta/E_d$	6.31	6.31	6.31
Ratio, $K^2 = E_\theta/E_r$	13.17	334	334
Ratio, $R = \gamma_d/\gamma_h$	1.195	1.222	1.226

TABLE 3 - OPTIMUM DESIGNS OF FLYWHEELS

Configuration No.	1	2	3
Composite Material	Carbon/Epoxy	Carbon/Urethane	High Strain Carbon/Urethane
Radius Ratio ( $c = a/b$ )	0.85	0.6	0.6
Interface Pressure Ratio ( $PL = p/\rho\omega^2 b^2$ )	0.0012	0.0021	0.0021
Maximum Stress Factors			
SLT	0.956	0.8577	0.8577
SLR	0.0082	0.00695	0.00695
SD	0.355	0.180	0.180
Maximum Stress Strength Ratios 10 <sup>-6</sup> /MPa (10 <sup>-6</sup> /psi)			
SLT/ $\sigma_{\theta 0}$	850.5 (5.86)	763.4 (5.26)*	545.7 (3.76)
SLR/ $\sigma_{r0}$	660.4 (4.55)	560.4 (3.861)	560.4 (3.861)*
SD/ $\sigma_{d0}$	920.2 (6.34)*	466.5 (3.214)	466.5 (3.214)
Maximum Energy Wh/kg (Wh/lb)	47.74 (21.7)	58.96 (26.8)	80.3 (36.5)
Failure Speed, RPM **	36,000	40,160	46,900

\* Indicates the failed part and the mode of failure.

\*\* Radius b of the flywheel is 22.48 cm (8.85 in.).

Figure 9 presents the maximum energy densities per unit weight for all three configurations as a function of the radius ratio  $a/b$ . The failure mode changes for different values of the radius ratio. It can be observed that failure occurs in the disk for all three configurations when the ring is thin. For thicker rings, the mode of failure shifts to circumferential rupture (radial stress) for the carbon/epoxy configuration. The energy density decreases rapidly at this point for a small increase in ring annular thickness. For a radius ratio less than 0.77, the failure mode of configuration No. 2 is a tangential stress failure with a constant energy density of about 58.3 Wh/kg. Configuration No. 3 (high strain carbon fiber) has the same characteristic for radius ratios less than 0.65. Its energy density is constant at 82.5 Wh/kg or 68% higher than the carbon/epoxy configuration.

### III. RESIDUAL STRESSES CAUSED BY MANUFACTURING PROCESSES

The manufacturing processes involved in fabricating a filament wound composite ring can create residual stresses in the flywheels. These stresses will have a detrimental effect on the performance of the flywheels if they are tensile in nature. Table 4 records the residual stresses in two carbon/epoxy rings and two carbon/urethane rings based on the calculations published in Reference 5.

It can be observed from Table 4 that as the thickness increases, the residual stresses also increase. In terms of ultimate strength it appears the radial stress is more harmful than the tangential stress. Even though analysis indicates a single ring having a small  $a/b$  ratio is feasible, manufacturing induced stresses may preclude this possibility. If so, it seems that two or three relatively thick rings with precompression will reduce the problem to a manageable level.

TABLE 4 - RESIDUAL STRESSES

Ring Number	Dimensions, cm (in.)			Material (V <sub>f</sub> )	Residual Stresses MPa (psi)		
	OD	ID	Thickness		(σ <sub>θ</sub> ) inside	(σ <sub>θ</sub> ) outside	(σ <sub>r</sub> ) middle
1(a)	53.34 (21.0)	50.8 (20.0)	1.27 (0.5)	Carbon/Epoxy (60%)	41.0 (5,940)	-39.6 (-5,750)	0.475 (69.0)
1(b)	53.34 (21.0)	50.8 (20.0)	1.27 (0.5)	Carbon/Urethane (46%)	31.7 (4,600)	-31.3 (-4,540)	0.455 (66.0)
2(a)	40.3 (15.87)	27.94 (11.0)	6.18 (2.44)	Carbon/Epoxy (60%)	87.7 (12,730)	-69.8 (-10,130)	6.7 (970.0)
2(b)	35.6 (14.0)	27.94 (11.0)	3.81 (1.50)	Carbon/Urethane (50%)	80.7 (11,710)	-70.4 (-10,210)	4.0 (580.0)

IV. FUTURE WORK

In this paper the performance improvement of a laminated disk/ring flywheel with a carbon/urethane ring over a flywheel with a carbon/epoxy ring has been demonstrated. There is, however, still a great deal of work to be done, such as:

- Optimum design of a disk/ring flywheel with a few rings assembled with an interference fit and possibly having different fibers and different resins at different fiber fractions (Figure 10).
- Materials data studies to determine the most suitable resin and fiber combination.
- Fiber sizing studies to optimize fiber/resin adhesion.
- Dynamic stability study.
- Spin test to burst.
- NDT evaluation.
- Deep cycle fatigue.

## V. SYMBOLS AND ABBREVIATIONS

a	radius of disk
b	radius of flywheel
c	ratio of disk radius to flywheel radius
$E_d$	elastic modulus of disk material
$E_r$	radial modulus of ring material
$E_\theta$	tangential modulus of ring material
ID	inside diameter
$K^2$	ratio of tangential to radial modulus of ring material
M	$E_\theta/E_d$
N	speed of flywheel, RPM
OD	outside diameter
PL	interface pressure, nondimensional; $PL = p/c_h \omega^2 b^2$
p	interface pressure,
R	$\sigma_d/\sigma_h$
r	radius
SD	maximum normalized stress factor
SLR	radial stress factor
SLT	maximum tangential stress factor
$V_f$	fiber volume section
$\gamma_d$	density of disk material
$\gamma_h$	weight of ring material
$\theta$	arbitrary position along circumference of ring
$\nu_d$	Poisson's ratio for disk material
$\nu_h$	Poisson's ratio for ring material
$\rho_d$	density of disk material
$\rho_h$	density of ring material
$\sigma_r$	radial stress in ring material
$\sigma_{ud}$	ultimate tensile strength of disk material
$\sigma_{ur}$	ultimate tensile strength of ring material in radial direction
$\sigma_{u\theta}$	ultimate tensile strength of ring material in tangential direction
$\sigma_\theta$	tangential stress in ring material
$\omega$	angular speed, rad/sec

Subscript:

max maximum



## VI. REFERENCES

1. Coppa, A.P. and Kulkarni, S.V.: Composite Flywheels Status and Performance Assessment and Projections, Proceedings of the Second European Symposium on Flywheel Energy Storage, Polytechnic of Tuon Turn, Italy, May 9 - 13, 1983
2. Nimmer, R. P., Torossian, K., and Wilkening, W. W.: Laminated Composite Disc Flywheel Development, Fourth Interim Report by General Electric Co., for Lawrence Livermore Laboratory, No. UCRL-15383, January 1981.
3. Gupta, B. P.: Elastic Constants of a Uniaxial Composite by Finite Element Energy Method, 19th Annual Meeting of the Society of Engineering Science, Inc. (University of Missouri-Rolla, Rolla, Missouri), October 1982.
4. Gupta, B. P. and Lewis, A. F.: Optimization of Hoop/Disk Composite Flywheel Rotor Designs. 1977 Flywheel Technology Symposium Proceedings, San Francisco, California, March 1978.
5. Dewey, B. R., and Knight, C. E., Jr.: Experimental and Theoretical Determination of Residual Stresses in Filament-Wound Rings, Rep. No. Y-1701, Union Carbide Corp., Oak Ridge, TN, 1970. (Available from NTIS.)

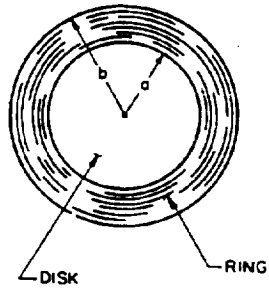


Figure 1.- Laminated disk/ring flywheel. Disk is solid and is made of an isotropic material, such as a laminated S2-glass/epoxy composite. A ring made of high-modulus high-strength fiber and flexible matrix composite is wound onto the disk. The fibers in the ring are directed circumferentially.

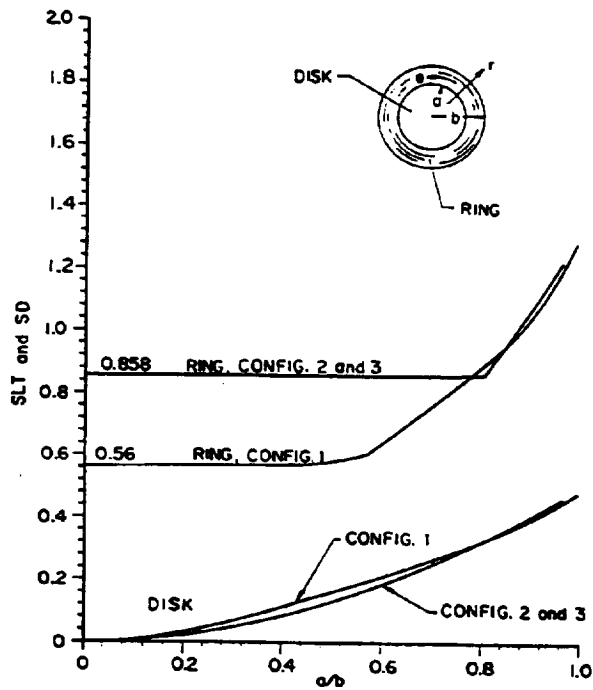


Figure 2.- Maximum tangential stress factors.

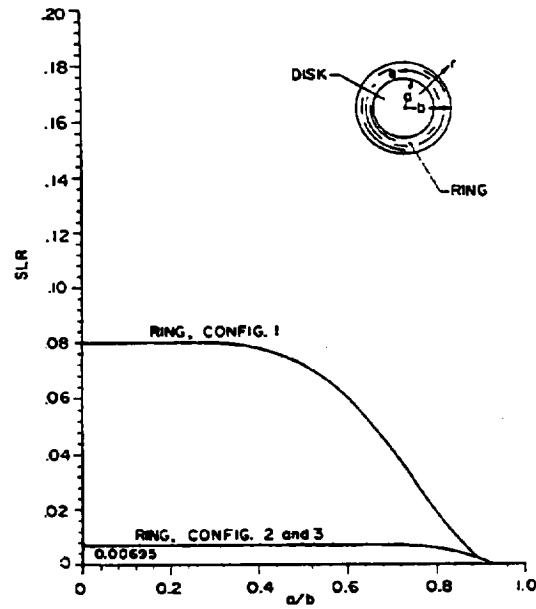


Figure 3.- Maximum radial stress factors.

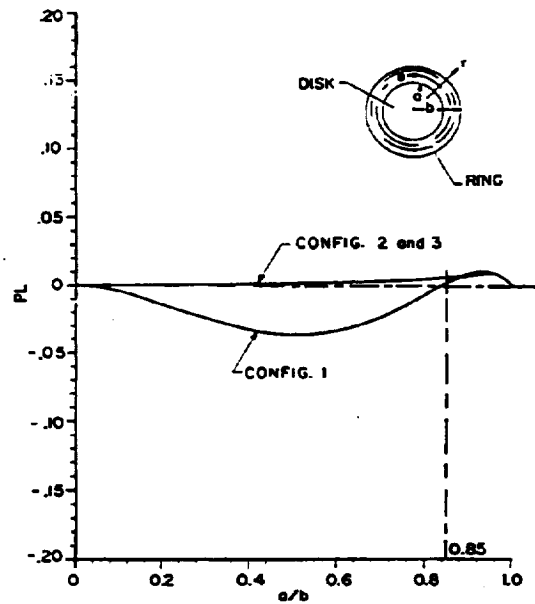


Figure 4.- Interface pressure factors.

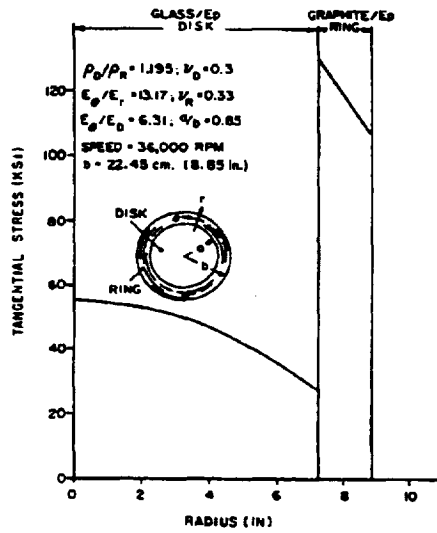


Figure 5.- Tangential stress along radius of flywheel. Configuration 1.

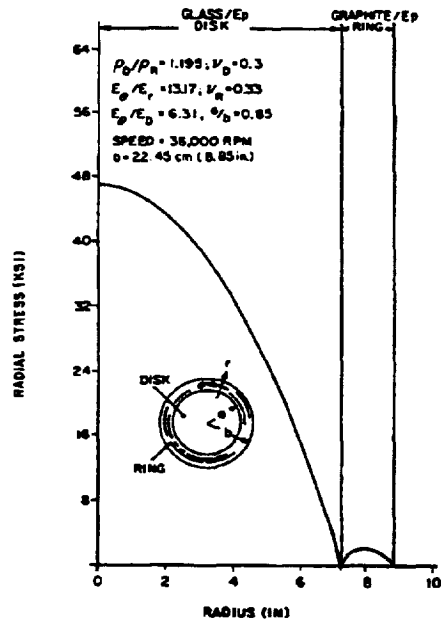


Figure 6.- Radial stress. Configuration 1.

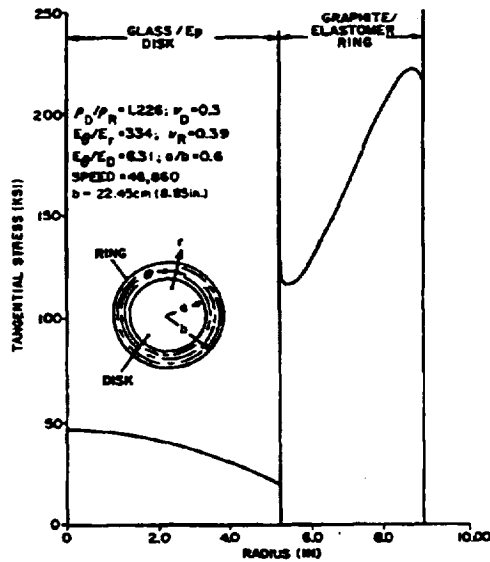


Figure 7.- Tangential stress. Configuration 3.

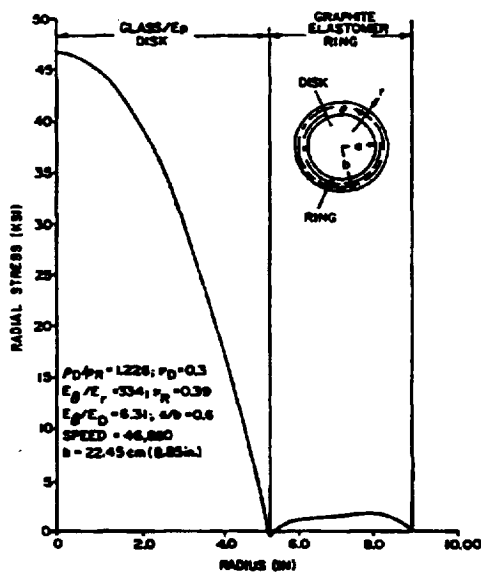


Figure 8.- Radial stress. Configuration 3.

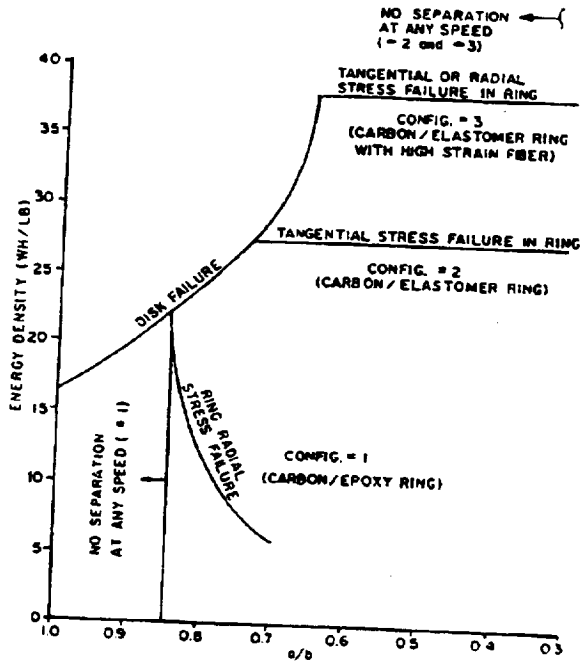


Figure 9.- Maximum energy densities and failure.

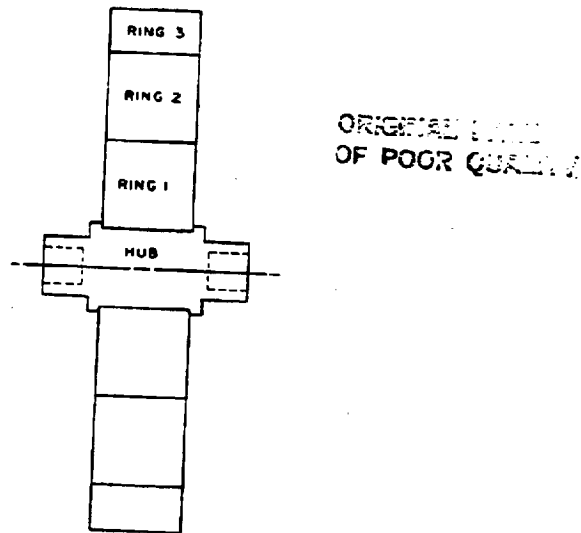


Figure 10.- Proposed flywheel construction.

N85

3867

INCLAS

N85 13867 019

GENERAL ELECTRIC COMPOSITE RING-DISK  
FLYWHEEL: RECENT AND POTENTIAL DEVELOPMENTS

Anthony P. Coppa  
General Electric Company  
Space Systems Division  
Philadelphia, Pennsylvania

PRECEDING PAGE BLANK NOT FILMED



## INTRODUCTION

During the past few years, an increasing recognition has developed of the important benefits that can be gained by utilizing high performance flywheel systems in spacecraft. While the case for flywheels for spacecraft power and combined power/attitude control was fairly well established by the 1974 NASA/Rockwell Study (Refs. 1-2), a more solid acceptance of it was inhibited by the then current state of technology, among other reasons. One of the key factors supporting the case for flywheels was (and is) the composite rotor, with its potential for very high density and manageable containment. Although flywheel systems incorporating then available metallic rotors appeared to be competitive with electrochemical energy storage systems for certain missions, a limited potential, certainly for long term performance growth, and an unresolved containment issue undoubtedly dampened significant system development.

The situation has, however, changed for the better in recent years due to important developments in composite rotor technology which have proceeded from the mechanical energy storage technology (MEST) program sponsored by the U.S. Department of Energy (DOE) and conducted by the Lawrence Livermore National Laboratory (LLNL). The primary objective of the program was to develop by 1984 an economical and practical composite flywheel having an energy density of 88 Wh/kg at failure with an operational range of 44-55 Wh/kg and an energy storage capacity of approximately 1 kWh. In addition, concerns regarding safety dictated the development of flywheel containment technology.

Initially, the DOE/LLNL program sponsored the development of 10 different composite rotor designs. Considerable data regarding the dynamics, failure modes, and containment behavior of the prototypes were obtained from spin testing. Also, some of the program goals were approached and exceeded (Garrett multi-ring rotor, which attained an ultimate energy density of 79.4 Wh/kg and a stored energy of 1.23 kWh). In addition, improved understanding of composite rotor design, structural behavior, material responses, and fabrication processing was obtained from prolonged association with the variety of materials, constructions, and design features embodied in the prototype rotors. Spin testing permitted evaluation of the effectiveness of intricate design features to obtain high storage performance (for example, rotors developed by the Garrett and Brobeck organizations). Tests also revealed surprisingly high performance in exceedingly simple design such as the constant thickness laminated disk.

Since it was not possible to continue the development of all the rotor designs, an evaluation/selection process was conducted to identify the most promising concepts for further development and testing. The designs selected were the Garrett multi-ring rim type rotor and the General Electric ring/disk hybrid rotor. Ten prototypes of each of these designs were fabricated and several were spin tested for ultimate and cyclic endurance in a laboratory environment. An AVCO design was also developed further.

In addition to the rotor developments, two parallel studies were initially performed to provide a design basis for composite rotor containment (Refs. 3-4). These studies included an assessment of available containment technology for metallic and composite rotors, examination of composite rotor burst test data, and definition of containment housing design concepts. The methodology and design concept produced by General Electric was subsequently selected for further development. Experimental containment housings for the Garrett and General Electric flywheels were fabricated and one containment test involving a complete burst of a General Electric rotor was

performed. This test was the first of its kind (i.e., a high performance burst within a housing of practical proportions) and revealed important realities of composite rotor containment processes.

This paper describes recent developments of the General Electric hybrid rotor design and discusses its relation to flywheel designs that are especially suitable for spacecraft applications. It also projects potential performance gains that can be achieved in such rotor designs by applying latest developments in materials, processing, and design methodology. Indications are that substantial improvements can be obtained.

Merit indices of composite flywheel performance include the following:

$$\begin{aligned} \text{Weight Energy - Density, } E_W &= \frac{\text{Stored Energy}}{\text{Total Rotor Weight}} \\ \text{Volume Energy - Density, } E_V &= \frac{\text{Stored Energy}}{\text{Rotor Swept Volume}} \\ \text{Cost Energy - Density, } E_C &= \frac{\text{Stored Energy}}{\text{Rotor Cost}} \end{aligned}$$

These indices may be related to an ultimate storage capacity based on short-term failure and an operational capacity based on cyclic life. Similar indices may, of course, also be defined on a system level by referring to the weight, enclosed volume, and cost of the entire energy storage system.

Another set of indices considers only the rotors and containment housing and is of particular value in designing an optimum flywheel system. This is because the various rotor designs under consideration may have widely different containment requirements. A high performance rotor design might, for instance, have a highly destructive failure mode, thereby requiring relatively heavy containment. Because of this, its combined rotor and containment energy density might be lower than that of a lower performance rotor which has a relatively benign mode of failure.

In contrast to metallic (isotropic) flywheels, whose weight energy-density can be expressed as

$$E_W = k \left( \frac{\sigma}{\rho} \right)$$

where  $k$  is the shape factor,  $\sigma$  the ultimate or operational strength, and  $\rho$  the mass density, the definition of a performance index is more complex for composite rotors. Such materials have distinctive and complex behaviors because of anisotropy and heterogeneity. The orthotropy in elastic moduli can introduce a strong coupling between geometry and material properties, the thin ring perhaps being an exception. Also, fiber composites have low strengths corresponding to failure modes that are controlled by matrix properties, and time-dependent properties can differ significantly from the static values usually quoted.

What is generally required for composite rotor designs is an accurate stress analysis of its component members and the identification of limiting failure modes. Each failure mode can be expressed in terms of a corresponding rotor peripheral speed.

Hence a set of limiting speeds can be defined for a given design, and from the lowest of these, minimum performance indications for the appropriate use conditions are determined.

#### DESIGN FEATURES OF THE HYBRID ROTOR

The hybrid rotor shown in Figure 1 is basically a solid, constant thickness disk configuration that consists of three parts: a central laminated disk, a filament-wound outer ring, and a small metallic hub that is attached to the disk. In the usual form of the design, the laminate is a quasi-isotropic layup of unidirectional plies of glass/epoxy prepreg material cured in a press. The fiber volume and void content have typically been 50 to 55 percent and 2 percent, respectively. The ring is usually constructed of high-strength type graphite/epoxy material with a fiber volume and void content of 60 percent and 1 to 25 percent, respectively.

The ring is fitted to the disk by means of a simple interference fit. Radial interferences of .001 to .002 in./in. of outside ring radius have been employed, with values in the lower range in more recent designs. The interference fit is accomplished by cooling the disk and ring. In the cooling process the disk diameter contracts while the graphite/epoxy ring remains dimensionally inert, thereby permitting the ring to be slipped over the disk. When the interference fit is in the vicinity of .002 in./in. mechanical pressing is required in addition to thermal action.

Stresses in the hybrid rotor are governed by the elastic properties of the disk and ring, the interference fit value, and the parameter  $\beta$  which is the ratio of the inner and outer radii of the ring. In previous prototype rotors,  $\beta$  values have ranged from about .73 to .82.

The ring serves the following functions: (1) it operates at high energy density; (2) the ring/disk interface pressure acts to reduce the disk tensile stresses slightly and also to reduce radial tensile stresses in the ring; (3) it prevents fraying and other edge effect problems of the disk, (4) it greatly improves the fatigue and creep performance of the disk because of the excellent fatigue and creep properties of graphite/epoxy and (5) it can alter the flywheel failure mode from disk rupture to a less severe ring burst mode.

A small aluminum hub/quill adapter is bonded elastomerically to the disk. The bond accommodates the large differential radial growth that occurs between the disk and hub adapter during rotation. It also provides damping, but this is probably a disadvantage because internal damping is known to have an adverse effect on dynamic stability.

In 1982, 14 hybrid rotors were produced by General Electric for LLNL for ultimate speed and cyclic endurance spin testing. Except for certain details the rotors were nominally identical in size and design energy storage capacity. Their properties are shown in Table 1. The storage capacities were nominally .5 kWh (ultimate) and .25 kWh at maximum operational speed. The differences among these rotors were due to the resin used for the matrix of the outer ring. The basic design (Type A) employed Epon 826 epoxy which had been used in previous hybrid rotors. Ten Type A rotors were produced. Types B and C used a high temperature epoxy (Ciba-Geigy CY-179) and a flexible polyurethane respectively. Two each of Types B and C were produced.

Table 1. Properties of General Electric Hybrid and Simple-Disk Flywheels

Parameter	Hybrid	Simple Disk
Rotor OD, in.	16.00	15.86
Ring ID, in.	12.80	-
Ring Thickness, in.	1.74	-
Disk Thickness, in.	1.67	1.70
Rotor Weight, lb.	22.33	23.44
Rotor Weight, less Hub, lb.	21.22	22.33
Polar Moment of Inertia, lb-in.-sec <sup>2</sup>	1.69	1.82
Swept Volume, ft <sup>3</sup>	.202	.194

Also, simple laminated disk rotors were produced (Table 1), mainly to obtain basic spin test data about failure stress levels and failure modes of the laminate. The rings and laminates were fabricated by the Lord Corp. and 3M Co., respectively.

#### PERFORMANCE TESTS

Two ultrarapid speed tests and one cyclic spin test were performed on hybrid rotors (Nos. H8/GE-F and H6/GE-J) and one ultimate speed and one cyclic test was conducted on a simple laminated disk rotor (D2/GE-D). The test conditions and performances are listed in Table 2. Rotors H8 and D2 were the only units that were subjected to the cyclic testing and both rotors successfully endured the required 10,000 spin cycles. Each cycle consisted of spinning between energy levels of 217 and 54.2 Wh over a 6.5 minute period for the hybrid rotor and between 190 and 47.4 Wh over an 8.0 minute period for the simple disk rotor. After completion of the cyclic tests, these same rotors were tested for ultimate burst capacity. Rotor H8 burst at an energy level of 650 Wh and energy density of 68.0 Wh/kg. The peripheral speed at failure was 1,010 m/sec, believed to be the highest value ever attained in a flywheel. Rotor D2 burst at an energy level of 529 Wh and energy density of 52.1 Wh/kg. The basis for computing the energy level and energy density is as defined in Ref. 4.

The only other hybrid rotor that was brought to its ultimate speed was rotor H6 which burst at an energy level of 648 wh and energy density of 67.0 Wh/kg. This result was most interesting for several reasons, first because rotor H6 had not been previously tested and yet its burst performance very nearly duplicated that of rotor H8 which had been cycled 10,000 times. Also, the failure mode of both rotors was the same (i.e., circumferential burst of the outer ring). This set of data provides

Table 2. Cyclic and Ultimate Spin Test Results  
for General Electric Hybrid and Simple Disk Flywheels

	Rotor Number (Type)		
	H8/GE-F (Hybrid)	H6-GE-J (Hybrid)	D2/GE-D (Simple Disk)
<u>Cyclic Test</u>			
No. of Cycles	10,000	-	10,000
Cycle Duration, minutes	6.5	-	8.0
Speed: rpm, max. (min.)	27,330(13,660)	-	24,600(12,300)
m/s, max. (min.)	583(292)	-	519(260)
Energy, Wh, max. (min.)	217(54.2)	-	190(47.4)
Weight, lb. <sup>(1)</sup>	21.27	21.32	22.38
$E_W$ , Wh/kg	22.5	-	18.7
$E_V$ , kWh/m <sup>3</sup>	37.9	-	34.6
<u>Ultimate Test</u>			
Ult. Speed, rpm (m/s)	47,058(1,010)	46,602(992)	40,638(867)
Energy, Wh	656	648	529
$E_W$ <sup>(2)</sup> , Wh/kg	68.0	67.0	52.1
$E_V$ <sup>(2)</sup> , kWh/m <sup>3</sup>	115	113	94

(1) Not including 1.11 lb Hub Arbor.

(2) Based on Dimensions at Ultimate Speed.

the only existing indication of the effect of significant spin-cycling on the ultimate performance of a composite flywheel. At least for these two test points, the performance appears to be rather unaffected by the cycling imposed.

Based on the high ultimate energy density exhibited in these tests the operational level of a hybrid rotor of the design represented here would appear to be about 40 Wh/kg. The operational level imposed in the cyclic test of rotor H8 reflected the lower ultimate performance that had been expected, as well as a degree of caution in approaching this unprecedented test. More will be said later about the significance of these test results.

Attempts to reach ultimate burst conditions were made unsuccessfully with three other duplicate hybrid rotors. The tests, however, were significant because they manifested the ruggedness of the rotor construction, especially the graphite/epoxy ring component, and contributed to a better understanding of the loose-rotor containment process. In each case, the rotors separated from the drive shaft due to a whirl resonance condition that developed prior to attainment of a burst speed condition. The speeds at which separation occurred ranged between 35,820 and 40,910 rpm or 769 and 878 m/sec. Subsequent to separation, the rotors spun within the containment ring, finally coming to rest within one minute. Except for some graphite/epoxy which had been smoothly ground away during the spin-down process, the rotors were recovered in an intact condition.

#### FAILURE MODES OF HYBRID ROTORS

A plane stress analysis considering a quasi-isotropic disk and orthotropic outer ring and a uniform interface pressure between the two is used to calculate the stresses and deformations of the hybrid rotor system. The analysis (Refs. 6-7) provides an accurate and convenient means of optimizing the design of hybrid rotors. This facility is due basically to the constructional simplicity and axial symmetry of the rotor. The result is that for given component materials, the rotor stresses, displacements, and interface pressure are expressible in terms of three design parameters, namely, the ring radius ratio,  $\beta = a/b$ , unit radial interference  $\bar{\delta} = \delta/b$ , and rotor peripheral speed,  $V$ . Here  $a$  and  $b$  are respectively the inside and outside radii of the ring and  $\delta$  the radial interference. Hence the maximum allowable speeds  $V_i$  can be determined with respect to each of the governing failure modes of the hybrid system for any set of values  $\beta$  and  $\bar{\delta}$ . These modes are as defined in Table 3, in which the starred quantities are the maximum allowable design stresses for ultimate or fatigue failure conditions. Symbols in the table are defined as follows: CRF, circumferential ring, PRF, radial (transverse) ring, and DF, disk failure; S, ring/disk separation; B, bearing failure;  $\sigma_{CR}$ , circumferential ring,  $\sigma_{rR}$ , radial ring, and  $\sigma_D$ , disk center stress or strength;  $\sigma_B$ , bearing strength at ring/disk interface; and  $P$ , interface pressure.

A composite plot of  $V_i$  vs  $\beta$  for the  $i$  failure modes clearly exhibits the allowable operational regime for rotor systems having a given value of  $\bar{\delta}$ . The rotor energy/weight ratio  $E_{w_i}$  (energy density), expressible in terms of  $\beta$  and  $V_i$ , is more usually plotted instead of  $V_i$ . The author has referred to such a representation as a Nimmer plot. Data for constructing Nimmer plots are obtained by means of a computer program which calculates the energy densities  $E_{w_i}$  for all failure modes and the interface pressure at rest,  $P_0$ , for a specified range of  $\beta$ . It also calculates, if applicable, the value of  $\beta$  above which the interface pressure increases with increasing rotor speed. In this particular  $\beta$  range, the ring will remain in contact with the disk even if the initial interference is zero.

Table 3. Definition of Governing Failure Modes of Hybrid Rotors

Failure Mode	Symbol	Condition for $V = V_i$
Circumferential Ring Failure	CRF	$\sigma_{\theta R} = \sigma_{\theta R}^*$
Radial Ring Failure	RRF	$\sigma_{rR} = \sigma_{rR}^*$
Disk Failure	DF	$\sigma_D = \sigma_D^*$
Ring/Disk Separation	S	$P = 0$
Interface Bearing Failure	B	$P = \sigma_{BR}^* \text{ or } \sigma_{BD}^*$

A meaningful interpretation of a Nimmer plot requires careful consideration of ring/disk loading interactions in the light of uncertainties in governing material property values. These uncertainties are due to (1) limited available standard specimen data, (2) fabrication process dependency, (3) size effects, and (4) variation of certain properties with load and time.

A Nimmer plot that was used for the initial design selection of the present hybrid rotors (Types A and B) is shown in Figure 2. It is based on moderately heavy interference fit of .002 in./in. and the materials data of Table 4. The plot shows energy density (Wh/lb) versus radius ratio  $\beta$  for the various governing failure modes and serves to identify the optimum range of  $\beta$ . The present hybrid rotors were designed with  $\beta = .8$ ; therefore, the limiting failure mode indicated is CRF for ultimate failure (solid curve) and either CRF or DF for the  $10^5$  cycle operational conditions (dashed curves). In most cases the failure modes for high  $\beta$  values (thin rings) is DF or CRF while for low  $\beta$  values (thick rings) it is RRF or S (the latter for light interference fits).

#### ANALYSIS OF SPIN TEST DATA

The design data of Table 4 were compiled from previous hybrid rotor developments (Refs. 6, 7 and 8), available rotor spin test (Refs. 8-9), specimen test data (Refs. 6-8, 10-13), and laminate analysis (Ref. 15). As more spin test data became available for hybrid and simple laminated disk rotors, they were studied by means of the rotor structural analysis to refine the assessment of material strength values. In doing this the older spin test data were reexamined to reduce all conclusions regarding strength to a reasonably consistent basis. This study, described in Ref. 16, led to several important conclusions. First, the elastic modulus of the laminated disk becomes degraded due to the development of distributed microcracks in the laminate resin as the stresses in the disk exceed threshold levels. In hybrid rotors, the principal effects of this are to reduce the stresses in the disk and increase the

Table 4. Properties of Prototype Rotor Materials: Disk (S-2 Glass/SP250 Epoxy); Ring (T-300 Graphite/Epon 826 Epoxy)

Item	Disk				Ring					
	$E_D'$ , msi*	$\sigma_D'$ , ksi	$\rho_D'$ , lb/in. <sup>3</sup>	$\nu_D$	$E_{\theta R}'$ , msi*	$E_{rR}'$ , msi*	$\sigma_{\theta R}'$ , ksi	$\sigma_{rR}'$ , ksi	$\rho_R'$ , lb/in. <sup>3</sup>	$\nu_R$
Ultimate	3.3	60	.066	.3	18.8	1.40	170	2.0-3.5	.0531	.3
10 <sup>5</sup> Cycles	2.55	25	.066	.3	18.8	1.40	117	1.2	.0531	.3

\*1 msi = 1,000,000 lb/in.<sup>2</sup>

circumferential stress ( $\sigma_{\theta R}$ ) and reduce the radial tensile stress ( $\sigma_{rR}$ ) in the ring. Second, as a direct consequence of this, when the failure mode is CRF, the strength  $\sigma_{\theta R}$  is greater than those values, based on the initial disk modulus, and when the mode is RRF, the tensile strength  $\sigma_{rR}$  is smaller.

The revised estimates of design strength values were inferred from the calculated stress results that correspond to observed failure modes of tested rotors. In some cases, a lower bound estimate was obtained for a particular failure mode that was not the actual mode of failure in the test. The stress results are summarized in Table 5, which embodies most of the available spin tests of hybrid and simple disk rotors having 0, 90, +45, -45° laminate ply construction. The stresses listed do not include residual stress. All the hybrid rotors except the second set of tests 80-3 and 80-4 have two listings of data, the first corresponding to the initial disk elastic modulus and the second to the reduced modulus. The most important effects of the reduced disk modulus pertain to the outer ring.

The radial tensile stress  $\sigma_{rR}$  is addressed first. Only in Tests No. 80-3 and 4 did the RRF mode actually occur. The average calculated stress for these tests at the location at which failure was observed to occur is 1.71 ksi for the reduced modulus and 2.66 ksi for the initial modulus. Adding to these an estimated .5 ksi due to fabrication-induced residual stress we obtain values of 2.2 and 3.2 ksi for the radial tensile strength. The lower value, especially as it is associated with the reduced disk modulus, is assumed to be the indicated  $\sigma_{rR}$  strength. In the H8 and H6 tests, in which RRF did not occur, the maximum calculated radial stress corresponding to the reduced modulus is 1.46 ksi and the calculated residual stress is .482 ksi (Ref. 16). Hence, the total  $\sigma_{rR} = 1.94$  ksi, which compared to the above strength value (2.2 ksi) is consistent with a non-radial failure condition. If, on the other hand, the calculated values of  $\sigma_{rR}$  for Tests No. 80-3 and 80-4 corresponding to the initial modulus were used as a basis for estimating the  $\sigma_{rR}$  strength, this would yield an average value of  $2.66 + .5 = 3.1$  ksi. But the average calculated  $\sigma_{rR}$  (based on the initial disk modulus and including residual stress) for the H8 and H6 tests is 3.5 ksi, or greater than the indicated strength. This would not be consistent with the fact that RRF did not occur in these latter two tests. Hence, the four tests taken together support the existence of a reduced disk modulus and an estimated  $\sigma_{rR}$  strength of about 2.2 ksi. In Ref. 16, transverse tensile test data obtained on specimens cut from rings identical to those used in the 80-3 and 4 tests yielded an average strength of 3.23 ksi. A



Table 5. Rotor Stresses Analytically Deduced from Spin Tests of Hybrid and Simple Disk Flywheels

Test No.	Type	$\beta$	$\delta$	Failure Mode	$E_D$	$\sigma_{\theta R}$	$\sigma_{rR}$	$\sigma_{D_0}$
80-3	Hybrid	.75	.002	RRF	3.0	134	1.9	33
					2.28	144	1.1	
80-4	Hybrid	.72	.002	RRF	3.0	149	3.5	38
					2.17	163	2.4	
80-3	Hybrid	.75	.002	NF	3.0	171	-	-
80-4					3.0	180	-	-
80-8	Hybrid	.82	.002	CRF	3.1	156	.7	47
					2.15	179	3.4	71
H-8	Hybrid	.80	.00111	CRF	3.3	239	1.6	64
					2.2	222	2.7	70
H-6	Hybrid	.80	.00168	CRF	3.3	239	1.3	61
					2.2			
80-2	Simple Disk	-	-	DF	-	-	-	106
D1	Simple Disk	-	-	NF	-	-	-	75
D2								81
D5	Simple Disk	-	-	NF	-	-	-	81

'size effect' factor accounting for the probability of internal flaws was applied to the raw data to yield an estimated strength of 1.6 ksi. Hence, the deduced strength 2.2 ksi (above) might indicate that the strength of the material in the ring state is greater than in the test coupon condition, with the computed 'size effect' of Ref. 6, maintained. Such a conclusion was reached in Ref. 15, also for the case of longitudinal (circumferential) strength, i.e.,  $\sigma_{\theta R}$  is greater in the ring than indicated by specimen tests.

Next the circumferential stress  $\sigma_{\theta R}$  is addressed. In the 80-3 and 80-4 tests, after the occurrence of RRF, the rotor speeds were subsequently increased until whirl-induced vibrations caused the rotor to separate from the drive shaft. During this interval of time, the graphite/epoxy ring in each case was divided into two ring portions mutually detached along the radial positions at which RRF occurred. In this condition interface pressure between the ring portions would not exist. Hence, the disk elastic modulus would not have any effect on the stresses in the outer ring portion. The second listing of  $\sigma_{\theta R}$  for these tests represents the maximum value in the outer ring portion at the highest speed attained (not including the residual stress, estimated to be about 4 ksi). Therefore, the  $\sigma_{\theta R}$  strength must have been greater than the listed value plus the residual stress, or greater than 175 (10-3) and 184 (80-4) ksi.

In Test No. 80-8, the ring failed in CRF. The calculated maximum value of  $\sigma_{GR}$  corresponding to the reduced modulus and including a residual stress of 7 ksi is 186 ksi. The rotor is suspected to have had an interference fit greater than the identified value of .002 in./in. because it required a heavy mechanical force in addition to thermal contraction of the disk to assemble the two components. Assembly with an interference fit of .0022 in./in. can be accomplished solely by thermal action. Accounting for this, it is estimated the ring manifested a strength of 190-195 ksi.

The circumferential ring strengths exhibited by these hybrid rotors produced in a previous program (Refs. 6-8) are substantially greater than the design value of 170 ksi used for the present rotors (Table 4). The tests of the present rotors, H8 and H6, also support these indications, except to a considerably greater extent. The  $\sigma_{GR}$  values corresponding to the reduced disk modulus for these rotors are identical, equal to 248 ksi (including a residual stress of 9 ksi determined in Ref. 16). The equality of the two values of  $\sigma_{GR}$  is in fact remarkable, considering the differences in  $\delta$ , densities of disk and ring materials, and failure speeds. These values were carefully determined and were used in the calculation of  $\sigma_{GR}$ . It is noted that the calculated values of  $\sigma_{GR}$  based on the initial disk modulus are not equal, and also that the values corresponding to the initial modulus are quite high (e.g.,  $222 + 9 = 231$  ksi for rotor H6). Hence, these unexpectedly high but plausible values of  $\sigma_{GR}$  are considered to be reasonably well established.

Another important point that can be made about the pair of tests is that rotor H8 is known to have possessed extensive resin microcracking prior to the performance of the ultimate speed test. This had developed during the 10,000 cycle spin test which preceded it. Visual examination of the lateral surfaces as well as ultrasonic C-scans of rotors D2 and H8 that were made after completion of the cyclic testing revealed this fact. Hence, ample evidence exists to support the assertion that a reduced modulus was indeed present in the disk during the subsequent burst test. The only question remaining is the exact value of it. However, any reduction in modulus whatever would result in an indicated  $\sigma_{GR}$  strength greater than 209 ksi. Also, the almost identical performance of rotor H6 which had not been tested in any way prior to its burst test would suggest that resin microcracking is a short-term phenomenon in a glass/epoxy laminate of the type represented here (i.e., it develops simultaneously with the onset of sufficiently high stresses).

The recently performed spin tests of simple laminated disk rotors (D1, D2, and D5) listed in Table 5 support the indication of the earlier test (80-2) that the biaxial strength of quasi-isotropic S-glass/epoxy laminates (0, 90, +45, -45°) is considerably higher than indicated by specimen tests (Table 4). The recent tests were specifically intended to show whether the high strength exhibited in Test No. 80-2 could be realized. The question was not answered because attempts to reach short-term burst were thwarted by separation failure of the rotor (D1 and D5) from the drive shaft following the development of a whirl resonance vibration. However, all the simple disk rotors exhibited strengths of at least 75-81 ksi at the maximum attained speed. This compares to the 60 ksi value used for the recent disk designs. The result of the D2 test, however, is very significant. The rotor successfully completed the 10,000 cycle test prior to undergoing the ultimate speed test that resulted in the burst. The peak center stress during the cyclic test was 30 ksi. Since the calculated center stress at burst was 81 ksi, it is probable that the short-term ultimate strength is considerably higher than this. In itself the D2 test indicates that the  $10^4$  cycle fatigue strength is probably considerably greater than 30 ksi.

Revised tentative design data based on Table 4 and Ref. 16 are shown in Table 6 for hybrid rotors of the type discussed herein. The  $10^5$  cycle fatigue values for  $\sigma_{OR}$  and  $\sigma_{DO}$  are multiplied by knock-down factors of .68 and .42 used in the recently tested rotor designs. The ultimate value of  $E_D$  reflects the conclusion stated above that the reduction in disk modulus due to resin microcracking is a short-term phenomenon.

Table 6. Revised Tentative Properties of Hybrid Rotor Materials:  
Disk (S-2 Glass/SP250 Epoxy); Ring (T-300 Graphite/Epon 826  
Epoxy); Poisson's Ratio = .3

Item	Disk			Ring				
	$E_D$ , msi <sup>*</sup>	$\sigma_D$ , ksi	$\rho_D$ , lb/in. <sup>3</sup>	$E_{OR}$ , msi <sup>*</sup>	$E_{RR}$ , msi <sup>*</sup>	$\sigma_{OR}$ , ksi	$\sigma_{RR}$ , ksi	$\rho_R$ , lb/in. <sup>3</sup>
Ultimate	2.2	>81	.067	18.8	1.4	248	2.2	.0535
$10^5$ Cycles	2.55	>34	.067	18.8	1.4	168	1.2	.0535

\* 1 msi = 1,000,000 lb/in.<sup>2</sup>

A Nimmer plot of designs based on the properties of Table 6 and an interference fit of .00168 in./in. is shown in Figure 3. The solid and dashed lines indicate the governing failure envelopes for ultimate and maximum ( $10^5$  cyclic life) operational speeds respectively. An optimum ultimate energy density of 30.3 Wh/lb (66.8 Wh/kg) occurs at  $\beta = .78$ . Designs with higher  $\beta$  values are governed by CRF and lower  $\beta$  values by RRF. The operational speed failure envelope is governed by DF on the left and RRF on the right and represents two different values of disk strength ( $10^5$  cyclic life) of 34 ksi (lower) and 42 ksi (upper). These values correspond to ultimate strengths of 81 ksi, discussed previously, and 100 ksi, a capability demonstrated in Test No. 80-2 (Table 5). The optimum operational energy densities for these values of  $\sigma_D$  are respectively 17.5 Wh/lb (45.2 Wh/kg) at  $\beta = .78$ . The design of rotor H6 is positioned on the plot at  $\beta = .8$ .

In addition to demonstrating high overall performance, the tests of rotors H8 and H6 yielded important data about the ultimate and cyclic energy storage capability of the graphite/epoxy ring component. These are summarized in Table 7, in which  $W_R$  and  $I_R$  are the weight and polar moment of inertia of the ring. The outer ring of rotor H8, which had been cycled 10,000 times between maximum and minimum energy density levels of 38.5 and 9.6 Wh/kg, later attained an ultimate energy density of 116 Wh/kg. Similarly, the previously untested ring of rotor H6 attained an ultimate value of 114 Wh/kg. Such high performance levels demonstrate the potential of flywheels that are constructed of similar filament-wound rings.

Table 7. Energy Storage Performance of the Ring Component of Rotors H8 and H6 as Obtained from Spin Tests

Rotor No.	Parameter					
	$W_R$ , lb	$I_R$ , lb-in.-sec <sup>2</sup>	Ultimate		10 <sup>5</sup> Cycles	
			E, Wh	$E_W$ , Wh/kg	E, Wh	$E_W$ , Wh/kg
H8	6.79	.922	358	116	119	38.5
H6	6.73	.913	348	114	-	-

#### TOWARD HIGH PERFORMANCE SPACE FLYWHEELS

It is desirable to employ designs that utilize radially thicker rings of such materials in order to obtain still higher energy density and an internal diameter that is more suitable for interfacing with other system components. Unfortunately, such designs are precluded due to the low radial tensile strength of present filament-wound materials. This characteristic is apparent in Figure 3 wherein the RRF mode governs designs having  $\beta < .77$ , or thickness  $t > .23 b$ , where  $b$  is the ring outside radius. Beyond this limit thicker ring designs are accompanied by steadily lower energy densities. Measures to remedy this limitation exist, however, at least theoretically. Two approaches have been discussed, namely, the multi-ring design (Refs. 17-18) and the flexible-matrix design (Refs. 19-20).

The multi-ring approach employs concentric rings that are assembled with suitable interference fits. The radial pressures thereby produced at the interfaces between rings set up initial radial compression stresses in the ring components. Under rotational conditions, these pre-stresses act to decrease the radial tensile stresses. Beneficial effects on the circumferential stresses can also be obtained by this method.

The other approach utilizes a flexible instead of rigid matrix in the ring material. Such construction results in a greatly reduced radial modulus of elasticity without affecting the circumferential modulus. Analysis shows that by proper construction, such a material can provide a radial strain capacity high enough to avoid radial failure even in very thick rings.

Another contribution to high performance rotor design is the utilization of new high strength (graphite, aramid) fibers that are now available. The graphite fibers have at least 50 percent greater strength than the type used in the present GE hybrid flywheels. This promises to yield a similar increase in energy density.

Up to the present time, two GE hybrid rotors incorporating flexible-matrix graphite fiber rings ( $\beta = .8$ ) have been fabricated. To the author's knowledge, no multi-ring rotors specifically utilizing graphite/epoxy rings have been produced.

Preliminary studies at General Electric have identified two generic flywheel designs that incorporate a thick, flexible-matrix ring, namely the concentric and tandem arrangements. They differ in the manner in which the motor/generator is mounted to the flywheel.

In the concentric arrangement the motor/generator is mounted and supported within the bore of the rotor ring, as shown in Figure 4. The advantages of this design are overall compactness and efficient placement of high energy density material within the assigned envelope. This is due to the absence of a central hub component. Disadvantages include limited design flexibility to incorporate other flywheel components and greater expected difficulty of cooling the rotating parts of the motor/generator.

Preliminary design estimates of rotors based on the concentric type ( $\beta = .5$ ) are listed in Table 8 for useful energy storage capacities of 2.5 and 5 kWh (75 percent depth of discharge (DOD)). The estimates are based on the high strain graphite fiber. The useful energy density is 79 Wh/kg and the energy densities at 100 percent operational and ultimate speeds are 105 and 155 Wh/kg respectively. These values are based on the rotor weight alone.

Table 8. Design Concept Estimates for Space Station Size Flywheels (Concentric Type)

Parameter	Operational Energy at 75% DOD	
	2.5 kWh	5.0 kWh
OD, in.	20.8	26.0
ID, in.	10.3	13.0
h, in.	5.2	6.5
W, lb	70	139
J, lb-in.-sec <sup>2</sup>	12.0	38.2
100% Op. Speed, RPM	40,100	31,800
E (75% DOD)	2.5	5.0
Useful Energy Density, Wh/kg (Rotor alone)	79	79

The tandem arrangement utilizes a relatively small diameter hub that is supported by means of a shrink fit within the rotor bore, as shown in Figure 5. Calculations show that it is feasible to employ a low weight metallic hub, a feature that greatly facilitates mounting of other components to the flywheel rotor. The tandem arrangement offers very significant advantages over the concentric type, namely enhanced design flexibility because it decouples the radial growth characteristics of the rotor bore and the motor/generator and does not restrict the selection of the latter's length/diameter ratio. In addition, cooling of the rotating portion of the motor/generator is facilitated due to its direct exposure to cooling sources. It also

permits greater bearing spans. The energy density that is estimated for the tandem design is somewhat less than that of the concentric type because of the presence of the hub. Performance estimates are listed in Table 9 for  $\beta$  ratios of .2 and .4. The respective useful energy densities being 76 and 70 Wh/kg.

Table 9. Calculated Energy Densities of Tandem Type Thick Ring Flywheel Rotors Constructed of High-Strain Graphite/Flexible Matrix Material

$\beta$	Rotor Energy Density (Wh/kg)		
	Ultimate	$10^5$ Cycles (100% DOD)	$10^5$ Cycles (75% DOD)
.2	146	101	76
.4	134	93	70

#### CONTAINMENT DESIGN APPROACH

Such high rotor performance levels indicate the growth potential offered by flywheels for space power applications. Recent experience has begun to show, however, that the weight penalties to provide for safe containment of a high energy rotor burst are likely to be prohibitive. It is important, therefore, to seek an early resolution to the issue of containment. Fortunately design and spin test experience, especially with ring/disk hybrid rotors, suggests that successful resolution of the issue may be obtained through proper rotor design.

The approach to this is to design rotors whose failure is accompanied by either zero or minor release of fragmentation. Such failure characteristics are theoretically obtainable in composite rotors by designing to a RRF mode or employing a flexible matrix in the ring construction. In the RRF mode, which is obtained with relatively thick, rigid-matrix rings, a circumferential crack is generated in the matrix between fibers. This does not significantly affect the circumferential strength of the ring but does disturb the rotor balance. The occurrence of RRF therefore produces a signal for initiating a safe shutdown of the rotor. There are at least two well documented instances in which RRF occurred in hybrid rotors (Tests No. 80-3 and -4 discussed previously). In each case the rotors were spun to considerably higher speeds after the occurrence of RRF. Subsequently they exhibited further ruggedness when they spun down to rest against the test chamber following separation from their drive shafts. Hence, there is good support for considering the RRF mode a practical basis for non-burst rotor design.

Flexible matrix rotor design has a potential for minor containment requirements because failure (CRF) should initiate very near the outside periphery of the rotor. In such an event, breaks in fibers would occur there, resulting in a disturbance of the rotor balance. This would provide a signal to shut down the unit. In the process it is quite possible that some minor fragmentation would be released from the outer surface of the rotor, thus necessitating use of a light-weight shield under certain

circumstances. The failure process, however, is considered to be self-arresting since the region radially inboard of the failure zone is at a lower stress level. This situation contrasts with the circumferential failure process involved in a rigid-matrix rotor ring. There, CRF occurs at the inside radius of the ring and material in the failed zone exerts its full centrifugal load on outer portions of the ring. Once this happens, the process can progress until the entire ring fails circumferentially. No test experience exists, however, for rotors utilizing flexible matrix rings.

Extensive testing is required to establish the practicality of high performance flywheel rotors whose failure is governed by zero or minor fragment-release modes. The technical grounds for expecting success are quite sound and the benefits of minimizing or eliminating the containment requirement manifold. If this can be achieved, a combined useful energy density of about 40 Wh/kg at 75 percent DOD (including motor-generator, bearings, and electronics) could result for the advanced space flywheel power system.

#### CONCLUSIONS

1. Of the two General Electric composite hybrid rotors that have been tested to ultimate speed, burst energy densities (and stored energies) of 67 Wh/kg (648 Wh) and 68 Wh/kg (656 Wh) have been obtained. Based on this, the  $10^5$  cycle operational energy density at 100 percent DOD is projected to be 40 Wh/kg.
2. One of the above flywheels (656 Wh, H8) completed 10,000 spin cycles, each involving a 6.5 minute duration and maximum and minimum stored energies of 217 and 54 Wh (75 percent DOD), prior to the ultimate speed test.
3. The pair of ultimate speed tests indicated no degradation in ultimate performance due to the  $10^4$  cycles.
4. The graphite/epoxy rings of the two rotors demonstrated ultimate energy densities of 114 and 116 Wh/kg. One of these (see conclusion no. 2) successfully completed 10,000 spin cycles at a maximum energy density of 38 Wh/kg (100 percent DOD) prior to the ultimate speed test. These data show the high potential of filament-wound graphite/epoxy ring components for use in flywheel space power systems.
5. Analysis of the high ultimate energy performance of hybrid rotors H6 and H8 has led to the conclusion that the circumferential strength of the T-300 graphite/Epon 826 epoxy composite rings used in the rotors is much greater than suggested by standard materials tests.
6. The low radial (transverse) tensile strength of filament-wound graphite/epoxy material limits the radial thickness to about 20 percent of the outside diameter. This can be extended somewhat by employing a radial compression pre-stress, as from a radial interference fit.
7. Large radial thicknesses are possible, however, when a flexible matrix is substituted for the standard rigid epoxy matrix of the ring. With this technique high energy densities are theoretically indicated.

8. Large, possibly prohibitive, penalties are associated with a requirement to contain a high energy composite rotor burst. A better approach is to design a rotor which is either fail-safe (no fragments released at failure) or releases a minor amount of fragmentation. Such failure characteristics are identified with particular rotor designs.
9. Utilizing a fail-safe rotor design and available 700 ksi graphite fibers in the ring component, advanced flywheels exhibiting operational energy densities as high as 105 Wh/kg (rotor alone and at 100 percent DOD) are indicated by design calculations.

#### REFERENCES

1. Notti, J.E., Cormack, A., III, and Schmill, W.C., "Integrated Power/Attitude Control System (IPACS) Study," Vol. I, NASA CR-2283, April 1974.
2. Notti, J.E., Cormack, A., III, and Schmill, W.C., "Integrated Power/Attitude Control System (IPACS) Study, Vol. II, NASA CR-2284, April 1974.
3. Coppa, A.P., "Energy Storage Flywheel Housing Design Concept Development", General Electric Company; LLNL, Report No. UCRL-15448, S/C 6624409, March 12, 1982.
4. Sapowith, A.D. and Handy, W.E., "Composite Flywheel Burst Containment", AVCO, Proceedings of the Mechanical, Magnetic, and Underground Energy Storage 1981 Annual Contractors' Review, Conf-810833, February, 1982.
5. Coppa, A.P. and Kulkarni, S.V., "Composite Flywheels: Status and Performance Assessment and Projections" Proceedings of the II European Symposium on Flywheel Energy Storage, G. Genta, Ed., Torino, Italy, May, 1983.
6. Nimmer, R.P., Torossian, K., and Wilkening, W.W., "Laminated Composite Disk Flywheel Development", General Electric Company Report No. SRD-81-051, Fourth Interim Report, Subcontract No. 2479309, January, 1981.
7. Nimmer, R.P., et.al., "Laminated Composite Disc Flywheel Development", General Electric Company Report No. SRD-79-016, January, 1979.
8. Nimmer, R.P., Torossian, K., and Hickey, J., "Laminated Composite Disk Flywheel Development", General Electric Company, Report No. SRD-80-091, 1980. (Also LLNL Report No. UCRL-15301, February 1980.)
9. Rabenhorst, D.W. and Wilkinson, W.O., "Prototype Flywheel Spin Testing Program", Johns Hopkins Applied Physics Laboratory; LLNL Report No. UCRL-15381, April, 1981.
10. Rotem, A. and Nelson, H.G., "Fatigue Behavior of Graphite-Epoxy Laminates at Elevated Temperatures", ASTM-STP-723, Fatigue of Fibrous Composite Materials, 1981.
11. Awerbuch, J. and Hahn, H.T., "Fatigue and Proof Testing of Unidirectional Graphite/Epoxy Composite", ASTM STP 636. Fatigue of Filamentary Composite Materials, 1977.
12. Davis, J.W. and Sundsrud, G.J., "Fatigue Data on a Variety of Non-Woven Glass Composites for Helicopter Rotor Blades", 34th Annual Technical Conference, 1979 Reinforced Plastics/Composites Institute, Society of the Plastics Industry, Inc., 1979.
13. Mandel, J.F., "Fatigue Behavior of Fiber-Resin Composites", MIT Research Report R81-2, April, 1981.



14. Kulkarni, S.V., Reifsnider, K.L., and Boyd, D.M., "Composite Flywheel Durability and Life Expectancy: Test Program," Proceedings of the Mechanical, Magnetic, and Underground Energy Storage 1981 Annual Contractors Review, U.S. Department of Energy CONF 810833, February 1982.
15. McLaughlin, P.V., Dasgupta, A. and Chun, Y.W., "Composite Failure Analysis for Flywheel Design Applications:", Villanova University; LLNL Report No. UCRL-15296, S/C 6448409, March, 1980.
16. Coppa, A.P., "Composite Ring - Disk Flywheel Design, Fabrication, and Testing", General Electric Company Document No. 83SDS4248, Final Report to Lawrence Livermore National Laboratory on Subcontract No. 6624409, Tasks 12-16, August, 1983.
17. Kirk, J.A., Studer, P.A., and Evans, H.E., "Mechanical Capacitor" NASA TN D-8185, November 1975.
18. Flanagan, R.C., Wong, J.M., and Munro, M.B., "Fibre Composite Rotor Selection and Design", 17th IECEC Proceedings, Vol. 4, pp. 1961-1966, August 1982.
19. Gupta, B.P. and Lewis, A.F., "Optimization of Hoop/Disk Composite Flywheel Rotor Designs", 1977 Flywheel Technology Symposium Proceedings, CONF-771053, pp. 111-118, October 1977.
20. Coppa, A.P., "Composite Hybrid Flywheel Rotor Development", Monthly Progress Report No. 6, LLNL Subcontract 6624409 Tasks 12-16, 28 February 1982.

### NOMENCLATURE

a,b	inside and outside radius of ring; $a/b = \beta$
B	bearing failure
CRF	circumferential ring failure
DOD	depth of discharge
DF	disk failure
E	energy
$E_C$	cost energy minus density
$E_D$	modulus of elasticity of disk material
$E_R$	modulus of elasticity of ring material
$E_{TR}$	modulus of elasticity of ring material in radial direction
$E_V$	volume energy minus density
$E_W$	weight energy minus density
$E_{\theta R}$	modulus of elasticity of ring material in tangential direction
h	height
$I_R$	polar moment of inertia
J	inertia
k	shape factor
P	interface pressure
RRF	radial (transverse) ring failure
S	ring/disk separation
V	rotor peripheral speed
$V_i$	maximum allowable speed
W	weight
$W_R$	weight of ring
$\beta$	ratio of inner to outer disk radius
$\delta$	radial interference
$\bar{\delta}$	unit radial interference; $\bar{\delta} = \delta/b$
$\nu_D$	Poisson's ratio for disk material
$\nu_R$	Poisson's ratio for ring material
$\rho$	mass density
$\rho_D$	density of disk material
$\rho_R$	density of ring material
$\sigma$	ultimate (operational) strength
$\sigma_B$	bearing strength
$\sigma_D$	strength of disk material

$\sigma_{DO}$

stress at center of disk

$\sigma_{rR}$

strength of ring material in radial direction

$\sigma_{\theta R}$

strength of ring material in tangential direction

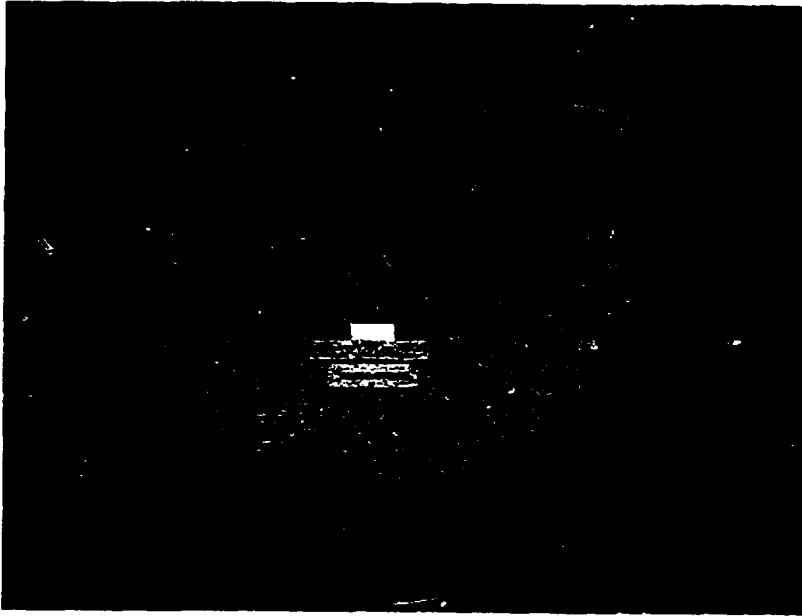
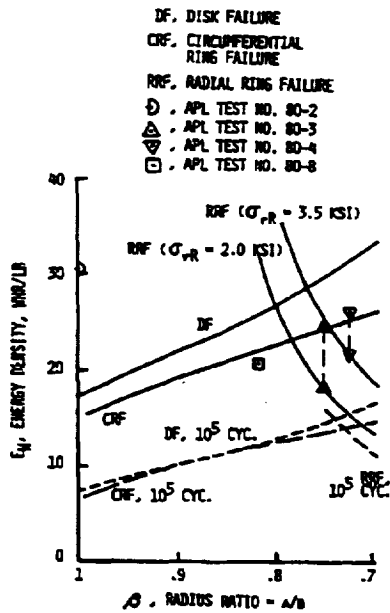


Figure 1.- Hybrid rotor no. H8-3M6-R14 after successful completion of 10,000-cycle 1083-hour spin test.



ORIGINAL PAGE IS  
OF POOR QUALITY.

Figure 2.- Hybrid rotor energy density vs radius ratio for governing failure modes ( $\delta = .002$ ).

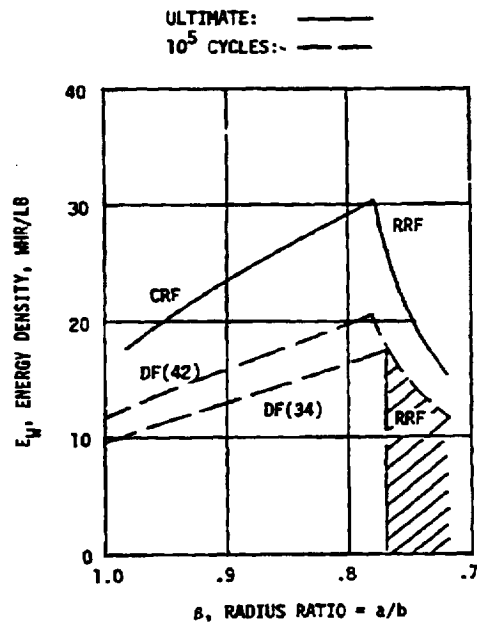


Figure 3.- Energy density vs radius ratio for improved hybrid rotor designs based on revised properties of Table 6.

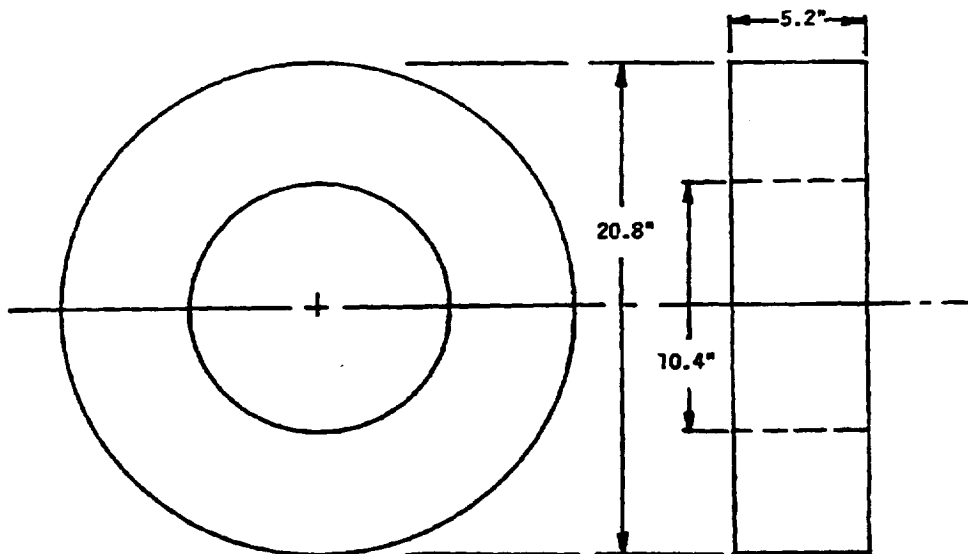


Figure 4.- Annular flywheel concept, concentric type (2.5 kWh). Rotor components mounted in bore.

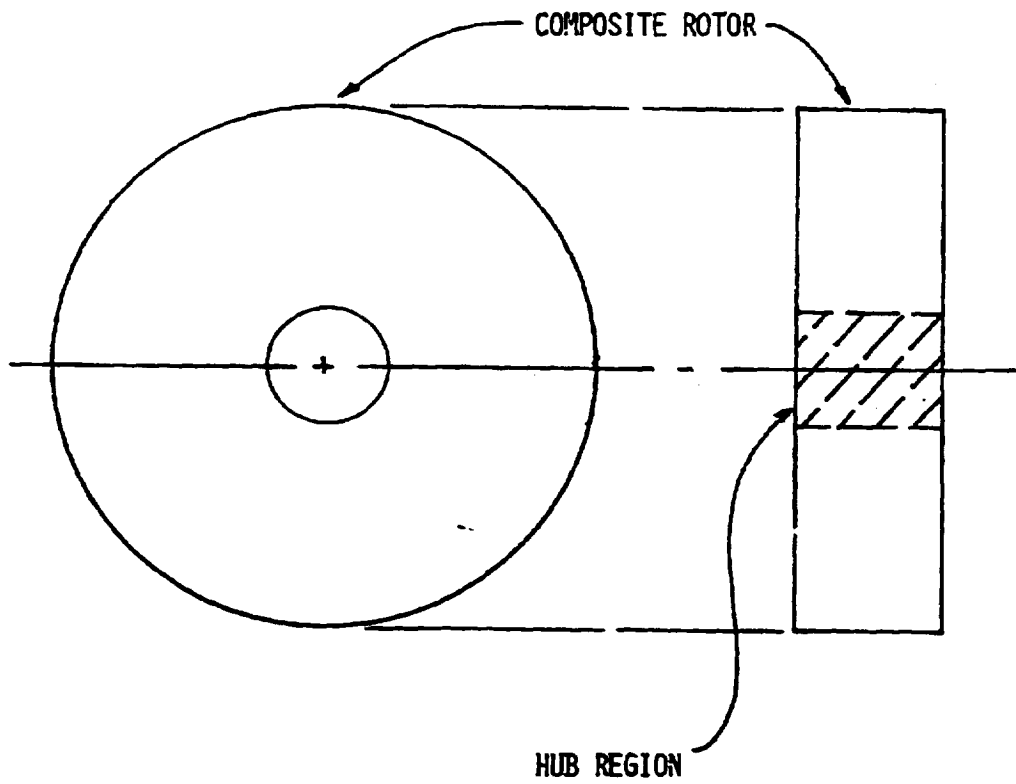


Figure 5.- Annular flywheel concept, tandem type, suitable for side mounting of rotor components.

N85

3868

UNCLAS

N85 13868 OR

THE  
MULTIPURPOSE  
COMPOSITE FLYWHEEL

B. R. Ginsburg  
Rocketdyne Division  
Rockwell International  
Canoga Park, Calif

PRECEDING PAGE BLANK NOT FILMED



## TWIN DISK COMPOSITE FLYWHEEL

The Twin Disk Composite Flywheel (Figure 1) represents a breakthrough in the state of the art of flywheels. It shows that the techniques that were developed at Rocketdyne to successfully design, fabricate and test high-speed rotating machinery (turbopumps) for rocket engines could be used to develop advanced flywheels. This flywheel not only demonstrates that successful mating of metal flywheel characteristics (high torque and ruggedness) and composite flywheel characteristics (lightweight and high energy density) can be achieved, but the unique design lends itself to easy adaptation to other configurations.



Figure 1

#### DESIGN CRITERIA

This flywheel was designed and fabricated under a DOE-Sandia contract (1978). It was the purpose of this contract to develop a composite flywheel for automotive use. The wheel was required to store between 1.0-5.0 kW-hr of useable energy to be dissipated through a 3:1 duty cycle. The envelope requirements were 0.6-m maximum diameter by 0.2-m maximum thickness. Two full-size, system ready units were made.

#### DESIGN CRITERIA

- USE NOMINAL MATERIAL PROPERTIES MINUS  $3\sigma$
- USE 2.0 FACTOR OF SAFETY (ULTIMATE)
- USE 1.5 FACTOR OF SAFETY (FATIGUE - 3:1 DUTY CYCLE)
- FLYWHEEL WEIGHT - 53 kg
- RATED SPEED - 22,000 RPM
  - 1.6 kW-hr ENERGY STORED
  - 30 W-hr/kg ENERGY DENSITY

## DESIGN FEATURES

- TWIN ALUMINUM DISKS
  - GIVES HIGH TORQUE CAPABILITY
- ALUMINUM MANDREL RING
  - AIDS FABRICATION
  - TRANSMITS TORQUE
- GRAPHITE/EPOXY RIM
  - HIGH ENERGY STORAGE
  - HIGH ENERGY DENSITY
- RADIAL PINS
  - CARRIES TORQUE
  - PERMITS RADIAL GROWTH



Figure 2

ORIGINAL PAGE IS  
OF POOR QUALITY

### FABRICATION, ASSEMBLY AND BALANCE

The aluminum parts were fabricated and assembled into a subassembly which was dynamically balanced. After the graphite/epoxy composite matrix was wound onto the wheel, the entire "composite flywheel" was dynamically balanced in bearings (Figure 3).

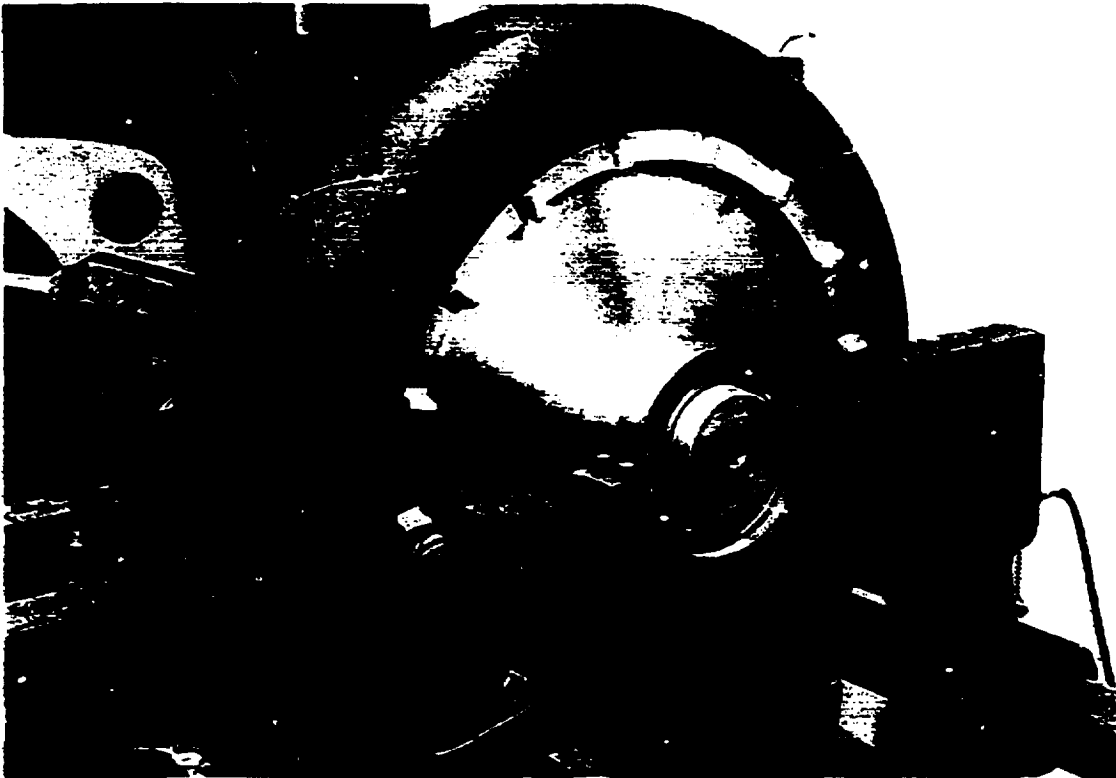


Figure 3

### TESTING AT DOE

The flywheel was tested by DOE at the Oak Ridge National Laboratory Spin Test Facility in August of 1980 and March of 1981. The results are summarized below

Test No.	Date	Top Speed RPM	Remarks
1	8/12/80	12,000	High-Speed Balance Checkout
2	8/14/80	17,040	Dynamically Stable
3	8/15/80	20,718	Dynamically Stable
4	8/18/80	6,000	Facility Checkout
5	8/19/80	22,000	Rated Operating Speed
6	8/20/80	22,920	30 minutes of successful operation over 22,000 RPM
7	3/05/81	6,000	Facility Checkout
8	3/06/81	15,000	High-Speed Balance Checkout
9	3/09/81	20,500	Test Terminated Pressure Rise
10	3/10/81	24,120	Test Terminated Facility Limitation
11	3/10/81	6,000	Data Verification

### TEST RESULTS

- DESIGN CONCEPT PROVEN
  - 11 TESTS AT DOE WITHOUT FAILURE
  - MAXIMUM SPEED OVER 24,000 RPM
  - OVER 2 kW-hr TOTAL STORED ENERGY
  - OVER 40 W-hr/kg ENERGY STORED (OPERATIONAL)
- HIGHER ENERGY VALUES NOW POSSIBLE
  - NEW MATERIALS (1978 VS 1985)
  - WIDER WHEEL - 2:1 ASPECT RATIO
  - 2:1 DUTY CYCLE

ORIGINAL PAGE IS  
OF POOR QUALITY

#### APPLICATIONS

The metallic twin disks allow this flywheel to be used in applications where a high torque capability is necessary. Attachment can be accomplished directly through couplings or splines, or a variety of clutches can be used (Figure 4).

#### HIGH TORQUE CAPABILITY

- ALLOWS DIRECT COUPLING WITH MOTOR/GENERATORS
- ALLOWS COUPLING TO SEPARATE MOTORS AND GENERATORS
- ALLOWS FOR DIFFERENT CHARGE/DISCHARGE RATES
- ALLOWS FOR HIGH POWER DENSITY DRAIN RATES

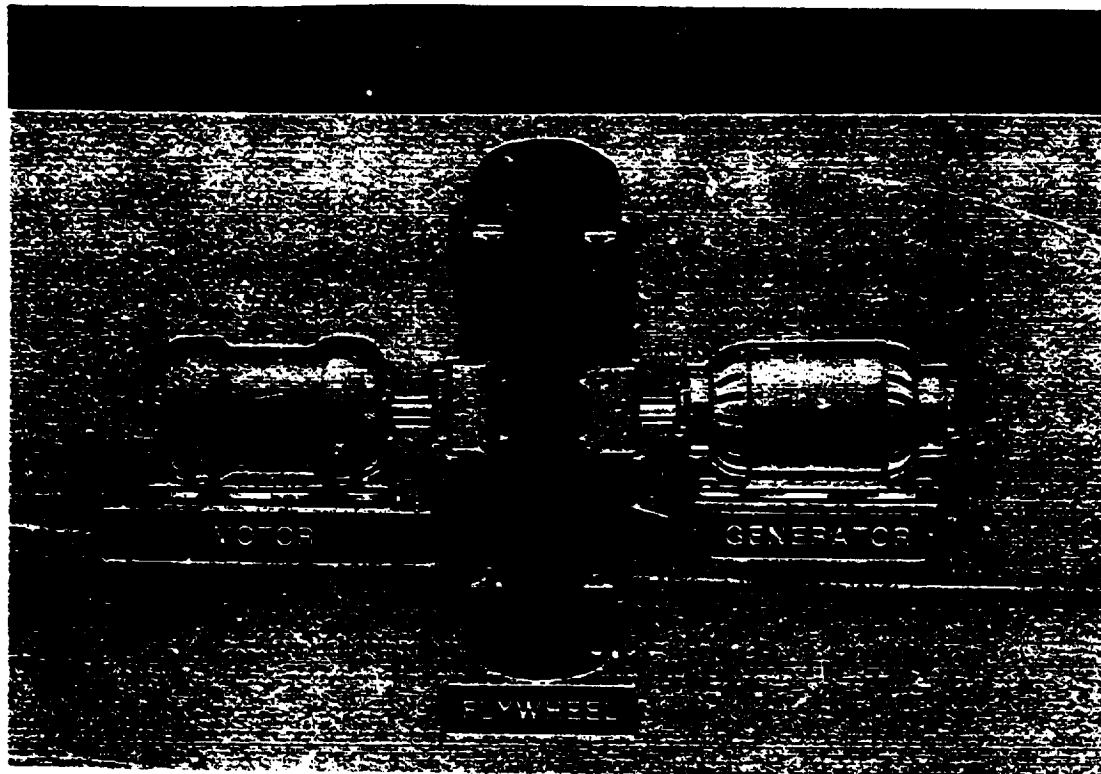


Figure 4

## SCALABLE AND STACKABLE

This design is both scalable and stackable. Design studies of similar wheels with energy storage capacities of 1 kW-hr to 1 MW-hr have been accomplished without difficulty. Identical disk profiles have been successfully stacked as part of Rocketdyne's RPE-13 Flywheel Power Module being used to power a coal mining shuttle car (Figure 5).

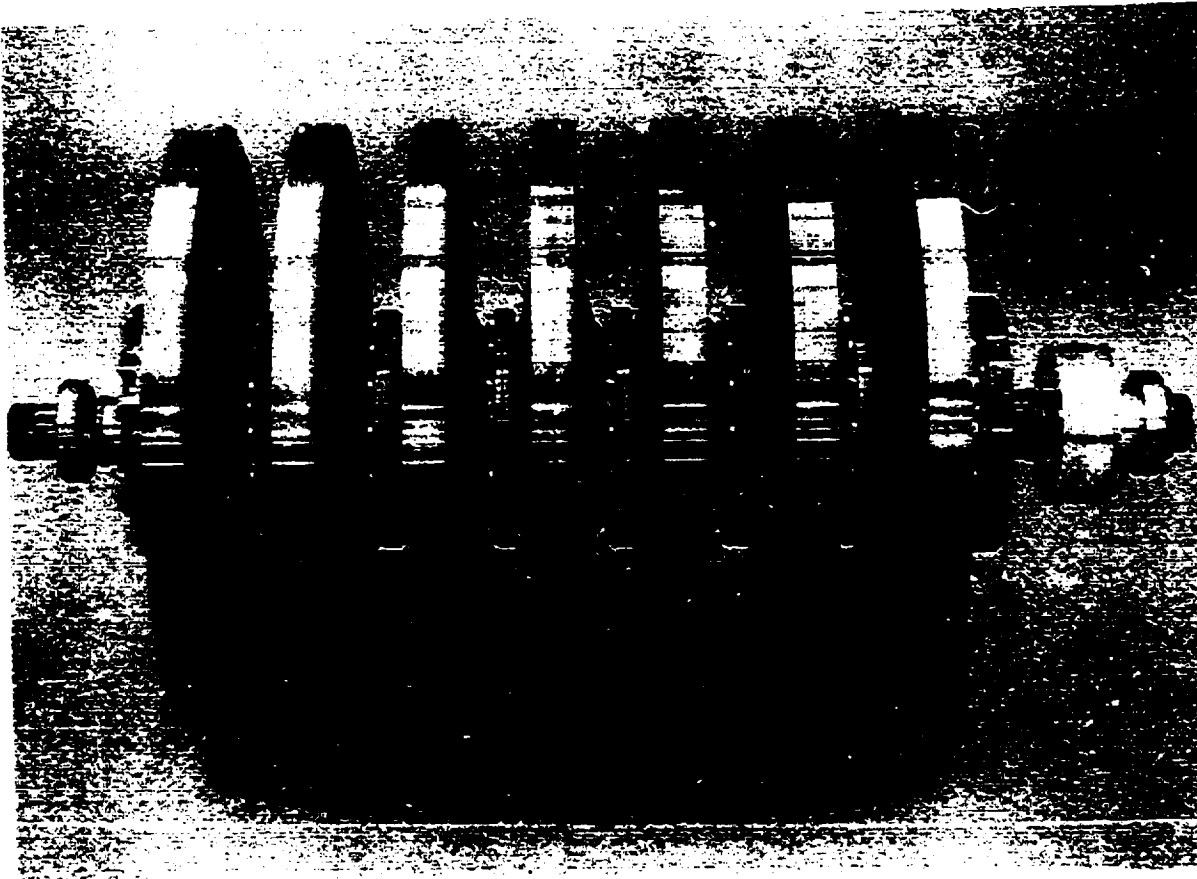


Figure 5

ORIGINAL PAGE IS  
OF POOR QUALITY

ADAPTABLE

ORIGINAL DESIGN  
OF POOR QUALITY

The unique design of this flywheel allows the side disks to be removed (Figure 6) leaving just the composite rim with the aluminum inner ring (Figure 7). This can then be readily adapted to other uses such as advanced AMCD or a brushless D/C motor/generator (Figure 8).



FIGURE 6



FIGURE 7

MOTOR/GENERATOR  
ELEMENT

CONTROL  
ELECTRONICS

FIGURE 8



## CONCLUSION

A composite flywheel has been designed, fabricated and tested by the same techniques used to successfully develop high-speed rotating machinery on various NASA programs. This flywheel is available for use in space-station proof-of-concept testing without further development.

- STATE-OF-THE-ART BREAKTHROUGH
- OVER 2 kW-hr STORED IN DOE TEST WITHOUT FAILURE
- HIGHER VALUES POSSIBLE NOW
- RUGGED CONSTRUCTION
- HIGH TORQUE CAPABILITY
- SYSTEM READY - DUAL BEARINGS
- SCALABLE
- STACKABLE
- ADAPTABLE
  - ADVANCED AMCD
  - ADVANCED BRUSHLESS MOTOR/GENERATOR
- AVAILABLE
  - FOR PROOF OF CONCEPT TESTING
  - WITHOUT FURTHER DEVELOPMENT

N85

3869

ENCLOS

N85 13869

D19

FLYWHEEL CONTAINMENT AND SAFETY CONSIDERATIONS

Anthony P. Coppa  
General Electric Company  
Space Systems Division  
Box 8555, Philadelphia, Pennsylvania

## INTRODUCTION

Considerable research and development work was directed during the past seven years to exploiting the large potential of flywheel energy storage systems [1-4]. These activities were spurred by the energy crisis and particular attention was focused on consumer passenger vehicle applications since these offered great promise of reducing petroleum fuel consumption on a world scale. In the United States, flywheel R&D programs were largely sponsored by the Department of Energy (DOE), through which the Lawrence Livermore National Laboratory (LLNL) played a principal role in directing and coordinating them. Under the Mechanical Energy Storage Technology (MEST) Project major advances were achieved in composite flywheel rotor design and fabrication technologies with a significant start in developing burst-containment design capability. A wide assortment of composite rotors featuring a variety of constructions and materials were produced during this effort. Table 1 lists some of these and identifies three generic rotor design categories, namely: rim, disk, and rim/disk hybrid types. In burst tests several rotors have demonstrated ultimate energy densities that approach the current DOE goal of 88 wh/kg for vehicular flywheels: The Garrett AiResearch multi-ring rim design obtained the best energy density, up to 79.4 wh/kg, and the General Electric ring/disk hybrid the best combination of weight and volumetric energy densities, i.e., 68.0 wh/kg and 115 kwh/m<sup>3</sup>. Also, progress was made in durability testing: A modified Garrett rotor design was tested for 2586 spin cycles at energy density levels between 44.1 and 11 wh/kg. The DOE goal for operational energy density is 44-55 wh/kg. Two General Electric flywheels survived 10,000 cycles at lower energy density levels and went on later to yield high ultimate performance, up to 68 wh/kg. In the area of operational safety, composite rotor burst and containment processes for a variety of rotor constructions are now better understood as a result of detailed studies of spin test data [5,6]. This led to definition of flywheel housing prototype designs.

In addition to obtaining high performance, composite has been preferred to metallic rotor construction because of the relatively benign containment processes that are associated with rotor burst. In the early stages of the MEST Project, this awareness was based principally on observation of post-burst debris which showed that composite rotors fragment to a much higher degree than metallic rotors and indicated a much lower capability to inflict damage on a containment housing. Much experience, however, was available with metallic rotor bursts which showed very severe containment processes. Estimates of containment weight requirements for metallic rotors often indicated values several times greater than the rotor weight itself. Although metallic flywheel rotors that are designed to release relatively low damage-potential fragmentation upon failure have been produced [7], such approaches were not emphasized in major MEST project developments that were aimed at transportation vehicle applications. Instead, composite construction was favored because of the promise of higher energy density and intrinsically safer containment.

Early assessments of composite-rotor containment processes led some to underestimate the need for substantial containment devices. Tests performed [8] during the past three years, however, have shown that composite-rotor bursts can produce impressive amounts of damage in heavy containment structures, although the damage is still well below that produced by a comparable metallic rotor burst. An optimum system would most likely incorporate rotor and containment housing designs which offer the best combination of performance indices (energy, density, durability, and cost). A fail-safe rotor, viz, one that fails in a non-burst mode, would be preferable to one that might have a higher energy density but simultaneously a catastrophic burst mode of failure.

Containment therefore became a strong driver in the development of a satisfactory vehicular flywheel system, and toward the end of the DOE program efforts were underway to perform experiments involving composite rotor bursts within realistic vehicular-type housings. The only such experiment that was conducted before termination of the program demonstrated the severity of a high energy burst containment process, but circumstances did not provide an opportunity to explore the problem further and develop a design solution. It is judged that acceptable housing designs for ground transportation vehicles could have been developed, drawing upon the lessons learned from the first containment test and others that would have followed had the program continued. It is less certain, however, whether containment of a high energy burst is a feasible design requirement to satisfy in a space flywheel system, in view of a much lower tolerance for the associated weight penalty. The importance of minimizing the degree of containment requirements in space systems through use of essentially 'fail-safe' or 'limited failure' rotor designs has become increasingly recognized and is a subject that deserves early and adequate attention.

#### THE FLYWHEEL SAFETY ISSUE

The issue of flywheel safety is a subject of growing interest. With greater quantification of composite rotor burst effects and corresponding containment requirements, attention is being focussed on possible development of 'limited failure' or 'fail-safe' rotor designs. In response to this concern, two specific design approaches based on the General Electric hybrid flywheel which feature such failure properties were outlined [9]. The hybrid flywheel consists basically of a central disk and a filament-wound ring interference-fitted to the disk at its periphery. In recent designs, the ring has an inside to outside radius ratio ( $\beta$ ) of .8. Spin tests performed on such rotors have demonstrated good ultimate energy densities ( $\sim 68$  wh/kg). The performance for this and other possible designs is shown in Figure 1, in which energy density is plotted against  $\beta$  for governing failure modes. Two sets of failure envelopes are shown, namely, short-time ultimate failure (solid curves) and  $10^5$  cyclic fatigue (dashed curves). For  $\beta = .8$ , the predicted failure modes are circumferential ring failure (CRF) and disk failure (DF) relative to ultimate and cyclic conditions respectively. Ultimate speed tests have in fact verified the CRF prediction. It would be desirable to avoid either type of failure in a space application because the associated containment weight penalty might be excessive. Designs based on values of  $\beta < .77$ , however, would be limited by the non-burst radial ring failure (RRF) mode for both conditions and at least theoretically would not require containment. Such a benefit would be gained at the expense of lower performance as evident in the Figure.

In order to establish an assured fail-safe composite rotor design practice along the lines illustrated in the previous example, material design properties will have to be established with greater reliability than presently available. Hence, materials specimen type as well as rotor spin tests, especially under cyclic conditions, should be initiated early in the process of developing composite rotors for space flywheel systems.

The above example is made to illustrate one of the trade-offs between performance and safety that can be systematically obtained through composite rotor design. Such an approach should be superior to one in which the rotor performance is merely

derated by a 'safety factor' in the attempt to obtain fail-safe operation because the latter practice would not intrinsically address a non-burst failure mode. Hence, an unresolved concern would exist about rotor safety for such a design in view of a possible, albeit improbable, burst failure event.

The second approach described in [9] illustrates the 'limited failure' rotor design technique. The example involves a radially thick filament-wound composite rotor ring which utilizes a flexible instead of a rigid matrix and its construction. For such a rotor, the limiting stress is confined to a relatively narrow radial zone at the outer periphery. Stresses inboard of this region are relatively low. Also, because of the large strain tolerance of the matrix, radial stresses would be held within acceptable bounds. Failure of such a rotor is expected to involve release of fragmentation only from the restricted region of maximum stress. The failure process would be self-arresting because of the lower interior stresses. Hence, containment would be required only for a relatively small portion of the rotor and the associated weight penalty would be acceptably low. Such an approach offers a high potential for energy storage performance in a space rotor. Spin tests, however, have not as yet been performed on such a design although rotors embodying flexible-matrix rings were produced under the DOE program.

By means of such design approaches as illustrated above, the issue of flywheel safety can be addressed systematically and ultimately resolved. The challenge will be to develop 'fail-safe' and/or 'limited-failure' rotor designs whose energy storage performance is not unduly compromised. Obviously, considerable testing will be required to demonstrate design reliability.

At least for the 'limited-failure' design approach, containment will have to be provided. Relative to the 'fail-safe' rotor approach, it remains to be seen whether in fact containment can be totally dispensed with. Design definition of containment requirements relative to the proposed rotor developments will be an important factor in determining the course of these developments. Hence, further growth in containment technology is seen to be vitally necessary to developing safe, high performance space flywheel systems.

#### PREVIOUS CONTAINMENT TECHNOLOGY DEVELOPMENTS

Most of the effort applied to developing containment design technology under the DOE/LLNL program was devoted to the radial burst problem [5]. This involves the response of the containment device (ring) to the radial impact of the bursting rotor and is aimed at defining the containment ring design. More recently, attention was given to the related problem of axial effects produced immediately subsequent to the radial burst actions [10]. These secondary effects can produce large loads on other parts of a containment housing, especially the end walls.

##### Radial Burst

Results of burst tests of composite rotors which had been performed at the Johns Hopkins U. Applied Physics Laboratory (APL) [8] were studied. The tests, listed in Table 1, involved a variety of rotor materials, constructions, and failure modes. The test results were especially useful because the rotors released a substantial and defined amount of fragmentation within containment rings that

were not excessively massive. Consequently, the rings were substantially deformed in the more severe bursts, while in the less severe ones, the rings, although not detectably deformed, nevertheless permitted deduction of an upper bound of containment severity. The tests provided a data base which helped in the development of the containment analysis.

When interacting with a containment ring, metallic fragments due to their material isotropy can exert contact pressures that exceed their yield stress. Also because of their high toughness, they typically remain intact during the entire process, thereby maintaining high bearing and shearing pressures. In contrast, composite fragments because of their relatively low transverse and interlaminar strengths cannot exert such high pressures. When pressures induced in the fragment exceed these strength limits, the matrix can be expected to break up, thereby releasing fibers or ribbons of fibers (filament-wound construction) or local delamination and crushing (laminated construction, edge loading). Rapid heating at the fragment/ring interface due to high pressure, high speed sliding also contributes to rapid fragment break-up. In some constructions, the initially released fragments may already be in a highly broken state prior to engagement.

Since the fragments are basically solid, as opposed to porous bodies, such action may be accompanied by the forcible ejection of material laterally from the fragment as the remaining fragment moves radially toward the containment structure. If the transverse strength is low, the fragment may continue this motion until its mass is expended. If the strength is high, however, the ejected mass may be appropriately less and a substantial portion of the original fragment remains after its radial velocity relative to the containment surface has vanished. Such residual fragments may continue to move tangentially after this time and exert centrifugal pressures against the containment ring.

An analysis, called the crushing fragment containment analysis (CFCA) was developed to calculate the containment ring response to such a loading process and is described in detail in [5]. Only a brief account is given here to provide a basis for describing the calculated results. The analysis (which neglects friction effects) assumes that at failure the rotor releases an axially symmetric distribution of fragments (See Fig. 2-I) which contacts the containment ring after moving through the radial clearance space,  $c$  that initially exists between the rotor and ring. At this instant (time,  $t = t_0$ ) the centroid of the fragment system has radial and tangential velocities  $V_{R0}$  and  $V_{\theta 0}$  respectively (Fig. 2-II). Subsequently, the fragment is further assumed to undergo a continuous radial crushing process, provided that the interface pressure that exists between the fragment and the ring exceeds a parameter  $p_0$ , called the apparent fragment crushing strength (Fig. 2-III). During the crushing process, the fragment system is assumed to eject material from its lateral (axial) faces, thereby losing mass and radial thickness, and its centroidal velocity,  $V_{Rt}$  may have increased or decreased from its initial value. Also the containment ring may have developed a velocity,  $\dot{R}_t$ . The interface pressure will be greater than  $p_0$  as long as  $V_{Rt} > \dot{R}_t$  (Fig. 2-III). When the quantity  $V_{Rt} - \dot{R}_t = 0$ , the fragment system remains rigid ( $t=t_p$ ). This begins the rigid phase (Fig. 2-IV), during which the fragment has only tangential velocity ( $V_{\theta p}$ ) relative to the ring and exerts centrifugal pressure against it. If  $V_{Rp} = 0$ , then the burst containment process is ended at this time, since both fragment and ring will be radially at rest. If

however  $V_{Rp} (=R_p) > 0$  is at the beginning of the rigid phase, then the ring (with the fragment still rotating relative to it) will either come to rest ( $t=t_f$ , Fig 2-V) within the allowable radial growth (containment), come to rest beyond the allowable growth but within the ultimate tensile growth (unacceptable containment), or exceed the tensile growth limit (non containment).

The interaction geometry is illustrated in Fig. 3 which shows how the fragment proceeds to move into the ring. The initial state of the fragment is indicated by its bounding radii  $R_I$  and  $r_{II}$ , thickness  $a_I$ , and centroid position,  $r_I$ . The initial total, radial and angular velocities are  $V_0$ ,  $r_I$ , and  $\omega_I$  respectively. These same quantities apply everywhere around the circumference since the fragment geometry and motion are considered to be axially symmetric. The various dashed lines indicate the trajectories of the fragment inner surface and mass center and the containment ring as time progresses. At a general instant, the fragment thickness is shown as having a centroidal radius,  $r$ , thickness,  $a$ , angular speed,  $\omega$ , and total and radial speeds  $V$  and  $r$ . It is noted that although  $V$  is always less than  $V_0$ , the radial speed may increase above the initial radial speed for a while. The final state of the fragment is depicted by the residual thickness,  $a_p$ , at the point where its radial velocity equilibrates with that of the containment ring.

The motion of the entire fragment is therefore characterized by that of the general mass center,  $m$ , whose variable mass per unit circumference  $2\pi$  is:

$$m = 2 \rho_f h(R-r), \quad (1)$$

where  $\rho_f$  is the distributed fragment density. The equations of motion of the fragment and containment ring (neglecting friction) are:

$$\text{Fragment: } \ddot{r} + \left( \frac{\dot{R} - \dot{r}}{m} \right) \dot{m} = \frac{H^2}{r^3} - \frac{p_0 h}{m} \quad (2)$$

$$\text{Ring: } \ddot{R} = \frac{2\pi}{M_C} \left[ (\dot{R} - \dot{r}) \dot{m} r + p_0 h r - \sigma T L_e \right] \quad (3)$$

where the single and double dots indicate first and second time derivatives respectively;  $H = \omega^2 r^2 = \text{constant}$ ;  $p_0$ , fragment crushing strength;  $h$ , rotor axial length;  $\sigma$ , dynamic tensile strength of ring;  $T$ , ring thickness; and  $M_C$  and  $L_e$ , the effective mass and length of the ring. Hence, the fragment is treated as a variable mass which transfers momentum loads,  $(R-r)\dot{m}$  and pressure loads,  $p_0 h$  (both per unit circumference) to the containment ring. The ring resists these loads by its plastic tensile resistance  $\sigma T L_e$ .

The initial conditions are:

$$\begin{aligned} \text{Fragment: } r(0) &= r_I, \quad \dot{r}(0) = V_{rI} \\ \text{Ring: } R(0) &= R_I, \quad \dot{R}(0) = 0 \end{aligned} \quad (4)$$



During the ensuing process, the condition  $\dot{r}_p = \dot{R}_p = V_{Rp}$  is reached, at which time and thereafter, the fragment is considered to be rigid. Subsequently, the fragment continues moving circumferentially at angular velocity  $\omega_p$  and exerting centrifugal pressure loading on the ring:

$$p_p = \frac{m_p (\omega_p r_p)^2}{F_p h} \quad (5)$$

During this time the radial motion of fragment and ring is governed by:

$$\ddot{R} = \frac{2\pi}{(M_c + M_p)} [p_p h r_p - \sigma T L_e] \quad (6)$$

where  $M_p = 2 \pi r_p m_p$ .

For present purposes, equation (6) was solved assuming the bracket term to be constant. Although not necessary to do this, it is conservative and it was convenient to do so. Hence the final time at which the radial velocity ceases is:

$$t_f = t_p + \frac{M_c + M_p}{2\pi} \left[ \frac{V_{Rp}}{\sigma T L_e - p_p h r_p} \right] \quad (7)$$

and the maximum radial deflection of the ring:

$$\Delta R_{max} = R_p - R_I + 1/2 V_{Rp} (t_f - t_p) \quad (8)$$

The ring deflection,  $\Delta R$ , applies to the effective length,  $L_e$ , which depends on the ring overhang/thickness ratio,  $a/T = (L-h)/2T$ . As described in [5],  $L_e = L$  for  $a/T \leq 3$  (narrow rings) and  $L_e = h+6t$  for  $a/T > 3$  (wide rings). These distinctions are based on [11]. Physical evidence shows that the axial deflection profile has a peak at the center of the ring, when the rotor is centrally situated. The peak deflection  $\Delta R'$  is estimated as follows [5]:

$$\text{Narrow Rings: } \frac{\Delta R'}{\Delta R} = \frac{h + 2a}{h + 2a(1-a/6T)} ; \text{ Wide Rings: } \frac{\Delta R'}{\Delta R} = \frac{h+6T}{h+3T} \quad (9)$$

CFCA has yielded some very interesting features of containment processes of composite rotors, features which appear plausible, especially when compared with experimental evidence of fragmentation as obtained for rotors of various constructions. The following results illustrate some of these features.

Figures 4 and 5 show plots of  $r$ ,  $\dot{r}$ ,  $R$ , and  $\dot{R}$  vs. time for the complete burst of a 0.25 kw.hr laminated glass/epoxy disk rotor, the principal differences being the fragment strength and ring thickness values:  $p_0 = 0$  and  $T = 0.22$  in. (Fig. 4)

and  $p_0 = 12$  ksi and  $T = 0.35$  in. (Figure 5). In each case,  $\dot{r}_I = 3847$  in/sec. initially (which corresponds to an initial radial clearance,  $c = 0.25$  in.) and subsequently rises to a peak value. The peak value of  $r$  is larger for  $p_0 = 0$  and occurs at a later time than for  $p_0 = 12$  ksi. Also,  $r$  approaches closer to  $R$  for  $p_0 = 0$  such that at the equilibration condition,  $\dot{r} = \dot{R} = V_{Rp}$ , the residual fragment thickness,  $a = 2(R - r)$  is much smaller than that of the stronger fragment. This is typical of fragment behavior as revealed by CFA. It is noted that even though  $p_0 = 0$ , substantial deformation is produced in the ring. This, of course, is attributable to the fragment momentum loading.

Another interesting result is to show that fragments having low strength can transmit substantial deformation to the ring even when the initial radial clearance is zero. An example is illustrated in Figure 6, which pertains to the same conditions as the previous figures except  $p_0 = 6$  ksi,  $T = 0.24$  in., and  $c = 0$ . Here  $\dot{r}$  is initially zero (because of the zero clearance) but rises to a peak value of 4,870 in/sec.  $\dot{R}$  remains at zero for the first 400  $\mu$  sec. and rises thereafter to a peak value of 1,570 in/sec., almost as high as for the case shown in Figure 4. The maximum ring deflection,  $\Delta R = 0.62$  in., compared to 0.60 in. (Figure 4). Since for these two cases, the ring thicknesses,  $T$ , are almost identical, it is seen that the effect of the higher fragment strength tends to be offset by the smaller clearance value.

The CFA was used to analyze the radial burst containment behavior of a variety of composite flywheels that had been spin tested [8]. The tests were performed within the confines of a steel ring which was used primarily to protect the test chamber from damage. To satisfy this need and also permit access to and visual coverage of the test chamber interior during the test, the radial and axial spaces between the flywheel and chamber walls were much larger than is representative of a practical containment housing design. Such tests provided the only available experimental base for studying composite rotor containment effects, however, and were so utilized despite the fact of their affording only a rough simulation of a realistic environment. Within these limitations, the CFA when applied to the tests permitted an evaluation of the apparent fragment crushing strength,  $p_0$  for such rotor components as laminated glass/epoxy and graphite/epoxy disks, chopped-glass fiber/SMC molded disks and filament-wound graphite/epoxy and aramid/epoxy rings. The resulting values of  $p_0$  which are dependent on the orientation of the composite component relative to the radial direction as well as the radial impact speed are listed in Table 2 along with other test data such as radial clearance  $C$ , and radial fragment speed at initial contact,  $V_{RI}$ . It is to be expected that the resulting values of  $p_0$  are affected by the testing environment as noted above and that they might be significantly different if evaluated in a more representative containment space. For example, two effects of excessive radial clearance would exert opposing influences on the value of  $p_0$ , namely, (1) it would facilitate the axial ejection of debris from the fragment crushing site and yield a lower value of  $p_0$  and (2) it would result in a larger radial fragment impact velocity and hence a higher value of  $p_0$ .

The two tests listed in Table 2, which involved aramid fiber/epoxy rings, viz. the Brobeck and Garrett flywheels, provide an example of how the evaluation of  $p_0$  is affected by test conditions. In the Brobeck rotor test, the clearance,  $C$

was 31 percent of the outside rotor radius whereas in the Garrett rotor test the corresponding value was only six percent. Also, the ratio of C to the rotor axial length for the two cases was 43 and 36 percent respectively. Assuming the material effects to be similar in the aramid/epoxy rings of these rotors, the above values would favor a lower evaluation of  $p_0$  for the Brobeck test on the basis of (1) above. On the other hand, the higher radial fragment speed in the Brobeck compared to the Garrett rotor tests (see Table 2) would contribute to a higher value of  $p_0$  for the former case. The Brobeck test correlation yielded a zero value of  $p_0$  and even further indicated that the rotor rim engaged the containment ring in discrete stages rather than all at once. For the Garrett test  $p_0$  was found to be 12,000 psi, indicating that the rim fragments engaged the ring in a much more contiguous state and required very high interface pressures to break them down.

An example of how the CFCA test correlation is done is given for the Garrett test. Calculations of peak containment ring growth were made for several assumed values of  $p_0$  which ranged from 0 to 21,000 psi. Results are shown in Figure 7 in which  $\Delta R'$  (equation 9) is plotted against  $p_0$ .  $\Delta R'$  (= .75 in.) of the actual ring was determined [12] by measuring the circumference near the ring axial center where the maximum deflection was present. A value of  $p_0$  equal to 12,000 psi was then picked off from Figure 7 for the measured value of  $\Delta R'$ .

An example of how the CFCA has been applied to design estimation is shown in Figure 8 which presents estimates of containment ring weight,  $W_C$  relative to the complete burst of a laminated glass/epoxy disk rotor at a stored energy of .25 kwh and whose OD and weight are 18 in. and 28.9 lb., respectively. The estimates are based on  $p_0 = 6$  ksi (rather than  $p_0 = 0$  as listed in Table 2), a conservative value to account for possible effects of fragment compaction in the small radial clearance assumed (three percent of rotor outside radius).  $W_C$  is plotted against the maximum radial ring growth for several ring materials. An advanced design incorporating an inner metallic liner over wound aramid fiber yarn is also shown. The dots on the curves indicate the maximum allowable ring growth which corresponds to an average tensile strain of 10 percent for the metallic rings and four percent for the aramid fiber/6061 aluminum ring. The burst performance of the latter ring construction is indicated to be 34 wh/lb (burst energy divided by ring weight). In contrast to this the performance of a low carbon steel ring (dynamic tensile strength of 85 ksi) is about 10 wh/lb.

#### Axial Effects

Although previous spin tests had shown evidence of important axial loading effects resulting from composite rotor bursts, not until the containment test of a General Electric hybrid flywheel were such effects amenable to detailed study. This particular test involved a high energy burst at a stored energy level of 648 wh within an experimental vehicular type housing and it remains the only such test ever performed. The housing failed to contain the burst due apparently to large axial loading effects that were further aggravated by asymmetric burst conditions. The containment ring which was a separate component within the housing assembly was, on the other hand, relatively unaffected by the burst except for small permanent out-of-roundness and radial expansion deformations.

A method for estimating the axial loads transferred to the housing end walls was devised using the crushing fragment analysis. In the CFCA the fragment system mass loss is accommodated by the axial ejection of crushed material, as previously noted. An upper bound estimate of the axial loading due to the flow of ejecta was made by assuming that the radial momentum of the entire crushed mass is conserved in the corresponding axial flow. The momentum of the crushed mass is obtained from the CFCA by summing up the products,  $\bar{V} \Delta m$  of the mass lost,  $\Delta m$ , in a given time interval and the average radial speed,  $\bar{V}$  of the contiguous fragment system at the beginning and end of the time interval. Actually, only a portion of the mass-loss momentum would be transferred to the end walls because some momentum would be dissipated in turning the velocity vector from the radial to the axial direction. The mass-loss momenta contributed by the rotor ring and disk components are plotted against time in Figure 9. The time base only signifies duration and does not chronologically relate the ring and disk portions. The contribution of the ring is quite small compared to that of the disk. This reflects the fact that the crushed mass of the ring is only 27 percent of the disk crushed mass. The disk contribution is shown for assumed values of  $p_0 = 0$  and 6 ksi. It is noted that the mass loss momentum corresponding to  $p_0 = 6$  ksi is the larger of the two. This is because the crushed mass is less for larger values of  $p_0$ , a fact due to the existence of the residual fragment (see Figure 2-V). This relationship holds even when the ultimate breakdown of the residual fragment is considered. For very large values of  $p_0$ , which characterize a rigid fragment system, the mass-loss momentum becomes negligible and hence the axial momentum associated with it as well. This behavior models that of rigid burst fragments which produce large radial loading effects but very small axial effects (assuming the motion remains in the plane of rotation).

The axial momentum as derived above from the mass-loss momentum can be applied to the end wall structures as an impulse load. This is justifiable because the duration of the crushing process is likely to be small compared to the period of the fundamental flexure vibration mode of the end wall. This was done in studying the behavior of the experimental housing during the General Electric hybrid rotor containment test. It was found the axial load due to the rotor ring mass-loss momentum was large enough to produce relatively minor plastic deflection of the end wall but insufficient to cause the observed level of damage. The load due to the disk mass-loss momentum, however, was found to be greater than necessary to produce damage.

It is noted that the above assessment of axial load effects represents but an initial attempt based on very limited test experience. It is viewed as being an overestimate of the load magnitude that can result from the primary breakdown of a composite rotor during the containment process. Other mechanisms are possible such as fragment debris compaction, which might produce large, localized loads and damage.

## CONCLUSIONS AND RECOMMENDATIONS

1. The preferred approach to developing high performance space flywheels is to utilize 'fail-safe' or 'limited-failure' rotor designs in order to minimize containment requirements. The penalty of having to contain a complete rotor burst, on the other hand, is very likely to be prohibitive.
2. 'Fail-safe' or 'limited failure' rotor concepts are available and their development should be pursued as a first step toward development of the flywheel power system. To establish assured designs will require a considerable extension of the mechanical properties data base of candidate rotor materials. Cyclic spin testing (adequately instrumented) of rotors or major rotor components should be emphasized.
3. Until assured 'fail-safe' rotor performance is demonstrated, containment is likely to be a design requirement for a manned environment. Meanwhile, containment requirements should be defined, where possible, on the basis of the failure modes of 'limited-failure' type rotor designs and appropriate shields designed.
4. Containment design technology is presently inadequate for defining an optimum housing design. The crushing fragment containment analysis (CFCA) can be applied to making preliminary designs which then should be subjected to rotor burst test conditions as a means of developing efficient hardware.
5. Containment technology development should be continued further, especially by means of coordinated experimental/analytical investigations of composite rotor containment test behavior. In support of this, rotor spin testing should be performed within a containment housing whenever possible.

## ACKNOWLEDGEMENT

This work was sponsored by the U.S. Department of Energy through the Lawrence Livermore Laboratory. The author gratefully acknowledges Drs. Satish V. Kulkarni and Carl Walter of the Lawrence Livermore Laboratory and Mr. J. F. Martin of the Oak Ridge National Laboratory (ORNL) for their generous support and Messrs. W. O. Wilkinson of Johns Hopkins University Applied Physics Laboratory, E. F. Babelay of ORNL, E.L. Gray of General Electric Space Systems Division, and to Dr. R. S. Steele, formerly of ORNL, for their technical contributions.

#### REFERENCES

1. "Proceedings, 1977 Flywheel Technology Symposium", U.S. Department of Energy, CONF-771053, March 1978.
2. "Proceedings, 1980 Flywheel Technology Symposium" U.S. Department of Energy, CONF-801022 (1980).
3. "Proceedings, Mechanical, Magnetic and Underground Energy Storage 1980 Annual Contractors' Review," U.S. Department of Energy, CONF-801128, November 1980.
4. "Proceedings, Mechanical, Magnetic and Underground Energy Storage 1981 Annual Contractors' Review," U. S. Department of Energy, CONF-810833, February 1982.
5. Coppa, A. P., "Energy Storage Flywheel Housing Design Concept Development", Lawrence Livermore National Laboratory, UCRL-15448, March 1982.
6. Sapowith, A.D., and Handy, W.E., "A Composite Flywheel Burst Containment Study", Lawrence Livermore National Laboratory, UCRL 15452, April 1982.
7. Davis, D., and Hodson, D., "Rocketdyne's High-Energy Storage Flywheel Module for U.S. Army", 1977 Flywheel Technology Symposium Proceedings, CONF-771053, UC-94b, 96, March, 1978.
8. Rabenhorst, D.W.; Wilkinson, W.O., "Prototype Flywheel Spin Testing Program", Johns Hopkins University, Applied Physics Laboratory Report No. SDO 5988, also UCRL-15381 (Lawrence Livermore National Laboratory, April 1981.
9. Coppz, A.P., "General Electric Composite Ring-Disk Flywheel: Recent and Potential Developments". Proceedings of the NASA Flywheel Inertial Energy Storage Workshop, February 7-9, 1984.
10. Coppa, A.P., "Flywheel Containment Design and Technology Developments", Proceedings of the DOE Physical and Chemical Energy Storage Annual Contractors' Review Meeting, CONF-830974, September 1983.
11. Hagg, A.C. and Sankey, G.O., "The Containment of Disk Burst Fragments by Cylindrical Shells", ASME Journal of Power, April 1974.
12. Wilkinson, W.O., "Final Report, Flywheel Burst Test Program, APL Spin Test Facility", Johns Hopkins University, Applied Physics Laboratory, Report No. JHU/APL AEO-83-57, June 1983.

Table 1. Flywheel Rotors Involved in the Data Correlation (8)

Rotor Description	$d_o$ in.	$W_R$ lb.	$KE_B$ kwh	$\omega_B$ rpm	Failure Mode	$W_F$ lb.
Hybrid Rotor: FW Graphite/Epoxy Ring; Laminated S-2 Glass/Epoxy Disk (General Electric)	17.68	23.3	0.459	35,040	Outer Ring Rupture	6.34
Disk Rotor: Laminated S-2 Glass/Epoxy Disk (LLNL)	15.00	5.2	0.156	49,320	Complete Disk Burst	5.2
Hybrid Rotor: FW Graphite/Epoxy Outer Ring; Molded Chopped Glass/SMC Disk (Owens Corning)	24.00	28.5	0.414	21,620	Complete Burst of Rim and Disk	28.5
Wound-Rim Rotor: FW Kevlar 49/Epoxy, Glass/Epoxy (Brobeck)	13.76	24.5	0.608	48,120	Rupture and release of 70% of Kevlar49/Epoxy Rim	6.76
Disk Rotor: Varying Thickness, Laminated Graphite/Epoxy	24.00	11.8	0.306	34,940	Complete Disk Burst	11.8

$d_o$ , OD,  $W_R$ , rotor weight;  $KE_B$ , energy at burst,  $\omega_B$ , burst speed,  $W_F$ , total fragment weight.

Table 2. Values of  $p_o$ , Fragment Crushing Strength as Obtained from Data Correlation of APL Rotor Burst Tests

Material	Form	Impact Direction	$P_o$ (psi)	C (in.)	$V_R$ (in/sec)
Graphite/Epoxy	Filament Wound Ring	Transverse	20,000	4.62	22,900
	Laminate	Longitudinal	45,000	1.50	15,790
S-2 Glass/Epoxy	Laminate	Longitudinal	0	1.50	16,470
Kevlar <sup>®</sup> 49/Epoxy	Filament Wound Ring	Transverse	0	2.12	21,540
		Longitudinal	12,000	0.75	12,000
Chopped Glass/SMC	Molding	Longitudinal	5,000	1.50	9,880

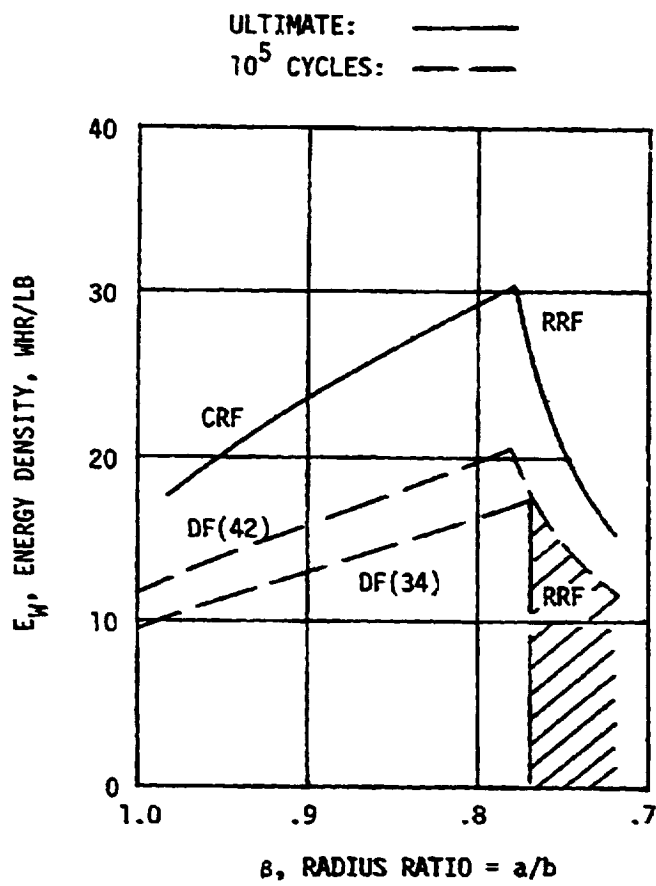
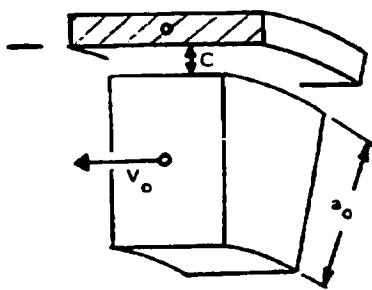
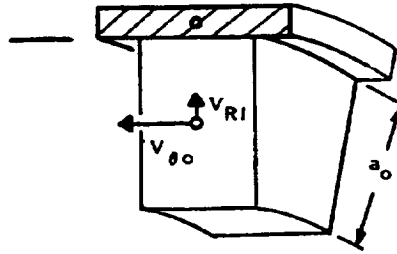


Figure 1. Hybrid Flywheel Energy Density vs. Radius Ratio

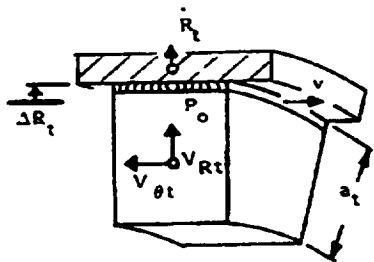




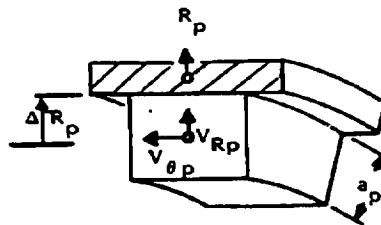
I. BEFORE ROTOR FAILURE



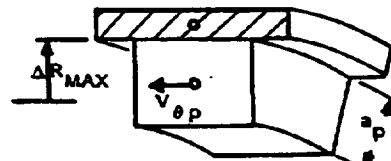
II. INITIAL FRAGMENT CONTACT:  $t = t_o$



III. FRAGMENT CRUSHING PHASE  
 $t_o < t < t_p; V_{Rt} > R_t$



IV. INITIATION OF RIGID MOTION PHASE:  
 $t = t_p; V_{Rp} = R_p$



V. END OF PROCESS:  $t = t_f; V_{Rf} = R_f = 0$

Figure 2. Diagram of Fragment Crushing Process Showing Five Phases

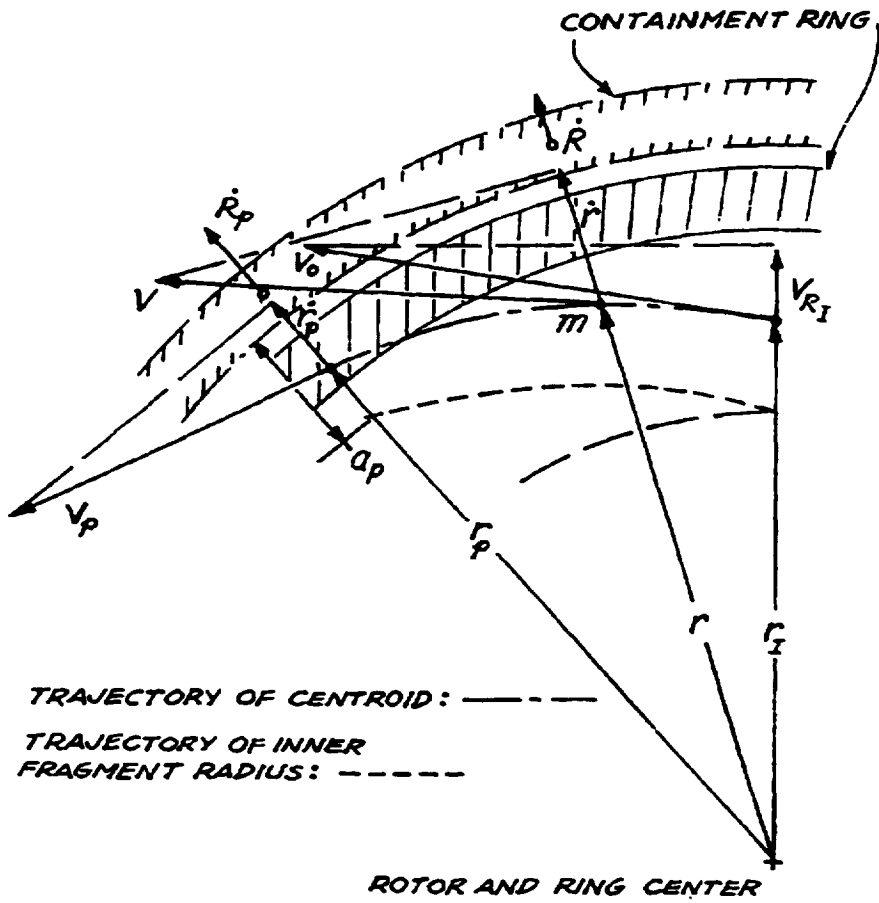


Figure 3. Crushing Fragment Interaction Schematic

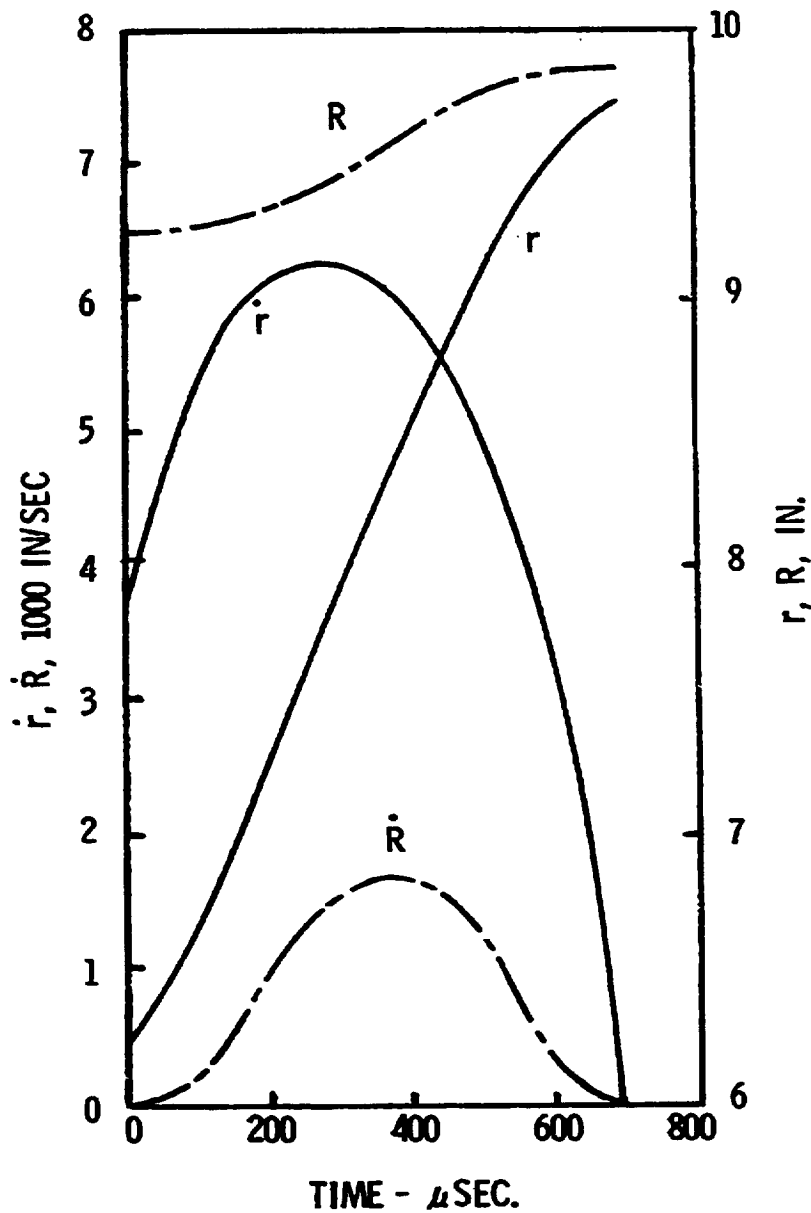


Figure 4. Calculated Fragment and Containment Ring Motions vs. Time for Complete Burst of a 0.25 kw Laminated Glass/Epoxy Disk Rotor.  $P_0 = 0$ ; 4130 Steel Ring ( $\sigma = 158$  ksi)

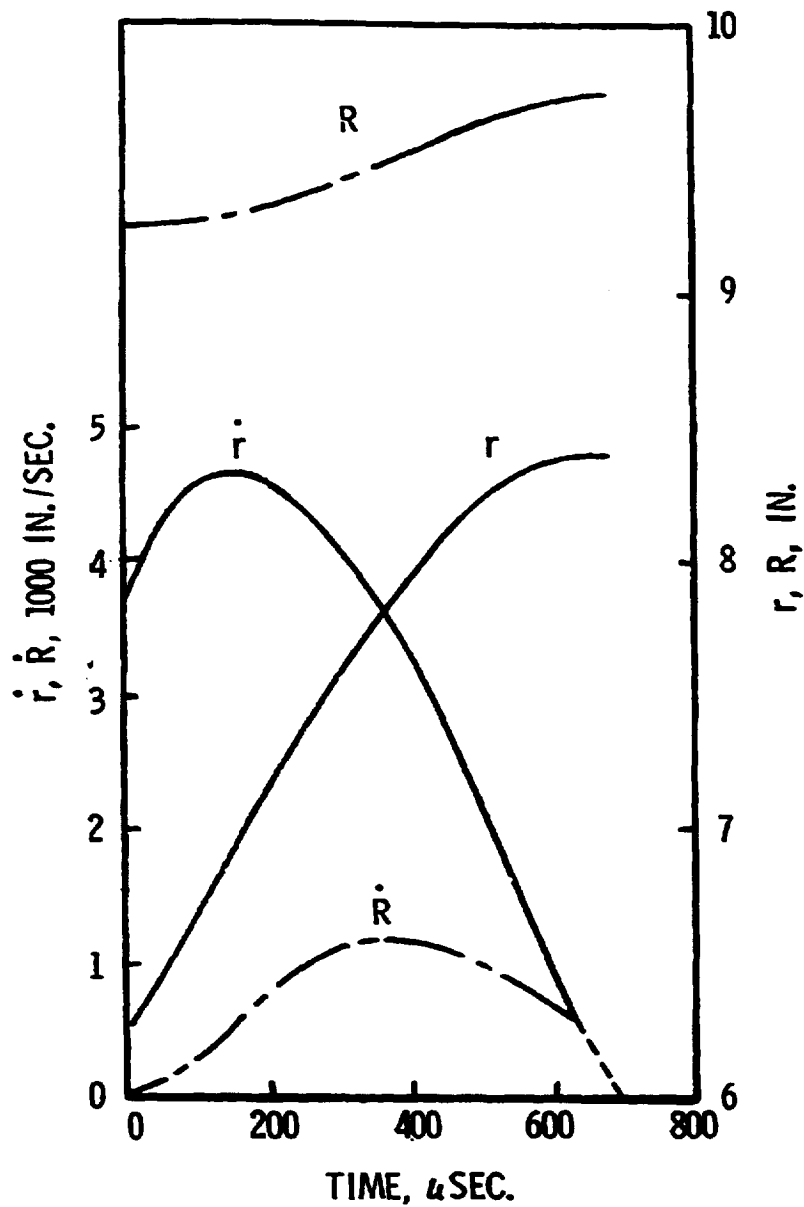


Figure 5. Calculated Fragment and Containment Ring Motions vs. Time for Complete Burst of a 0.25 kw Laminated S-Glass/Epoxy Disk Rotor.  $p = 12,000$  psi, 4130 Steel Ring ( $\sigma = 159$  ksi)

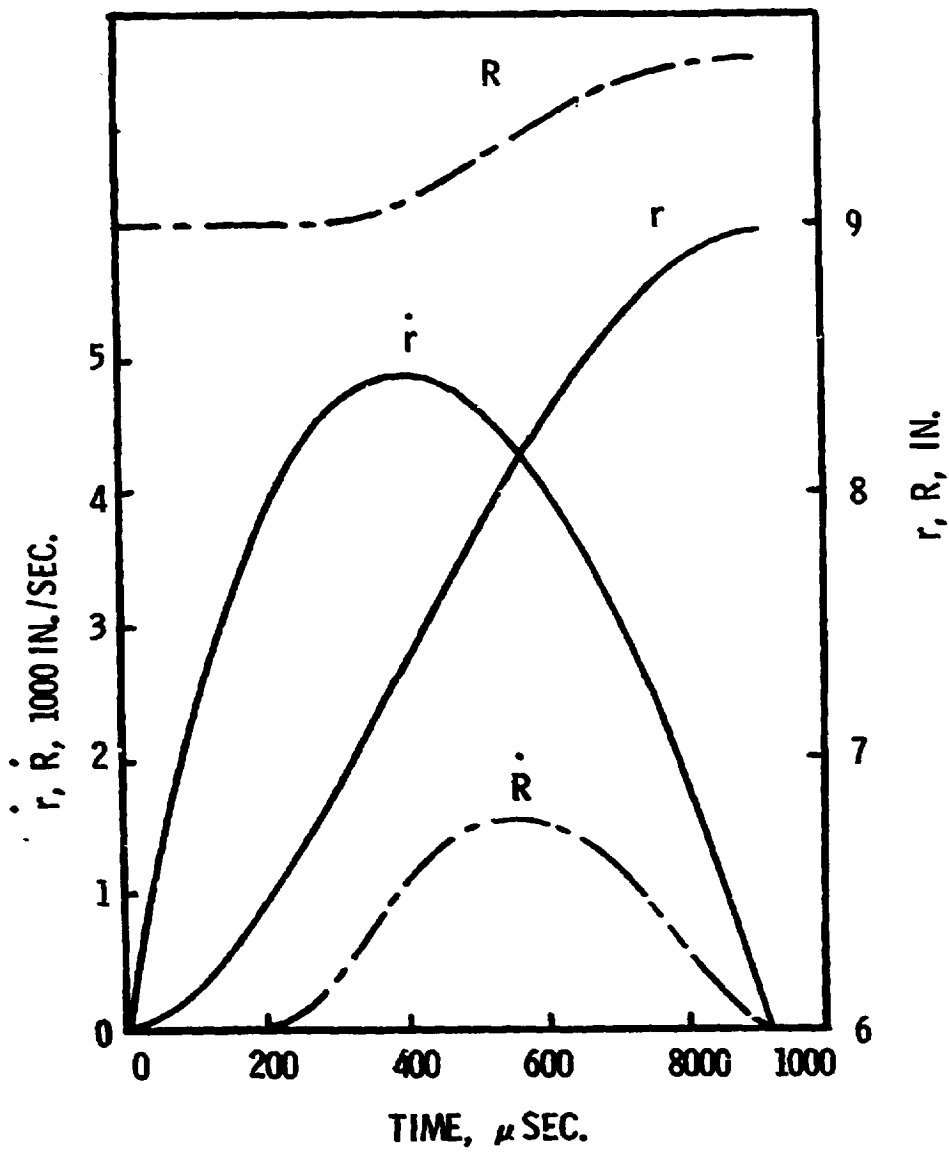
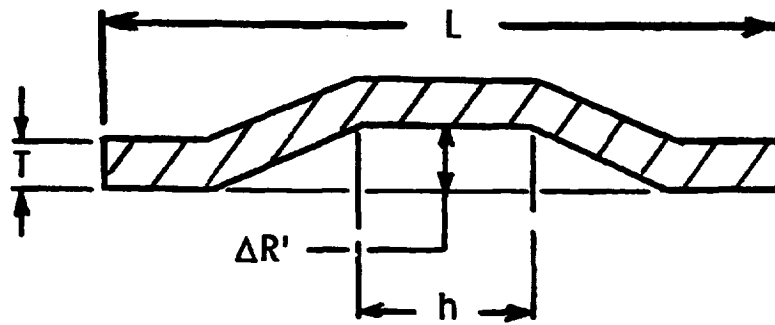


Figure 6. Calculated Fragment and Containment Ring Motions vs. Time for Complete Burst of a 0.25 kw/h Laminated S-Glass/Epoxy Disk Rotor,  $P_0 = 6,000$  psi. Radial Clearance,  $C = 0$ , 4130 Steel Ring ( $\sigma = 158$  ksi)



DEFLECTED RING SECTION

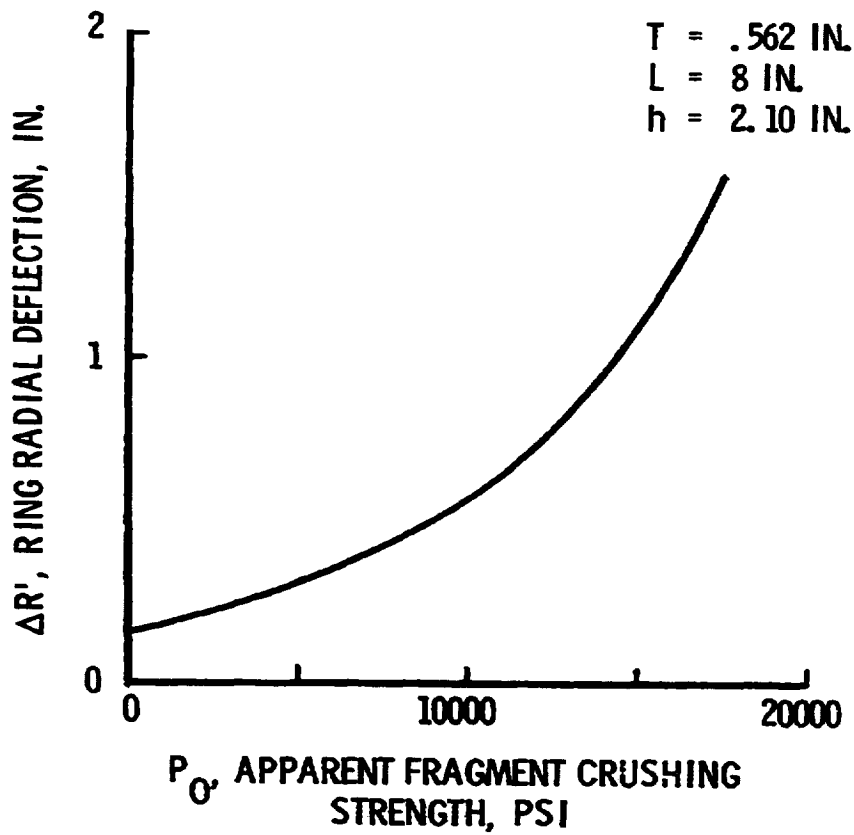


Figure 7. Calculated Peak Radial Deflection,  $\Delta R'$  vs. Crushing Strength,  $P_0$  for Aramid/Epoxy Filament Wound Rim (Garrett Flywheel)

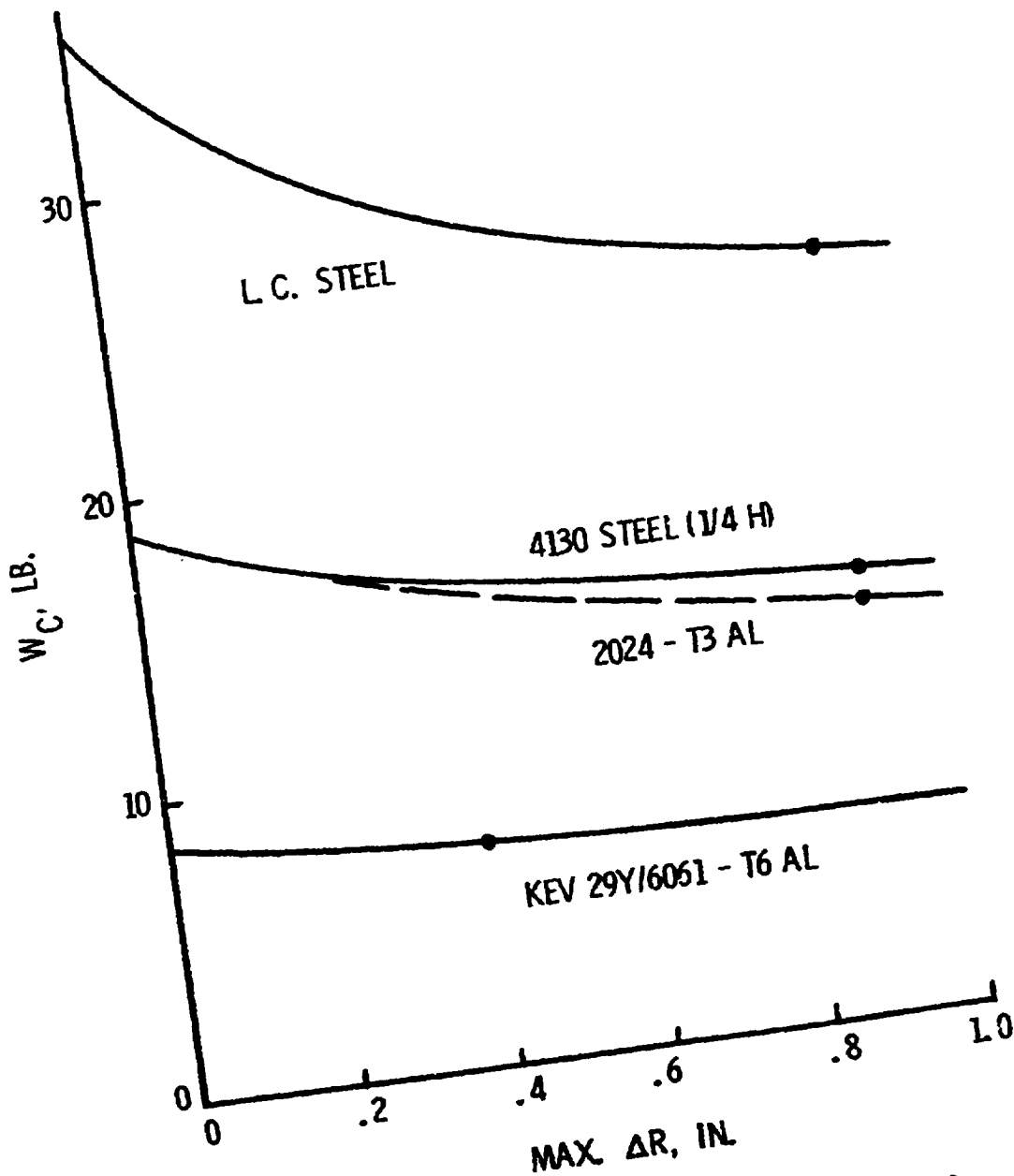


Figure 8. Containment Design Curves:  $W_c$  vs.  $\Delta R_{max}$  for Complete Burst of an 18 in. OD, 0.25 kw Laminated S-Glass/Epoxy Disk Rotor for Several Containment Ring Materials

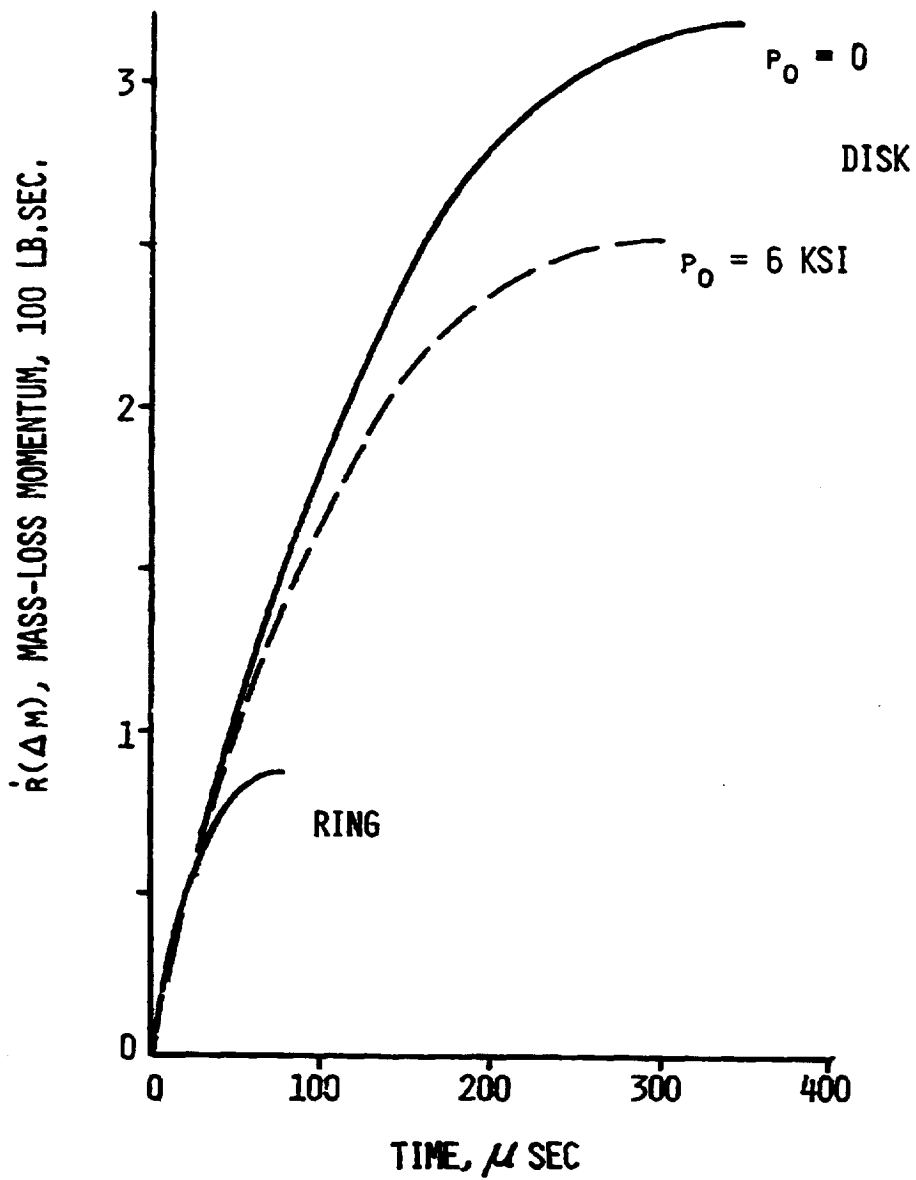


Figure 9. Calculated Mass-Loss Momentum During Containment of a GE Hybrid Flywheel at 648 wh Stored Energy



1

N85

3870

UNCLAS

N85 13870 D20

**MAGNETICALLY SUSPENDED  
REACTION WHEEL ASSEMBLY**

**George Stocking  
Sperry Corporation  
Flight Systems  
Phoenix, Arizona**



## INTRODUCTION

The Magnetically Suspended Reaction Wheel Assembly (MSRWA) is the product of a development effort funded by the Air Force Materials Laboratory (AFML) at Wright Patterson AFB. The specific objective of the project was to establish the manufacturing processes for samarium cobalt magnets and demonstrate their use in a space application. The development was successful on both counts.

This presentation emphasizes the application portion of the program, which involves the magnetically suspended reaction wheel assembly. The requirements for the reaction wheel were based on the bias wheel requirements of the DSP satellite.

The work was performed during the period of May 1976 through June 1980. The tasks included the design, fabrication, and test of the unit to the DSP program qualification requirements.

## AFML PROGRAM SCOPE

- **Establish Manufacturing Processes For the Production of a Magnetically Suspended Reaction Wheel Assembly (MSRWA) Consisting of Two Subassemblies, Mechanical and Electrical.**
- **Work to be Completed Includes:**
  - **Electrical/Mechanical Design**
  - **Electrical/Mechanical Subassembly Production and Assembly**
  - **Engineering Model Assembly**
  - **Engineering Test and Evaluation**
  - **Quality Control and Test**

Figure 1

## **RADIATION FACTOR**

One of these unique requirements is the radiation-hardened electronics factor. Under this type of requirement, designing involves additional analytical effort because of severe derating and the need to limit current. Once designed, however, the electronics proved to be the most reliable portion of the system.

## **AFML PROGRAM SCOPE (CONT'D)**

- **Radiation Hardened Electronics**
  
- **Four Phase Program**
  - **Phase I Thru III Includes Design, Manufacturing Methods Development, Production and Test of Subassemblies, and Fabrication of an MSRWA**
  
  - **Phase IV Includes Testing and Evaluation of the Engineering Model**

**Figure 2**

## **PROGRAM REQUIREMENTS**

The overall program goal was to demonstrate that magnetic suspension was a viable concept, capable of meeting realistic space program requirements.

## **PROGRAM GOALS**

- **Elimination of Lubrication Requirements**
- **Increased Speed Capability**
- **Reduction of Temperature Sensitivity**
- **Reduction of Running and Noise Torques**
- **Reduction of Power Requirements**
- **Elimination of Single Point Failures**

**Figure 3**

## MECHANICAL ASPECTS

ORIGINAL DOCUMENT  
OF PGR CONTROL

The mechanical portion of the system is patterned after our successful line of control moment gyros (CMGs), using a shell rotor and housing. Each end of the shaft assembly houses a magnetic bearing, a motor, a velocity sensor, and a position sensor. The normal mode of operation is to control the axial position from one end.

AFML  
MAGNETIC SUSPENSION  
REACTION WHEEL  
500-1000 RPM-sec

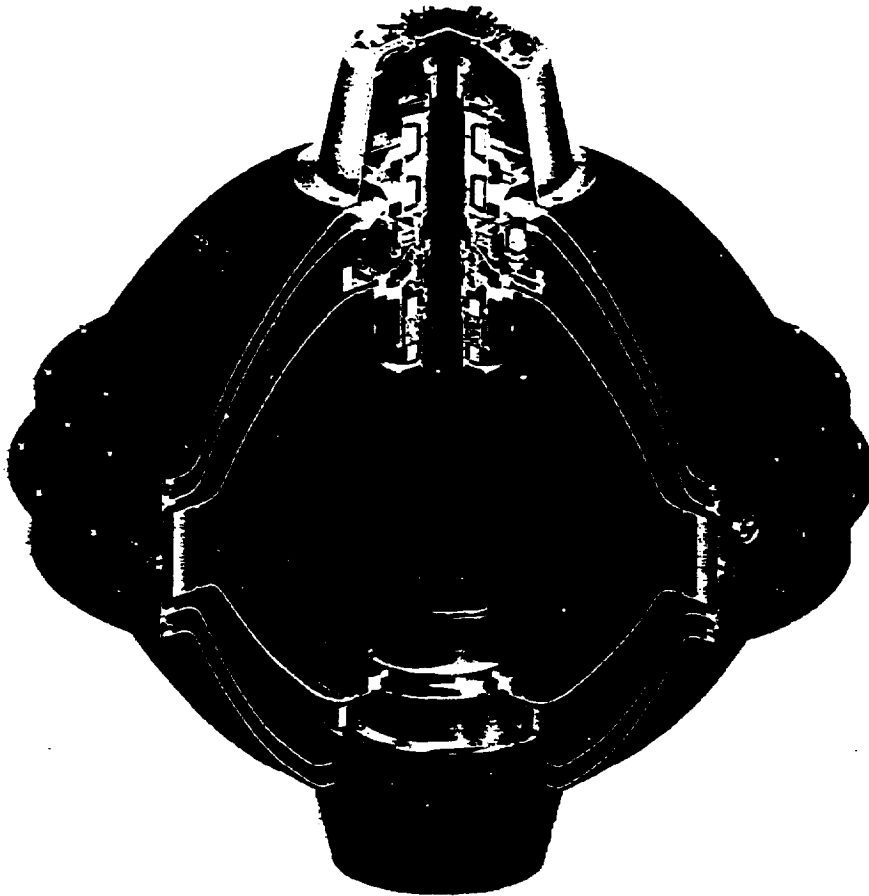


Figure 4

## RELIABILITY

The high reliability and insensitivity to thermal conditions are the principal advantages of permanent magnetic suspension. Thus the limitations of permanent magnetic suspension do not present the serious threat to space-station type applications that they would present in high-rate and acceleration systems.

## MAGNETIC SUSPENSION CHARACTERISTICS

### ADVANTAGES

- High Reliability
  - No Wearout Mechanisms
  - No Lubrication
  - No Fatigue
- Low Torque— Starting, Drag and Ripple
- High Speed Capability
- Performance Independent of Time
- No Single Point Failures (With Redundant Electronics)
- Insensitive To Thermal Conditions
- High Momentum Capacity
- Low Induced Vibration

### LIMITATIONS

- Lower Stiffness
- Low Cross Axis Torque Capacity
- Suspension Control Electronics Required
- Added Bearing Weight

Figure 5

## **HARDWARE**

The hardware designed to meet the DSP requirements did not require any major developments. During the development phase we learned that a combined structural/vacuum shell was not practical, and the design was changed accordingly.

## **RESULTING HARDWARE FEATURES**

- **Passive Radial, Active Axial, Attractive Mag Suspensions**
- **3 Loop Magnetic Circuit**
- **Titanium Shell Rotor**
- **AC Induction Motor**
- **Radiation Hardened Electronics**
- **Ball Bearing Backup or Touchdown System**
- **Samarium Cobalt Magnets**
- **Rate and Position Feedback**

**Figure 6**



## MAJOR COMPONENTS

The cutaway (Fig. 7) shows the major components of the design. The rotor was designed for momentum efficiency, but it could just as easily be made to accommodate energy storage. A complete set of electromagnetic components is located at each end of the rotor shaft to provide the redundancy needed for long missions.

## AFML—MSRWA

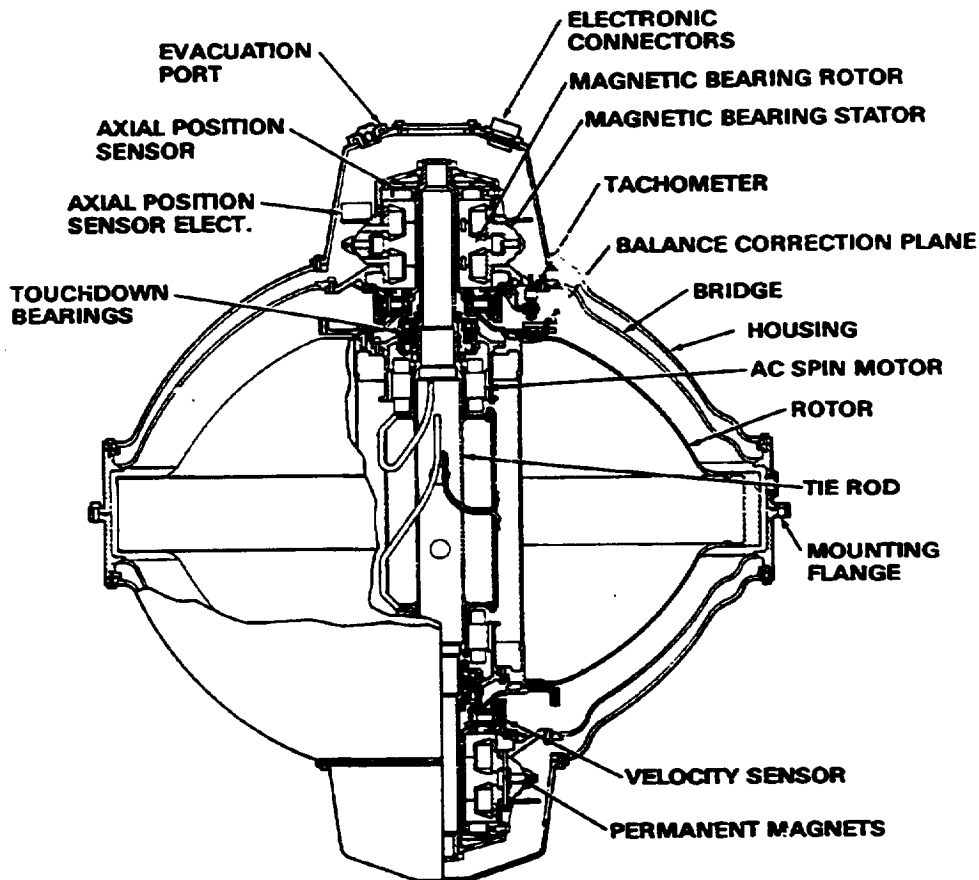


Figure 7

## PERFORMANCE

The performance of the unit met all program requirements, with the exception of the cross-axis rate. A capability of 3 degrees per second was desired, but the weight impact precluded achieving this capability.

### AFML MSRWA PERFORMANCE CHARACTERISTICS

- **Momentum**                      1000 FPS @ 10,000 RPM  
    500 FPS @ 5,000 RPM
  
- **Cross-Axis Rate**                2°/Sec.
  
- **Spin System**
  - Motor                              Dual 6 Pole 2 $\phi$  Induction
  - Control                            Constant Power/Constant Slip
  - Torque                             7 Oz-In @ 5000 RPM
  
- **Suspension System**
  - Control                            Axially Active with Position and Velocity Feedback
  
  - Stiffness
    - Radial                                2000 Lb/In
    - Angular                              4.3 X 10<sup>5</sup> In-Lb/Rad.
    - Axial                                  32,000 Lb/In
  
- **Drag Torque**                    .05 Oz-In/1000 RPM

Figure 8

The system is capable of being run up with either one or two spin motors. Since weight was not a major design goal, there is approximately a 10 percent improvement available.

## **AFML MSRWA PERFORMANCE CHARACTERISTICS (CONT)**

- **Power**
  - Steady State**                    **17 Watts @ 1000 FPS**
  - Run-Up**                            **110/220 Watts**
  
- **Weight**                            **145 Lb Mech (RWMS)**  
    **65 Lb Rotating Assy—Total**
  
- **Envelope**                         **27 In. Dia X 30 In. High**
  
- **Life**                                 **No Single Point Failure,  
    **Hardened Electronics****

Figure 9

## TEST SEQUENCE

The conducted test sequence was based on program qualification requirements. No major problems were encountered during the environmental tests. However, it was discovered that motor heating was higher than predicted, which would be revised if the unit were prepared for flight.

## AFML—MSRWA TEST ENVIRONMENTS

Test	Level
● Thermal-VAC	Ambient, -35°C, +71°C
● Sine Vibration	±1.0 g, 20-2000 Hz, 1 Oct/Min, 2 Axes
● Random Vibration	
— Acceptance	8.5 g-rms, 0.08 g <sup>2</sup> /Hz pk, 1 Min/Axis, 3 Axes
— Qualification	17.0 g-rms, 0.32 g <sup>2</sup> /Hz pk, 3 Min/Axis, 3 Axes

Figure 10

## MAGNETIC BEARINGS

The magnetic bearing characteristics that were measured were very close to the design goals established early in the program. Especially encouraging was the drag torque, which makes this type of suspension attractive for energy storage. Ball bearings for this application would produce 10 oz-in drag torque.

## MAGNETIC BEARING CHARACTERISTICS

- **Stiffness**
  - Radial 2000 Lb/Inch Per End
  - Angular 430,000 In-Lb/Rad
  - Axial 32,000 Lb/In
- **Capacities**
  - Radial 50 Lb
  - Angular 450 In-Lb
  - Axial >65 Lb
- **Weight**
  - Stators (2) 10 Lb
  - Rotors (2) 22 Lb
- **Current**
  - Lift-Off 8 Amp
  - Steady State .07 Amp
- **Drag Torque** < 0.5 Oz-In  
@ 10 K Rpm

Figure 11

C-4

## MODEL CORRELATION

This figure shows the open-loop axial characteristic from an analytical model. The structural modes of the system are phase-stabilized.

### AFML ANALYTICAL AXIAL MODEL

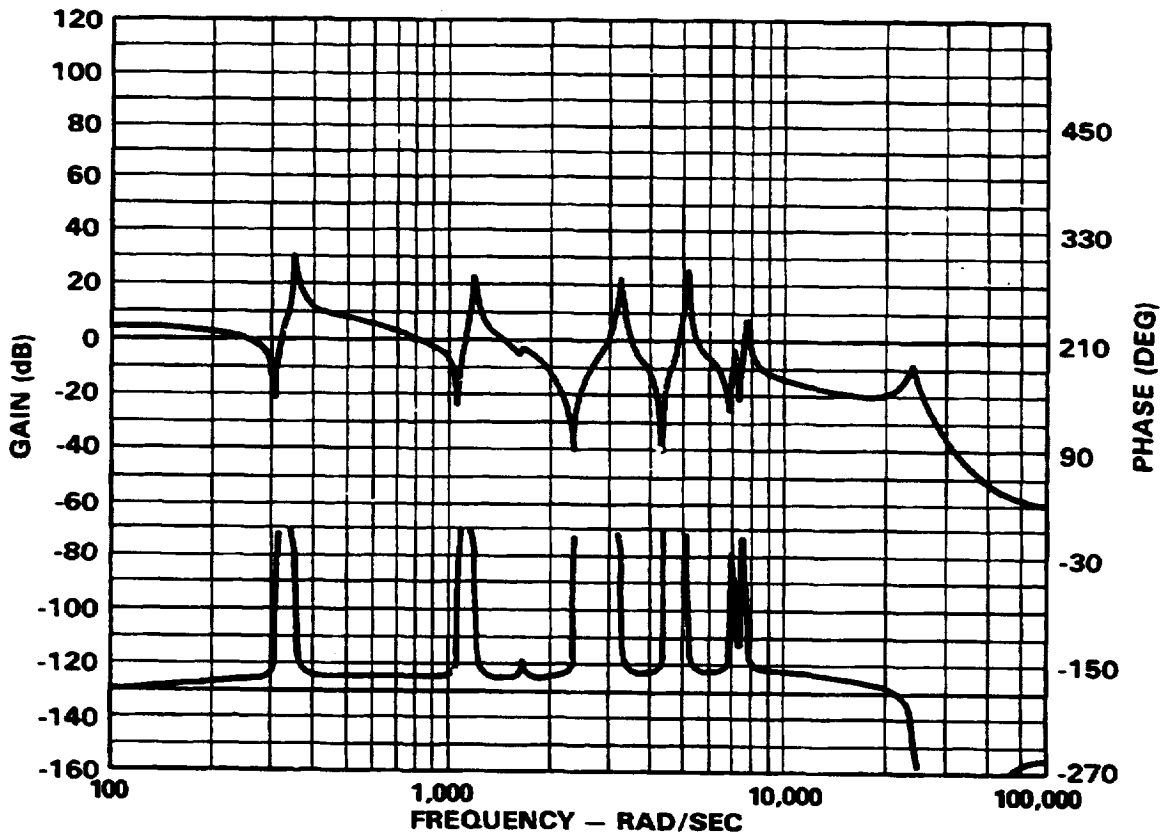


Figure 12

### RESULTS

Fig. 13 shows the results obtained by measuring the open-loop characteristic of the hardware. The correlation with the analytical model was quite good.

### AFML AXIAL CONTROL SYSTEM RESPONSE

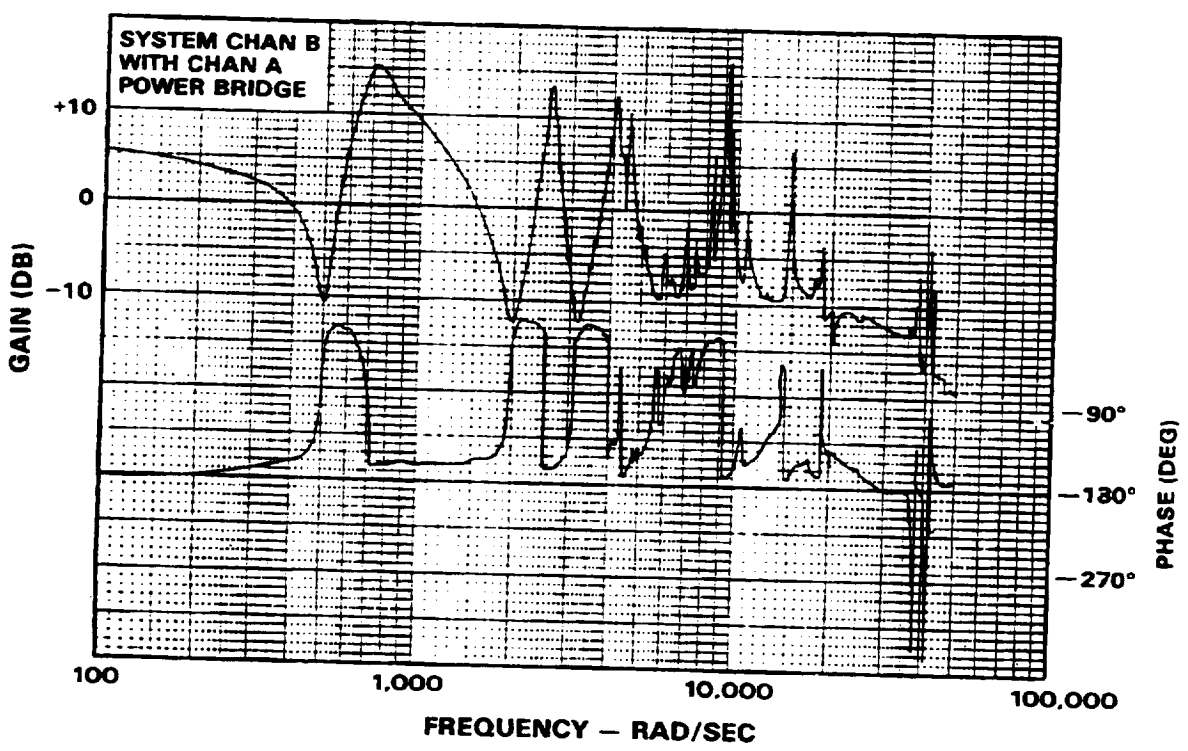


Figure 13

## SUMMARY

The unit demonstrated that permanent magnetic suspension of this type provides a definite advantage over ball bearings for energy storage efficiency. The low radial stiffness would have to be evaluated for each application.





N85

3871

UNCLAS



N85 13871 021

MAGNETIC SUSPENSION OPTIONS  
FOR  
SPACECRAFT INERTIA-WHEEL APPLICATIONS

J. R. Downer  
The Charles Stark Draper Laboratory, Inc.  
Cambridge, Massachusetts

PRECEDING PAGE BLANK NOT FILMED

Listed below are the criteria that should be used when evaluating a suspension system for an inertia wheel in a spacecraft environment. The suspension must be compatible with a vacuum environment. It must exert minimal drag torques on the wheel and must consume only small amounts of power. The suspension must be capable of extended life with little or no attention. Additional functions that could be performed by the suspension include pointing the wheel's angular momentum vector to achieve active attitude control and precisely measuring the torques exerted on the wheel so that an attitude reference signal can be obtained.

### DESIGN CRITERIA FOR SPACECRAFT INERTIA-WHEEL SUSPENSIONS

- VACUUM COMPATIBLE
- LOW LOSSES
  - DRAG
  - POWER CONSUMPTION
- LONG LIFE
- LOW MAINTENANCE
- HIGH RELIABILITY
- ANGULAR MOMENTUM VECTOR POINTING CAPABILITY (OPTIONAL)
- CALIBRATION CAPABILITY (OPTIONAL)

The primary advantage of utilizing a magnetic suspension for a spacecraft inertia-wheel application is the lack of physical contact between the rotor and the stator. This leads to extended suspension life and reduced drag. The tolerances that must be allowed in construction of the suspension can be reduced from those required of other suspension system types such as precision ball and gas bearings. Reduced vibration and structural interaction can also be obtained. Since magnetic suspensions require no lubricant, they are quite compatible with a vacuum environment. Properly designed magnetic suspensions also allow the functions of attitude control and attitude rate sensing to be performed.

### **ADVANTAGES OF MAGNETIC SUSPENSIONS OVER OTHER SUSPENSION TYPES FOR SPACECRAFT INERTIA-WHEEL APPLICATIONS**

- **NO ROTOR/STATOR CONTACT**
  - EXTENDED LIFE
  - REDUCED DRAG
  - REDUCED TOLERANCES
  - REDUCED MECHANICAL VIBRATION
  - REDUCED STRUCTURAL INTERACTIONS
- **NO PROBLEM OF PROVIDING LUBRICATION IN A VACUUM**
- **POTENTIAL TO ELIMINATE MECHANICAL GIMBALS**
- **POTENTIAL FOR ESTIMATING SATELLITE RATES**

A magnetic suspension system may perform one or more of the following functions: rotor support, torquing, and torque measurement. Regardless of function, the suspension design is typically driven by the inertia wheel precession torques, the stiffness of the surrounding structure, and by the angle through which the rotor must be tipped.

- **FUNCTIONS PERFORMED BY MAGNETIC SUSPENSION**

- BEARING
- TORQUER (OPTIONAL)
- RATE SENSOR (OPTIONAL)

- **FACTORS AFFECTING MAGNETIC BEARING DESIGN**

- WHEEL ANGULAR MOMENTUM
- REQUIRED SLEW RATES OF SATELLITE
- STRUCTURAL COMPLIANCES AND INTERACTIONS
- MAXIMUM TILT ANGLE



There are four common designs for magnetic suspensions. The oldest type, the passive dynamic field bearing (ref. 1), is stabilized by tuning circuit parameters for a particular excitation frequency. This type typically consumes excessively high power for a spacecraft inertia-wheel application. Earnshaw's theorem states that a body in a static magnetic field is stable in at most two axes. The stiffness along passively stable axes is typically low. Many designers utilize active control of passively unstable axes to achieve a stable system. Several advantages exist for actively controlling all axes with servo control. These are addressed in detail on the next viewgraph.

**MAGNETIC BEARING TYPES**

<u>TYPE</u>	<u>COMMENTS</u>
PASSIVE DYNAMIC FIELD	● HIGH POWER CONSUMPTION
PASSIVE STATIC FIELD	● STABLE IN AT MOST TWO AXES (EARNSHAW'S THEOREM)
	● LOW STIFFNESS
PASSIVE/ACTIVE	● UNSTABLE AXIS OF PASSIVE SYSTEM ELIMINATED WITH SERVO CONTROL
ACTIVE	● SERVO CONTROL REQUIRED
	● POTENTIAL FOR ADVANCED CONTROL STRATEGIES
	● POTENTIAL FOR ELIMINATION OF MECHANICAL GIMBALS



An actively controlled magnetic suspension will typically be much stiffer than a passive suspension. The advantages of a high dc stiffness include more repeatable performance and reduced core losses due to changing flux in the rotor as it spins. Stiff suspensions are required if conventional electrical machines (such as induction motors), which produce significant sideload forces, are to be utilized.

Actively controlled magnetic suspensions may be used to provide set point control of the inertia wheel's angular momentum vector to provide attitude control with mechanical gimbals. By actively varying the damping of the suspension, performance near rotor critical speeds may be improved. Advanced control and estimation techniques aimed at suppressing whirl instabilities can also be applied.

## **ACTIVELY CONTROLLED MAGNETIC SUSPENSIONS**

- **HIGHER dc STIFFNESS THAN PASSIVE MAGNETIC SUSPENSIONS**
  - MORE REPEATABLE PERFORMANCE
  - LOWER DRAG LOSSES
  - UTILIZATION OF CONVENTIONAL ELECTRICAL MACHINES POSSIBLE
- **POTENTIAL FOR UTILIZING ADVANCED CONTROL STRATEGIES**
  - SET POINT CONTROL OF ANGULAR MOMENTUM VECTOR
  - ACTIVE VARIATION OF DAMPING
  - WHIRL MODE SUPPRESSION

Magnetic suspensions exert forces either through the attraction of a ferromagnetic body or by the Lorentz force.

Ferromagnetic attraction type magnetic suspensions can be further classified by the manner through which the magnetic field is produced. Purely electro-magnetic suspensions have very low gain near zero current and are highly non-linear. Permanent magnet biased electromagnets, however, possess relatively high gain near zero current and are more nearly linear.

Magnetic suspensions that produce forces by the Lorentz force across a fixed length air gap have an advantage in terms of core loss since the core material sees a constant flux. Lorentz force suspensions are very nearly linear. By utilizing a permanent magnet rather than a wound core to produce the magnetic field, copper losses are reduced.

## ACTIVE MAGNETIC BEARING DESIGNS

- FERROMAGNETIC ATTRACTION
  - PURE ELECTROMAGNET
    - LOW GAIN
    - NON-LINEAR
  - PERMANENT MAGNET (PM) BIASED ELECTROMAGNETS
    - HIGH GAIN
    - LINEAR
- LORENTZ FORCE
  - FIXED GAP LENGTH
    - ELIMINATES CORE LOSSES
    - LINEAR
  - PERMANENT MAGNET FIELD
    - REDUCES COPPER LOSSES



The Charles Stark Draper Laboratory (CSDL) has been involved in magnetic suspension technology for more than 30 years. The definitive reference on float suspensions was written by three CSDL engineers in 1974 (ref. 1). A 5-axis actively controlled flywheel suspension supporting a 12 lb rotor was constructed in 1978 (refs. 2, 3, 4). A magnetic suspension system for removing all but a nominal preload from the ball bearing support of a 200 lb flywheel was constructed in 1981.

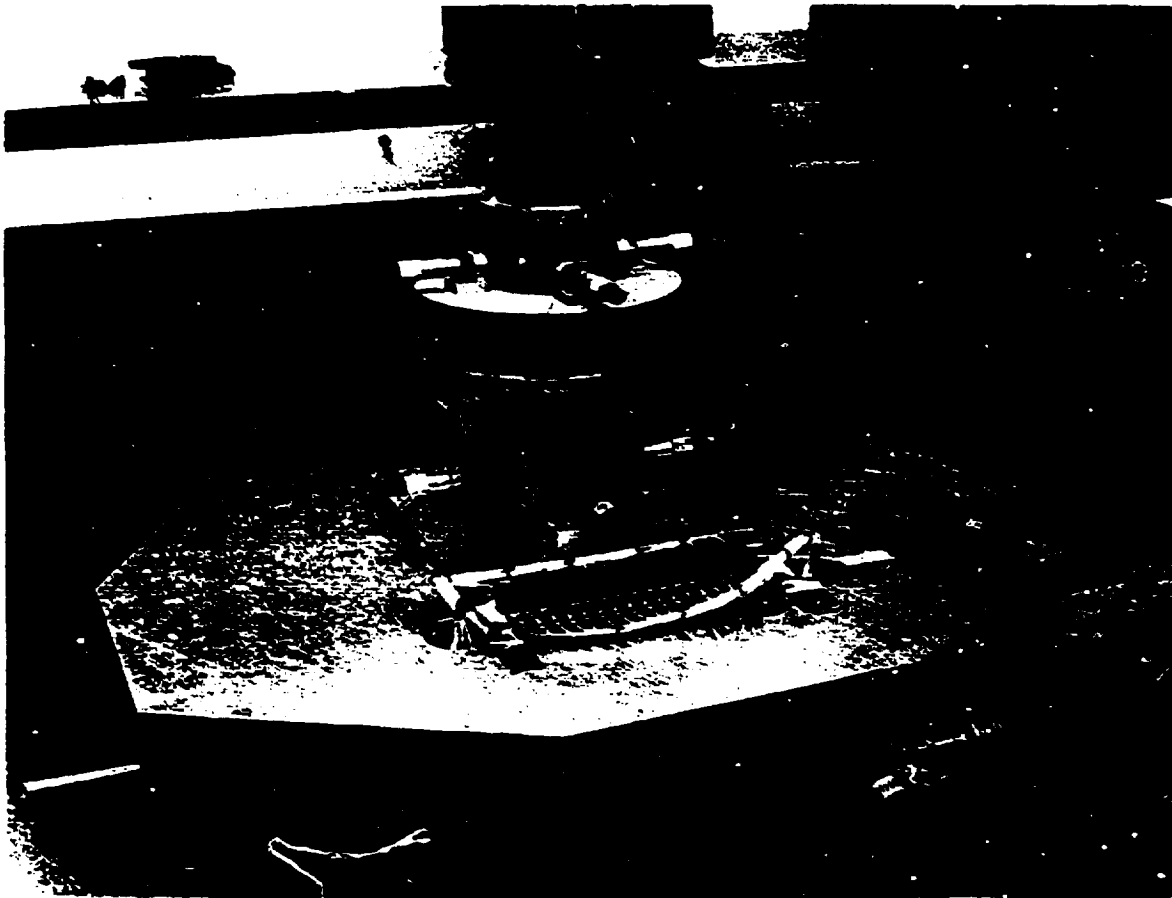
There are currently three advanced magnetic suspension programs at CSDL. A single axis actively controlled magnetic vibration-isolator and a magnetically suspended inertial reference unit are being constructed and tested. A study of a Combined Attitude, Reference, and Energy Storage (CARES) system (ref. 5) is also in progress. The goal of this study is to demonstrate the feasibility of performing the energy storage, attitude control, and attitude reference functions of a satellite with high energy density, magnetically suspended inertia wheels. A novel Lorentz force type magnetic suspension is being constructed and tested as part of this program.

## **DRAPER LAB MAGNETIC SUSPENSION EXPERIENCE**

- **FLOAT SUSPENSIONS**
- **5 AXIS ACTIVELY CONTROLLED FLYWHEEL SUSPENSION  
(12 lb WHEEL)**
- **HYBRID FLYWHEEL SUSPENSION (200 lb WHEEL)**
- **PRECISION ACTIVE MAGNETIC VIBRATION ISOLATION**
- **MAGNETICALLY SUSPENDED INERTIAL REFERENCE UNIT**
- **COMBINED ATTITUDE, REFERENCE, AND ENERGY  
STORAGE (CARES) SYSTEM**

As an example of a typical flywheel magnetic suspension, the 5-axis actively controlled flywheel shown here will be discussed.

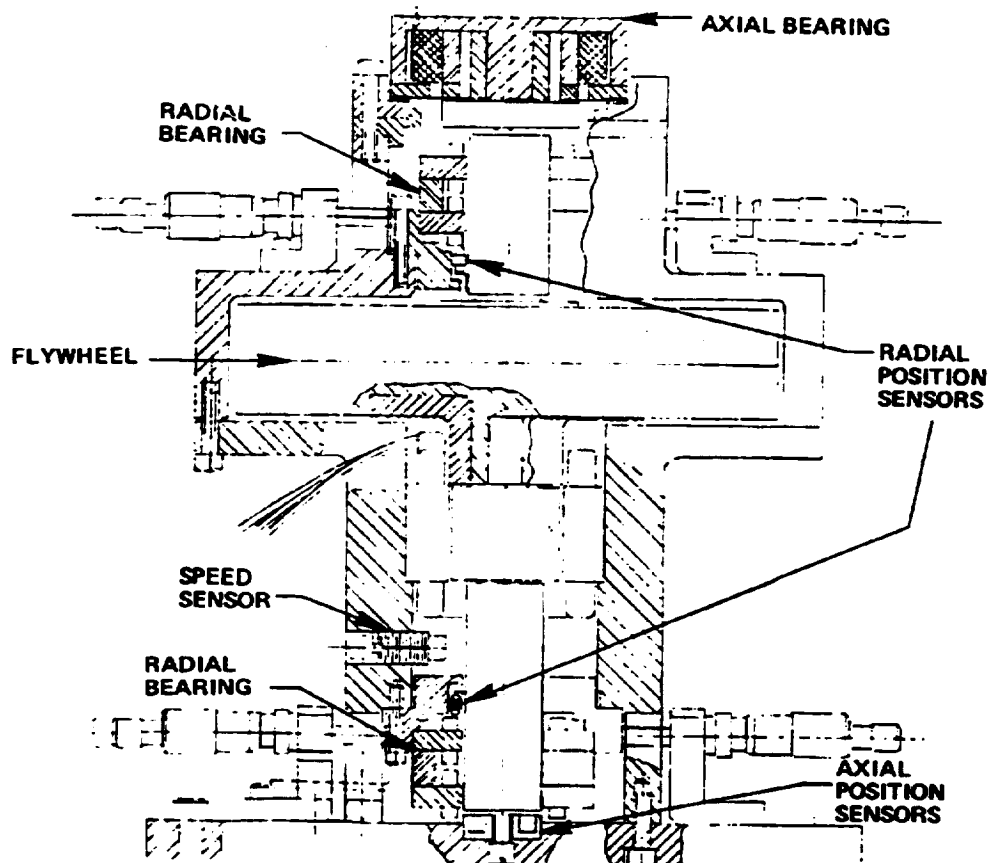
ORIGINAL  
OF POOR QUALITY





The figure below shows the internal arrangement of components. This system uses three actively controlled bearing elements, two radial and one axial, to control five degrees of freedom. Three inductive position sensors and an optical speed sensor are also used.

The flywheel module was designed to have a vertical spin axis so that the suspension that supported the weight of the wheel would not see changing fluxes due to rotor eccentricity and thereby reduce losses.

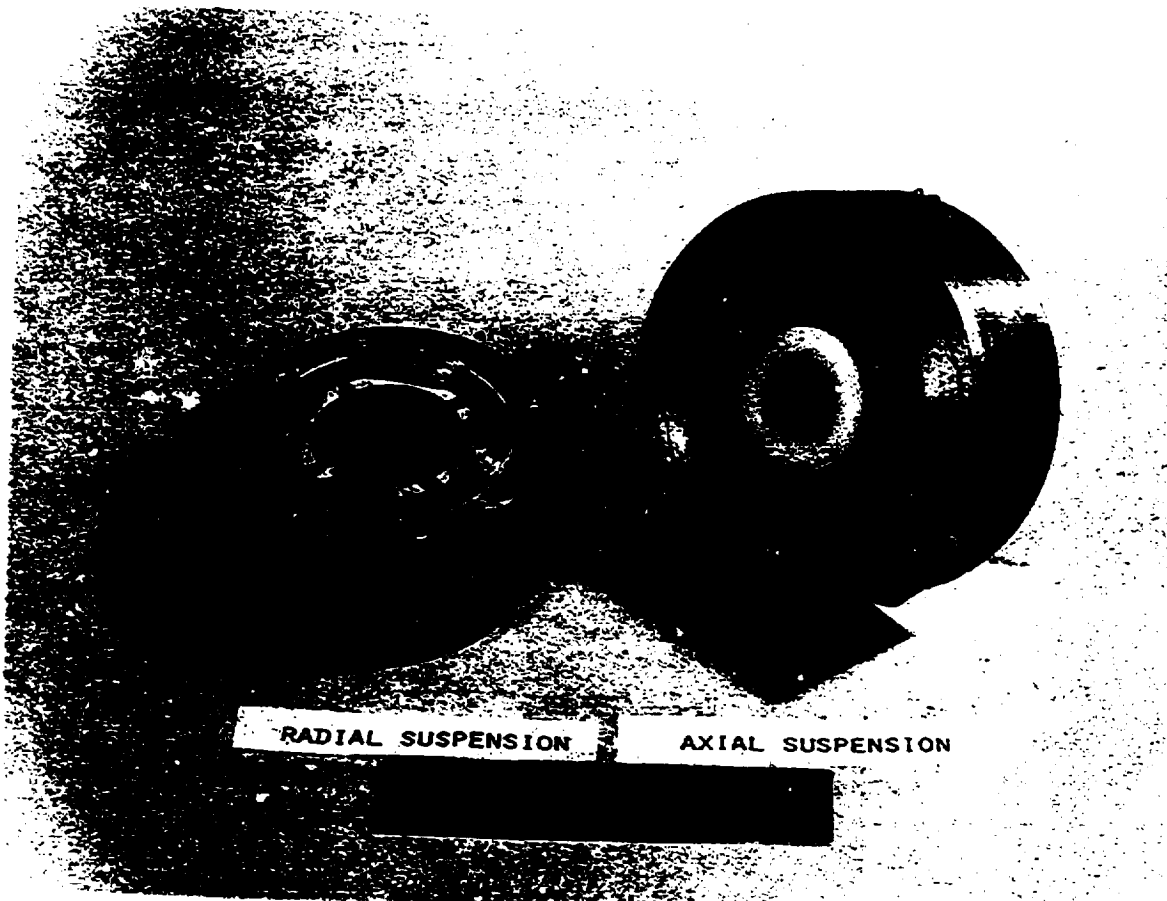


ORIGINAL PAGE IS  
OF POOR QUALITY

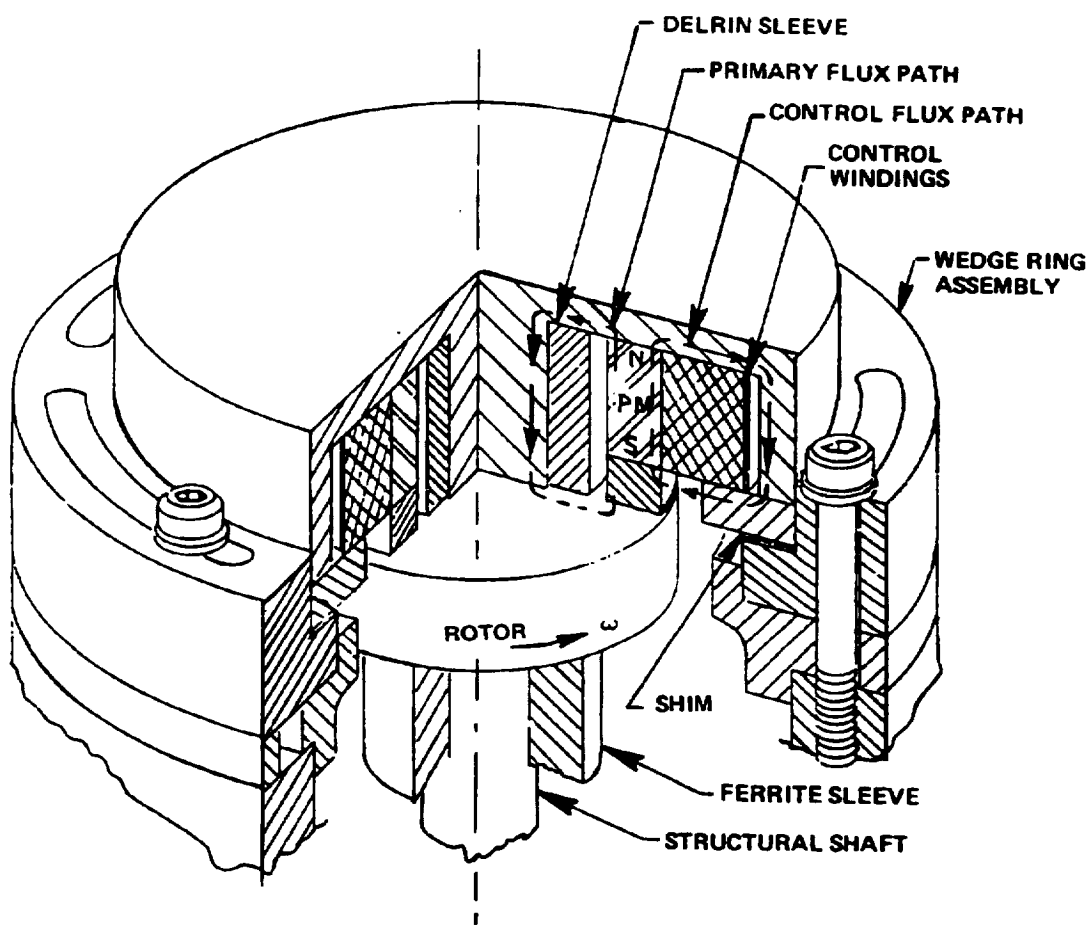


The photograph below shows the magnetic actuators that were used in the 5-axis actively controlled flywheel. Each is a permanent magnet biased electromagnet which uses a permanent magnet to produce a biasing field and control coils to obtain active control.

ORIGINAL COPY  
OF POOR QUALITY

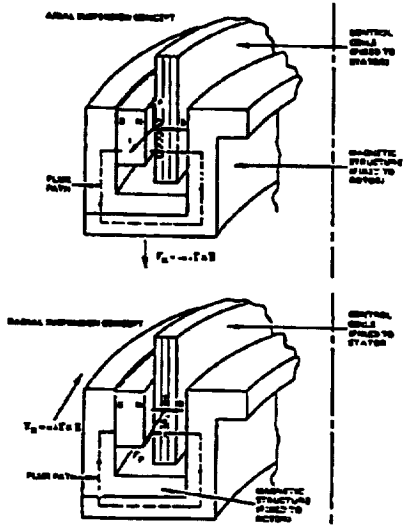


As an example of the operation of a permanent magnet biased magnetic suspension, consider the axial bearing of the 5-axis actively controlled flywheel that is shown below. The primary flux for suspension is provided by an axially oriented permanent magnet. Control of the air gap flux is obtained by using a control coil to shunt flux through an alternate flux path that has been provided in the magnet housing.



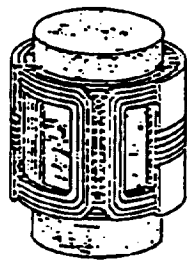


The CARES system magnetic bearing is shown below. Forces are exerted on the flywheel due to the interaction of rotating permanent magnets and stationary control coils. The figure also shows the winding configuration required to produce these forces. The windings of the control coil structure are shown assembled and in exploded form.

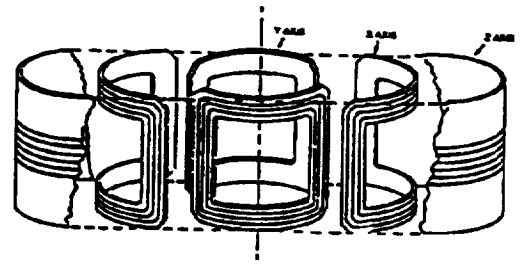


CARES MAGNETIC SUSPENSION CONCEPT

WINDING CONFIGURATION OF CONTROL COILS



CONTROL COILS ASSEMBLED



CONTROL COILS DETAILED



Proper material selection in terms of either permanent magnets or core materials is critical to a successful magnetic suspension design.

When selecting a permanent magnet, maximum energy product is of primary importance since this directly affects the magnet size. The proper mix of remanence and coercivity must also be considered to make a small cross sectional area or long air gap design work. The relative ease with which a permanent magnet can be machined should also be considered.

Core materials are typically selected on the basis of their core loss characteristics (as measured by their hysteresis loop and volume resistivity) but ease of magnetization must also be considered. Ease of magnetization is measured by a material's permeability (one of three types, depending on application). Operating a core material in its saturation region is typically wasteful of power.

## MATERIAL CONSIDERATIONS

### ● PERMANENT MAGNETS

- MAXIMUM ENERGY PRODUCT
- PERMANENT FLUX DENSITY
- COERCIVE FORCE
- MACHINABILITY

### ● CORE MATERIALS

- HYSTERESIS LOOP
- RESISTIVITY
- PERMEABILITY
  - INITIAL
  - MAXIMUM
  - INCREMENTAL
- SATURATION FLUX DENSITY

It is safe to conclude that the basic technology required to utilize an actively controlled magnetic suspension system in a spacecraft inertia wheel has been satisfactorily demonstrated, and that the design and control experience necessary to produce this hardware is available.

In addition, there is currently in progress a great deal of effort aimed at improving magnetic materials. These advances are taking place in the areas of high energy product rare earth/cobalt magnets and low loss ferroceramic core materials. These advances are certain to facilitate magnetic suspension design.

## CONCLUSIONS

- **THE BASIC TECHNOLOGY REQUIRED FOR MAGNETIC SUSPENSION OF A SPACECRAFT INERTIA WHEEL EXISTS:**
  - SUSPENSION DESIGN EXPERIENCE
  - CONTROL TECHNOLOGY
- **RECENT ADVANCES IN MAGNETIC MATERIALS FACILITATE MAGNETIC SUSPENSION DESIGN**



#### REFERENCES

1. Frazier, R.; Gillinson, P.; and Oberbeck, G.: Magnetic and Electric Suspensions, Cambridge, MA, The MIT Press, 1974.
2. Eisenhaure, D.; Oberbeck, G.; and Downer, J.: "Development of a Low-Loss Flywheel Magnetic Suspension," Proceedings of the 14th Inter-Society Energy Conversion Engineering Conference, American Chemical Society, Vol. 1, 1979, pp. 357-362.
3. Downer, J.: Analysis of a Single Axis Magnetic Suspension System, MS Thesis, MIT, 1980.
4. Eisenhaure, D.; Downer, J.; and Hockney, R.: "Factors Affecting the Control of a Magnetically Suspended Flywheel," Proceedings of the 1980 Flywheel Technology Symposium, The American Society of Mechanical Engineers, Vol. 1, 1980, pp. 380-391.
5. Eisenhaure, D.; Downer, J.; Bliamptis, T.; and Hendrie, S.: "A Combined Attitude Reference, and Energy Storage (CARES) System for Satellite Applications," AIAA-84-0565, The American Institute of Aeronautics and Astronautics, 1984.

N85

3872

UNCLAS

N85 13872

D-22

OVERVIEW OF MAGNETIC BEARING CONTROL  
AND LINEARIZATION APPROACHES  
FOR ANNULAR MAGNETICALLY SUSPENDED  
DEVICES

Nelson J. Groom  
Langley Research Center  
Hampton, VA 23665

## INTRODUCTION

The purpose of this paper is to present an overview of magnetic bearing control and linearization approaches which have been considered for annular magnetically suspended devices. These devices include (Fig. 1) the Annular Momentum Control Device (Ref. 1) and the Annular Suspension and Pointing System (Ref. 2).

### ANNULAR MAGNETICALLY SUSPENDED DEVICES FOR CONTROL AND POINTING APPLICATIONS

- ANNULAR MOMENTUM CONTROL DEVICE (AMCD)
  - Momentum Storage Device
- ANNULAR SUSPENSION AND POINTING SYSTEM (ASPS)
  - Auxiliary Pointing System

Figure 1

## CONTROL AND LINEARIZATION APPROACHES

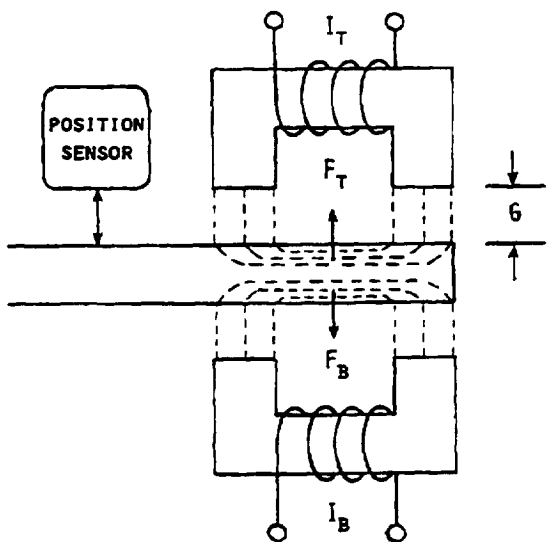
In order to define the basic type of magnetic bearing actuator being discussed, the simplified schematic diagram of Figure 2 is introduced. Shown are two electromagnets, with currents  $I_T$  and  $I_B$ , producing forces  $F_T$  and  $F_B$  on a suspended element positioned at a gap distance  $G$  from the top electromagnet pole face. A position sensor is shown and is required both for some of the linearization approaches to be discussed and for the magnet suspension control system. Under ideal assumptions, the force produced by a given electromagnet is directly proportional to the square of the coil current and inversely proportional to the square of the electromagnet gap. Since the electromagnet produces an attractive force only, two are required to produce a bidirectional force capability. Two approaches have been investigated for controlling this type of magnetic actuator. One approach involves controlling the upper and lower electromagnets differentially about a bias flux. The bias flux can either be supplied by permanent magnets in the magnetic circuit or by bias currents. In the other approach, either the upper electromagnet or the lower electromagnet is controlled depending on the direction of force required. One advantage of the bias flux approach is that for small gap perturbations about a fixed operating point, the force-current characteristic is linear. However, if a requirement for a linear force characteristic over a wide gap range exists, as for example in the ASPS, bias currents which are varied as a function of measured gap are used. Linearization approaches investigated for individual element control include an analog solution of the nonlinear electromagnet force equation and a microprocessor-based table lookup method.

### MAGNETIC BEARING CONTROL APPROACHES

- BIAS FLUX
- INDIVIDUAL ELEMENT CONTROL

### MAGNETIC BEARING LINEARIZATION APPROACHES

- BIAS FLUX
  - PERMANENT MAGNETS
  - FIXED BIAS CURRENTS
  - VARIABLE BIAS CURRENTS
- INDIVIDUAL ELEMENT CONTROL
  - ANALOG SOLUTION OF BEARING ELEMENT FORCE EQUATION
  - MICROPROCESSOR CONTROL (TABLE LOOKUP)



$$F = K \frac{I^2}{G^2}$$

Figure 2

## PERMANENT MAGNET FLUX-BIASED MAGNETIC ACTUATOR

In order to describe the operation of a permanent magnet flux-biased magnetic actuator, the simplified schematic drawing of Figure 3 is introduced. The figure shows a single actuator, for control along a single axis, which consists of a pair of magnetic bearing elements with permanent magnets mounted in the cores. The bearing elements are connected in a differential configuration. That is, for a given input the amplifier driver shown in the figure produces current in a direction to aid the permanent-magnet-produced flux in one element while at the same time producing equal current in a direction to subtract from the permanent-magnet-produced flux in the other element. This results in a net force produced on the suspended mass in a direction dependent on the polarity of the input to the amplifier driver.

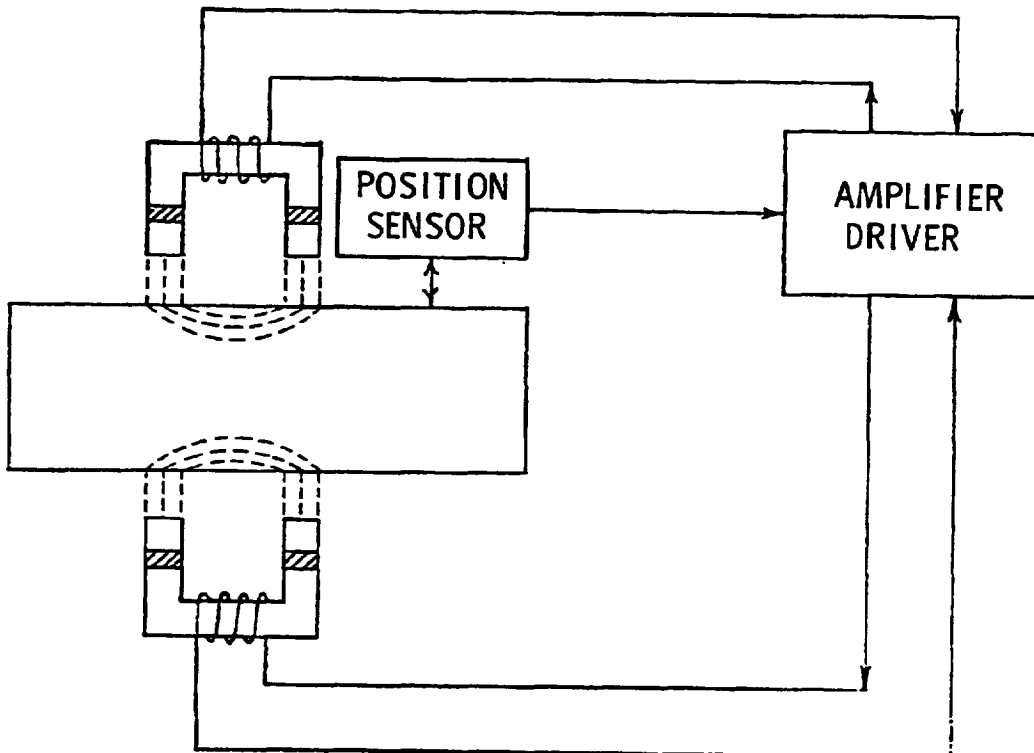


Figure 3

## FLUX-BIASED MAGNETIC ACTUATOR FORCE CHARACTERISTIC

The composite force-current characteristic of a flux-biased magnetic actuator with the suspended mass centered in the actuator gaps is shown in Figure 4. This figure illustrates a linear electromagnet gain of the actuator at a given gap position. By performing a first order linearization of the actuator force equation about a fixed operating point the actuator force as a function of differential coil current and displacement can be written as

$$F = K_B I + K_M G$$

where  $K_B$  is an equivalent electromagnet gain and  $K_M$  is an equivalent bias flux stiffness. These gains would be different for different operating points. Permanent magnet flux-bias was the control approach used in the original magnetic suspension system for the laboratory test model AMCD (Ref. 3).

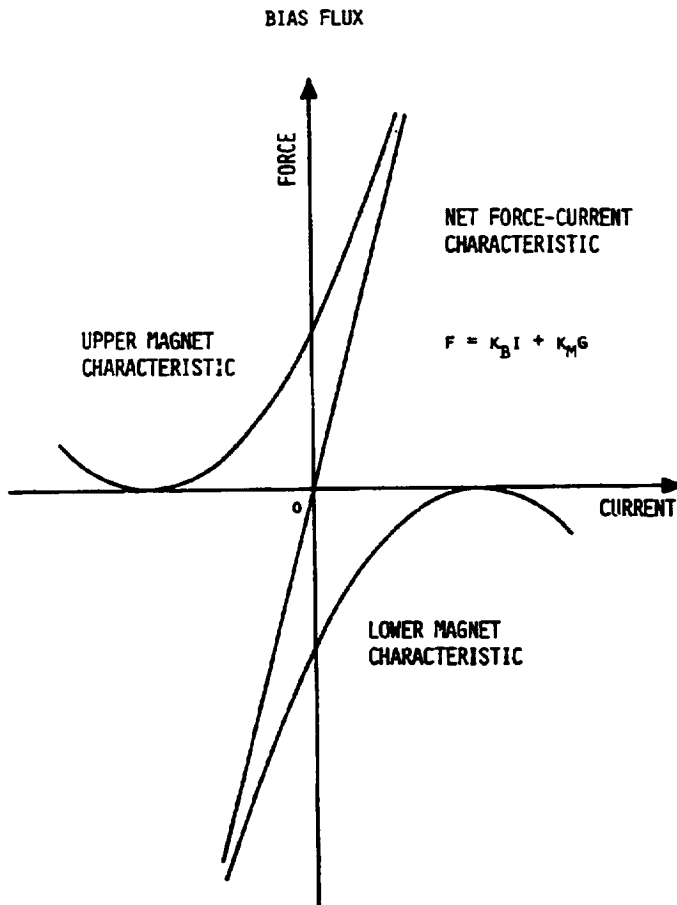


Figure 4

### VARIABLE BIAS CURRENT APPROACH

Figure 5 is a simplified block diagram of a variable bias current approach which was implemented for the ASPS. As can be seen by working through the block diagram, the bias current and control currents of the upper and lower electromagnets are adjusted so that the bias force produced by each and the net force produced by a given command force are equal no matter where the suspended mass is in the gap. The unbalanced bias flux stiffness is thus eliminated and the electromagnet gain is constant. For more detail on the implementation of this approach, see Reference 4.

#### DIFFERENTIAL CONTROL OF ELEMENTS ABOUT BIAS FLUX VARIABLE BIAS CURRENT APPROACH

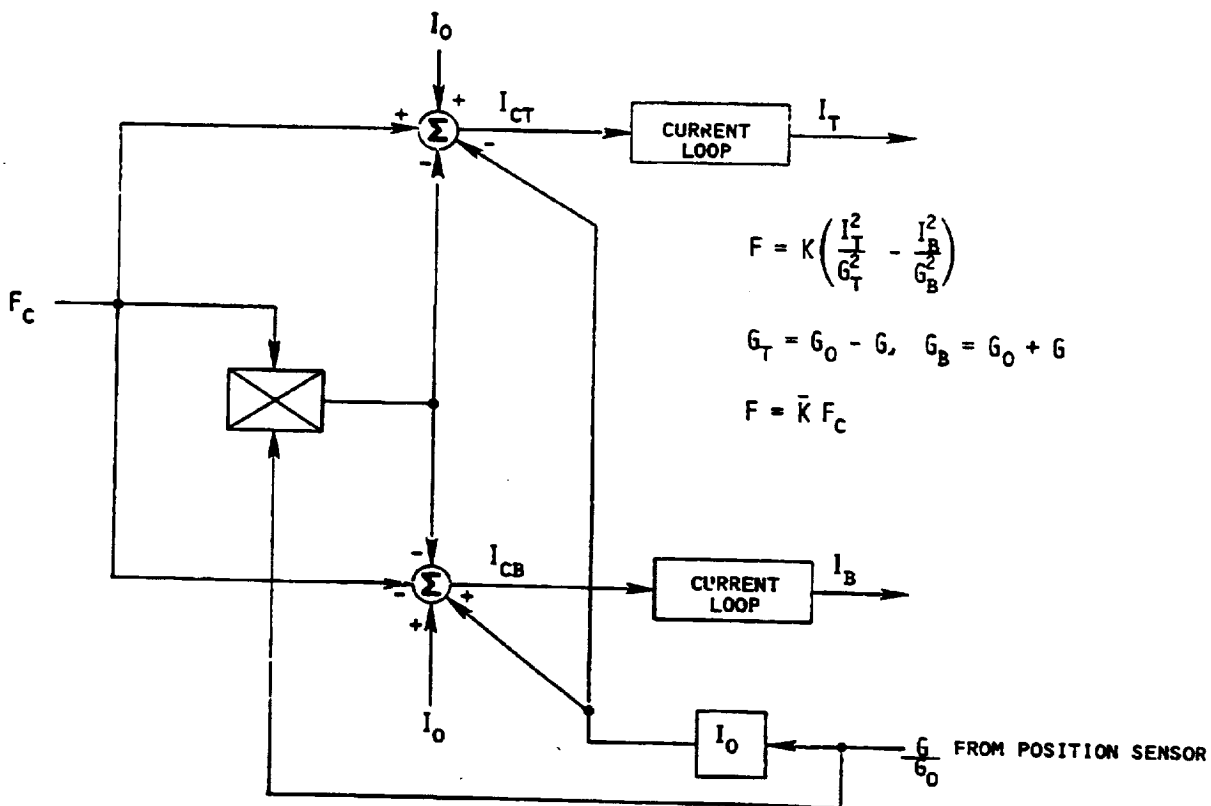


Figure 5



### INDIVIDUAL ELEMENT CONTROL FORCE CHARACTERISTIC

The composite force-current characteristic of a magnetic actuator with individual element control and with the suspended mass centered in the actuator gaps is shown in Figure 6. This figure illustrates the highly nonlinear force characteristics of an uncompensated actuator.

### INDIVIDUAL ELEMENT CONTROL

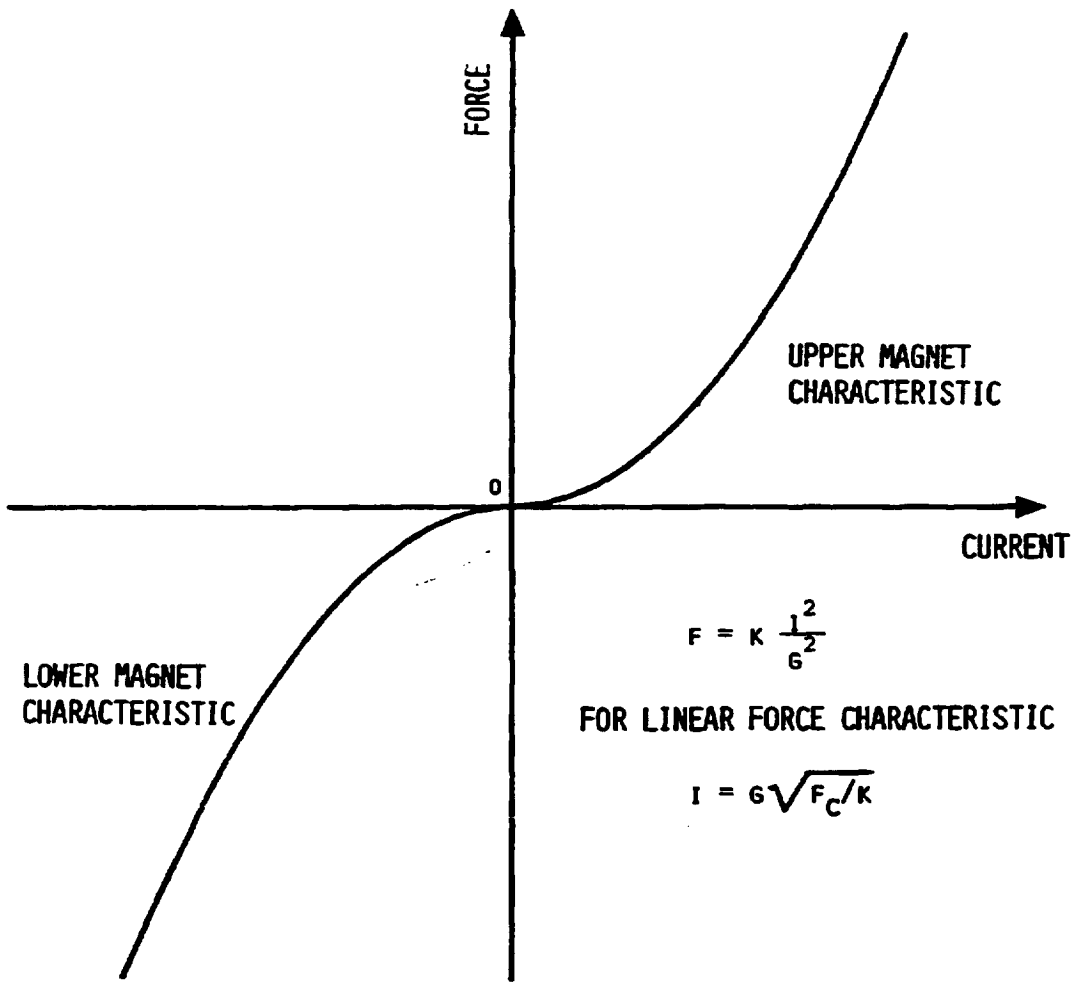
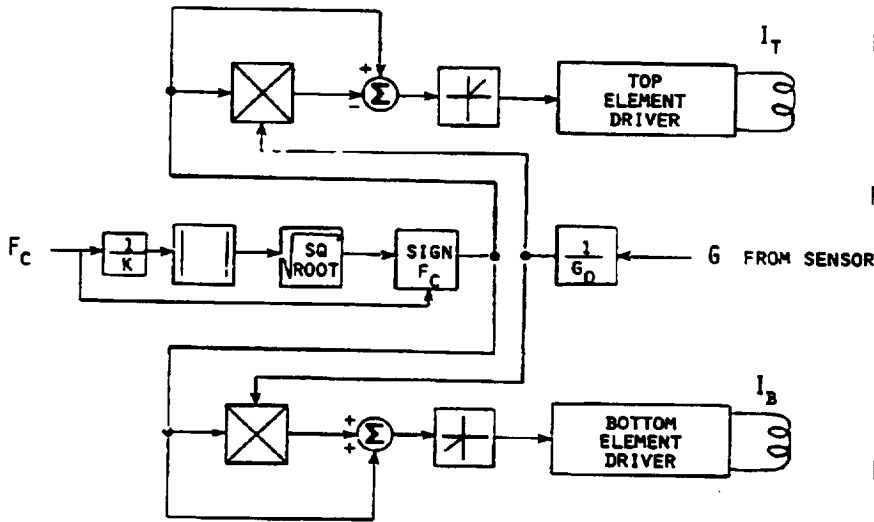


Figure 6 .

### ANALOG SOLUTION OF FORCE EQUATION FOR INDIVIDUAL ELEMENT CONTROL

Figure 7 is a simplified block diagram of an analog implementation of the solution of the force equation for a magnetic actuator with individual element control. This approach was implemented for a magnetic suspension system for the laboratory test model AMCD. For more detail on the implementation of this approach, see Reference 5.

#### INDIVIDUAL ELEMENT CONTROL ANALOG APPROACH (SOLUTION TO FORCE EQUATION)



$$F_T = K \frac{I_T^2}{G_T^2}, \quad G_T = (G_0 - G)$$

$$I_T = \frac{1}{G_0} \sqrt{\frac{F_C}{K}} (G_0 - G)$$

$$F_T = \bar{K} F_C$$

$$F_B = K \frac{I_B^2}{G_B^2}$$

$$F_B = K \frac{I_B^2}{G_B^2}, \quad G_B = (G_0 + G)$$

$$I_B = \frac{1}{G_0} \sqrt{\frac{F_C}{K}} (G_0 + G)$$

$$F_B = \bar{K} F_C$$

Figure 7

## TABLE LOOKUP APPROACH FOR INDIVIDUAL ELEMENT CONTROL

The last magnetic bearing linearization and control approach to be discussed is a microprocessor-based table lookup linearization approach for individual bearing element control and is shown in Figure 8. This approach was bench tested but has not been used in the AMCD laboratory model suspension system to date. In this approach, actual calibration data for a given bearing element pair are used to build a lookup table which is stored in the memory of a microprocessor system. Using the force command and gap position as input data, the correct value of current input to the coil, for the suspended element centered in the actuator gaps, is obtained by using a table lookup routine. This current is compensated for displacement from center by multiplying by the calculated gap. This approach is described and test results from bench tests are presented in Reference 6.

### INDIVIDUAL ELEMENT CONTROL MICROPROCESSOR APPROACH (TABLE LOOKUP)

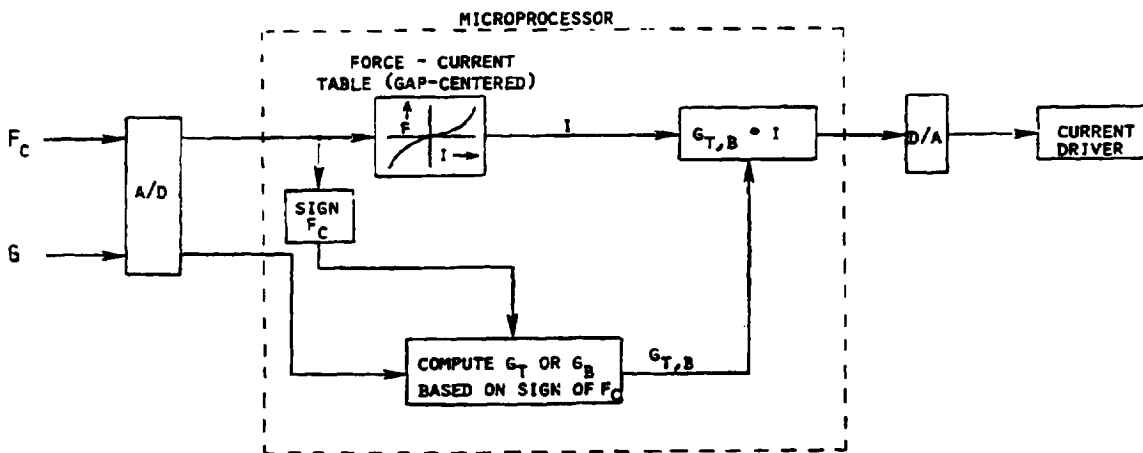


Figure 8

## REFERENCES

- (1) Anderson, Willard W.; and Groom, Nelson J.: The Annular Momentum Control Device (AMCD) and Potential Applications. NASA TN D-7866, 1975.
- (2) Anderson, Willard W.; Groom, Nelson J.; and Woolley, Charles T.: Annular Suspension and Pointing System. J. Guid. & Control, Vol. 2, No. 5, Sept.-Oct. 1979, pp. 367-373.
- (3) Ball Brothers Research Corp.: Annular Momentum Control Device (AMCD). Volumes I and II. NASA CR-144917, (1976).
- (4) Cunningham, D. C., Gismondi, T. P., and Wilson, G. W.: "System Design of the Annular Suspension and Pointing System (ASPS)," AIAA Paper 78-1311, AIAA Guidance and Control Conference, Palo Alto, CA, August 1978.
- (5) Khetarpal, M. : Magnetic Suspension System for an Annular Momentum Control Device (AMCD). NASA CR-159255, 1979.
- (6) Groom, Nelson J; and Miller, James B.: A Microprocessor-Based Table Lookup Approach for Magnetic Bearing Linearization. NASA TP-1838, 1981.

N85

3873

UNCLAS

D-23

N85 13873

MAGNETICALLY SUSPENDED FLYWHEEL SYSTEM STUDY

J. A. Kirk and D. K. Anand  
University of Maryland  
College Park, Maryland

H. E. Evans  
Advanced Technology and Research, Inc.  
Burtonsville, Maryland

G. E. Rodriguez  
NASA Goddard Space Flight Center  
Greenbelt, Maryland

ABSTRACT

The Goddard Space Flight Center (GSFC) and the University of Maryland (UM) Mechanical Engineering Department have a common interest in flywheels and have cooperated since the mid-1970's in designing and testing flywheel components. GSFC/UM is currently involved in studying application of a graphite/epoxy, magnetically suspended, pierced disk flywheel for the combined function of spacecraft attitude control and energy storage (ACES).

Past achievements of the GSFC/UM magnetically suspended flywheel program include design and analysis computer codes for the flywheel rotor, a magnetically suspended flywheel model, and graphite/epoxy rotor rings that have been successfully prestressed via interference assembly. All hardware has successfully demonstrated operation of the necessary subsystems which form a complete ACES design.

Areas of future GSFC/UM work include additional rotor design research, system definition and control strategies, prototype development, and design/construction of a UM/GSFC spin test facility.

The results of applying design and analysis computer codes to a magnetically suspended interference assembled rotor show specific energy densities of 42 Wh/lb (92.4 Wh/kg) are obtained for a 1.6 kWh system.

## INTRODUCTION

The Goddard Space Flight Center has been active in the development of high efficiency motor/generator and magnetic suspension systems since the early 1960's. One outcome of this work resulted in a magnetically suspended momentum wheel for spacecraft application [1,2,3]\*.

Based upon this early work at GSFC it appeared useful to consider a system which can provide for the joint functions of attitude control and energy storage. Since the mid-1970's GSFC and the University of Maryland have been active in a joint program on the various aspects of a magnetically suspended flywheel system. Recently GSFC/UM has addressed the problems of the joint solution of attitude control and energy storage. The program is termed ACES (Attitude Control and Energy Storage) and it involves hardware definition and problem identification/solution of all aspects of a magnetically suspended flywheel system.

The purpose of this paper is to provide a brief review of the GSFC/UM ACES effort, to present some of the hardware currently undergoing testing, and to identify the areas of future work.

---

\* Brackets denote references at end of paper.



## SYSTEMS BACKGROUND

In designing a magnetically suspended flywheel system, GSFC/UM has concluded [4,5,6] that a pierced disk of uniform thickness provides a desirable rotor geometry from both a performance and manufacturing point of view.

Shown in Figure 1 is a cross-sectional view of the original GSFC/UM magnetically suspended flywheel design. The original design consists of 2 rings with the outermost ring being made of a filamentary wound composite material and the inner ring being made of continuous iron bonded to the filamentary wound ring. The stator of this design fits in the "hole" of the 2 ring rotor and it carries the magnetic suspension and motor/generator electronics. The original GSFC/UM design was configured around a homopolar permanent magnet motor/generator with variable field flux for maintaining constant voltage output as rotational speed varies [4]. The magnetic suspension system is an integral part of the motor/generator design and it utilizes permanent magnets to establish a steady state magnetic flux, which is then modulated via sensor feedback [4].

Shown in Figure 2 is a photograph of the current test system which GSFC/UM is using to establish rotational losses and efficiencies for the motor/generator and magnetic suspension concepts embodied in the original GSFC/UM design. Testing is currently under way on this first generation ACES design and preliminary results are encouraging and support the performance projections previously presented in the literature [4,6].

## ROTOR DESIGN CONSIDERATIONS

RCA [7] and J.A. Kirk, under contract to GSFC, have done additional work on the original GSFC/UM design. It was concluded that a multiring, interference assembled rotor, such as shown in Figure 3, would provide for substantial improvements over the original GSFC/UM design. The modified GSFC/UM design, shown in Figure 3, differs from the original GSFC/UM design in the following areas:

1. The rotor is composed of a number of individual filamentary wound rings, rather than being one continuous ring.
2. The inside diameter (ID) to outside diameter (OD) rotor ratio (ID/OD) is smaller than the original GSFC/UM design.
3. The innermost ring is made of iron and is segmented into discrete pie-shaped "chunks".

Each of the above changes was made in the original GSFC/UM design in order to improve the overall performance of the system. The reasoning behind the changes has been documented by Kirk and Huntington [8,9,10,11] and a brief explanation follows:

1. The rotor is made of a number of composite material rings which are interference assembled. The reason behind this change is to favorably prestress the rotor so higher rotational speeds and energy densities can be obtained before a limiting performance constraint is encountered.
2. The ID/OD ratio has been lowered. The reason behind this change is that the original GSFC design was of a "thin hoop" type and suffered excessive "gap" growth between the rotor and the stator as it spun.

Since gap growth will degrade electrical performance, it must be controlled, and the best way to achieve this control is by decreasing the ID/OD ratio.

3. The innermost ring must be made of iron and is now segmented instead of being continuous. This change has been made because the iron ring would always reach its limiting strength long before the filamentary wound composite ring(s) reached their strength limit. To overcome this limitation a "segmented" inner ring is now proposed for use on the magnetically suspended flywheel system. The important point to note is that the inner iron ring will have all the necessary magnetic properties but will consist of a number of pie-shaped segments which are bonded to the inside diameter of the first filamentary wound ring. The iron ring thus has no stiffness in a "hoop" or tangential direction and presents an "inner loading" on the filamentary wound composite ring to which it is attached.

The three changes described above have no impact on the motor/generator or magnetic suspension system. The effect that these changes have on the projected system performance is dramatic and has been documented via a recent GSFC contractor report [12].

#### ROTOR ANALYSIS TOOLS

GSFC/UM realize that the final rotor design dimensions must evolve in parallel with the magnetic suspension and motor generator designs (as they impact on the dimensions and weight of iron inner ring). Obviously then, the most useful rotor design and analysis tools are those which most closely model the real physical system and are convenient to apply as the iron inner ring

design evolves. GSFC/UM has developed two (2) design and analysis tools for this purpose. Both tools are computer codes which perform detailed stress analysis and final dimension selection (including component tolerances) for all the components of the ring rotor. The analysis code is called FLYANS (FLYwheel ANalySis) and the sizing code is called FLYSIZE (FLYwheel SIZE). The interested reader will find a description of these codes in References 8 and 12.

Shown in Figure 4 is a schematic diagram of the multiring rotor which is modeled by the FLYANS and FLYSIZE codes. Each of the rotor rings is the same axial thickness and the stresses in each ring consist of a hoop or tangential stress ( $\sigma_{\theta}$ ) and a radial stress ( $\sigma_r$ ). If power is being put in or taken out of the system there is an additional shear stress ( $\tau_{r\theta}$ ) in each ring. It is assumed that the flywheel rings are in a state of plane stress, meaning that there is no variation of the  $\sigma_{\theta}$  and  $\sigma_r$  stresses in the axial direction.

The materials which comprise the multiring rotor are modeled as homogeneous, linearly elastic, orthotropic materials [13], with material properties specified in the radial and tangential direction. The current GSFC/UM design is based on Celion 6000/epoxy for the filamentary wound composite rings [12]. It should also be pointed out that any new or hypothetical materials can easily be added to the computer code data base with minimal effort.

The total stress distribution in one ring of the multiring flywheel is the superposition of the five stress distributions due to the following:

1. Rotation of the ring at constant angular velocity.
2. Interaction with adjoining rings due to rotational expansion.

3. Interference assembly of the rings.
4. Residual stresses due to curing.
5. Angular acceleration of the entire assembly.

The stress distribution for the entire flywheel is the summation of the above 5 stresses for each flywheel ring.

Of the 5 stress distributions given above, no. 3, interference assembly, is under the direct control of the designer. The FLYANS code provides an algorithm for the selection of interference pressures in order to optimize the stored energy per unit weight of the rotor.

It will be instructive at this point to consider the hypothetical example of how interference stresses interact with rotational stresses in a simple 2 ring "pierced disk" rotor.

Shown in Figure 5 is the stress distribution which occurs when 2 rings of the same material are interference assembled. When the interference stress distribution is added to the rotational stress distribution the net result is as shown in Figure 6. In Figure 6 the stresses have been made nondimensional by the factor

$$\rho_1 \omega^2 b^2 \text{ (units are psi)}$$

where

$\rho_1$  = mass density for the first ring of the assembly (value is weight density in lb/in<sup>3</sup> divided by  $g = 386 \text{ in/sec}^2$ )

$\omega$  = rotational speed (rad/sec)

$b$  = outer radius of the flywheel (inches)

The solid line shown in each of the plots in Figure 6 represents the stress

distribution which occurs when the 2 rings are spun without any interference assembly present. The dotted lines show the stress distribution when the 2 rings are interference assembled and then spun. Consider the lower plot in Figure 6. If the working tangential stress of the material,  $\sigma_\theta$ , is constant, then the limiting value of  $\sigma_\theta/\rho_1\omega^2b^2$  is = 0.97 with no interference present, and 0.94 with interference present. For a fixed value of  $b$  and  $\sigma_\theta$  it is clear the interference assembled flywheel has a larger  $\omega$ , and therefore a larger kinetic energy per unit weight over the non-interference assembled flywheel.

GSFC/UM has done preliminary testing of interference assembly of composite rings and has found that a conical taper of approximately 1 degree between the inside diameter and outside diameter of adjacent rings will permit press assembly of the rings. Shown in Figure 7 are two graphite epoxy rings that were assembled and pressed together at the Hercules Alleghany Ballistics Laboratory (Cumberland, MD) in 1978. The two rings are 8 inches in OD, 7 inches in ID and are each 1/2 inch in radial thickness. The two rings have approximately 0.3% interference and the ring interface was lubricated with epoxy before pressing together. The collection of wires shown in Figure 7 is for strain gage instrumentation placed on the rings. The ring assembly shown in Figure 7 was donated to the University of Maryland and is currently undergoing further testing as part of the GSFC/UM ACES program.

The results of applying the FLYANS and FLYSIZE computer codes to a 1.6 kWh GSFC/UM design [12] have shown that it is possible to design a 6 ring rotor with an iron inner ring. The rotor has an inside diameter of 8 inches and an outside diameter of 20 inches. Using Celion 6000/epoxy for all the filamentary wound composite material rings, the projected specific energy density is 41.9 Wh/lb

(92.2 Wh/kg) and the inner radius displacement (i.e., air gap growth) will not exceed .040 inch (from 0 to burst speed).

#### CURRENT WORK

GSFC and UM are currently engaged in a detailed study which will significantly advance understanding of the magnetically suspended flywheel for ACES. The following three major tasks are currently being worked on:

1. Rim research requirements
2. Systems research requirements
3. UM/GSFC prototype development and spin test facility.

#### Task 1: Rim Research Requirements

The purpose of this task is to conduct a detailed analytical analysis of the mechanical properties and stresses of a composite material rim.

Specifically the analysis will include:

- Analytical determination of the stress distribution in the rim. This will include the loading of the iron at the inner radius. The simulation of the stress distribution will be initially represented by closed form solutions, although standard finite element codes may be applied if the authors feel their use is warranted.
- Determination of the effect of mechanical stresses on the magnetic properties of the iron with specific consideration of hysteresis.
- Identification of optimum materials and manufacturing/assembly methods for present and future rims with an aim towards maximizing performance.
- The use of multirings that are interference assembled for prestressing.
- Identification of detection mechanisms for rotor failure and system

shutdown prior to destructive failure.

The overall goal is to clearly define the present state of technology and future problems that must be solved for a viable design.

### Task 2: System Research Requirements

The purpose of this task is to conduct a study in order to establish the feasibility of the complete ACES system. Three major sub-tasks have been identified. These are:

- System definition
- Control strategies
- System testing

System definition includes the characterization of the subsystems needed for the entire system. This includes specifying, at least generally, the requirements of commutation, microprocessing, containment and interactions, and identifying the problems of failure and shutdown. The identification of control strategies for the system is quite unique. Certainly the inertial coupling and control of the momentum require careful analysis. The interaction of the magnetic field and other perturbations on stability and attitude control are also important areas requiring careful characterization.

The system testing component of this task is specifically concerned with testing the GSFC/UM model. This model will be modified for maximum performance by redesigning the rotor initially. The primary thrust of this exercise is to identify important parameters that must be studied for future component and system design.

### Task 3: UM/GSFC Prototype Development and Spin Test Facility

An important adjunct to the current research tasks is to foster continued



long-term involvement between the University of Maryland and GSFC. At the end of FY 84 it is envisioned that GSFC/NASA Headquarters will continue UM funding for development of the ACES system. In particular, the next phase of the work will involve development of a 500 watt hour ACES system along with design and construction of test facilities suitable for evaluating the 500 watt hour system. The proposed UM test facilities will provide for experimental monitoring of the performance of the rim, motor/generator, and magnetic suspension systems. The 500 watt hour system will be designed for ease in the replacement of all components. It is expected that the 500 watt hour system will serve the purpose of both a showpiece working model and a facility to try out enhancements which can improve system performance. Not only will UM be a NASA/GSFC resource but, in addition to that, NASA contractors producing deliverable magnetically suspended flywheel systems will find UM to be a valuable analysis, test, and evaluation facility.

#### CONCLUSIONS

The concept of using a magnetically suspended flywheel for the combined function of spacecraft attitude control and energy storage (ACES) is extremely viable. Several pieces of hardware have been built and are undergoing testing to evaluate the various subsystems used in ACES. Based upon reasonable and well founded projections, an ACES magnetically suspended flywheel system could easily store 1.6 kWh with a rotor specific energy density of 42 Wh/lb (92.2 Wh/kg).

The areas of study which will be required to integrate the ACES subsystems into a complete working system have been identified and are currently under detailed study. The results of the current study will project a workable

5-year plan between UM and NASA/GSFC to turn the already documented successes of the magnetically suspended flywheel system into a complete ACES system.

## REFERENCES

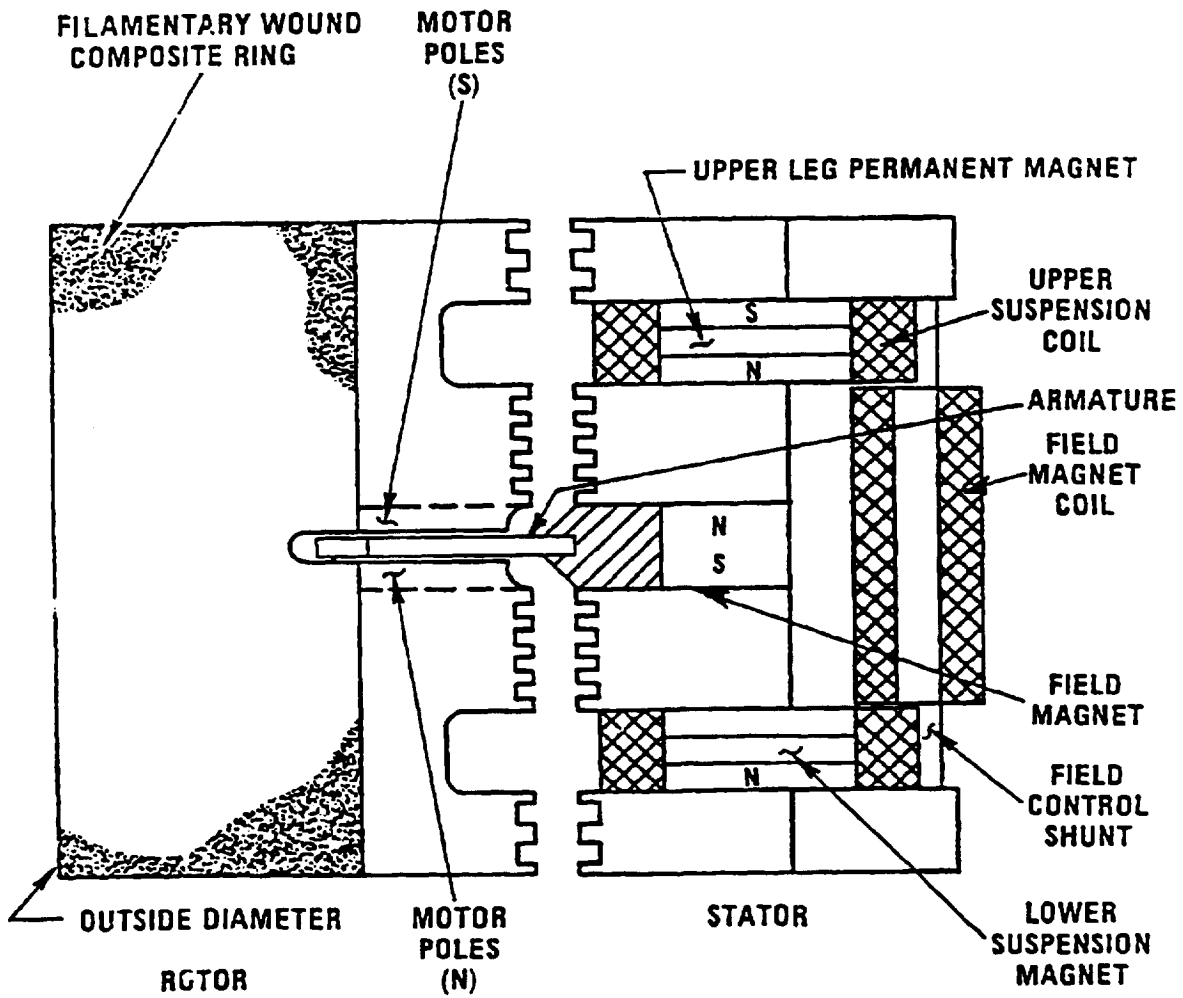
1. Studer, P.A., "Magnetic Bearing", U.S. Patent 3,865,442, February 11, 1975.
2. Studer, P.A., "Magnetic Bearings for Spacecraft", Goddard Space Flight Center, TM X-66111, January 1972.
3. Studer, P.A., "Electric Motive Machine Including Magnetic Bearing", U.S. Patent 3,694,041, September 26, 1972.
4. Kirk, J.A., Studer, P.A. and Evans, H.E., "Mechanical Capacitor", NASA TND-8185, March 1976.
5. Kirk, J.A., "Flywheel Energy Storage - Part I, Basic Concepts", International Journal of Mechanical Sciences, Vol. 19, 1977, pp. 223-231.
6. Kirk, J.A. and Studer, P.A., "Flywheel Energy Storage - Part II, Magnetically Suspended Superflywheel", International Journal of Mechanical Sciences, Vol. 19, 1977, pp. 233-245.
7. Michaelis, T.D., Schlieben, E.W. and Scott, R.D., "Design Definition of a Mechanical Capacitor", Contractor Report NASA CR-152613, May 1977.
8. Kirk, J.A. and Huntington, R.A., "Energy Storage - an Interference Assembled Multiring Superflywheel", Proceedings of the 12th Intersociety Energy Conversion Engineering Conference, Aug. 28-Sept. 2, 1977, pp. 517-524.
9. Kirk, J.A. and Huntington, R.A., "Stress Analysis and Maximization of Energy Density for a Magnetically Suspended Flywheel", ASME paper 77-WA/DE-24, 1977.
10. Kirk, J.A. and Huntington, R.A., "Stress Redistribution for the Multiring

Flywheel", ASME paper 77-WA/DE-26, 1977.

11. Huntington, R.A., "Stress Analysis and Maximization of Performance for a Multiring Flywheel", M.S. Thesis, University of Maryland, Mechanical Engineering Department, Jan. 1978. Thesis advisor: J.A. Kirk.
12. Kirk, J.A. and Evans, H.E., "Inertial Energy Storage Hardware Definition Study -- Ring Rotor", NASA CR-175217, 1984.
13. Ashton, J.E., Halpin, J.C. and Petit, P.H., Primer on Composite Materials: Analysis, Technomic Publishing Co., Stamford, Conn. 1969.

Figure 1

Original GSFC/UM Design



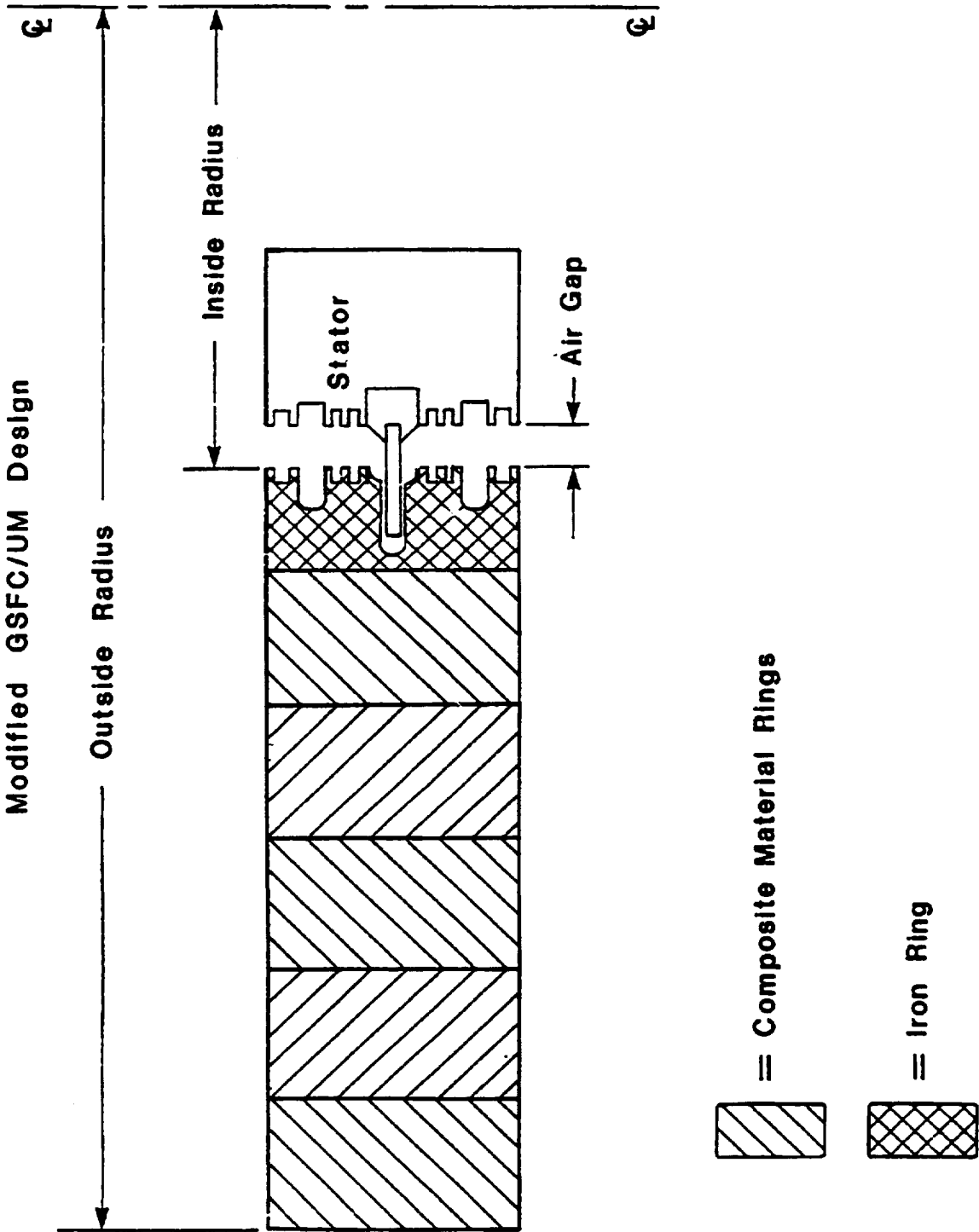
ORIGIN  
OF POCN QUANTITY

Figure 2

The GSFC/UM test system



**Figure 3**  
**Modified GSFC/UM Design**



**Figure 4**  
**Ring Rotor Model**

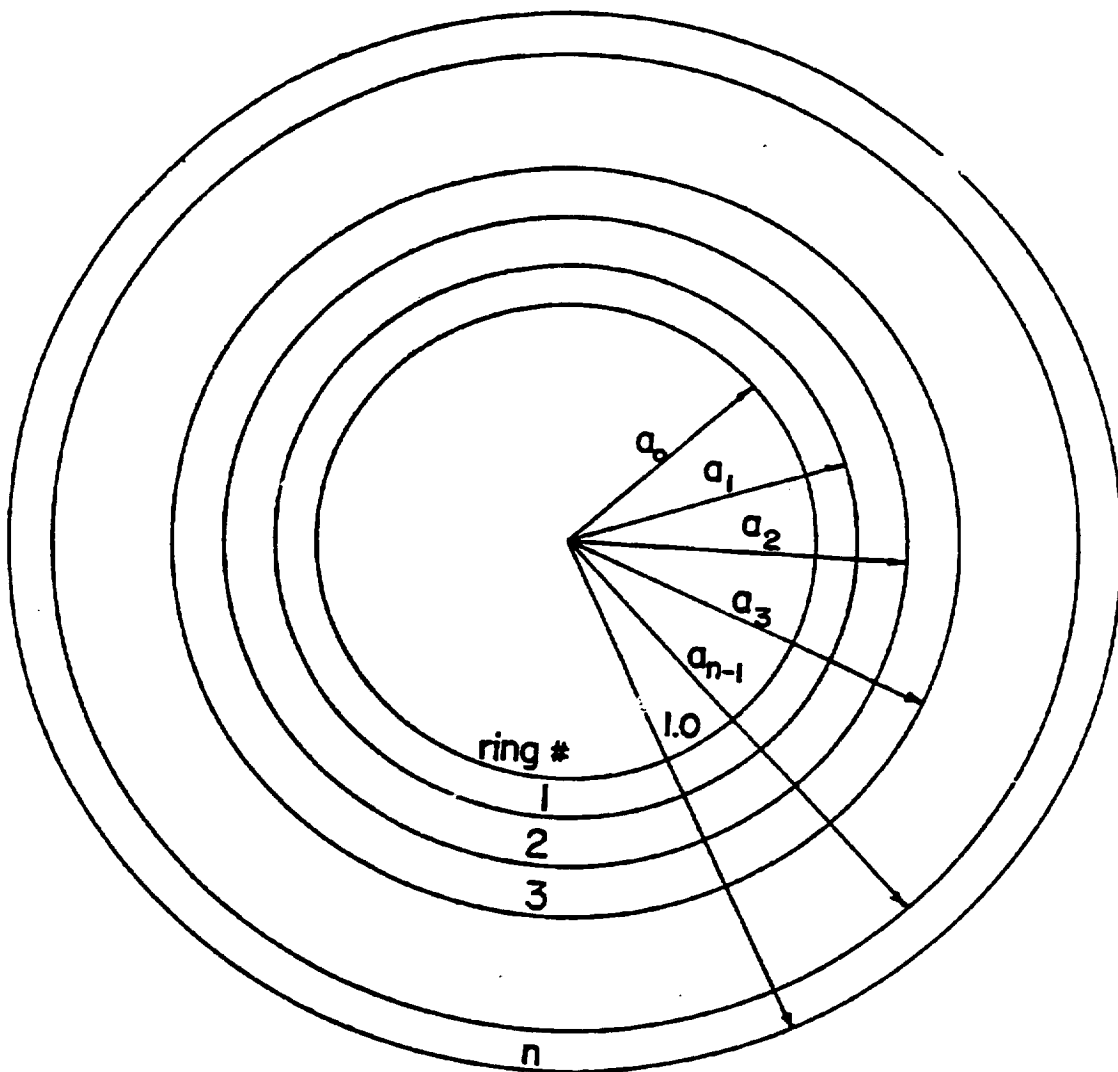
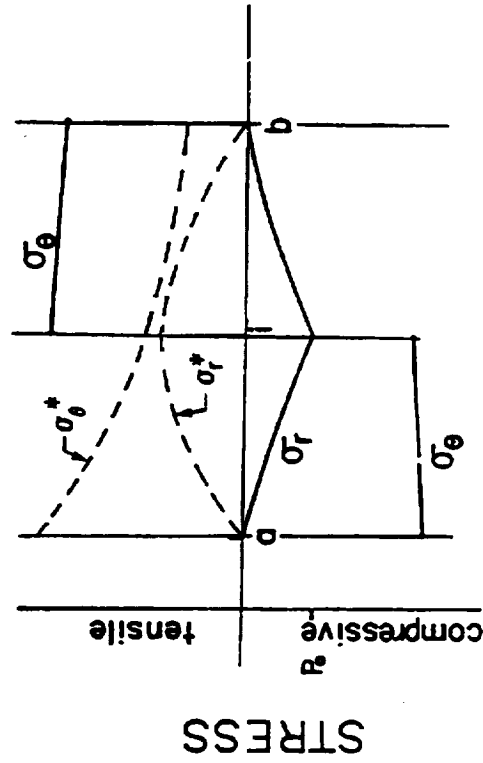
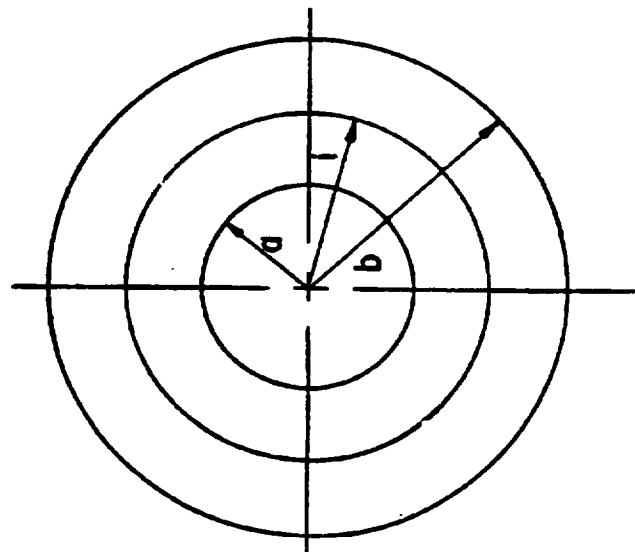




Figure 6

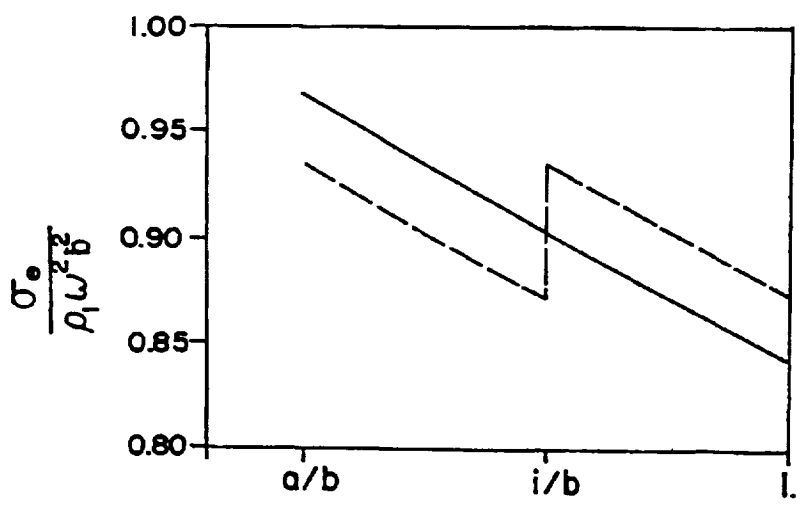
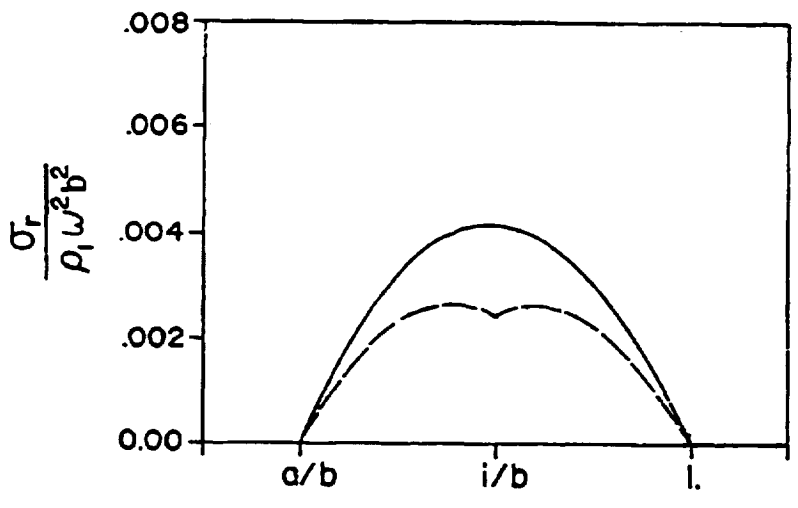
# INTERFERENCE ASSEMBLY



$\sigma_\theta^*$ ,  $\sigma_r^*$  - Rotational Stresses

Figure 6

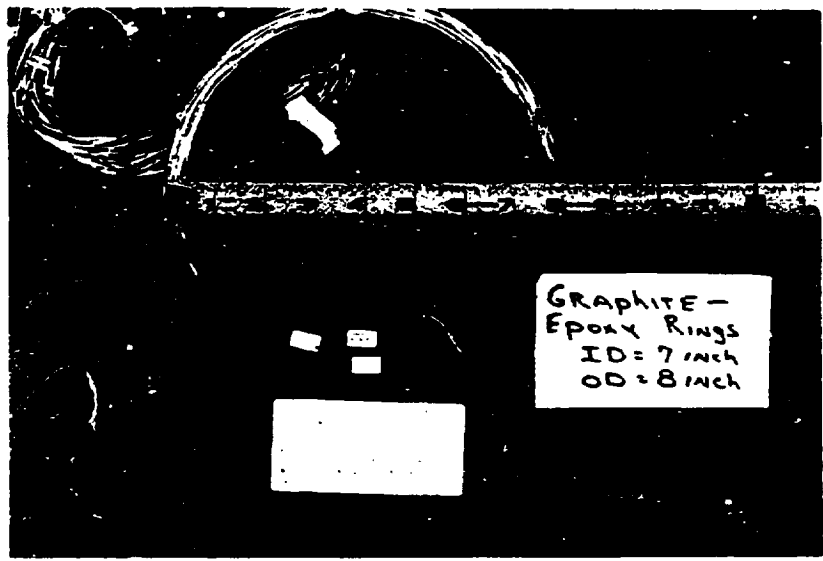
STRESS VS. RADIUS  
2 RING



———— = No Interference  
----- = With Interference



Figure 7  
Graphite/epoxy press fit rings



N85

3874

UNCLAS

0-24

N85 13874

REACTION WHEELS FOR KINETIC ENERGY STORAGE

Philip A. Studer  
NASA Goddard Space Flight Center  
Greenbelt, Maryland

## ABSTRACT

In contrast to all existing reaction wheel implementations, an order of magnitude increase in speed can be obtained efficiently if power to the actuators can be recovered. This will allow a combined attitude control-energy storage system to be developed with structure mounted reaction wheels.

Combining reaction wheels with energy storage wheels may seem an unlikely marriage between two elements with opposing requirements. This paper will show that they are not incompatible. The power required for control torques is a function of wheel speed but this energy is not dissipated; it is stored in the wheel. The  $I^2R$  loss resulting from a given torque is shown to be constant, independent of the design speed of the motor. What remains, in order to efficiently use high speed wheels (essential for energy storage) for control purposes, is to reduce rotational losses to acceptable levels.

Progress has been made in permanent magnet motor design for high speed operation. Variable field motors offer more control flexibility and efficiency over a broader speed range. Research necessary to reach the goal of efficient kinetic energy storage will have generic benefits to spacecraft attitude control systems and dynamic power systems. (See fig. 1.)

## REACTION WHEELS for ENERGY STORAGE

### AC/ES

- + REGENERATIVE TORQUE CONTROL
- +  $I^2R$  INDEPENDENT OF SPEED

### MOTOR TECHNOLOGY

- + IRONLESS ARMATURE
- + PERMANENT MAGNETS
- + VARIABLE FIELD-CONSTANT VOLTAGE

Figure 1

## REACTION WHEELS FOR KINETIC ENERGY STORAGE

Energy storage in flywheels has had a long and successful history in machines as simple as grandmother's spinning wheel to current automotive engines. It has recently been studied and found potentially competitive for applications in which the desired output is electrical as an alternative to electrochemical batteries. Rotating machinery has not had a significant role in aerospace power systems, whereas attitude control systems have used flywheels for stabilization and control since the early days of space flight. Combining these functions could potentially reduce the weight of two of the heaviest elements in both of these systems. Power used for attitude control has not been recovered in the past. Brushless DC motor drives make it possible to recover energy previously lost, improving system efficiency.

Merging these two subsystem functions and recovering energy used for control radically change the tradeoffs used to size and set the speed limits on reaction wheels. It will be shown that several improvements in technology have the effect of raising the optimum design speed of reaction wheels with a consequent reduction in control system mass. Likewise, the further evolution of wheel technology necessary to make flywheels competitive with batteries will have a beneficial effect on all future attitude control systems.

Historically, reaction wheels have been low speed devices. They are generally operated at nominally zero speed and are able to store momentum by rotating in either direction. The maximum speed is set by the cyclic momentum expected in one orbit. The rotational motion of the wheel is a

mirror image of the motion of the spacecraft (or what that motion would be if unopposed). The amplitude of the angles, rates, and accelerations are proportional to the ratio of the inertia of the wheel to inertia of the spacecraft about the axis of control. The stored momentum is the product of wheel inertia and angular rate. Therefore, a tradeoff is routinely run between Reaction Wheel Assembly (RWA) weight and power as a function of maximum speed to find a minimum effective weight which will meet the mission momentum requirement. (See fig. 2.)

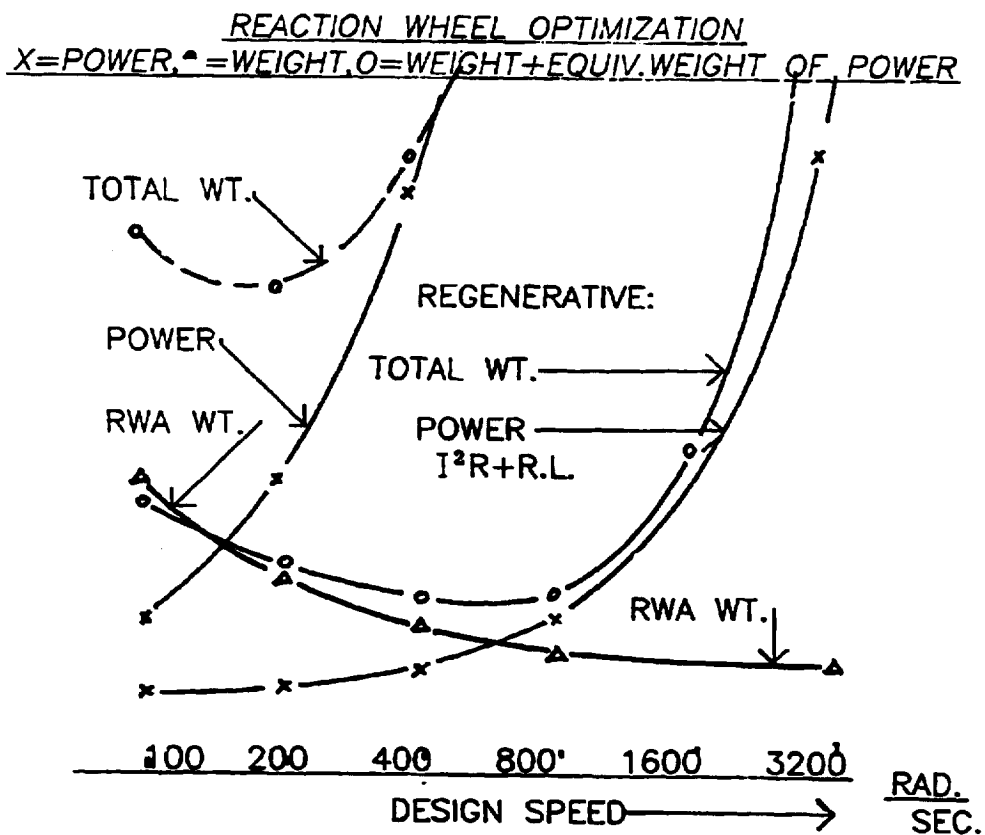


Figure 2



This proportionality between power and maximum speed is based on the physical law relating power to speed and torque (figure 2). The motor constant  $K_T$ , torque per ampere, is equal to  $K_V$ , volts per rad/sec. We cannot change these physical relationships but we note that this energy is not dissipated, it is stored in the wheel. In the case of a combined attitude control/energy storage (ACES) system, we have simply transferred energy from one storage element to another where it remains available to the power system. Since reaction wheel control handles cyclic torques, the wheel will be called on to slow down as often as to accelerate. The drive must be a motor/generator to efficiently recover the stored energy and transfer it to the spacecraft electrical load. The permanent magnet dc motor is an efficient transducer. It behaves equally well as a generator and as a motor. This power recovery has not generally been implemented in spacecraft control systems because the energy was relatively small and the voltage variation was 100 percent, making efficient recovery very difficult. For high speed energy storage wheels, the energy involved will be larger and the voltage variation much smaller.

The efficient transfer of power requires a careful look at the amount of power dissipated in the process. As we have seen earlier, the motor constant  $K_T$  decreases in proportion to the increased no-load speed of the motor. At first glance, an order of magnitude increase in the current to produce a given torque looks alarming, recognizing that  $I^2R$  is the power dissipated.

However, (figure 3) the number of turns (armature conductors) necessary to achieve  $K_v$  and  $K_t$  are lower by the same proportion. Also, if the motor in question is the same size, the diameter of the conductors can also be proportionally increased. Therefore,  $R$  decreases as fast as  $I^2$  increases and the internal dissipation is the same for all design speed ranges.

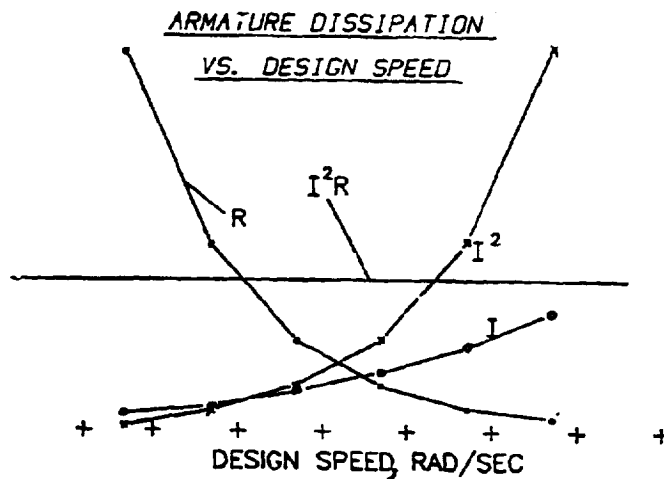


Figure 3

A more difficult challenge is posed by the rotational losses. At peak efficiency the rotational losses are equal to the  $I^2R$  losses (figure 3). Furthermore, these are not all linearly related to speed. There are components which are speed independent, such as hysteresis in motor laminations, and some which increase faster than the square of the speed such as windage. It is necessary to isolate and eliminate as many sources of parasitic loss as possible if efficient high speed operation is to be achieved<sup>(1)</sup>. There follows a list of losses not associated with power into or out of a dc motor generator (see fig. 4):

ROTATIONAL LOSSES

SOURCES: \_\_\_\_\_ SOLUTIONS:

BRUSHES,  
    MECH. \_\_\_\_\_  
    ELEC. \_\_\_\_\_ POWER FETS  
WINDAGE, \_\_\_\_\_ VACUUM  
"CORE" LOSSES,  
    HYSTERESIS \_\_\_\_\_ IRONLESS ARMATURE  
    EDDY CURRENTS \_\_\_\_\_  
ARMATURE,  
    EDDY CURRENTS \_\_\_\_\_ "LITZ" WIRE  
    CIRCULATING CURRENTS \_\_\_\_\_ "WYE" WINDING

Figure 4

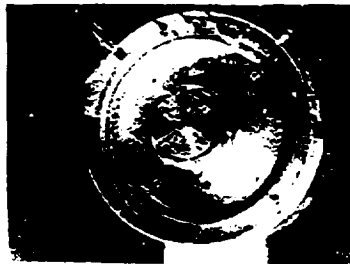
Electronic commutation has eliminated the mechanical drag torque associated with carbon brushes. There are electrical losses due to leakage currents in power switches and diodes, logic circuit power drain, and rotor position sensors. All of these occur independent of the power demand on the motor/generator. They are also independent of the operating speed of the motor and will not be considered further here.

Windage loss is extremely speed dependent; but the solution is straightforward. Reduction of enclosure pressure to  $10^{-5}$  torr can make this loss negligible over the entire speed range.

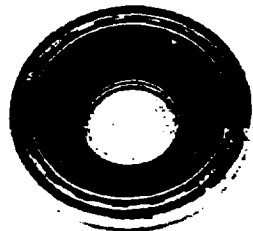
Bearing drag torques for mechanical bearings have both coulomb and viscous components. The power loss is therefore proportional partly to speed and partly to the square of wheel speed. Magnetic bearings offer somewhat lower torques having the same effects due to hysteresis and eddy currents. Treating magnetic bearing torques adequately would require a full discussion in another paper. For the purpose of this discussion, let us assume that the bearing torque loss can be held to small enough levels so as not to drive the choice of operating speed.

For conventional dc motors, the hysteresis and eddy current losses are much larger than bearing losses for the power and torque levels required for either energy storage or reaction wheel control. These losses occur in the laminated magnetically soft iron into which the armature conductors are wound. Although the potential of newly developed amorphous steel alloys, such as Metgas (a trademark of Allied Corp.), have not been fully explored, the power losses of this type of motor would likely be prohibitively high at the upper end of the speed range.

Fortunately another dc motor construction is available. These so-called "ironless armature" dc motors have the armature conductors in the magnetic air gap<sup>(2)</sup> (figure 5).



MOTOR ARMATURE (IRONLESS)  
& MAGNETIC BEARING STATOR



PERMANENT MAGNET SmCo<sub>5</sub> MOTOR ROTOR  
& MAGNETIC BEARING SUSPENSION RING

Figure 5

The entire "iron" and permanent magnet field assembly is on the rotor and there is no relative motion between it and any stationary iron. Therefore, there is no hysteresis loss. There remains eddy current loss within the armature conductors themselves, but even this can be reduced by known methods such as subdividing each conductor into finer strands ("litz" wire)<sup>(3)</sup>. Further gains can be expected by pole shaping to make the field pole flux vary sinusoidally since the flux gradient creates the eddy currents. Neither of these techniques drastically affects the performance or sizing of the motor. Therefore, very high efficiency, high speed motor design can be approached with confidence when the necessary analytical and experimental resources are applied.

There are a few other sources of parasitic power losses such as circulating currents within the armature windings and eddy currents in various structural and mechanical parts which require careful engineering attention because they are generally ignored in less demanding applications.

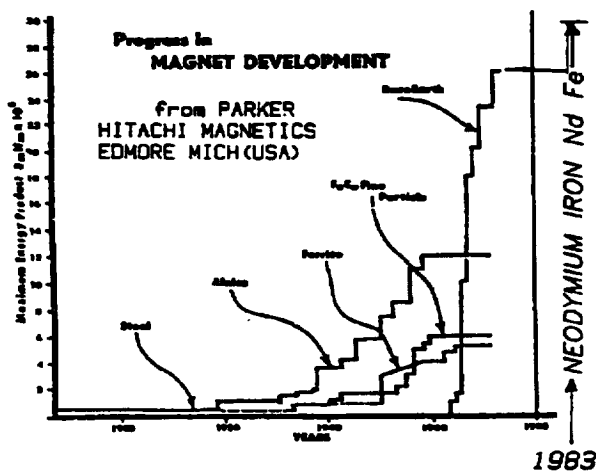


Figure 6

Permanent magnet motors have improved significantly in the past 25 years (figure 6) and each of these steps has allowed efficient operation at a higher speed regime. Higher speed puts more energy into a smaller lighter package. This has a visible impact in attitude control technology—the NOAA series of spacecraft utilize brushless dc reaction wheels with a no-load speed of 10,000 RPM. Neither ironless armature motors nor magnetic bearings have yet been applied to flight spacecraft systems by American aerospace manufacturers. In spite of many feasibility demonstrations, the required depth of engineering analysis and design has not been applied. However, given the technology program needed to accomplish the kinetic energy storage task, generic improvements in attitude control systems will result.

All of the earlier discussion focused on permanent magnet motors. Would field motors offer greater control flexibility, the ability to vary the peak of the efficiency point to match the load, and produce constant voltage over a range of speeds. (See fig. 7.)

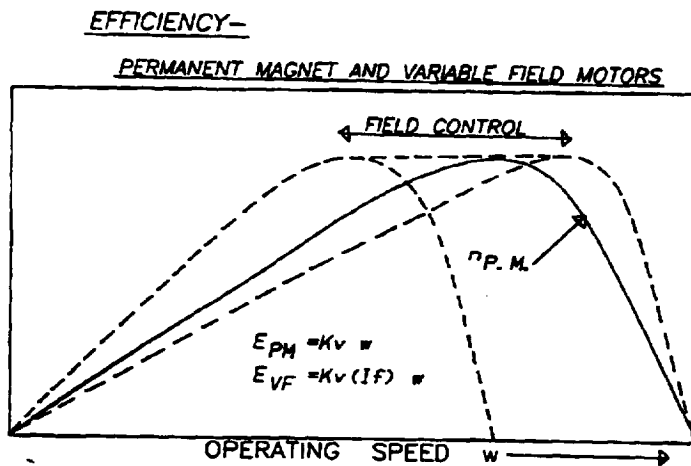


Figure 7

This technology was explored briefly in the 1960's and is applicable to combined energy storage and attitude control systems. The value of wound field motors increases at higher power levels now being considered. NASA owns the patents on this design approach<sup>(4,5)</sup>. To improve balance stability both the field and the armature windings are on the stator. The rotor is entirely a magnetically soft ferro-magnetic alloy, which has the requisite strength properties for use on energy storage wheels. Since the field flux is induced into the rotor via an auxiliary airgap(s), the magnetic suspension can be integrated into the motor design with a sizeable weight savings since they utilize a common "iron" path. Integration of these two prime functions adds a significant challenge to the engineering design task. The payoff is a vastly superior product.

In conclusion, the GSFC is already operating reaction wheels in space with good reliability at speeds as high as 10,000 RPM. The technological path which will allow quadrupling this speed to make kinetic energy storage competitive with electrochemical systems has already been charted. If the decision is made to proceed with development and use of ACES, a significant advance will be achieved in two primary spacecraft subsystems. If the United States does not meet this challenge, someone else will; the Europeans<sup>(6)</sup> and the Japanese<sup>(7)</sup> are already proceeding with developments of energy storage flywheels.

Efficient recovery of the energy stored in a flywheel is implicit in a kinetic energy storage system. When this mode of operation is incorporated into the reaction wheel sizing and speed selection tradeoffs, much different results are obtained.

The technological development program to make efficient reliable energy storage wheels will have substantial intermediate benefits in attitude control and dynamic power systems generally. Power efficient lightweight high-speed control and momentum storage wheels will improve spacecraft "bus" performance, increasing payload mass fraction and available power for instruments. Combining the functions of control actuators and energy storage as in ACES focuses the technology on two of the more massive elements in spacecraft and can be of particular value in large scale long-life systems where resource sharing, distributed control, and unlimited cycle life are essential.

#### REFERENCES

1. Kuhlman, John H.: Design of Electrical Apparatus, Third ed., chap. 7, J. Wiley & Sons, Inc., 1950.
2. Studer, P. A.: A New DC Torque Motor. Second Int. Workshop on R.E. Cobalt Magnet Applications, Univ. of Dayton, Dayton, Ohio, June 8-11, 1976.
3. Roters, Herbert C.: Electromagnetic Devices. J. Wiley & Sons, Inc., 1941.
4. Studer, P. A.: Direct Current Motor With Stationary Armature and Field. U.S. Patent 3,569,804, Aug. 1968.
5. Studer, P. A.: Electric Motive Machine Including Magnetic Bearing. U.S. Patent 3,694,041, Jan. 1971.
6. Napolitano, L. G.: Space 2000. 33rd Int. Astronautical Congress, Paris, France, Sept. 27 - Oct. 2, 1982.
7. Murakami, C.: Development Activity on Magnetic Bearings for Space Use in the National Aerospace Lab of Japan. Sixth Int. Workshop on R.E. Cobalt Magnet Applications, Baden/Vienna, Austria, Aug. 31 - Sept. 3, 1982.



N85

3875

UNCLAS

D-25

N85 13875

**ADVANCED HIGH-POWER TRANSFER  
THROUGH ROTARY INTERFACES**

**Pete Jacobson  
Senior Staff Engineer  
Sperry Corporation  
Flight Systems, Space  
Phoenix, Arizona 85036**

## ROLL-RING CONFIGURATION

The successful flights of space shuttles Columbia and Challenger initiated an entirely new generation of space research. The opportunity now exists to build and maintain a variety of strategically important space structures. A large percentage of these spacecraft will have one or more rotating interfaces through which signal and/or power current must be conducted. New demands for high-voltage and high-current transfer, at up to 200-kilowatt (kW) power levels, have been forecast, particularly in the area of solar power arrays.

Considerable research has been conducted to determine the operational advantages and disadvantages of a variety of rotating electrical interface devices. The majority of this effort has been expended on a wide variety of slip-ring designs, power rotary transformers, and the roll ring. The latter device is the subject of this paper.

The patented roll ring, a concept with over 550,000 circuit hours of test in 400 circuits, is a device that performs the same function as a slip ring/brush assembly, but does so by means of rolling instead of sliding electrical contact. The roll ring consists of two concentric conductive rings and at least one rolling flexible conductive element. This latter flexure is fitted to and captured in the annulus space between the two rings. When the rings are suitably attached to two structures aligned with a common axis, the flexure provides a precise electrical coupling between the two. Figure 1 shows a photograph of the circuit components of a typical roll-ring circuit. This particular design has been used to conduct up to 15 amperes of current.

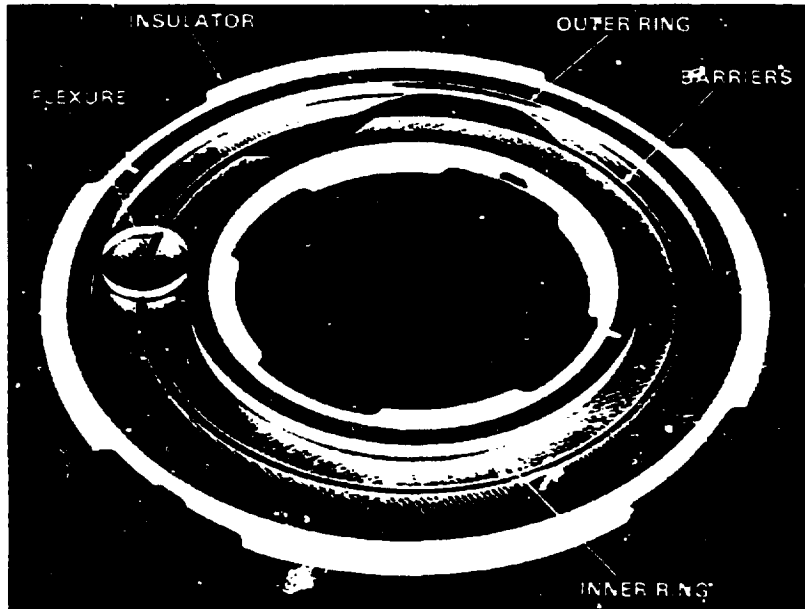


Figure 1: Single Roll-Ring Circuit

## DESIGN FEATURES – CURRENT CAPACITY

When transfer currents exceed 15 amperes, the roll-ring design is modified and the number of flexures is increased to divide the total current. The flexure design parameters are also modified to accommodate a transfer current greater than 15 amperes.

Another design consideration is the fact that sliding contact is undesirable in any device that operates in hard vacuum. When more than one flexure is used, the high-power design includes idlers between adjacent flexures to minimize interface sliding. These idlers are guided by a set of rails that are mechanically attached to the inner ring assembly. This arrangement is shown schematically in Figure 2.

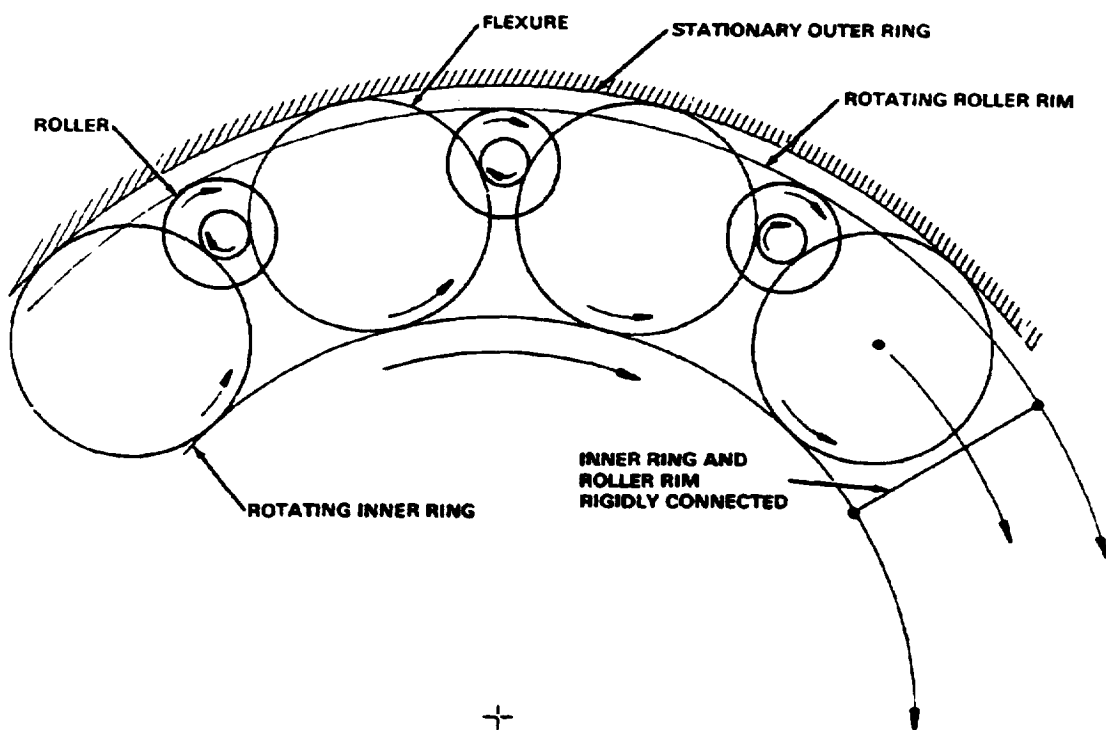
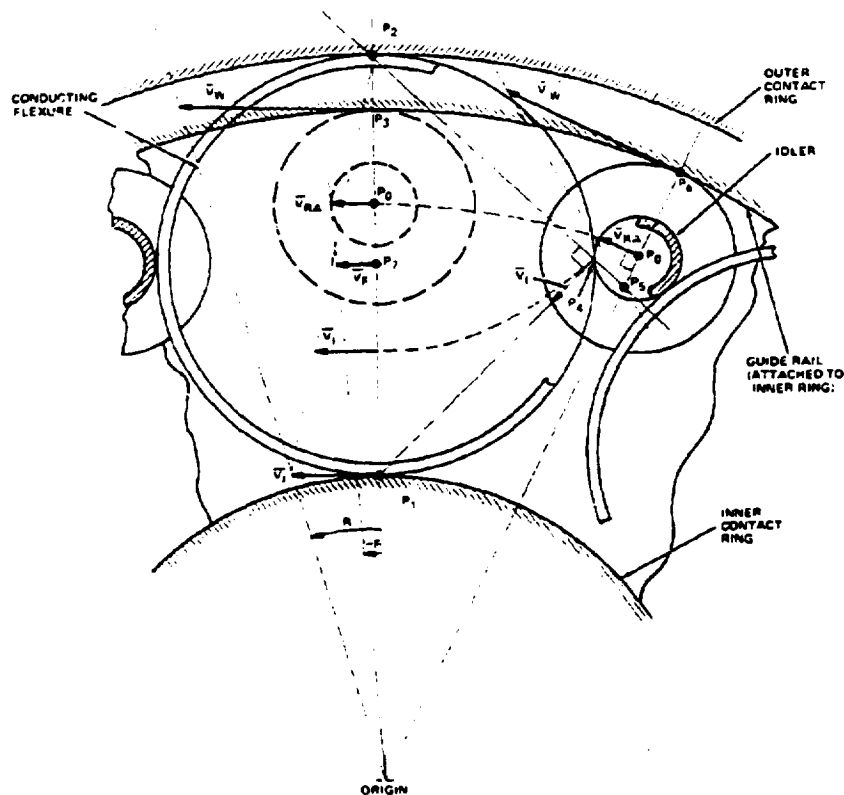


Figure 2: Multiple Flexure Idler Configuration

## DESIGN FEATURES — ROLLING INTERFACES

The idlers that maintain the spacing between adjacent power flexures roll on a rim that is rigidly connected to the inner ring assembly. This nonconductive, disc-like mount acts in conjunction with the outer ring spacer/insulators to provide an effective labyrinth between adjacent ring sets. This labyrinth acts primarily to inhibit arcing and corona formation at higher voltages. It also effectively controls debris, and even though debris generated by roll-ring components is almost nonexistent, these barriers also prevent external debris from entering the circuit cavities.

In any given high-power, roll-ring design, the size of all roll-ring components is selected by simultaneous solution of the interface velocity equations of these components so that the relative velocity of the two contacting surfaces at each interface is zero. Figure 3 is a graphic representation of these various velocity vectors.



**Figure 3: Velocity Vector Diagram**

## HIGH-CURRENT PROTOTYPES

An initial design was generated on Sperry IR&D funding for a multiflexure high-current test module that incorporated idlers to maintain the spacing between adjacent flexures. This configuration fulfills a need for high-current transfer for both oscillating and rotating applications. This design requires that a full complement of flexures exist in the annulus between the rings. Two iterations of this device have been evaluated to date. The measured contact resistance of a ring set (circuit) is less than .6 milliohm ( $m\Omega$ ). The unit has been tested at up to 200 amperes in  $10^{-3}$  torr vacuum at 10 volts. The unit has been operated for >300,000 revolutions without showing measurable wear. A photograph of the original two-circuit prototype test module is shown in Figure 4. The latest version of the original prototype has demonstrated that weight-to-power ratios as low as .07 kilogram/kilowatt are achievable, even for only two-circuit configurations.



Figure 4: High-Current Test Module

## PREVIOUS PERFORMANCE

The modified two-circuit prototype was tested in a  $10^{-3}$  torr vacuum, and evaluations were made at various current levels up to 185 amperes, the limit of the power supply. The transfer efficiency, defined as the percentage of current conducted through the rotating interface without thermal loss, was derived from these tests. The mean terminal-to-terminal resistance of the prototype was measured as  $6 \times 10^{-4}$  ohm. This roll-ring design can be configured to accommodate high voltages, which makes it feasible to include this parameter in the potential transfer efficiency optimization. The governing equation is

$$e_T = \frac{EI - I^2R}{EI} = \frac{E - IR}{E}$$

where

- E = Source Potential
- I = Conducted Current
- R = Effective Terminal-to-Terminal Resistance

This relationship is plotted in Figure 5 for the device resistance of  $6 \times 10^{-4}$  ohm.

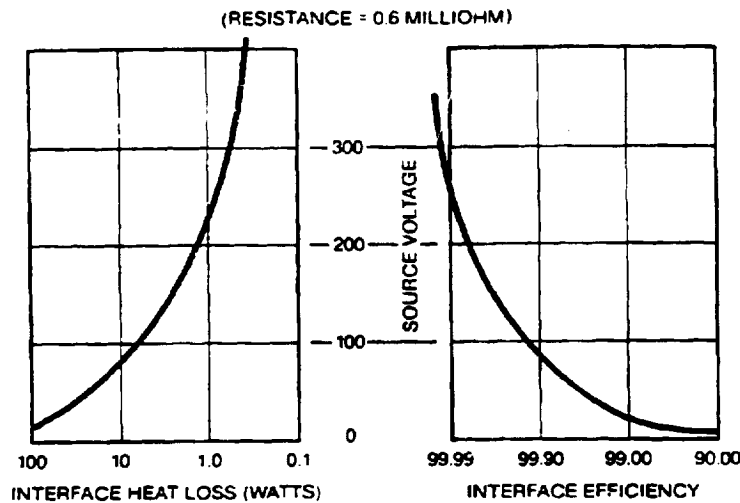


**Figure 5: Electrical Transfer Characteristics at 10 kW**

## FUTURE EVALUATION REQUIREMENTS

The design of a "latest generation" high-power roll-ring test unit has been initiated to evaluate both high-current and high-voltage current transfer. The objective of this roll-ring power transfer assembly is to ultimately conduct up to 200 amperes of current at 500 volts dc. This represents 100 kW of power transfer per circuit.

It would be expensive and difficult to evaluate a power transfer unit under high-current and high-voltage conditions simultaneously because of the size of both the power source and the power load required. However, the unit can be satisfactorily evaluated by monitoring the performance at high voltage with reduced current, and again at high current with reduced voltage. High-voltage tests evaluate the voltage breakdown characteristics of the insulating materials as well as corona and arcing susceptibility. High-current tests evaluate the thermal properties of the unit and contact characteristics. Both test configurations evaluate the transfer efficiency of the unit. By using this approach to test a power transfer assembly, a much lower power expenditure is achieved with essentially the same results. When conducting 200 amperes at 20 volts dc, a power of only 4000 watts must be converted to thermal energy by the load. When operating at 500 volts dc and 500 milliamperes, only 250 watts must be transformed.

Figure 6 is a cross section of a representative power/signal transfer module. An evaluation module of the power transfer section of this device is now being developed under a NASA/Lewis Research Center contract to bring this technology to a more mature status.

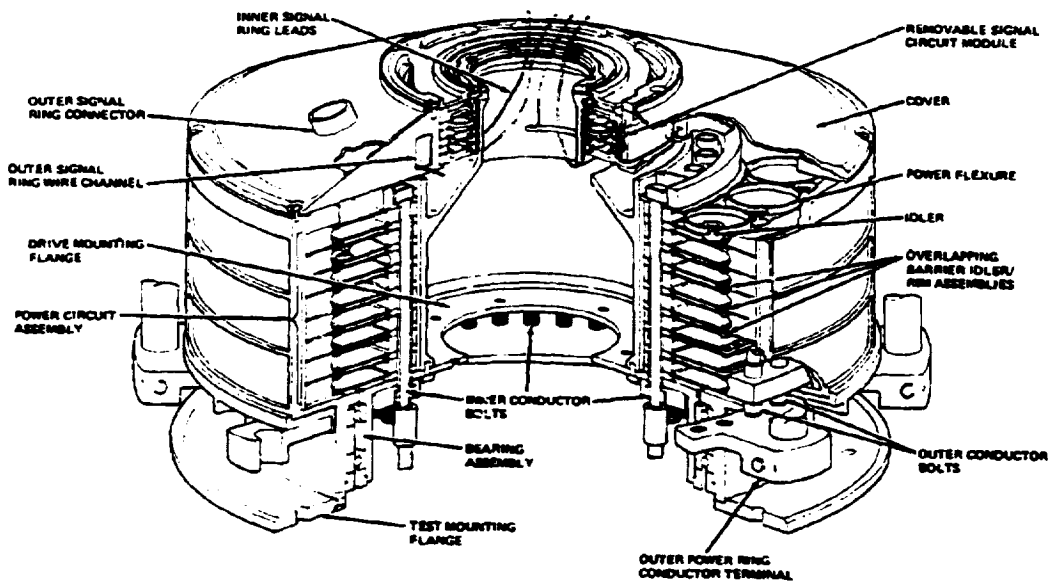


**Figure 6: High-Power/Signal Test Unit**



## SUMMARY

- Sperry has extensively evaluated a patented roll-ring design that is uniquely suited for rotary signal/power transfer in space applications.
- Two high-power configurations of the roll ring have been developed.
- Present lab-proven hardware is available with power transfer capability of 2 kW at 200 amps.
- Higher power units with 100-kW capability are presently in design.
- Theoretical analysis has indicated that power levels of >100 kW are possible, which will keep pace with spacecraft requirements for the 1990's and beyond.



N85

3876

UNCLAS

D-26

N85 13876

HIGH-EFFICIENCY POWER CONVERSION OPTIONS  
FOR  
FLYWHEEL ENERGY STORAGE SYSTEMS

R. L. Hockney  
The Charles Stark Draper Laboratory, Inc.  
Cambridge, Massachusetts

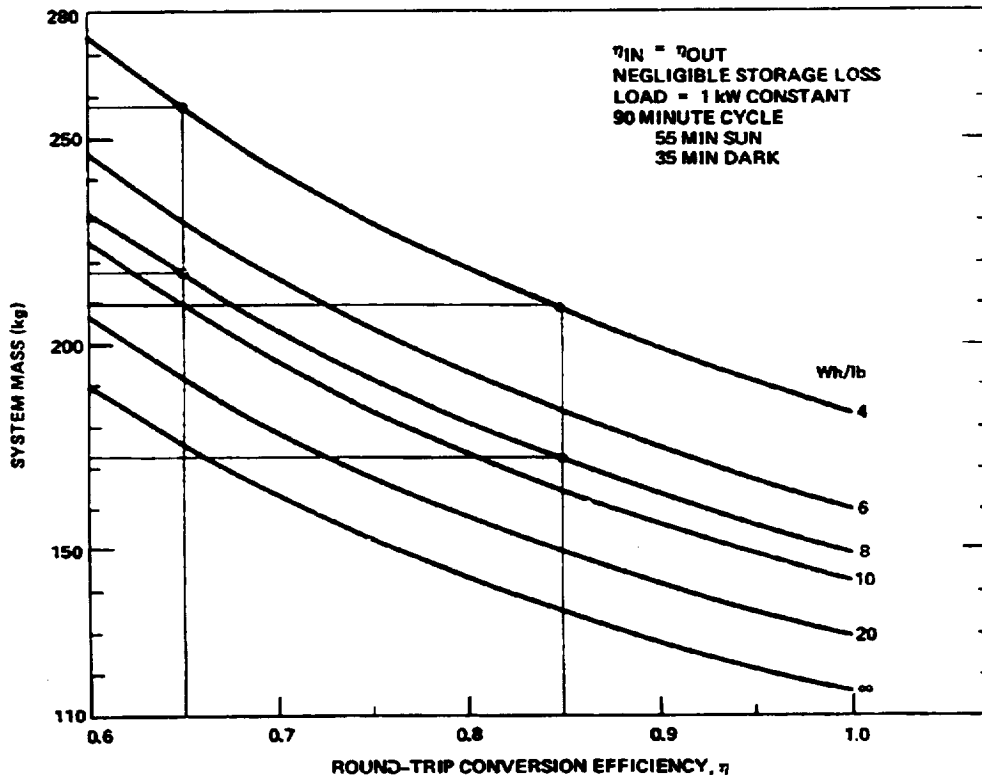
This presentation includes a discussion of the impact of efficiency on the power system; how efficiency is affected by component types; some ac and dc bus configurations; and systems developed at CSDL; and concluding remarks.

**HIGH-EFFICIENCY POWER CONVERSION OPTIONS  
FOR  
FLYWHEEL ENERGY STORAGE SYSTEMS**

- **EFFICIENCY**
  - SEMICONDUCTOR
  - MACHINE
- **CONFIGURATIONS**
- **CSDL EXPERIENCE**
- **CONCLUSIONS**

### SYSTEM MASS VS EFFICIENCY

This graph (ref. 1) shows the mass of a satellite energy system as a function of conversion efficiency and energy density for a system that supplies a 1-kW steady-state load aboard a satellite in low Earth orbit. The satellite energy system consists of a photovoltaic array and an energy storage element, such as a battery or flywheel. The mass of the photovoltaic array is the product of the required capacity and the power density of the array material. The mass of the storage element is the product of the required storage capacity and the energy density of the storage element.



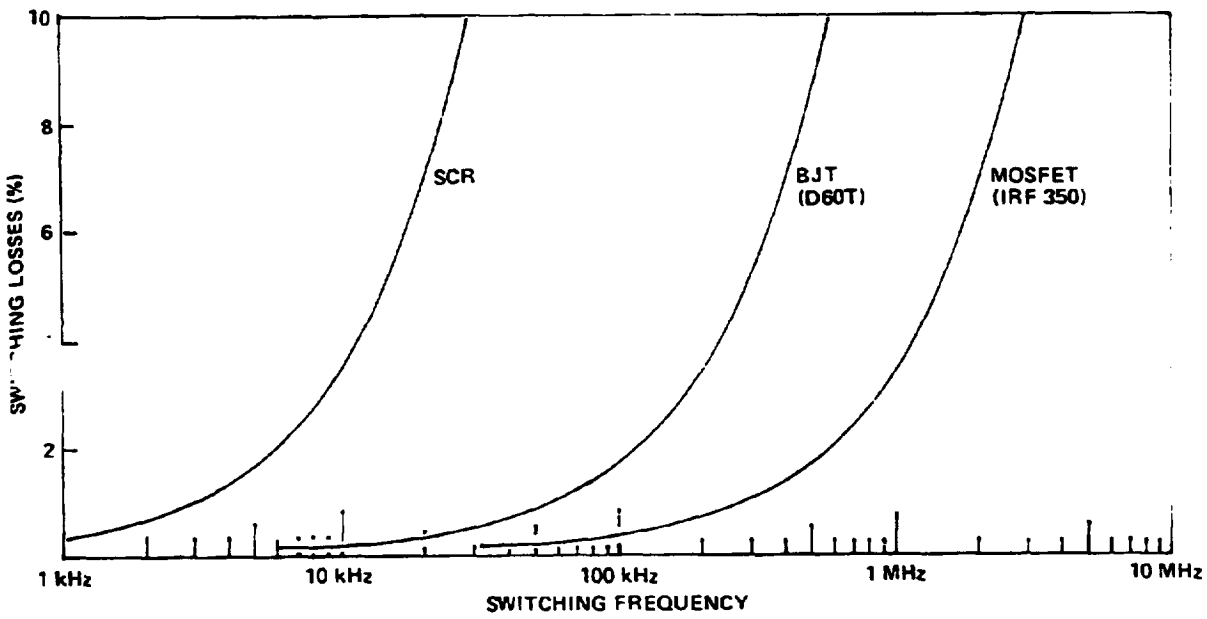
A relative comparison of each semiconductor technology reveals their strengths weaknesses. The IGT is an Insulated Gate Transistor, a relatively new technology.

### SEMICONDUCTOR TYPES

	SCR	BJT	FET	IGT
"ON" LOSS	$I \times V_D$	$I \times V_D$	$I^2 \times R_D$	$I \times V_D$
SPEED	SLOW	FAST	VERY FAST	MED
DRIVE	LATCH	CURRENT	VOLTAGE	VOLTAGE
POWER	VERY HIGH	HIGH	MED	LOW

### SWITCHING LOSS

The relative switching efficiencies of the three most popular types of power semiconductor devices including FETs, bipolar junction transistors (BJT), and silicon controlled rectifiers (SCR) are indicated. The FETs clearly give superior performance throughout, and will efficiently operate in regions which are not possible for SCRs and even BJTs.



The design parameters of the candidate machine types can be compared in order to trade off performance with simplicity.

### MACHINE TYPES

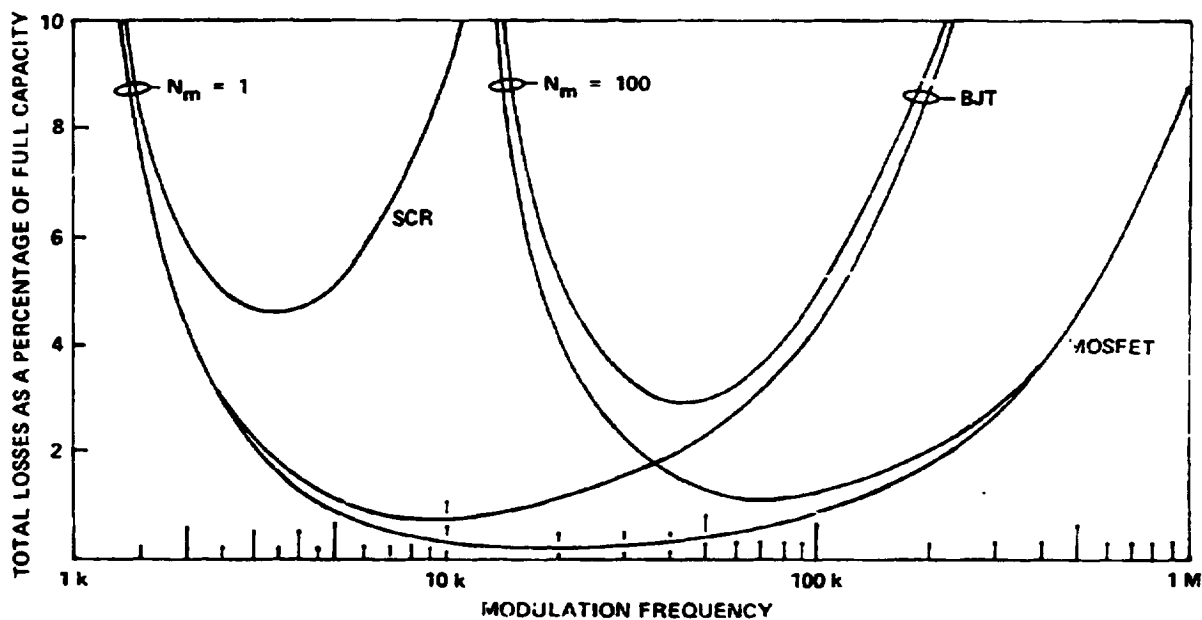
	PM BRUSHLESS	PM "IRONLESS"	INDUCTION	WOUND- FIELD
TORQUE	$KI$	$KI$	$KI^2$	$KI_A I_F$
LOSS	IRON	MED	VERY LOW	LOW
	COPPER	$I^2 R_W$	$I^2 R_W$	$I^2 (R_S + R_R)$
SIDE-LOAD	YES	NEGLIGIBLE	YES	YES
FEEDBACK	POSITION	POSITION	SPEED	POSITION
COMPLEXITY	MED	HIGH	LOW	MED

ALL REQUIRE CONTROLLED-CURRENT, VARIABLE-FREQUENCY DRIVE



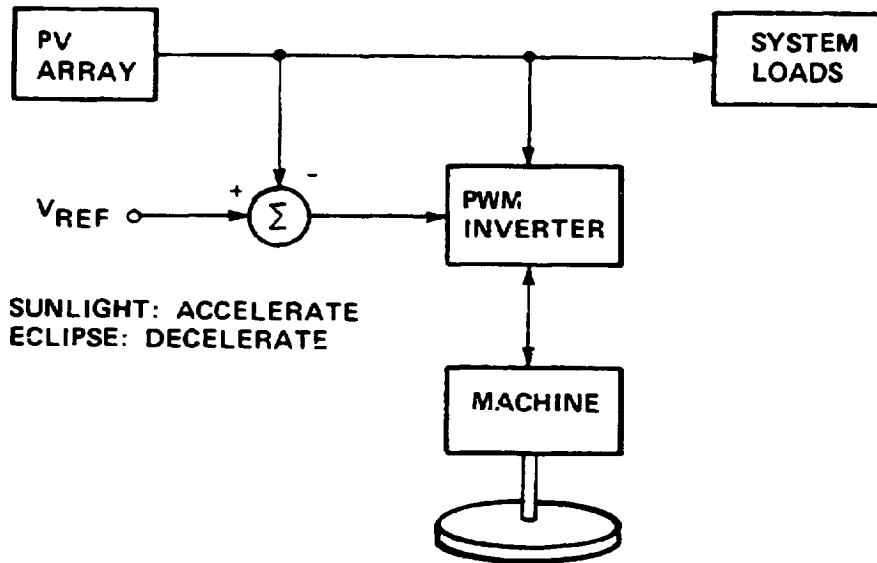
### TOTAL LOSS

PWM losses are minimized by selecting a carrier frequency which is a trade-off between the decreasing harmonic losses and increasing switching losses with increased carrier frequency. The combined effect of harmonic and switching losses is plotted for differing values of a machine normalization quantity,  $N_m$  (ref. 2). These curves demonstrated that FET devices are advantageous for all applications. They do, however, have particular advantages for high  $N_m$  and, therefore, PM motors.



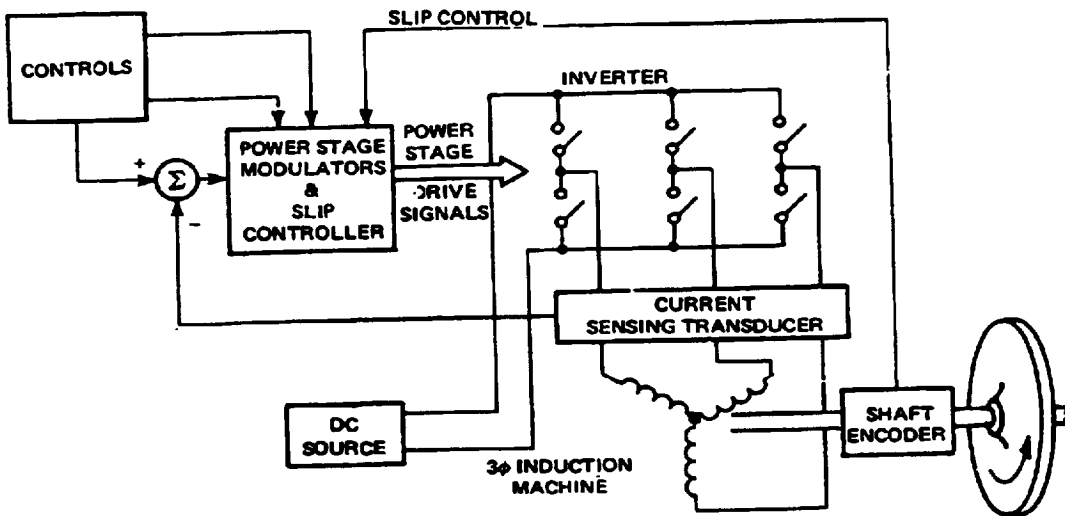
In the first dc configuration, a high-frequency pulse-width modulated inverter controls the rate and direction of power flow. The rate is determined by the voltage regulation control loop.

### DC BUS CONFIGURATION



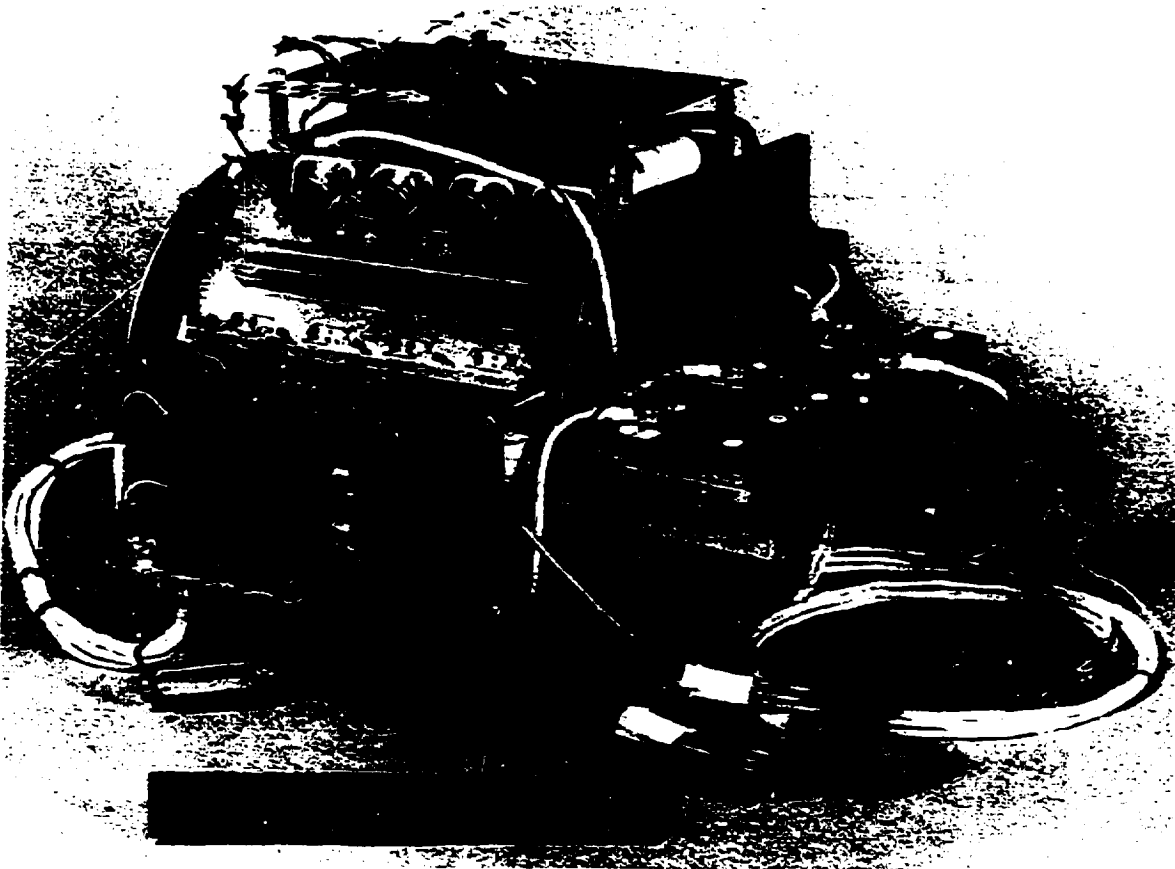
### PWM INVERTER

This is the block diagram of a 10-kW three-phase motor controller developed at CSDL (ref. 2). It utilizes MOSFET's in the power stage and employs pulse-width modulation to produce a variable frequency, variable current drive. It was used to develop the slip-control algorithm for optimum-efficiency operation of an induction motor.

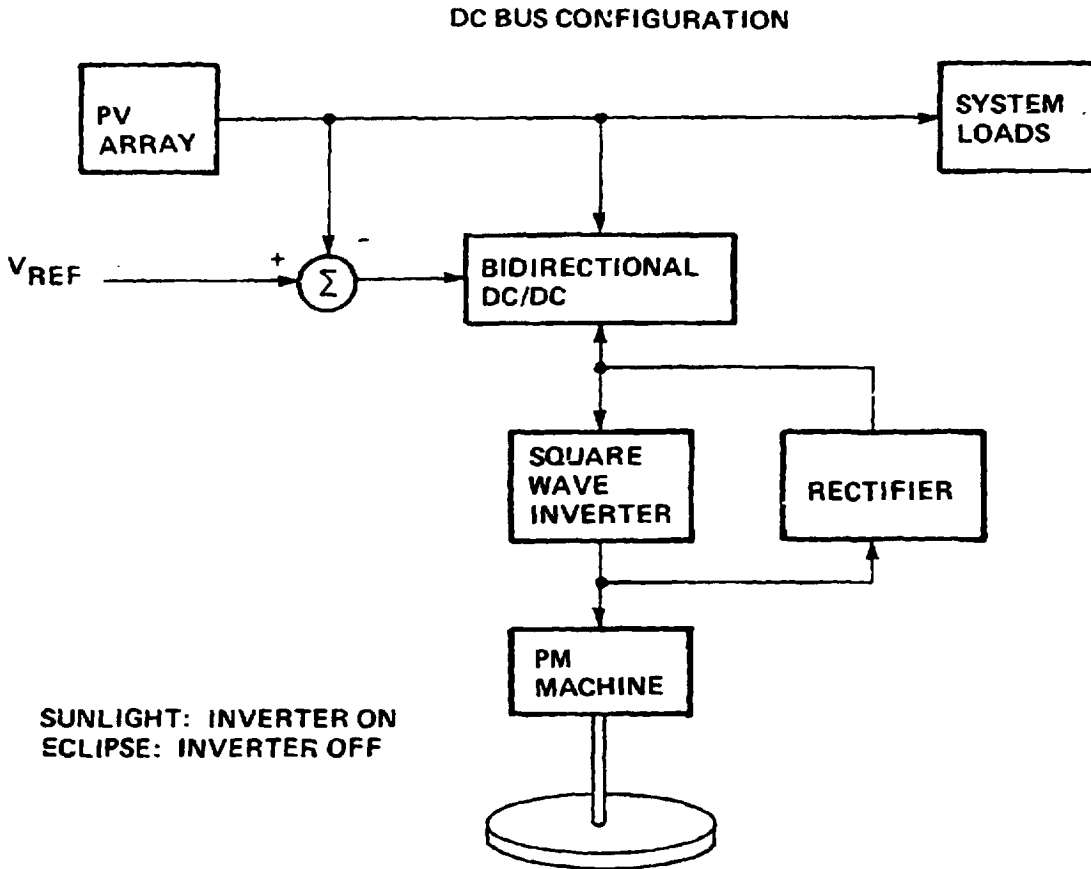


POWER STAGE

The power stage of the 10-kW three-phase inverter comprised 24 MOSFET's and their associated drivers on a forced-air cooled heat sink.

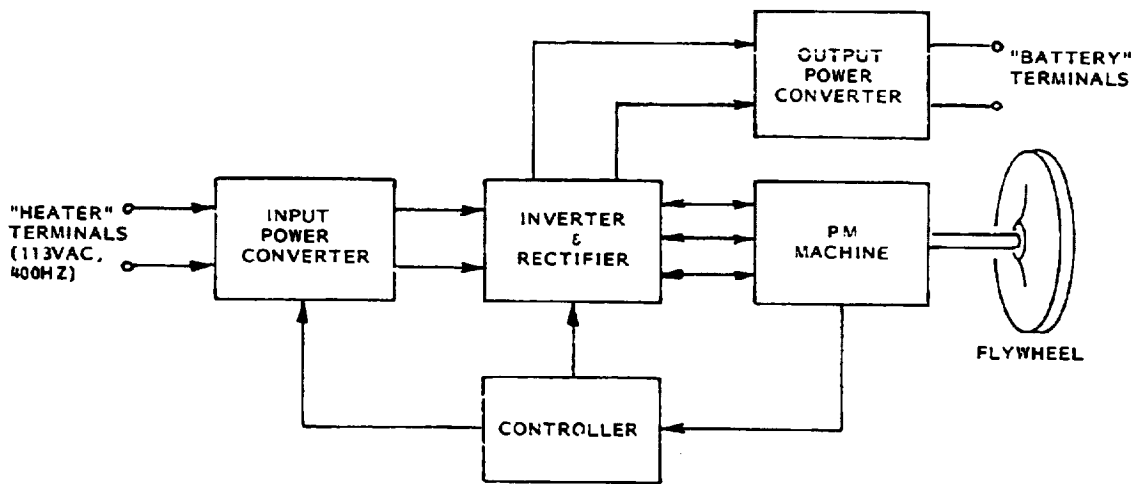


In an alternate dc configuration, the high-speed switching can be performed in a one- or two-switch converter rather than the six-switch inverter.



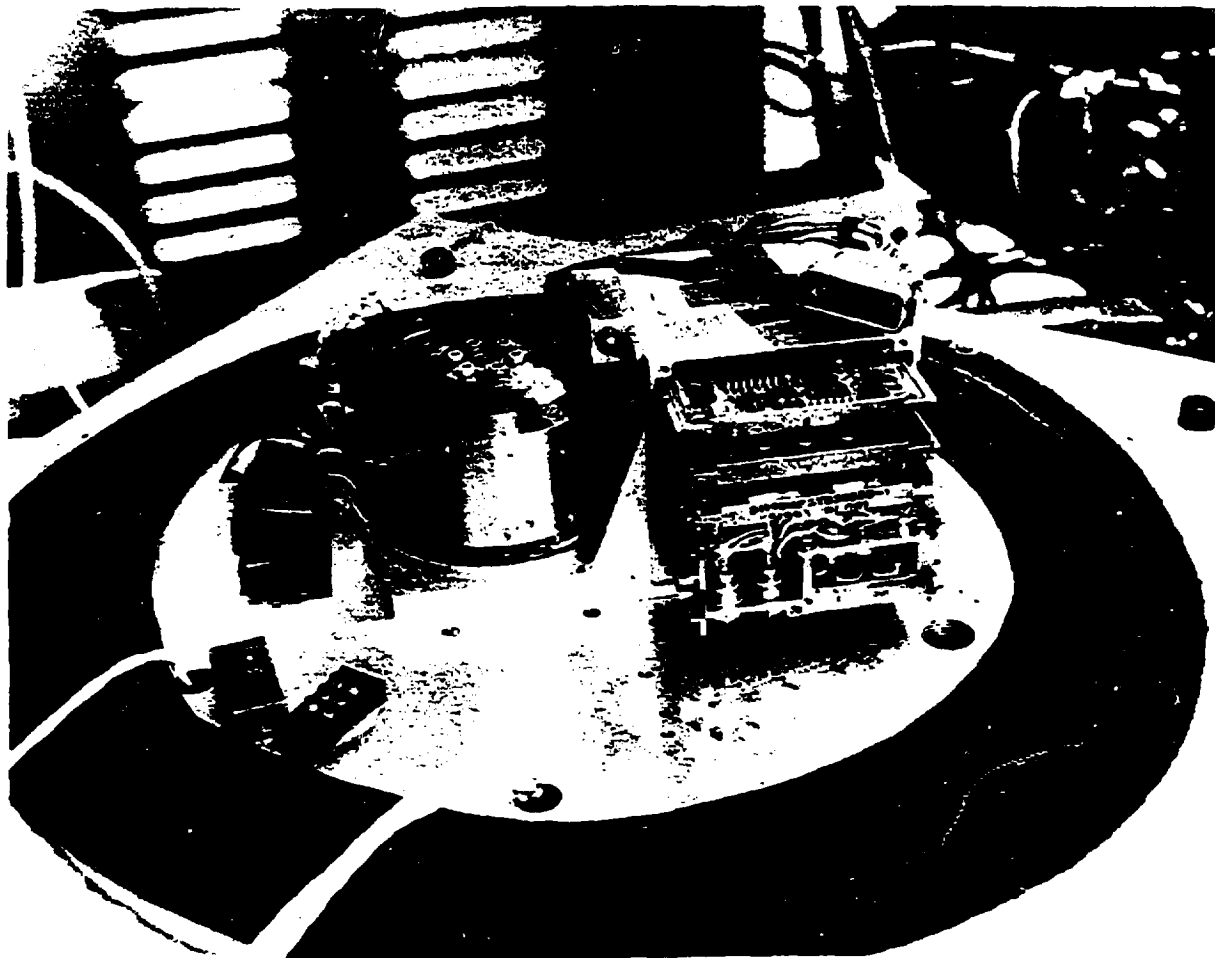
### SQUARE-WAVE INVERTER

This figure is the block diagram of the Inertial Power Storage Unit (IPSU) developed at CSDL as a battery replacement. It utilizes a permanent magnet (PM) machine wound to produce square-wave back-EMF and separate input and output converters.



ENGINEERING MODEL

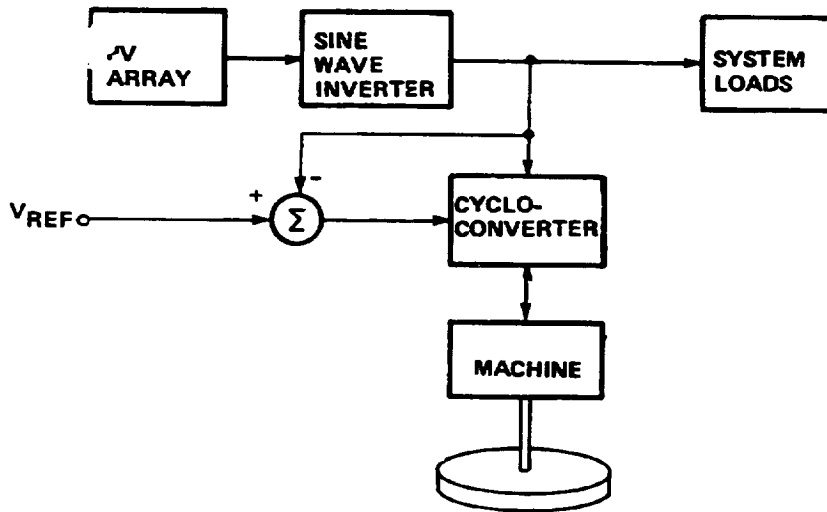
The flywheel/machine module and electronics module for IPSU have to perform as a form, fit, and function replacement for the NiCd battery in fighter aircraft.



OF FOUR

In the first ac configuration, bi-directional power flow through the cyclo-converter will require forced commutation in at least one direction.

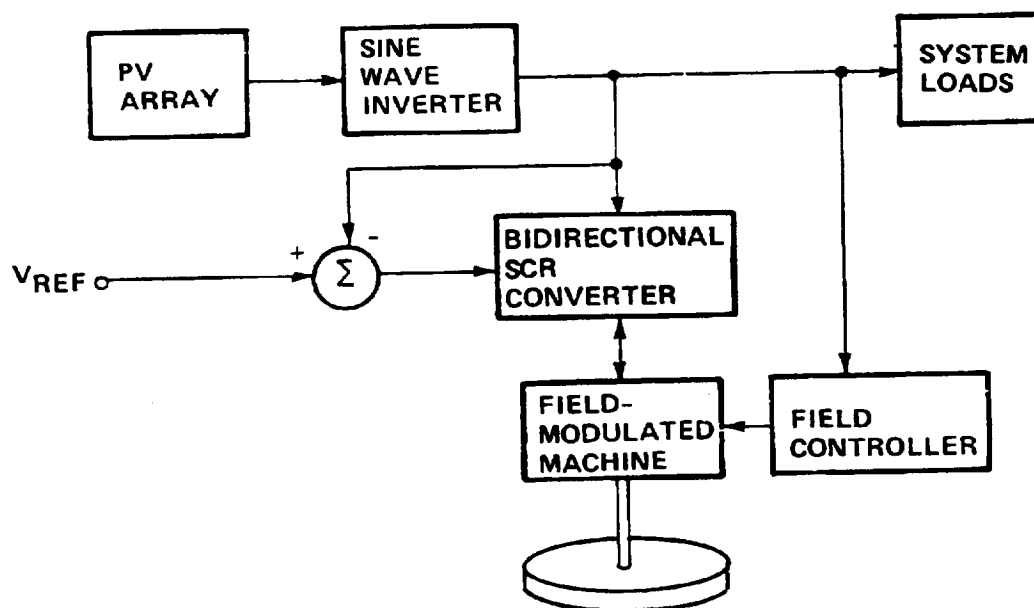
### AC BUS CONFIGURATION





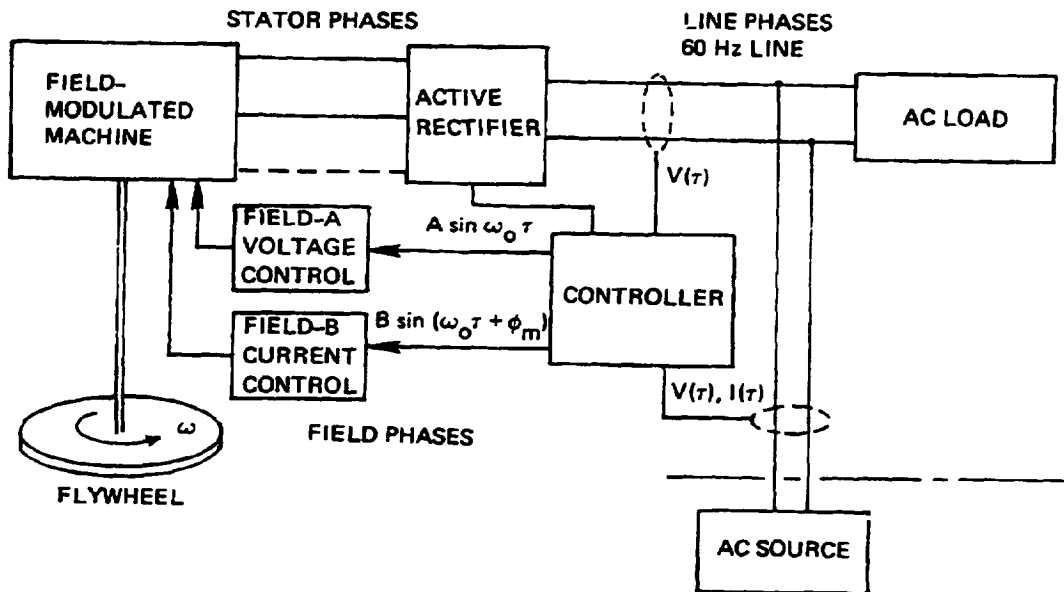
In the alternate ac configuration, a field-modulated machine allows bi-directional power flow through naturally commutated SCR's.

### AC BUS CONFIGURATION



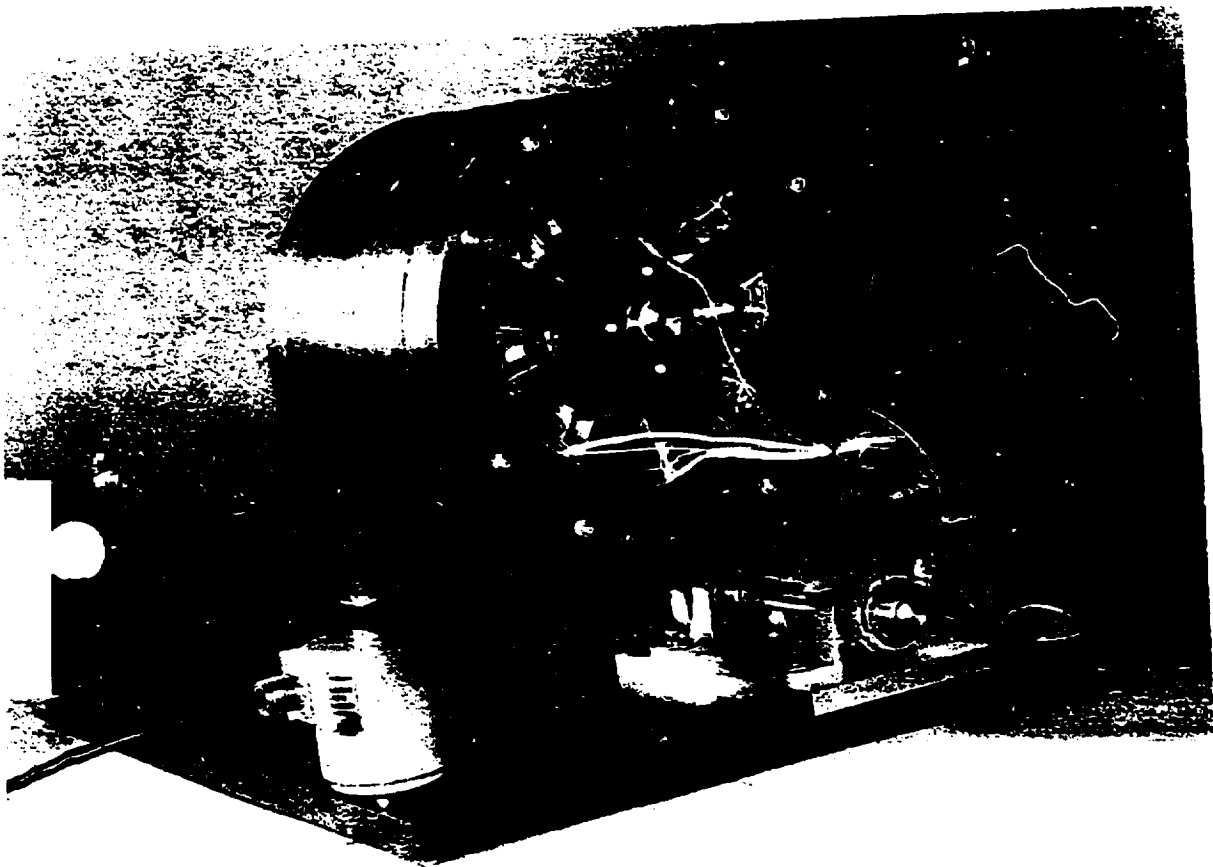
### FIELD MODULATION

This power-conversion system uses a CSDL-developed machine (ref. 3) utilizing two independently controlled field windings on the stator. The system includes an SCR switching circuit that demodulates the high-frequency armature waveform to produce the lower-frequency bus voltage.



PROTOTYPE MACHINE

The multi-field machine (right) is shown on its testbed with a dc machine which regulates the flywheel as both load and drive.



Improvements in component technology in recent years have increased the attractiveness of flywheel energy storage. A technology development program is required to determine the optimum configuration.

## CONCLUSIONS

- TECHNOLOGY EXISTS FOR PRACTICAL SYSTEM
- RECENT ADVANCEMENTS INCREASE SYSTEM VIABILITY
- SPECIFIC IMPLEMENTATION DEPENDS UPON
  - POWER
  - VOLTAGE
  - AC/DC BUS
- ADVANCED DEVELOPMENT PROGRAM INDICATED

#### REFERENCES

1. Eisenhaure, D. B.; Downer, J. R.; Bliamptis, T.; and Hendrie, S. D.: "A Combined Attitude, Reference and Energy Storage System for Satellite Applications," AIAA-84-0565, Jan. 1984.
2. Eisenhaure, David; Stanton, William; Hockney, Richard; and Bliamptis, Tim: "MOSFET Based Power Converters for High-Speed Flywheels," 1980 Flywheel Technology Symposium, Rep. No. CONF-801022, Dep. Energy, 1980, pp. 363-370.
3. Eisenhaure, David; Stanton, William; St. George, Emery; and Bliamptis, Tim: "Utilization of Field-Modulated Machines for Flywheel Applications," 1980 Flywheel Technology Symposium, Rep. No. CONF-801022, Dep. Energy, 1980, pp. 353-362.

D-27

N85 13877

DEVELOPMENTS IN  
SPACE POWER COMPONENTS  
FOR  
POWER MANAGEMENT AND DISTRIBUTION

David D. Reuz  
NASA Lewis Research Center  
Cleveland, Ohio

PRECEDING PAGE BLANK NOT FILMED

C-5

**Power Electronic Component Development  
at Lewis Research Center**

Advanced power electronic component development for space applications has been going on at NASA Lewis for more than a decade (Fig. 1). A wide range of development work has been done, including transformers and inductors, semi-conductor devices such as transistors and diodes, remote power controllers, and supporting electrical materials development. Present power component capability for space applications is about 25 kW. Work in the early and middle 1980's should raise this capability up to 100 kW and begin work toward a megawatt.

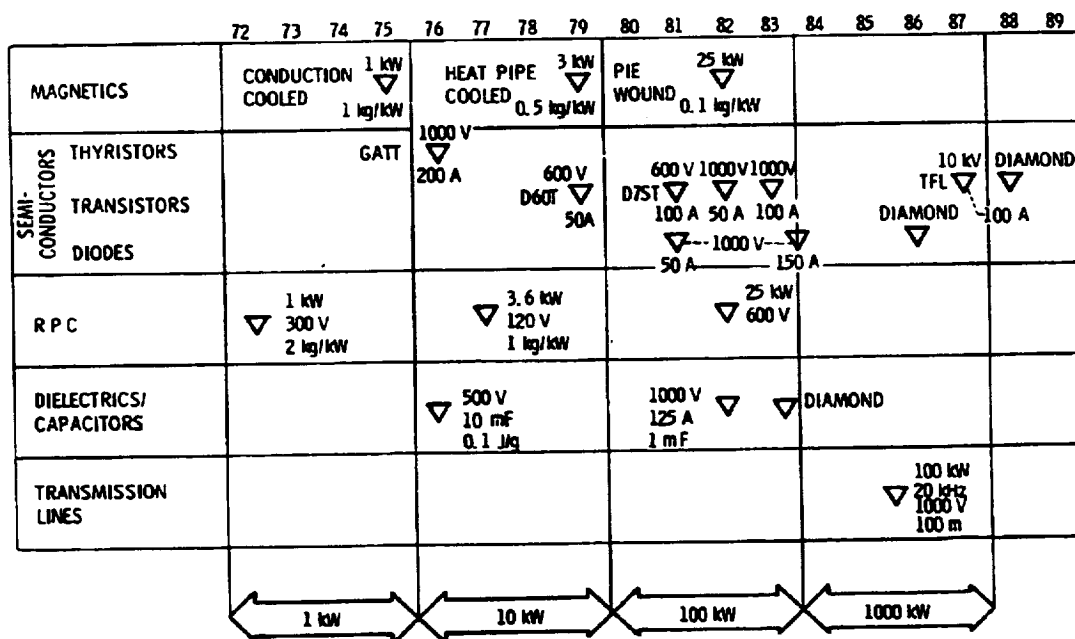


Fig. 1

## D60T Transistor

Against the backdrop of a circuit diagram for a solid-state remote power controller a technician holds a D60T (Fig. 2) ready for assembly in a stud package (ref. 1). In her right hand the interdigitated silicon wafer may be seen inside the base. The emitter-base contacts are visible in the ceramic-to-metal top held in her left hand. To the left of the picture are shown three package types. From the top are a special flat base package (a modification of the stud package), a stud package and a disc-type package. This transistor is rated at 400 to 500 volts, 100 amperes continuous (200 A peak) collector currents with switching frequency of 20 to 50 kHz. This device can be used in DC-DC inverters, DC-AC converters, DC motor controllers and remote power controllers.



Fig. 2

RESEARCH AND  
DEVELOPMENT



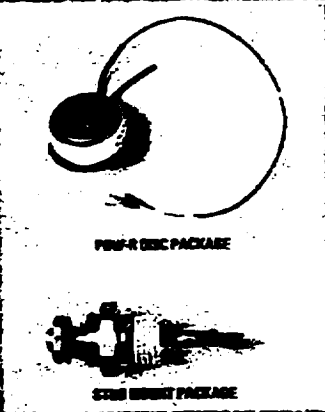
## High Current Power Switching Transistor

Figure 3 shows the Westinghouse D7ST (ref. 2), which is now being marketed as a direct transfer of technology from a research contract supported and directed by NASA LeRC. The two package types available are shown in the center photograph. Surrounding the picture are listed the features and applications of the D7ST. The primary benefit of the new transistor to NASA is the extension of the power handling capability to 50 kW without paralleling of transistors. This opens new areas of application and directions for future space power system design.

**WESTINGHOUSE MODEL D7ST  
(HIGHER CURRENT VERSION OF D60T)**

**FEATURES**

- VOLTAGE: 400 TO 500 VOLTS
- CURRENT: 100 TO 150 AMPERES @ CASE OF 30 AND AMPERES PDM
- POWER HANDLING: 50 KILOWATTS
- POWER DISSIPATION: 2 KW @ 25°C
- RISE AND FALL TIMES: 0.25 MICROSECOND
- STORAGE TIME: 4 MICROSECONDS
- LOW SATURATION AND PER CYCLE SWITCHING LOSSES



PNP-R DISC PACKAGE

STUD MOUNT PACKAGE

**APPLICATIONS**

- 5-20 MHz HIGH FREQUENCY INVERTERS
- VSCF CONVERTERS IN MILITARY AIRCRAFT
- ELECTRIC VEHICLE MOTOR CONTROLLERS
- DC MOTOR CONTROLLER FOR SPACE SHUTTLE ACTUATOR
- 100 MW VLF TRANSMITTERS
- 50 MW RF INDUCTION HEATERS
- POWER SUPPLIES FOR CONSUMER AND INDUSTRIAL APPLICATIONS

**BENEFITS TO NASA**

- EXCEEDS CAPABILITY OF PREVIOUS 10-150 AMPERE WIRING BOX TRANSISTOR
- COMMERCIALLY AVAILABLE IN QUANTITY AT REASONABLE COST
- MAKES POSSIBLE 50 MW SPACE POWER SYSTEM CONVERTERS AND POWER CONTROLLERS WITHOUT PARALLELING OF TRANSISTORS
- DIRECT IMPROVEMENT ALSO IN AIRCRAFT POWER DISTRIBUTION AND CONTROL
- ESTABLISHES TECHNOLOGY FOR LARGER AREA, HIGHER POWER TRANSISTORS

Fig. 3

ORIGINAL PAGE IS  
OF POOR QUALITY

### Augmented Power Transistor Specifications

Figure 4 shows the ratings and main characteristics of a research contract now underway at Westinghouse (ref. 3). Transistors from this program are now available. The two significant developments of this program were the demonstration of glass passivation of the wafer to provide hermetic sealing of the junctions and a new package that isolates the thermal and electrical interfaces.

VOLTAGE: 800 TO 1000 VOLTS

CURRENT: 70 TO 112 AMPERES (GAIN OF 10)  
400 AMPERES PEAK

POWER HANDLING: 75 KILOWATTS

POWER DISSIPATION: 1.25 KILOWATTS AT 75°C

RISE AND FALL TIMES: 0.5 MICROSECOND

STORAGE TIME: 2.5 MICROSECONDS

Fig. 4

## Fast Recovery, High Voltage Power Diode

Figure 5 shows the benefits to NASA, the features and general applications of a newly developed 50 ampere, 1200 volt fast recovery power diode (ref. 4). Power Transistor Company developed the new diode on contract to NASA LeRC. Because of the large demand for such a device commercially in motor controllers, Power Transistor Company is already marketing the product as their PTC 900 series Power Rectifier. A 150 ampere device (ref. 5) has also been developed but is not shown.



Fig. 5

ORIGINAL PAGE IS  
OF POOR QUALITY

ORIGINAL FILED  
OF POOR QUALITY.

120 VDC, 30 Amp, Solid State Remote Power Controller

Figure 6 shows the 30 ampere version of the 120 VDC solid state RPC (ref. 6) developed for NASA LeRC by Westinghouse Aerospace Division. This version incorporates  $I^2t$  trip characteristics rather than current limiting. It may be noted that this version has a single layer substance 6 x 7 cm and weighs about 7 ounces.

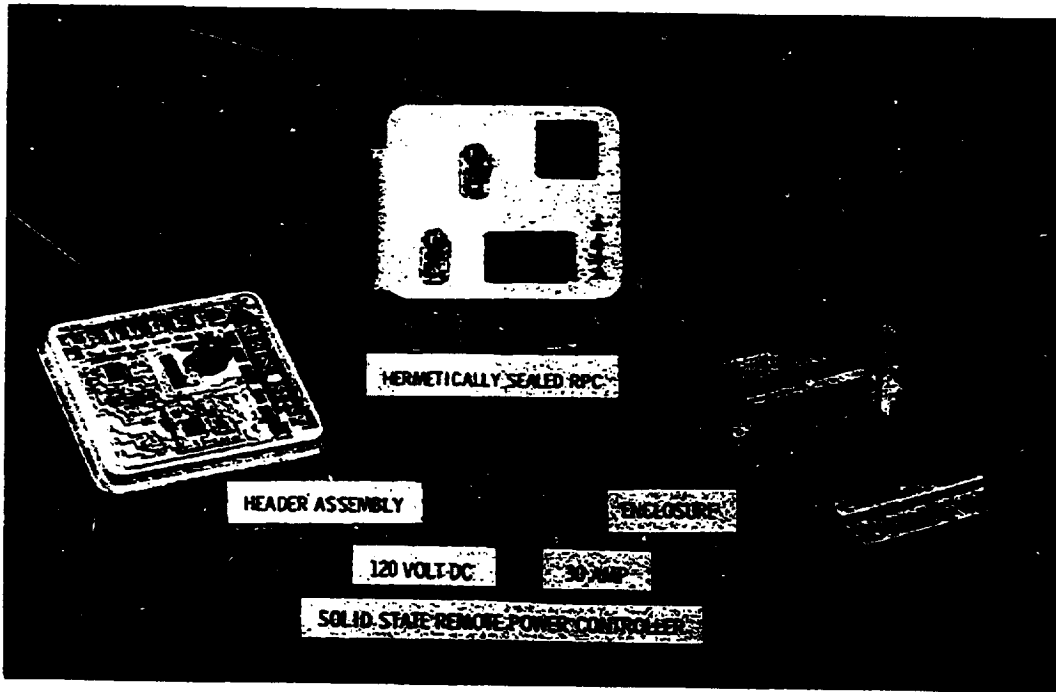


Fig. 6

ORIGINAL PAGE IS  
OF POOR QUALITY

NASA High Voltage, High Power Circuits

Figure 7 shows an SCR switched solid state circuit breaker breadboard for 1000 volts DC and 25 amperes (ref. 7). This is an early model developed for use with ion thruster power supplies by John Sturman of Lewis Research Center. With the development of the 1000 volt D7 size transistor, a transistorized version is now available as symbolized by the circuit schematic on the right. Three advantages are listed, also. Solid state circuit breakers at high voltage DC have other significant advantages over conventional electromechanical circuit breakers. These include: arcless circuit interruption, long life (no contact wear), reliability, 99% efficiency, and universal source, load, computer interface compatibility.

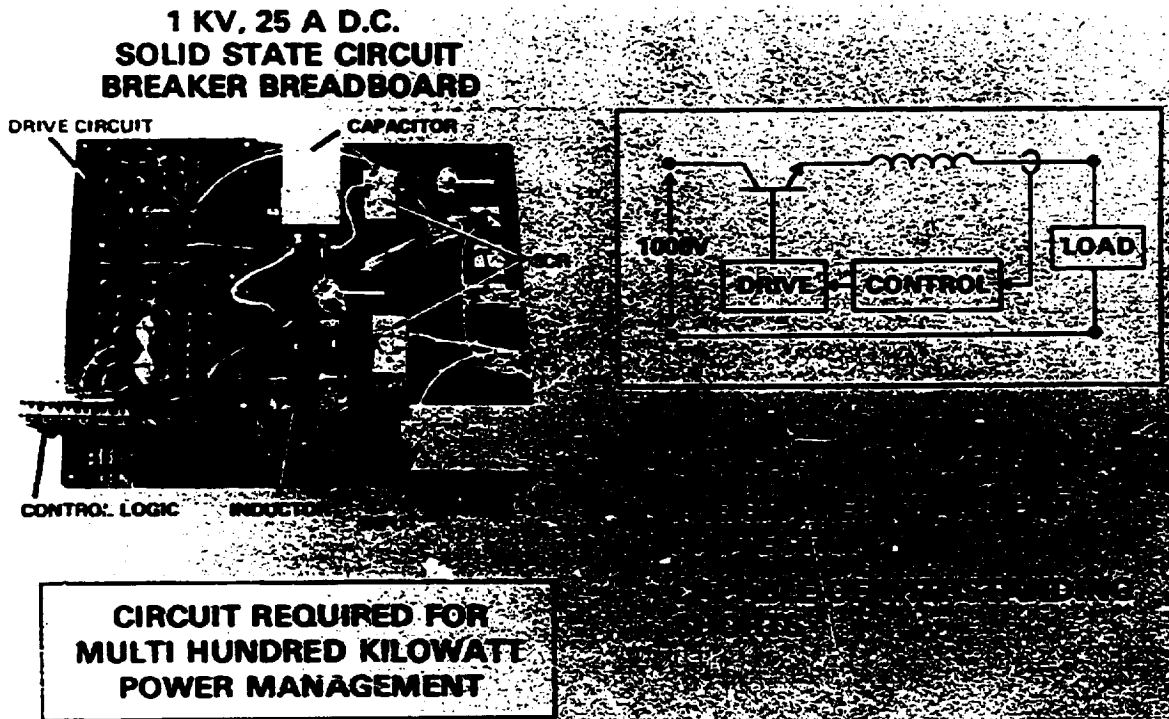


Fig. 7

ORIGINAL FACILITY  
OF POOR QUALITY

### Heat Pipe Cooled Transformer

Using heat pipe cooling permits about a 30% reduction in transformer weight in the transformer shown (ref. 8). Lifetime is also probably improved, as the maximum temperature rise above baseplate is only half as much. The transformers shown in Figure 8 have a nominal 2.2 kW power rating and a power density of 0.6 kg/kW at an operating frequency of 10 kHz.

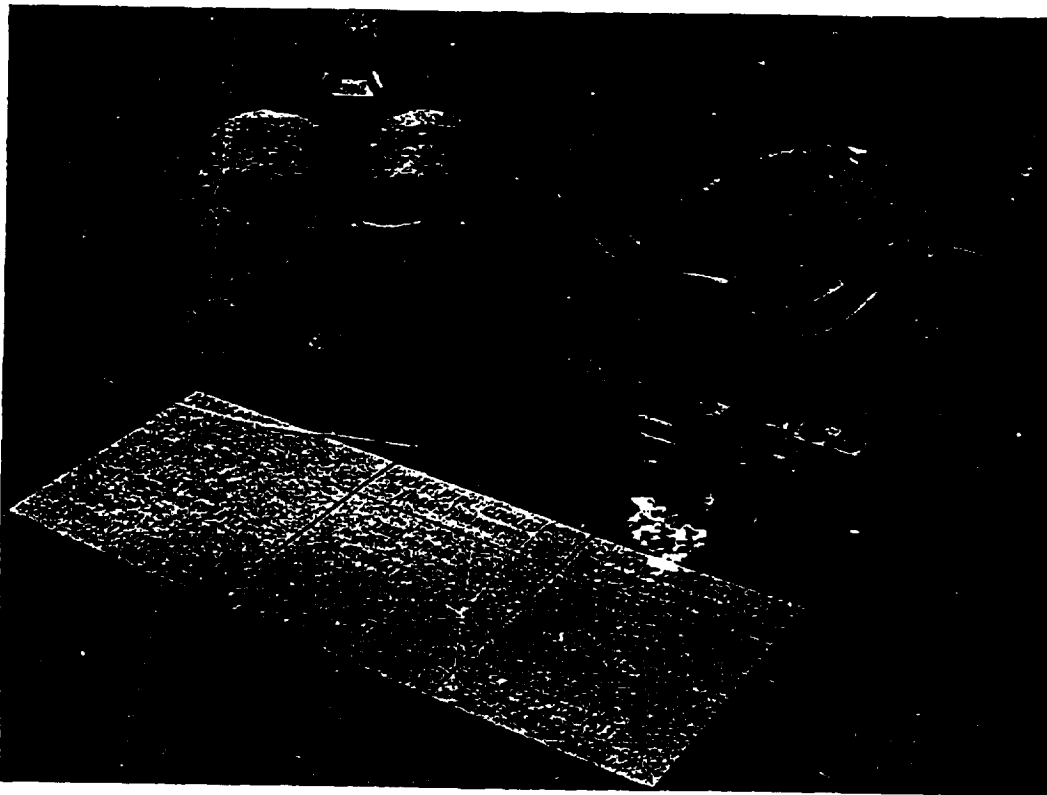


Fig. 8

ORIGINAL QUALITY  
OF POOR QUALITY

Comparison of Space-Type and Commercial Transformers

The significant weight and size reductions which can be realized by going to high frequency operation and unique thermal control techniques are clearly illustrated in Figure 9. Of major importance also is the fact that the 25 kVA space-type transformer (ref. 9) is more than 1% more efficient and has a 35°C lower temperature rise than the commercial transformer. The specific weight of the space-type 25 kVA, 20 kHz transformer is 0.28 lb/kVA, while that of the commercial 25 kVA, 60 Hz transformer is 16 lb/kVA. The very good maintainability and easy serviceability of the space-type transformer are additional outstanding features. The advanced technology which the space-type transformer exemplifies is not limited to power transformers but should be applicable to other power magnetic components. Power systems utilizing this type of magnetic components should show marked improvement in system weight, size, efficiency and reliability.

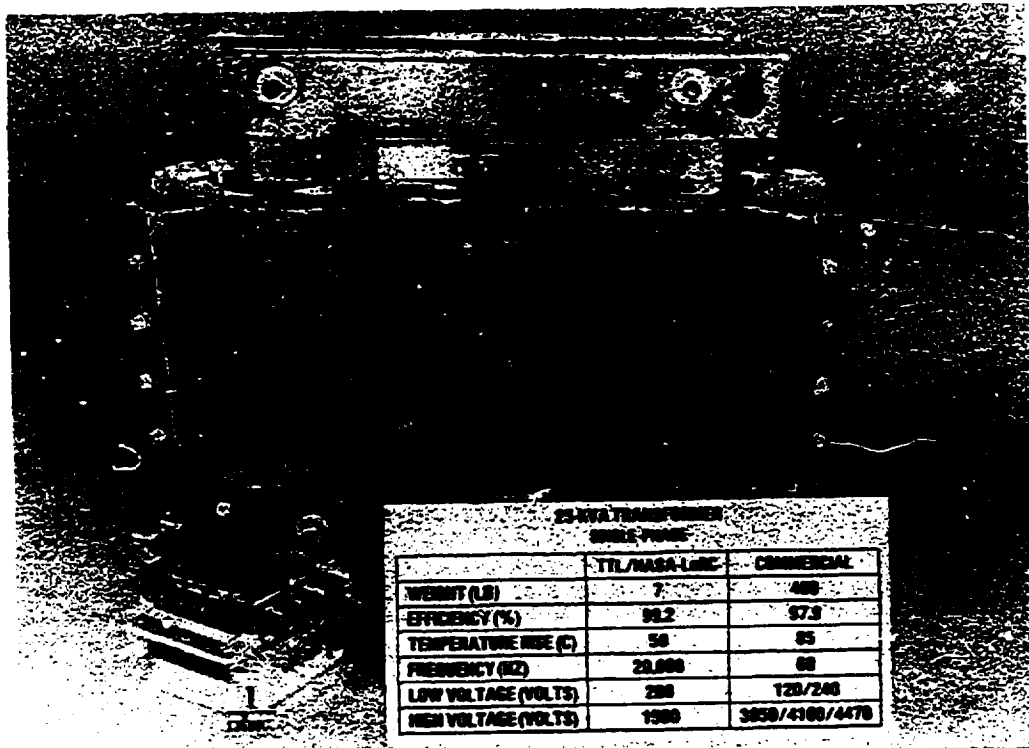


Fig. 9

ORIGINAL FILED  
OF POOR QUALITY

### 25 kVA Space-Type Transformer

Shown in Figure 10 is a close up photograph of the 25 kVA high frequency transformer shown on the previous page. Pie or pancake-type coils bonded to metallic conduction plates are the basic building blocks for constructing the primary and secondary windings. Very low leakage inductance is possible by placing a primary pie coil on one face of the metallic conduction plate and the secondary pie coil on the opposite face. Good thermal control is realized since the coil's  $I^2R$  loss is uniformly transmitted directly to the metal coil plates which then conduct the heat directly to the heat sink baseplate. In this transformer, the 8 primary pie coils for a 200 V input are connected in parallel and the ends of each pie-coil terminate on copper tabs which become an integral part of the primary bus bars located on top of the transformer. The 8 secondary pie coils for a 1500 V output are connected in series, and again the ends of each pie-coil terminate on copper tabs which become an integral part of the secondary bus bars located below the primary bus bars.

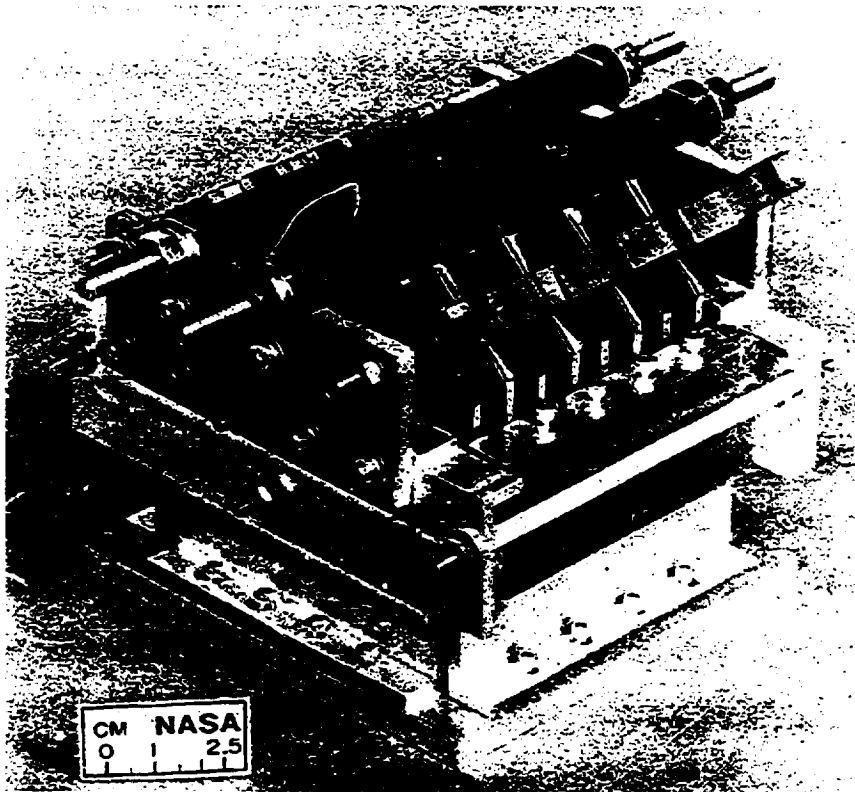


Fig. 10



### High Power High Frequency Lightweight Capacitor

The smaller capacitor is a nominal microfarad, 600 volt capacitor with a maximum current capability of 125 A at 40 kHz (ref. 10). The dielectric is polypropylene. The losses at maximum operating conditions are 22 watts, which may be compared to the 75 kVA rating of the capacitor. The small capacitor developed for NASA applications as shown in Figure 11 is compared to a typical commercial 40 kHz capacitor, which has a rating of 1.8 kVAR per pound. The NASA capacitor, as developed by Maxwell Laboratories, Inc., has a power density of 11 kVAR per pound. This represents a decrease in size and weight by a factor of seven.



Fig. 11

### Lightweight Filter Using Heat Pipe Cooled Inductor

Figure 12 shows a factor of two reduction in weight resulting from the use of heat pipe cooled inductors (ref. 8) in the first stage input filter in a DC-DC converter. Both capacitor and inductor weights are reduced, because the lightweight inductor allows the use of a large inductance value, and therefore a smaller capacitance.

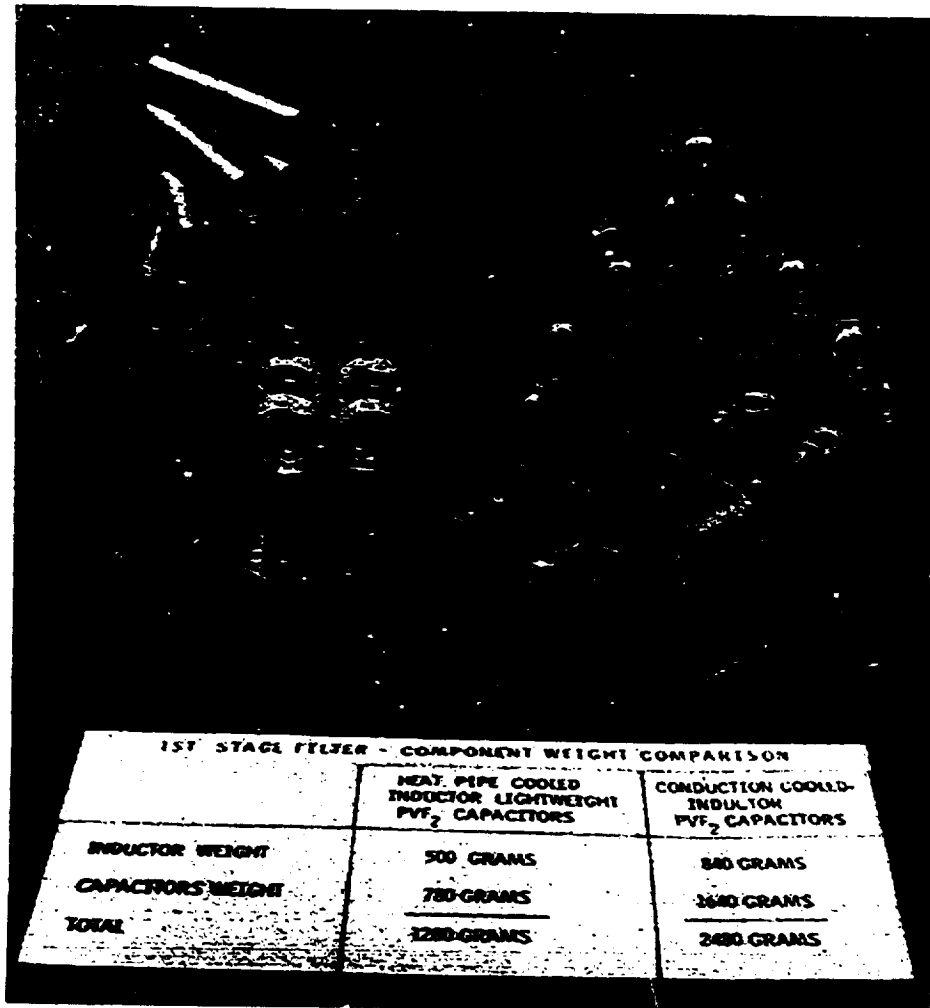


Fig. 12

### Power Processor for Ion Rockets, Functional Model

The power processor for a pair of 30 cm ion thrusters (ref. 11) is shown in Figure 13 in its package form. Included in this functional model is Lewis developed new technology in both circuits and electronic components. Circuit development includes the series resonant inverter, which through zero current turn off and turn on of switches allows low stress long life operation. Components developed at Lewis and incorporated in this model include heat pipe cooled lightweight transformers and inductors, polyvinylidene fluoride capacitors, and gate assisted turn-off thyristors. The power level is about 6 kW.



Fig. 13

ORIGINAL PHOTO  
OF POOR QUALITY

## **Rotary Power Transformer**

Two studies were conducted by General Electric for Lewis Research Center. The first study designed a 100 kW rotary transformer (ref. 11) which had an axial gap (axial symmetric) and utilized four 25-kW modules placed along the shaft axis. The second study (ref. 12) was to investigate a radial gap (vertical gap) rotary transformer and compare its characteristics with those of the axial gap configuration. The conclusion of the study was that the radial gap rotary transformer is the most feasible method for transferring electrical power of 100 kW or more across a rotary joint. The rotary transformer program is shown in Figure 14.

### PAST

#### STUDIES

- A) 100 KW (GENERAL ELECTRIC)
- B) > 100 KW (GENERAL ELECTRIC)
- 2 KW, 2 KHz SQUARE-WAVE DEMONSTRATION MODEL

### PRESENT

#### TRANSFORMER CHARACTERIZATION

### FUTURE

#### BUILD PROTOTYPE MODEL

- A) 25 KW
- B) 20 KHz
- C) 1000 VOLTS

Fig. 14

## Roll Ring

The Roll Ring is a device that transfers electrical power across a rotating joint through rotating flexures between concentric conductors (Fig. 15). The advantages of the Roll Ring over the slip ring are the elimination of sliding friction and the low torque needed to rotate the device. The Roll Ring can transfer both AC and DC power and will be more efficient than the rotary transformer. Lewis Research Center is purchasing a multi-kilowatt device from Sperry Flight System, Phoenix, Arizona for in-house component testing. Each power circuit will be capable of conducting 200 amperes at 500 volts DC.

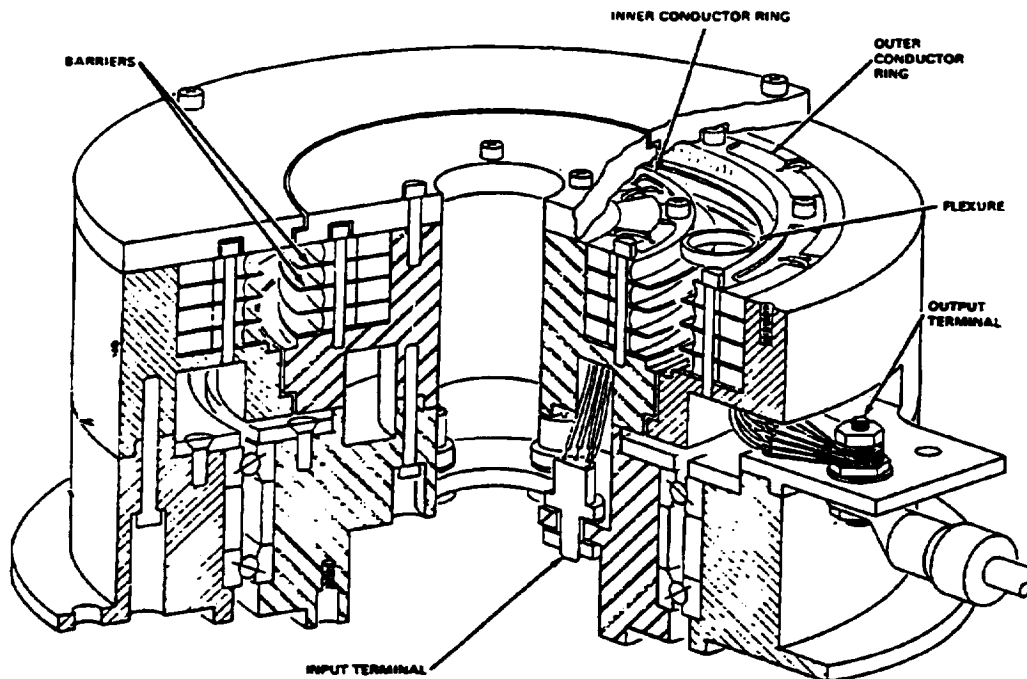


Fig. 15

## Transmission Lines

Lewis Research Center is presently preparing an RFP for a high power, high frequency transmission line. The specifications of the line will be 1000 volts, 100 amperes at 20 kHz. The output of the contract will be a 50 meter transmission line that will be tested to determine the line characteristics. Fig. 16 shows two possible configurations of a high frequency transmission line.

### HIGH-POWER HIGH-FREQUENCY TRANSMISSION LINE

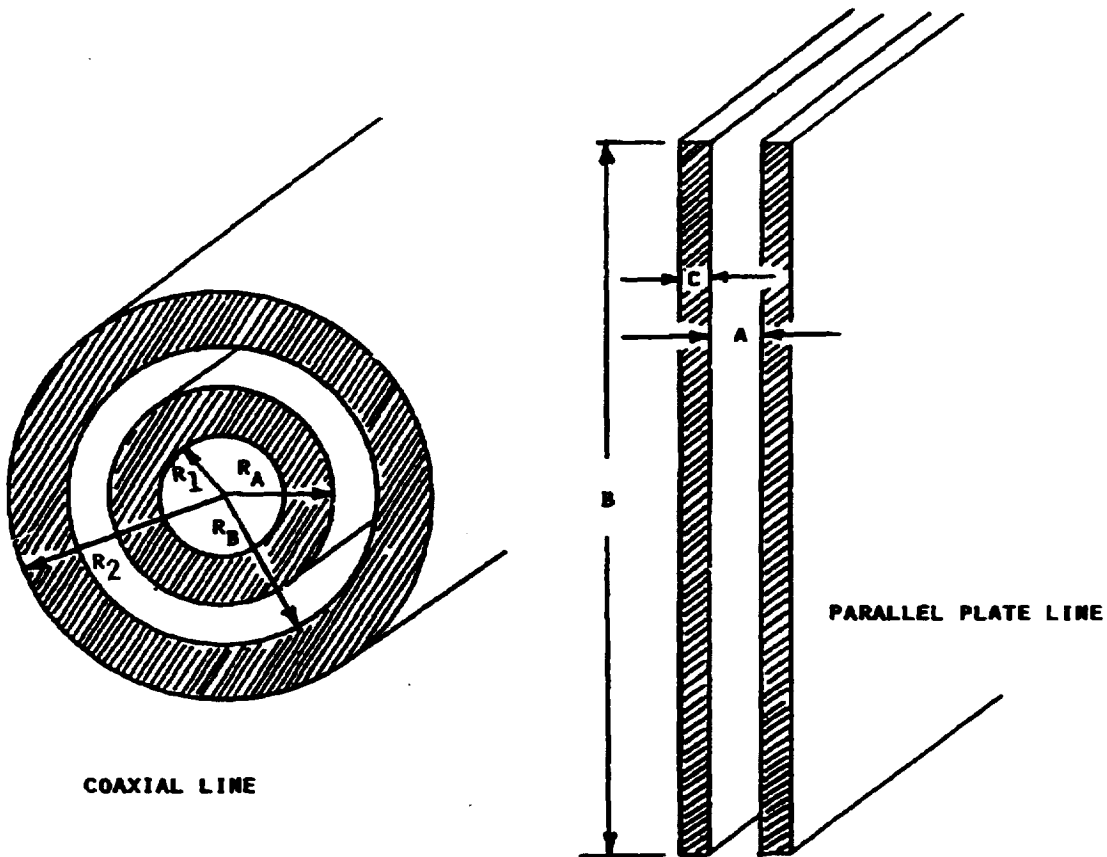


Fig. 16

## Power Management

For the last 15 years, Lewis Research Center has been developing power processors for space flights. The current development is a 25 kW series resonant DC/DC converter which is at the prototype level (ref. 13). With today's component technology, the power level of space power processors could reach 50 kW. These 50 kW modules could then be paralleled, which could increase the power system size to 250 kW or larger (Fig. 17).

STATUS: 25 KW DC/DC CONVERTER - PROTOTYPE

TODAY'S TECHNOLOGY: 50 KW POWER PROCESSORS (AC OR DC)  
(USING NEW POWER COMPONENTS)

SYSTEM SIZE: BY USING 25 TO 50 KW MODULES IN PARALLEL, SYSTEM  
SIZES >250 KW ARE REASONABLE

Fig. 17

## References

1. Hower, P. L.; and Chu, C. K.: Development and Fabrication of Improved Power Transistor Switches. NASA CR-159524, 1979.
2. Hower, P. L.: High-Current, Fast-Switching Transistor Development. NASA CR-165372, 1981.
3. Geisler, M. J.; Hill, F. E.; and Ostop, J. A.: Development and Fabrication of an Augmented Power Transistor. NASA CR-168262, 1983.
4. Berman, A. H.; Balodis, V.; et al.: Development and Fabrication of a Fast Recovery, High Voltage Power Diode. NASA CR-165411, 1981.
5. Berman, A. H.; Balodis, V.; et al.: Development and Fabrication of a High Current, Fast Recovery Power Diode. NASA CR-168196, 1983.
6. Mitchell, J. T.: Aerospace Technology Development of Three Types of Solid State Remote Power Controllers For 120 VDC With Current Ratings of Five and Thirty Amperes, One Type Having Current Limiting. NASA CR-135216, 1977.
7. Mitchell, J. T.: Kilovolt DC Solid State Remote Power Controller Development. NASA CR-168041, 1982.
8. Chester, M. S.: Heat Pipe Cooled Power Magnetics. NASA CR-159659, 1979.
9. Welsh, J. P.: Design and Development of Multi-kW Power Electronic Transformers — for Long Duration Space Applications. NASA CR-168082, 1983.
10. White, C. W.; and Hoffman, P. S.: High Frequency, High Power Capacitor Development. NASA CR-168035, 1983.
11. Weinberger, S. M.: Preliminary Design Development of 100 kW Rotary Power Transfer Device. NASA CR-165431, 1981.
12. Weinberger, S. M.: Design Study of a High Power Rotary Transformer. NASA CR-168012, 1982.
13. Hughes Aircraft Company: 25-kW Series-Resonant dc/dc Power Converter. NASA CR-168273, 1984.



N85

3878

UNCIALS

D-28

N85 13878

MOTOR/GENERATOR AND ELECTRONIC CONTROL CONSIDERATIONS  
FOR ENERGY STORAGE FLYWHEELS

Frank Nola  
NASA Marshall Space Flight Center  
Huntsville, Alabama

PRECEDING PAGE BLANK NOT FILMED

389

## REQUIREMENTS

Requirements of the system are to accelerate the momentum wheel to a fixed maximum speed when solar energy is available and to maintain a constant voltage on the spacecraft bus under varying loads when solar energy is not available.

- SOLAR POWER AVAILABLE

ACCELERATE MOMENTUM WHEEL TO 35,000 RPM

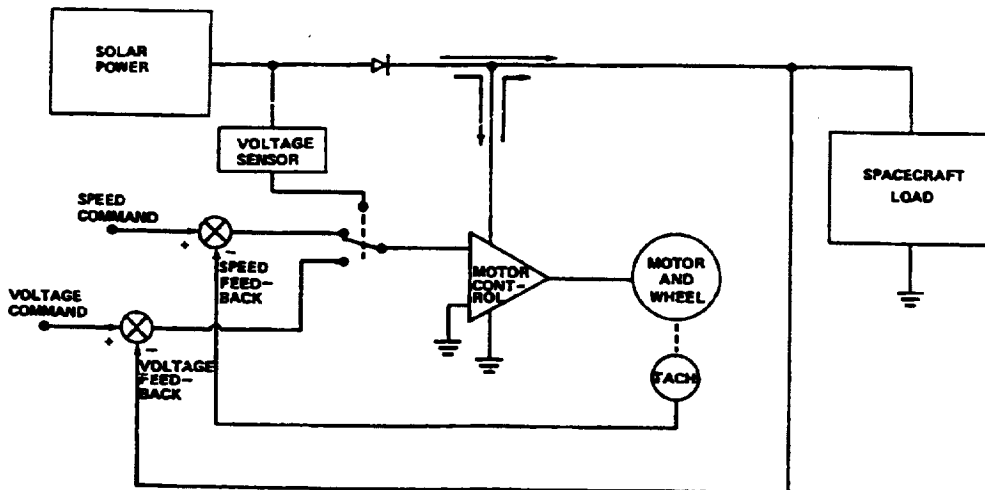
MAINTAIN CONSTANT SPEED IF EXCESS ENERGY AVAILABLE

- NO SOLAR POWER

DECELERATE WHEEL - PROVIDE ELECTRICAL ENERGY TO SPACECRAFT -  
MAINTAIN CONSTANT REGULATED SUPPLY VOLTAGE OVER VARIABLE POWER  
OUTPUT RANGE.

## ENERGY FLOW CONTROL

This is a simplified energy flow control diagram. The motor controller senses the voltage level from the solar power source and compares it to a threshold. Voltage above the threshold indicates the availability of solar energy and the controller is switched to a speed control mode for accelerating the flywheel. Solar energy is being supplied to the IPACS and to the spacecraft in this mode. Voltage below the threshold indicates insufficient solar energy and switches the controller to a voltage control mode. In this mode, energy is being supplied to the spacecraft only by the IPACS and the voltage is held constant by the voltage feedback loop.



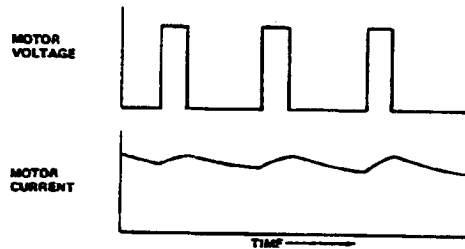
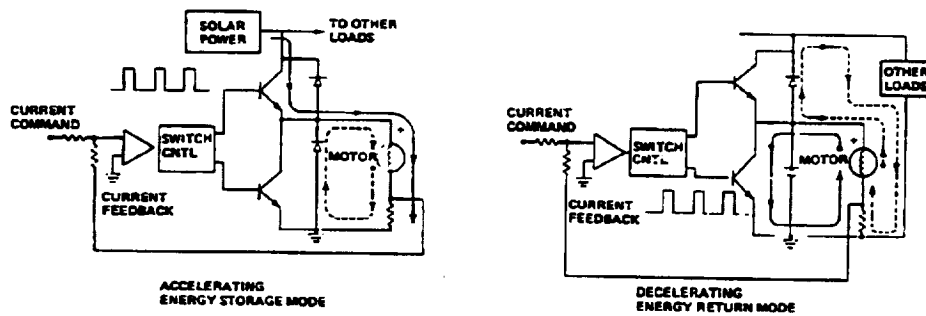
## CANDIDATE MOTOR TYPES

Candidate motor types are discussed. Permanent magnet brushless DC motors and variable frequency AC induction motors are the only two considered for IPACS. The brushless DC motor is favored because of its high torque to weight ratio and high efficiency.

- SELF-SYNCHRONOUS PERMANENT MAGNET BRUSHLESS DC MOTOR
  - CONVENTIONAL STATOR
  - IRONLESS STATOR
- VARIABLE FREQUENCY AC INDUCTION MOTOR
  - BOTH ARE ESSENTIALLY AC MOTORS
    - DC LINE VOLTAGE CONVERTED TO AC FOR ACCELERATION
    - AC MOTOR VOLTAGE CONVERTED TO DC FOR ENERGY RETURN
    - COMMON CONTROLLER ACCOMPLISHES BOTH/CONTROLLER ALSO REGULATES LINE VOLTAGE IN GENERATOR MODE
  - AC INDUCTION MOTOR
    - MOST RUGGED
    - REQUIRES NO POSITION SENSORS
    - REQUIRES SPEED SENSOR
  - BRUSHLESS DC MOTOR
    - HIGHEST TORQUE TO WEIGHT RATIO
    - HIGHEST EFFICIENCY - PERMANENT MAGNET IS LOSS LESS
    - BETTER REDUNDANCY POTENTIAL
    - REQUIRES ROTOR POSITION SENSORS
    - SAMARIUM COBALT MAGNETS INSURE RUGGEDNESS
    - 140 HP, 20,000 RPM MOTOR DEMONSTRATED (G.E.)

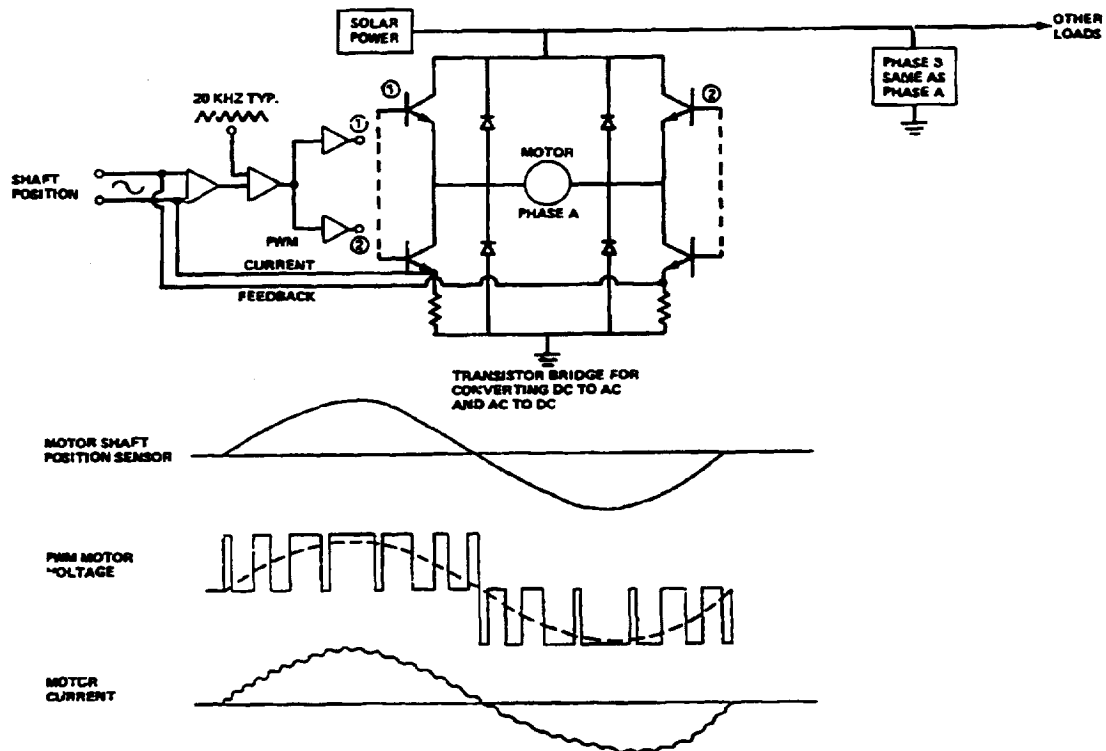
## PULSE WIDTH MODULATED CURRENT CONTROL

Simplified diagrams show the path of current flow in the pulse width modulated (PWM) controller for both the accelerating and decelerating mode. Diagrams show how both are accomplished in a common controller. Transistor switches are either full on, dissipating very low power; or full off, dissipating no power, resulting in high efficiency.



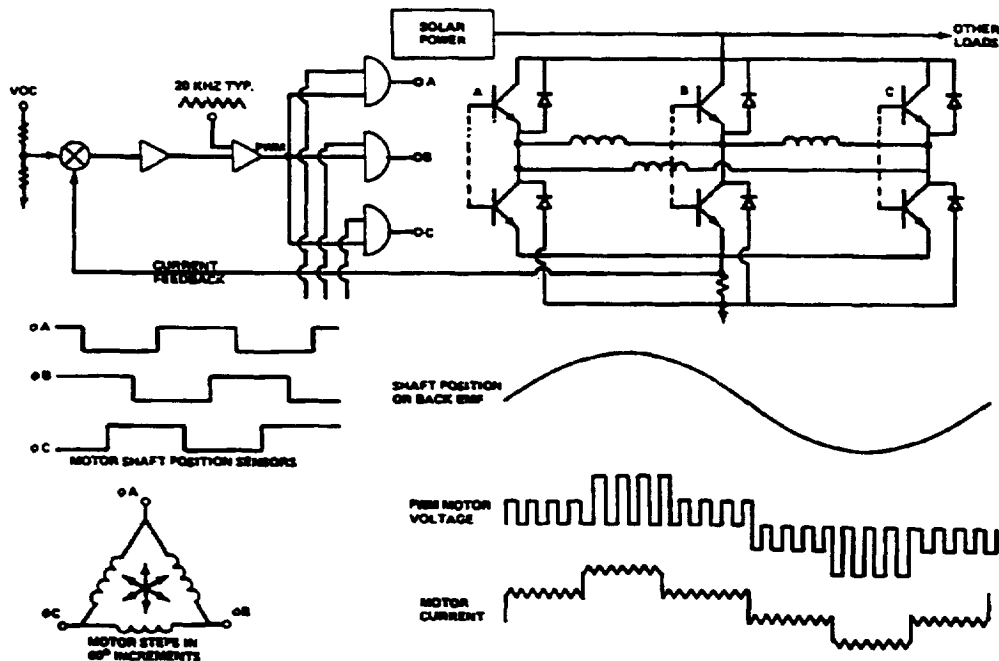
## TWO-PHASE SINUSOIDAL PWM CONTROL - BRUSHLESS DC

A transistor bridge provides bi-directional current flow for converting DC to AC in the motor mode and AC to DC in the generator mode. In the two-phase system, sinusoidal outputs of the shaft position transducers are pulse width modulated as indicated to produce sinusoidal motor currents. Linear current feedback is used to control the amplitude of the current and to force it to be in phase with the position transducer. Maintaining sinusoidal motor currents essentially eliminates harmonic losses.



### THREE-PHASE PWM CONTROL - BRUSHLESS DC

In the three-phase controller, the shaft position sensors are converted to square waves which, after conditioning, switch a square wave of current to the motor to essentially step the motor in 60 degree increments. In the accelerating mode, one top transistor is switched at the PWM frequency while one bottom transistor is switched on for a full 120 degrees to provide a path for "free wheeling" current. In the generating mode, one bottom transistor is switched at the PWM frequency to instantaneously short out the back EMF. The "free wheeling" current supplies power to the bus through one upper and one lower diode. Voltage appearing across the current sampling resistor is DC and is consistent with the DC current command voltages.





## EFFICIENCY CONSIDERATIONS

Sources of power loss which affect the efficiency are listed. Included are the motor, the electronic controller, and bearings.

- SOURCES OF LOSS
  - MOTOR
  - ELECTRONIC CONTROLLER
  - BEARINGS - BALL OR MAGNETIC
- MOTOR EFFICIENCY OPTIMIZED BY INCREASING WEIGHT
  - REDUCES COPPER LOSS
  - LOWER FLUX DENSITY IN IRON REDUCES CORE LOSSES
  - IRONLESS STATOR ELIMINATES CORE LOSSES
- CONTROLLER EFFICIENCY OPTIMIZED BY OUTPUT POWER OF SYSTEM AND BY LINE VOLTAGE CONSISTENT WITH AVAILABLE TRANSISTORS
- EFFICIENCY DECREASES SIGNIFICANTLY WITH DEPTH OF DISCHARGE
  - CURRENT DOUBLES AT HALF SPEED
  - MOTOR  $I^2R$  LOSS INCREASES BY AT LEAST A FACTOR OF FOUR
  - CONTROLLER LOSS AT LEAST DOUBLES

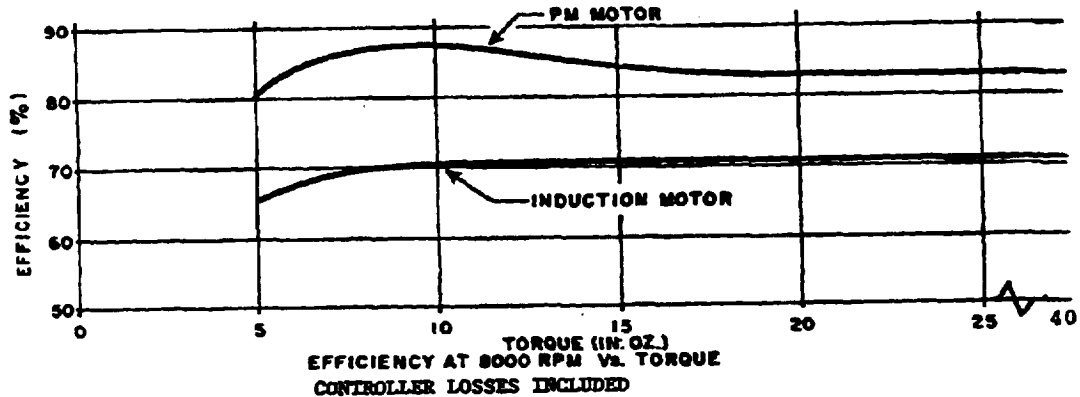
## BRUSHLESS DC MOTOR WITH IRONLESS STATOR

In the ironless stator motor below, the flux return path rotates with the permanent magnet rotor. Since there is no relative motion between the flux and the iron, core losses are eliminated. In high speed fly wheels, the return path may be the inner rotor and the magnets mounted in the outer structure to take advantage of the support provided by the wheel. The low inductance resulting from this type of structure may require external chokes for proper controller operation.



### COMPARISON OF INDUCTION AND PERMANENT MAGNET (PM) MOTORS

A variable frequency AC induction motor and a brushless PM motor were designed to be interchangeable on the shaft of a control moment gyroscope. Both were tested with a common controller with only minor modifications to the input circuitry as required by each motor. The lower efficiency resulting from rotor excitation losses in the induction motor is clearly indicated. Also, the higher inductance of the induction motor forces a lower back EMF and torque constant than for an equivalent PM motor resulting in a higher current capacity controller.



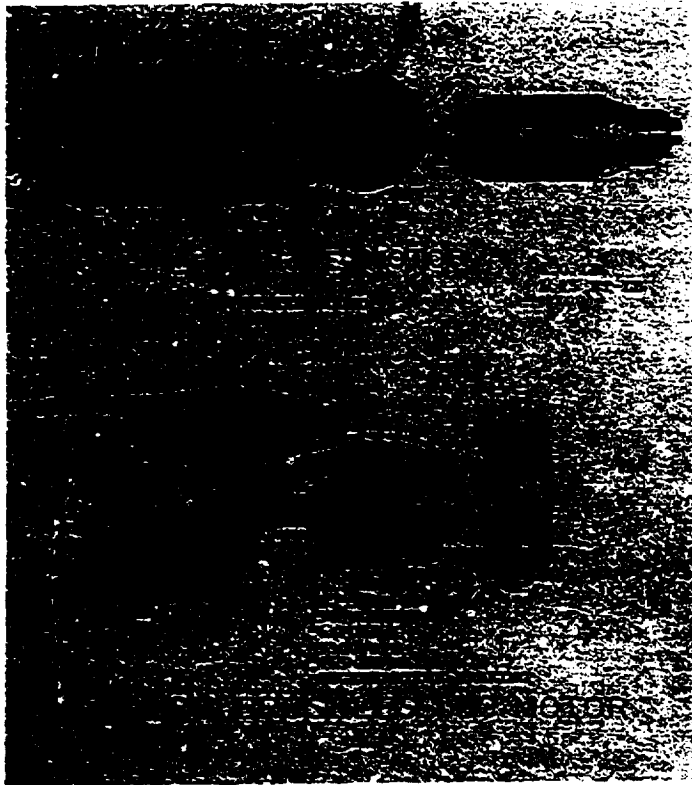
PM MOTOR  
 28 VOLTS  
 5.7 LB  
 .17 OHM/PHASE  
 .6 MILLIHENRY/PHASE

INDUCTION MOTOR  
 28 VOLTS  
 7.2 LB  
 .26 OHM/PHASE  
 1.2 MILLIHENRY/PHASE

ORIGINAL FILED  
OF POOR QUALITY

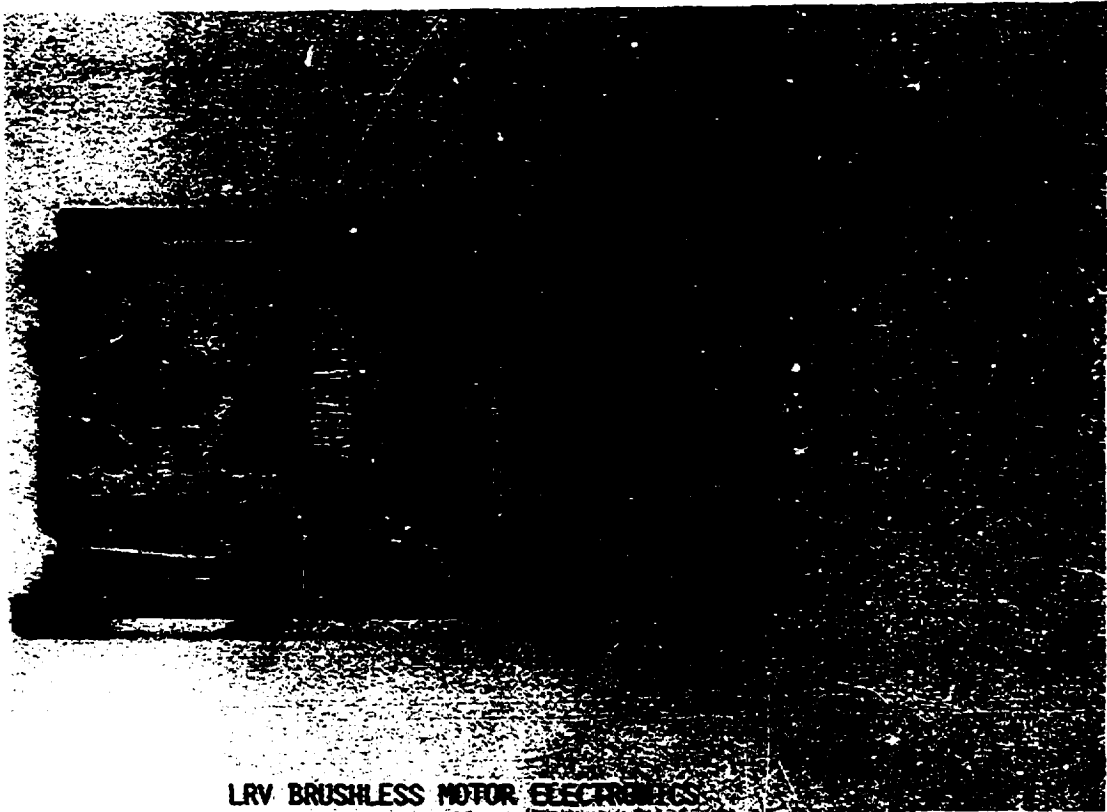
### LUNAR ROVING VEHICLE (LRV) MOTORS

Both a series wound motor and a brushless permanent magnet (PM) motor were developed for the Lunar Roving Vehicle. The series motor completed qualification first and was incorporated in the flight system. The PM motor was used in other off-road vehicle programs. The regenerative braking feature and 465 hertz excitation frequency (equivalent to 27,900 RPM, 2-pole motor) of the PM motor are similar to the requirements for a high speed energy storage flywheel application. Because of its low inductance, small external chokes were used (as opposed to raising the PWM frequency) for smoothing the PWM current.



## LRV BRUSHLESS MOTOR ELECTRONICS

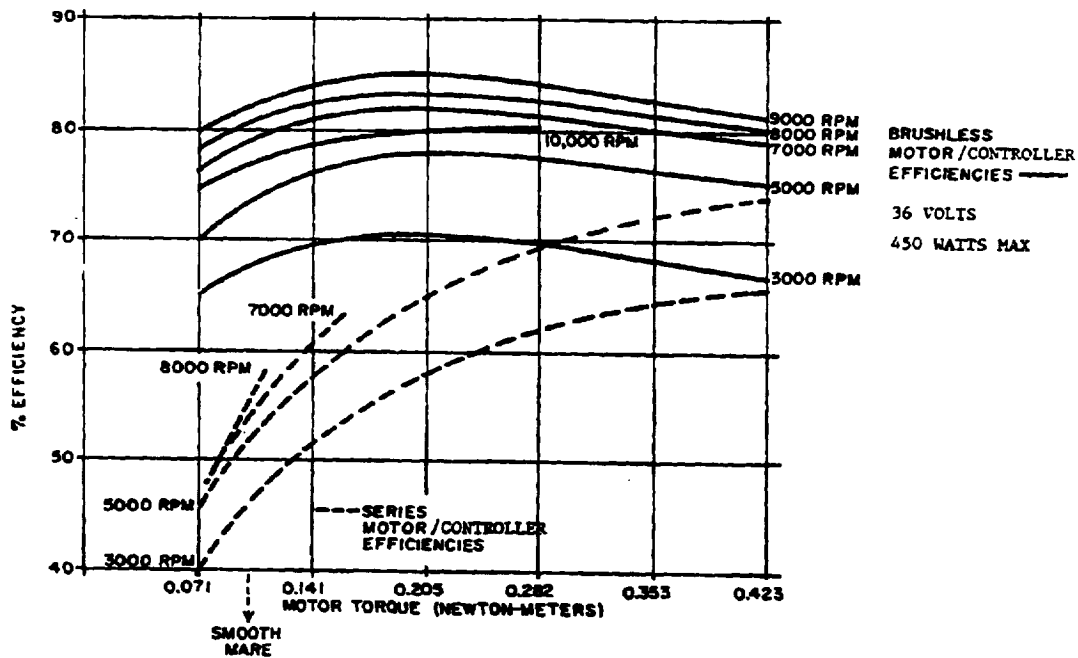
The electronic controller developed by Marshall Space Flight Center for the LRV included regenerative braking similar to that required for energy storage flywheels as well as electronic gearings. The motor winding was tapped at one-fourth of its turns. The vehicle started with the full winding applied to the controller for high accelerating or climbing torque. At one-fourth maximum speed, the controller automatically switched to the one-quarter turns tap for high speed, low torque operation. This reduced the current handling requirement of the controller by 75 percent.



LRV BRUSHLESS MOTOR ELECTRONICS

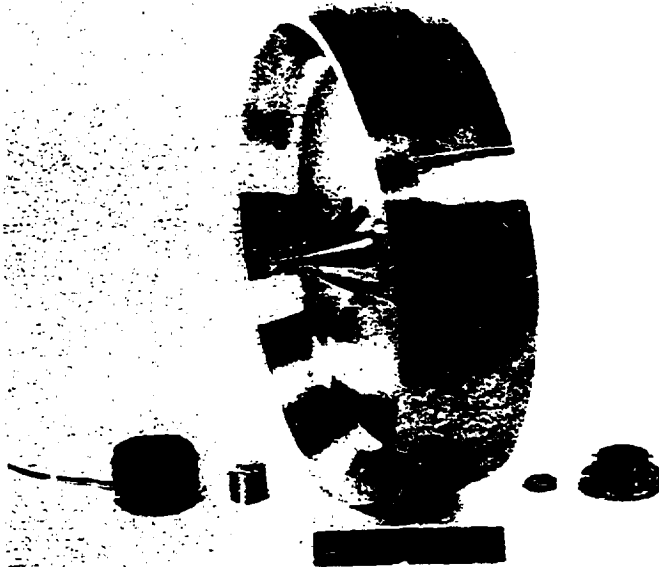
### EFFICIENCY VS TORQUE OF LRV MOTORS

Peak motoring efficiencies of 85 percent were obtained for the LRV motor and electronic controller. Efficiencies shown are for a 36-volt system. The motor was weight critical and was not optimized for efficiency. Increased motor weight and higher line voltage would result in a significant increase in efficiency.



## BRUSHLESS DC MOTOR AND FLYWHEEL

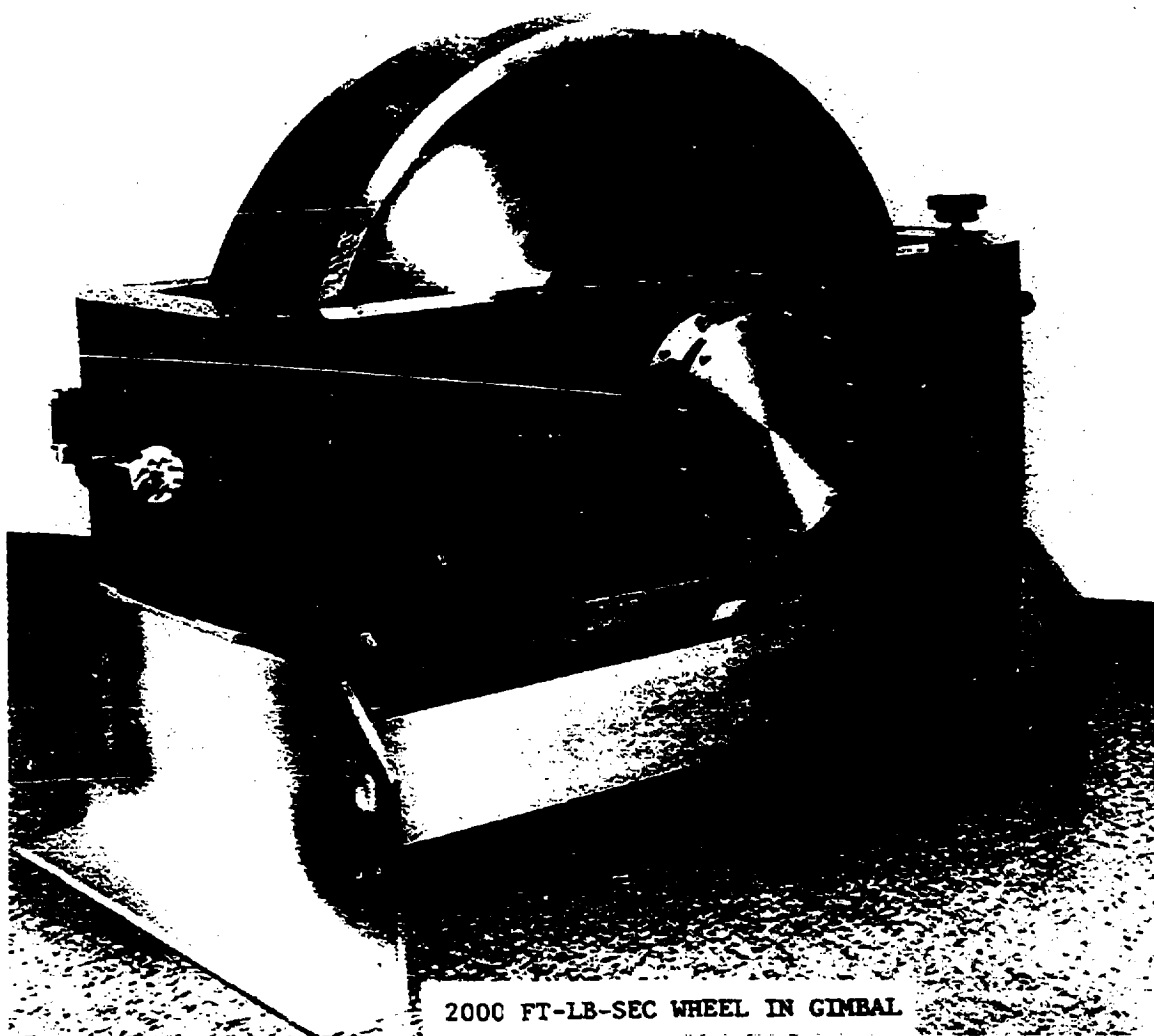
The brushless DC motor and flywheel shown below were fabricated early in the SKYLAB program (1967) to investigate control concepts for high speed brushless motors driving momentum storage wheels. The 162-pound wheel has an angular momentum of 2000 ft-lb-sec at 8000 RPM and stores 315 watt-hours of energy. While the motor exhibits efficiencies in excess of 95 percent, it operates from a 28-volt source resulting in an overall efficiency of slightly greater than 80 percent when controller losses are included. Bearing losses are also appreciable. Although the system is not optimized for efficiency, it is presently in use at MSFC for developing motor/generator concepts related to integrated flywheel systems.



FLYWHEEL MOUNTED IN GIMBAL

ORIGINAL PART IS  
OF POOR QUALITY

The flywheel is shown mounted in its gimbal support and vacuum enclosure assembly.

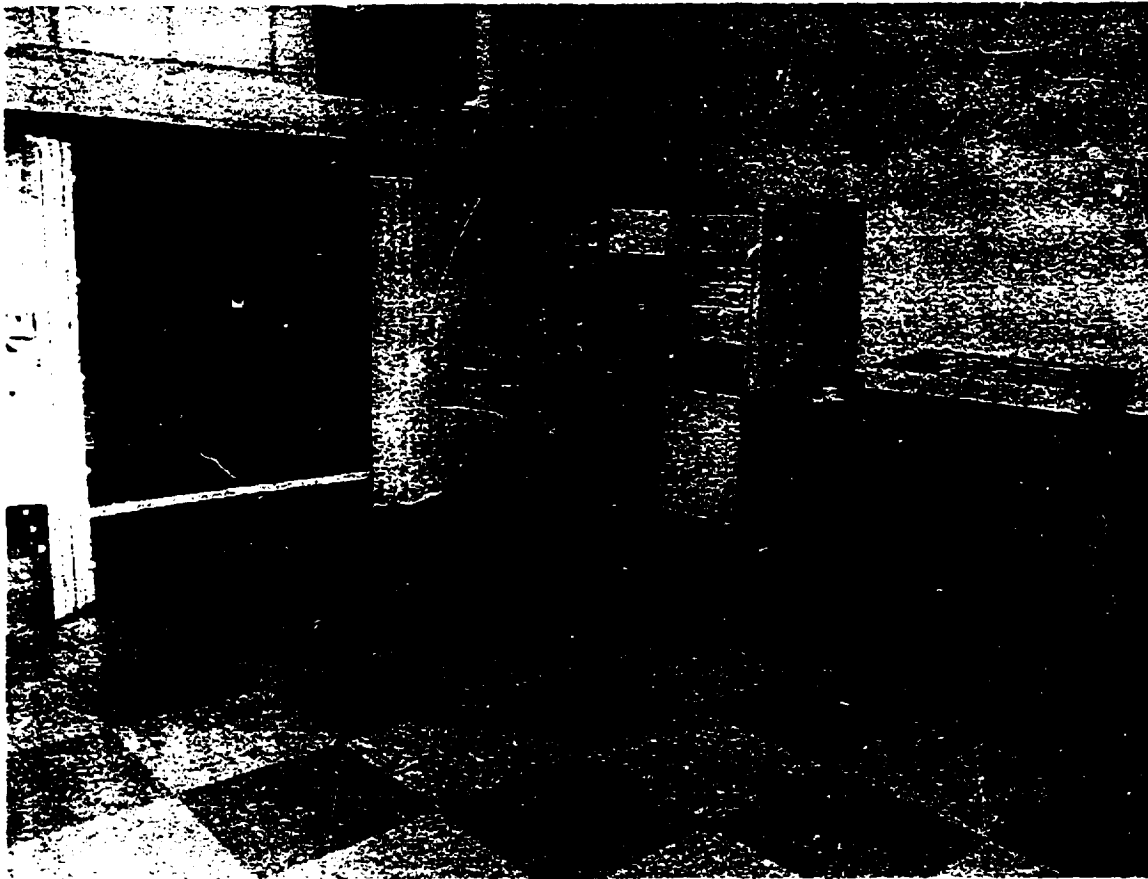


2000 FT-LB-SEC WHEEL IN GIMBAL



## HIGH ENERGY FLYWHEEL TEST VAULT

Control concepts for storing energy in flywheels and for converting stored energy to supply a constant bus voltage under varying load and wheel speed conditions are being tested in the vault shown below.



ORIGINAL PAGE IS  
OF POOR QUALITY

## TECHNOLOGY ASSESSMENT

An assessment of the technology related to motors/generators and electronic controls for high speed flywheels is presented in the comments below.

- PRESENT MOTOR TECHNOLOGY ADEQUATE - TRADE-OFFS MAY BE REQUIRED TO ACHIEVE ULTIMATE IN EFFICIENCY
- PWM TECHNIQUES FOR CONTROLLING POWER IN BOTH THE MOTOR AND GENERATOR HAVE BEEN WELL DEVELOPED AND DEMONSTRATED
- HIGH EFFICIENCY (> 95%) ELECTRONIC CONTROLLERS IN THE 1/2 TO 1 KW RANGE HAVE BEEN DEMONSTRATED
- DESIGN AND TRADE-OFF STUDIES FOR HIGHER POWER SYSTEMS WILL BE REQUIRED TO MAINTAIN HIGH EFFICIENCY. SWITCHING LOSSES IN HIGHER POWER BIPOLAR TRANSISTORS BECOME APPRECIATIVE AT PWM FREQUENCIES REQUIRED FOR HIGH WHEEL SPEED OPERATION
  - POSSIBILITIES INCLUDE:
    - USE OF NEW MOSFET POWER TRANSISTORS
    - MOTORS WITH MULTIPLE PARALLEL WINDINGS AND MULTIPLE TRANSISTOR BRIDGES FOR CURRENT SHARING
- REDUNDANCY MANAGEMENT TECHNIQUES FOR MULTIPLE WHEEL OPERATION NEED TO BE DEVELOPED
  - FOR MOST EFFICIENT OPERATION ALL WHEELS SHOULD SWITCH FROM MOTOR TO GENERATOR MODE AND VICE VERSA SIMULTANEOUSLY
  - ALL WHEELS SHOULD SHARE A COMMON ERROR VOLTAGE TO INSURE THEY SHARE EQUALLY IN SUPPLYING THE SPACECRAFT LOAD
  - NEAR EQUAL WHEEL SPEEDS MAY SIMPLIFY MOMENTUM MANAGEMENT CONTROL LAWS

N85

3879

UNCLAS

D-29

N85 13879

TORQUE COMMAND STEERING LAW  
FOR  
DOUBLE-GIMBALED CONTROL MOMENT GYROS  
APPLIED TO  
ROTOR ENERGY STORAGE

Ha. F. Kennel  
Systems Dynamics Laboratory  
NASA George C. Marshall Space Flight Center  
Marshall Space Flight Center, Alabama

PRECEDING PAGE BLANK NOT FILMED

## INTRODUCTION

As space vehicles become larger and mission times become longer double-gimbaled control moment gyros (CMGs) will be used more and more for attitude control, angular momentum storage and energy storage. Therefore, a need exists for a simple, but universally applicable CMG steering law which takes the control torque command and generates gimbal rate commands in such a way that, in spite of the highly nonlinear CMG behavior, the resulting torque on the vehicle is ideally equal to the commanded one. Furthermore, this steering law should allow the use of any number of CMGs, which allows the tailoring to the angular momentum requirement while at the same time making the failure accommodation a built-in feature. It should also allow the mixing of CMGs of different momentum magnitudes to the extent that some or all CMGs could be used for energy storage. It also should allow adding energy storage flywheels to the mix.

A steering law is presented here, which has all these features, assuming the CMG outer gimbal freedom is unlimited (however, the range of the outer gimbal angle readout should be:  $-\pi \geq \beta_1 > +\pi$ ; the inner gimbal angle should be hardware limited to  $\pm\pi/2$ ). The reason is the idea of mounting all the outer gimbal axes of the CMGs parallel to each other. This allows the decomposition of the steering law problem into a linear one for the inner gimbal angle rates and a planar one for the outer gimbal angle rates. The inner gimbal angle rates are calculated first, since they are not affected by the outer gimbal angle rates. For the calculation of the outer rates, the inner rates are then known quantities. An outer gimbal angle distribution function (to avoid singularities internal to the total angular momentum envelope) generates distribution rates next, and finally the pseudoinverse method is used to insure that the desired total torque is delivered.

This paper is a revision of Reference 1.

## PARALLEL MOUNTING ARRANGEMENT

The proposed mounting, with all outer gimbal axes parallel, is shown in Figure 1 (for convenience only, the outer gimbal axes are also shown colinear). This mounting arrangement has many advantages. The mounting interfaces can be identical, i.e., the mounting brackets and hardware, cable harnesses, etc. There is no need to individually identify the CMGs, and the on-board computer can assign an arbitrary label to any CMG, which could be changed from one computation cycle to the next. This simplifies the steering law and the redundancy management. The parallel mounting in conjunction with a steering law that accepts any number of CMGs makes failure accommodation a built-in feature. However, if increasing angular momentum requirements during the design of a space vehicle demand it (and the moments of inertia always tend to increase), additional CMGs can be added with minimum impact on the hardware and almost none on the software. The parallel mounting also makes the visualization of the system operation exceedingly simple (especially when compared with the momentum envelopes and saturation surfaces of skewed mounted single-gimbaled CMGs).

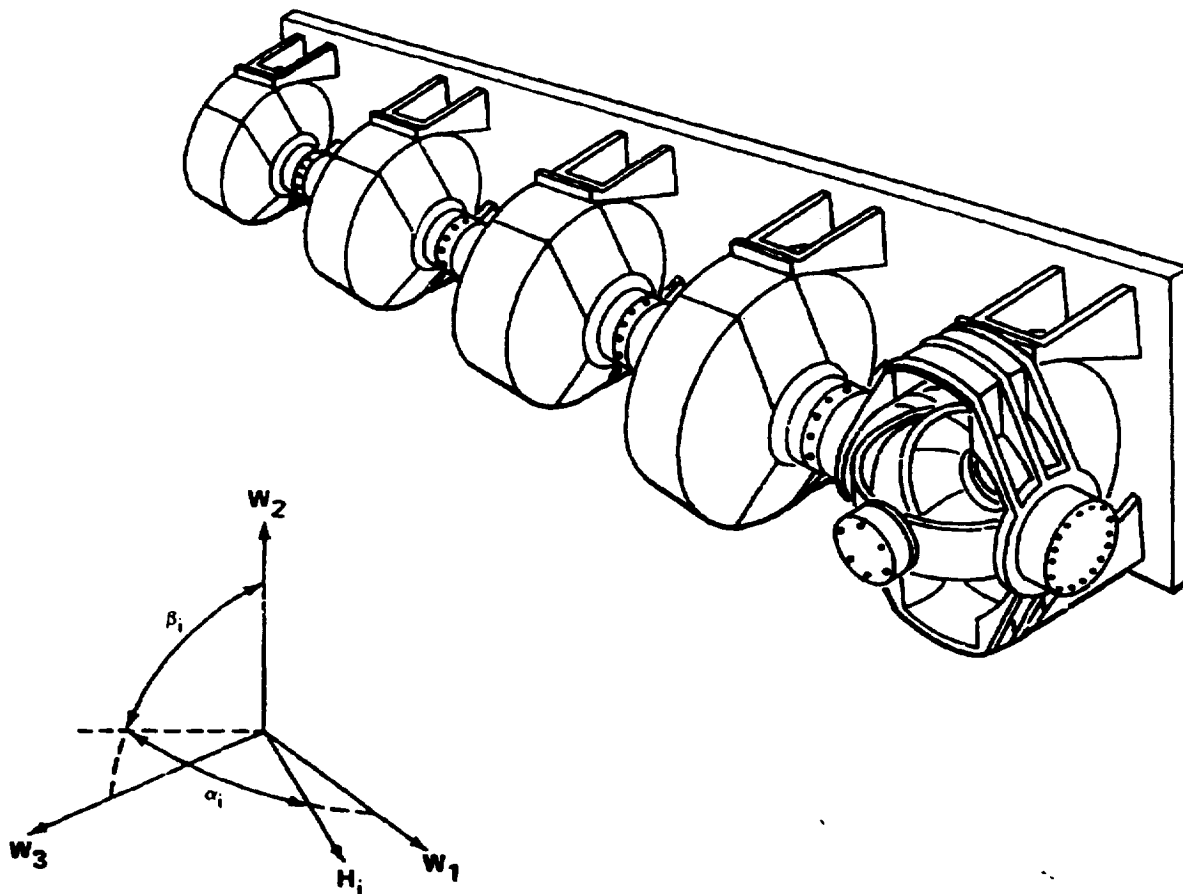


Figure 1.-Proposed mounting.

### TOTAL ANGULAR MOMENTUM AND TORQUE COMMAND

Given a CMG coordinate system W, Figure 1 shows the inner and outer gimbal angles  $\alpha_i$  and  $\beta_i$  of the  $i$ th CMG. With this definition, the angular momentum of  $n$  CMGs is ( $i$  ranges from 1 to  $n$ ,  $H_i$  is the momentum magnitude):

$$\underline{H}_G = \begin{bmatrix} H_{G1} \\ H_{G2} \\ H_{G3} \end{bmatrix} = \begin{bmatrix} \sum_i H_i s\alpha_i \\ \sum_i H_i c\alpha_i c\beta_i \\ \sum_i H_i c\alpha_i s\beta_i \end{bmatrix} \quad (1)$$

The CMG angular momentum change is

$$\dot{\underline{H}}_G = \begin{bmatrix} \sum_i H_i c\alpha_i \dot{\alpha}_i \\ \sum_i (-H_i s\alpha_i c\beta_i \dot{\alpha}_i - H_i c\alpha_i s\beta_i \dot{\beta}_i) \\ \sum_i (-H_i s\alpha_i s\beta_i \dot{\alpha}_i + H_i c\alpha_i c\beta_i \dot{\beta}_i) \end{bmatrix} + \begin{bmatrix} \sum_i \dot{H}_i s\alpha_i \\ \sum_i \dot{H}_i c\alpha_i c\beta_i \\ \sum_i \dot{H}_i c\alpha_i s\beta_i \end{bmatrix} \quad (2)$$

We can assume that the  $\dot{H}$  terms are known (from power demand or the difference between present and past value of  $\underline{H}$ ) and it is accounted for in the torque command:

$$\underline{T} = \dot{\underline{H}}_G - \underline{\dot{H}} = \begin{bmatrix} \sum_i H_i c\alpha_i \dot{\alpha}_i \\ \sum_i (-H_i s\alpha_i c\beta_i \dot{\alpha}_i - H_i c\alpha_i s\beta_i \dot{\beta}_i) \\ \sum_i (-H_i s\alpha_i s\beta_i \dot{\alpha}_i + H_i c\alpha_i c\beta_i \dot{\beta}_i) \end{bmatrix} \quad (3)$$

The task is now to find a set of gimbal angle rate commands  $\dot{\alpha}$  and  $\dot{\beta}$  which when inserted into equation (3) will satisfy the torque command, while at the same time utilizing the excess degrees of freedom to distribute the gimbal angles such that the momentum singularities are avoided.

## DESIRABLE INNER GIMBAL ANGLE DISTRIBUTION

The  $n$  double-gimbaled CMGs have  $2n$  degrees of freedom. Three are needed to satisfy the torque command; the excess of  $2n-3$  degrees of freedom is utilized to achieve a desirable gimbal angle distribution. Before one can decide on a desirable distribution, the characteristics of a double-gimbaled CMG have to be considered.

The inner gimbal angle rate needed to produce a given torque perpendicular to the inner gimbal axis is independent of the inner and the outer gimbal angles. However, the outer gimbal angle rate needed to produce a given torque perpendicular to the outer gimbal axis is inversely proportional to the cosine of the inner gimbal angle. Therefore, it is desirable to keep the cosine of the inner gimbal angle large, i.e., it is desirable to minimize the largest inner gimbal angle. This then reduces to outer gimbal angle rate requirements. The largest inner gimbal angle is minimized when all inner gimbal angles are equal to the inner gimbal reference angle, cf. equation (1),

$$\alpha_R = \sin^{-1} \left\{ \left( \sum_i H_i \cos \alpha_i \right) / \left( \sum_i H_i \right) \right\} \quad (4)$$

Inner gimbal angle redistribution should be made without resulting in a torque along the  $W_1$  axis. This implies [cf. equation (3)]

$$T_{D1} = \sum_i H_i \cos \alpha_i \dot{\alpha}_{D1} = 0$$

For simplicity we select the distribution rate as  $\dot{\alpha}_{D1} = K_a (\alpha_o - \alpha_i)$ . The  $W_1$  torque is now

$$T_{D1} = \sum_i H_i \cos \alpha_i K_a (\alpha_o - \alpha_i)$$

Setting this torque to zero results in

$$\alpha_o = \left( \sum_i H_i \cos \alpha_i \alpha_i \right) / \left( \sum_i H_i \cos \alpha_i \right) \quad (5)$$

When all  $\alpha_i = \alpha_o$ ,  $\alpha_o$  has converged to its ideal value of equation (4). However, a torque does result in the  $W_2$ - $W_3$  plane and it will be treated in conjunction with the outer gimbal angle distribution.



## DESIRABLE OUTER GIMBAL ANGLE DISTRIBUTION

The situation is not as clear-cut with respect to the desirable outer gimbal angle distribution. However, for double-gimbaled CMGs a singular condition inside the total angular momentum envelope can only occur when some of the momentum vectors (at least one) are antiparallel and the rest parallel to their resultant total angular momentum vector. Maintaining adequate and more or less equal spacing between the vectors will therefore eliminate the possibility of a singularity. Many distribution functions are possible and the goal is to find one which minimizes the software requirements. The selected distribution function requires no transcendental functions or divisions and allows CMG failures or resurrections any time. The distribution function uses repulsion between all possible CMG pairs, i.e., proportional to the product of the angular momentum magnitudes and proportional to the supplement of the outer gimbal angle differences. Therefore, the repulsion ranges from a maximum (for equal outer gimbal angles) to zero (for antiparallel momentum vector components). Since the repulsion is generated by pairs (and all possible pairs are treated equally), no sorting is necessary. However, due to the stronger repulsion of the immediate neighbors, the outer gimbal angles act as if sorting had been done. A failed CMG is simply ignored (its angular momentum magnitude is set to zero) since it does not generate a repulsion. Any number of CMGs can be failed or resurrected at the beginning of any computation cycle. The rates due to this distribution function are (with  $-\pi \leq \beta_i < +\pi$ )

$$\dot{\beta}_{Di} = -K_b \sum_j \{H_i H_j [\beta_i - \beta_j - \pi \operatorname{sgn}(\beta_i - \beta_j)] (1 - \delta_{ij})\} \quad (6)$$

Without any momentum constraint the CMG outer gimbals would come to rest when they are separated by an angle of  $2\pi/n$ , assuming identical angular momentum magnitudes. (This would not make any sense for two CMGs since they would be antiparallel. However, two CMGs have only one excess degree of freedom and it is taken up by the inner distribution, and no distribution is possible for the outer gimbals.)

### INNER GIMBAL RATE COMMANDS

The change of the  $W_1$  angular momentum component is not a function of the outer gimbal rates [equation (3)],

$$\dot{H}_{G1} = T_{G1} = \sum_i H_i c\alpha_i \dot{\alpha}_i$$

Since all inner gimbal angles should be equal (enforced by the inner gimbal distribution), an inner gimbal rate command for all CMGs of

$$\dot{\alpha}_C = T_{C1} / \sum_i H_i c\alpha_i \quad (7)$$

will result in  $T_{G1} = T_{C1}$ , if it is assumed that the actual and the commanded gimbal rates are equal. For the total inner gimbal angle rate command we have then [cf. equation (5)],

$$\dot{\alpha}_i = K_a (\alpha_0 - \alpha_i) + T_{C1} / \sum_i H_i c\alpha_i \quad (8)$$

where it should be remembered that the distribution rates are non-torque-producing with respect to the  $W_1$  axis. The effect of the total inner gimbal angle rates on the  $W_2$  and  $W_3$  momentum components is treated later. Gimbal rate limiting will be discussed after the outer gimbal rate commands have been treated.

### OUTER GIMBAL RATE COMMANDS

The outer distribution rates of equation (6) as well as the total inner gimbal angle rate commands of equation (8) generate a torque in the  $W_2$ - $W_3$  plane. This torque is

$$\begin{bmatrix} T_2' \\ T_3' \end{bmatrix} = \begin{bmatrix} -\sum_i H_i (c\alpha_i s\beta_i \dot{\beta}_{Di} + s\alpha_i c\beta_i \dot{\alpha}_i) \\ \sum_i H_i (c\alpha_i c\beta_i \dot{\beta}_{Di} - s\alpha_i s\beta_i \dot{\alpha}_i) \end{bmatrix}$$

and the  $W_2$ - $W_3$  torques must be modified as follows:

$$\begin{bmatrix} T_{CM2} \\ T_{CM3} \end{bmatrix} = \begin{bmatrix} T_{C2} - T_2' \\ T_{C3} - T_3' \end{bmatrix}$$

To generate the modified torque, we now apply the pseudo-inverse method to get a unique set of outer gimbal rate commands

$$\begin{bmatrix} \dot{\beta}_{C1} \\ \dot{\beta}_{C2} \\ \vdots \\ \dot{\beta}_{Cn} \end{bmatrix} = [B]^T \{ [B][B]^T \}^{-1} \begin{bmatrix} T_{CM2} \\ T_{CM3} \end{bmatrix}$$

where

$$[B] = \begin{bmatrix} b_{11} & b_{12} & \dots & b_{1n} \\ b_{21} & b_{22} & \dots & b_{2n} \end{bmatrix} \quad \begin{matrix} (b_{1i} = -H_i c\alpha_i s\beta_i) \\ (b_{2i} = H_i c\alpha_i c\beta_i) \end{matrix}$$

The total outer gimbal rate commands are then

$$\dot{\beta}_i = \dot{\beta}_{Di} + \dot{\beta}_{Ci}$$

### PROPORTIONAL GIMBAL RATE LIMITING

The gimbal torques will have a definite torque limit,  $T_{LIM}$ . In order not to exceed this limit, we need to know the torque demand on the torquers due to the gimbal rate commands. Setting the outer gimbal angle to zero we get for the torque of the  $i$ th CMG [equation (3)],

$$\begin{bmatrix} T_{1i} \\ T_{2i} \\ T_{3i} \end{bmatrix} = H_i \begin{bmatrix} c\alpha_i \dot{\alpha}_i \\ -s\alpha_i \dot{\alpha}_i \\ c\alpha_i \dot{\beta}_i \end{bmatrix}$$

The torque  $T_{1i}$  is the torque load on the outer gimbal torquer and  $T_{3i}$  is the torque load on the inner gimbal torquer. Assuming the same torque limits for both inner and outer gimbal torquers, we get for the gimbal rate limits

$$\dot{\alpha}_{TLIM} = \dot{\beta}_{TLIM} = K_i / c\alpha_i$$

with  $K_i = T_{LIM} / H_i$  a CMG design constant, more or less the same for all double-gimbaled CMGs. There are also other rate limits ( $\dot{\alpha}_{LIM}$ ,  $\dot{\beta}_{LIM}$ ) due to hardware limits like gimbal rate tachometer limits, voltage limits, etc.

To reduce the magnitude of the actual torque only, but keep the same direction as the commanded torque, a proportional scaling of all gimbal rates by dividing by DIV is done, where:

$$DIV = \text{MAX} \left\{ 1, \frac{|\dot{\alpha}_1|}{\dot{\alpha}_L}, \frac{|\dot{\alpha}_2|}{\dot{\alpha}_L}, \dots, \frac{|\dot{\alpha}_n|}{\dot{\alpha}_L}, \frac{|\dot{\beta}_1|}{\dot{\beta}_L}, \frac{|\dot{\beta}_2|}{\dot{\beta}_L}, \dots, \frac{|\dot{\beta}_n|}{\dot{\beta}_L} \right\}$$

with

$$\dot{\alpha}_L = \text{MIN} (\dot{\alpha}_{TLIM}, \dot{\alpha}_{LIM})$$

$$\dot{\beta}_L = \text{MIN} (\dot{\beta}_{TLIM}, \dot{\beta}_{LIM})$$

## PERFORMANCE DISCUSSION

As implied by the discussion of the desirable gimbal angle distribution, there is no need for a strict adherence to the ideal distribution. For the inner distribution gain  $K_a$  this means that its value can be chosen over a wide range up to  $1/\Delta t$  where  $\Delta t$  is the computer cycle time, especially since the torque producing portion of the inner gimbal rate command tends to keep the inner gimbal angles on their distribution. To select the outer gimbal distribution gain we have to remember that the maximum magnitude of the outer distribution rate can be as large as [cf. equation (6)].

$$\dot{\delta}_{D\text{MAX}} = K_b \pi H_i \sum_j H_j (1 - \delta_{ij})$$

For a desired maximum outer distribution rate of 0.02 rad/s and with 5 CMGs of an angular momentum magnitude of 3000 Nms we get for example,

$$K_b = 1.8\text{E-}10$$

No special effort has to be made to "unhook" the CMG momentum vectors when, after bunching up due to saturation, the torque command is such that the momentum magnitude is reduced. In the real world, the gimbal angle readouts are noisy enough to introduce unhooking. Therefore, if a simulation is too ideal and problems are encountered, some noise should be added to the gimbal angles. The same considerations apply for starting up from an internal singularity (the distribution functions prevent any later internal singularities from occurring).

While any number of double-gimbaled CMGs can be accommodated (two CMGs are the minimum), the cycle time might become a problem for very large numbers of CMGs. Since any angular momentum magnitude is allowed, there is then the possibility to group several CMGs, add their angular momentum, and consider the group as one CMG as far as the steering law is concerned. The group is then commanded to its combined outer and inner gimbal angle. Setting the angular momentum magnitude of any CMG to zero is a convenient way of signaling that the CMG has failed.

The general logic flow, including the input and output parameters for the steering law is shown in Figure 2. The implementation for the high level language APL is shown in Figure 3 and a detailed flow in Figure 4.

<b>INPUTS</b>	$T_C$	Nm	TORQUE COMMAND ( $T_{C1}, T_{C2}, T_{C3}$ )
	$\alpha_i$	rad	INNER GIMBAL ANGLES
	$\beta_i$	rad	OUTER GIMBAL ANGLES
	$s\alpha_i, c\alpha_i$		SINES & COSINES OF THE $\alpha_i$ 'S
	$s\beta_i, c\beta_i$		SINES & COSINES OF THE $\beta_i$ 'S
	$H_i$	Nms	CMG ANGULAR MOMENTUM MAGNITUDES
<b>OUTPUTS</b>	$\dot{\alpha}_{Ci}$	rad/s	INNER GIMBAL RATE COMMANDS
	$\dot{\beta}_{Ci}$	rad/s	OUTER GIMBAL RATE COMMANDS

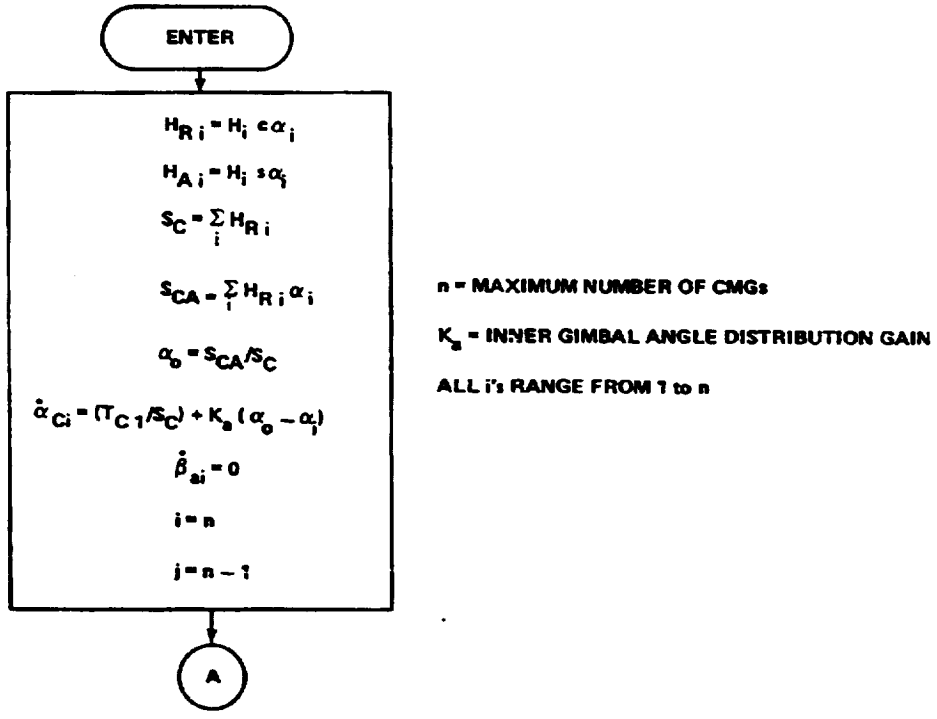


Figure 2.-Steering law logic flows.

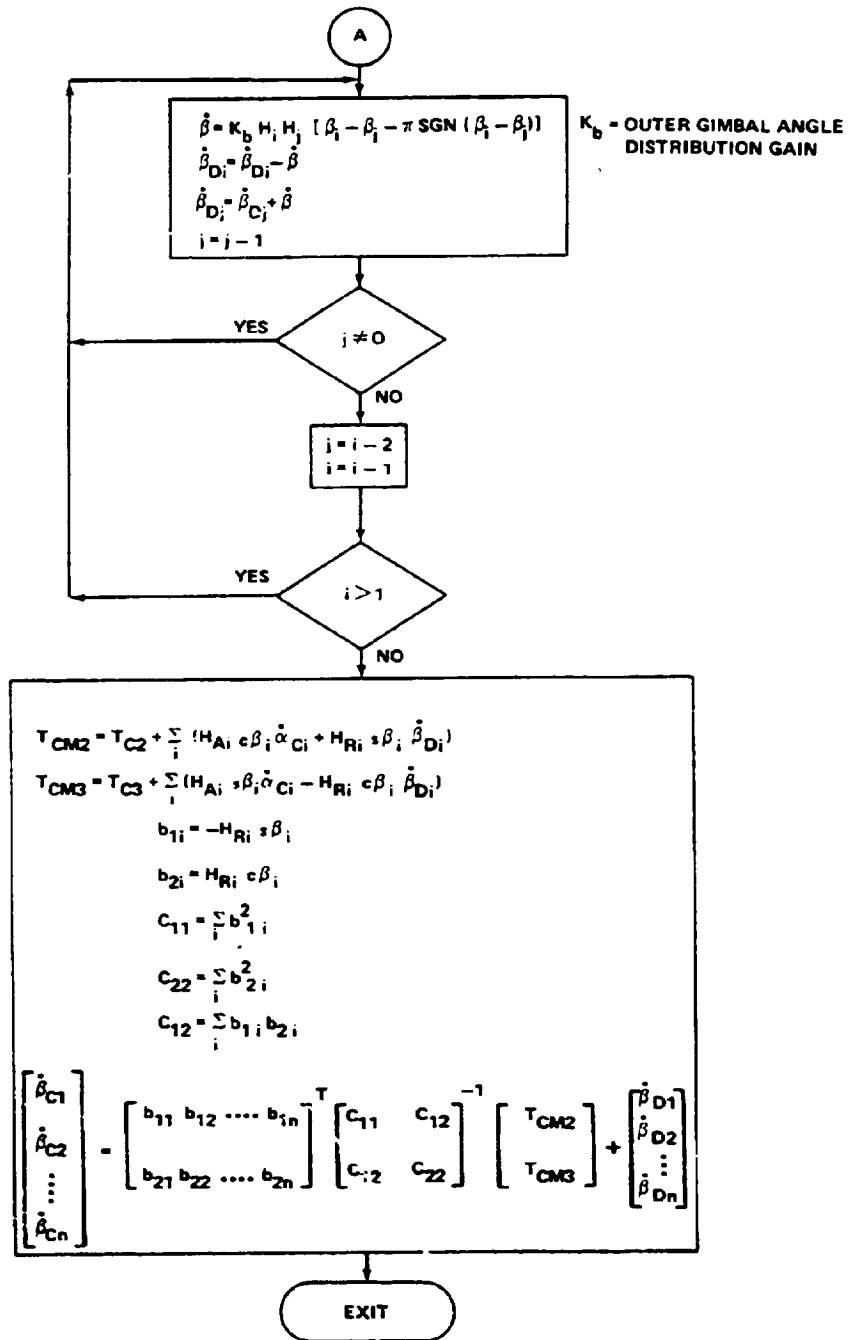


Figure 2.-Concluded.

```

▽ STLAW;HA;HR;SC;T ;BD;B;M
(1) A
(2) A
(3) A
(4) A
(5) A
(6) A
(7) A
(8) A
(9) A
(10) A
(11) A
(12) A
(13) A
(14) A
(15) A
(16) A
(17) A
(18) A
(19) A
(20) A
(21) A
(22) A
(23) A
(24) A
(25) A
(26) A
(27) A
(28) A
(29) A
▽
      ***** STEERING LAW FOR N DOUBLE *****
      ***** GIMBALED CONTROL MOMENT GYROS *****

INPUT_PARAMETERS:  TC = TC1 TC2 TC5
                  AL = α1 α2 ..... αn
                  BE = β1 β2 ..... βn
                  H  = H1 H2 ..... Hn

LOCAL_VARIABLES:  HA, HR, SC, T, BD, B, M

ALD+(TC(1)+SC)-KA*AL-(+/HR*AL)÷SC+*/HR-H*2OAL
BD+KB*+/(M*OM+(N,N)PH)*B-PI*x*B+B-OB+(N,N)PBE
T+TC(2 3)÷((/HA*ALD*2OBE)+HR*BD*1OBE),÷/((HA+H*1OAL)*ALD*1OBE)-HR*BD*2OBE
BED+BD+(OB)÷*(OB+*OB+(2,N)P(-HR*1OBE),HR*2OBE)÷.*T

QUIPUI_PARAMETERS:  ALD = α1 α2 ..... αn
                   BED = β1 β2 ..... βn

```

Figure 3.-Steering law for n double-gimbaled control moment gyros.



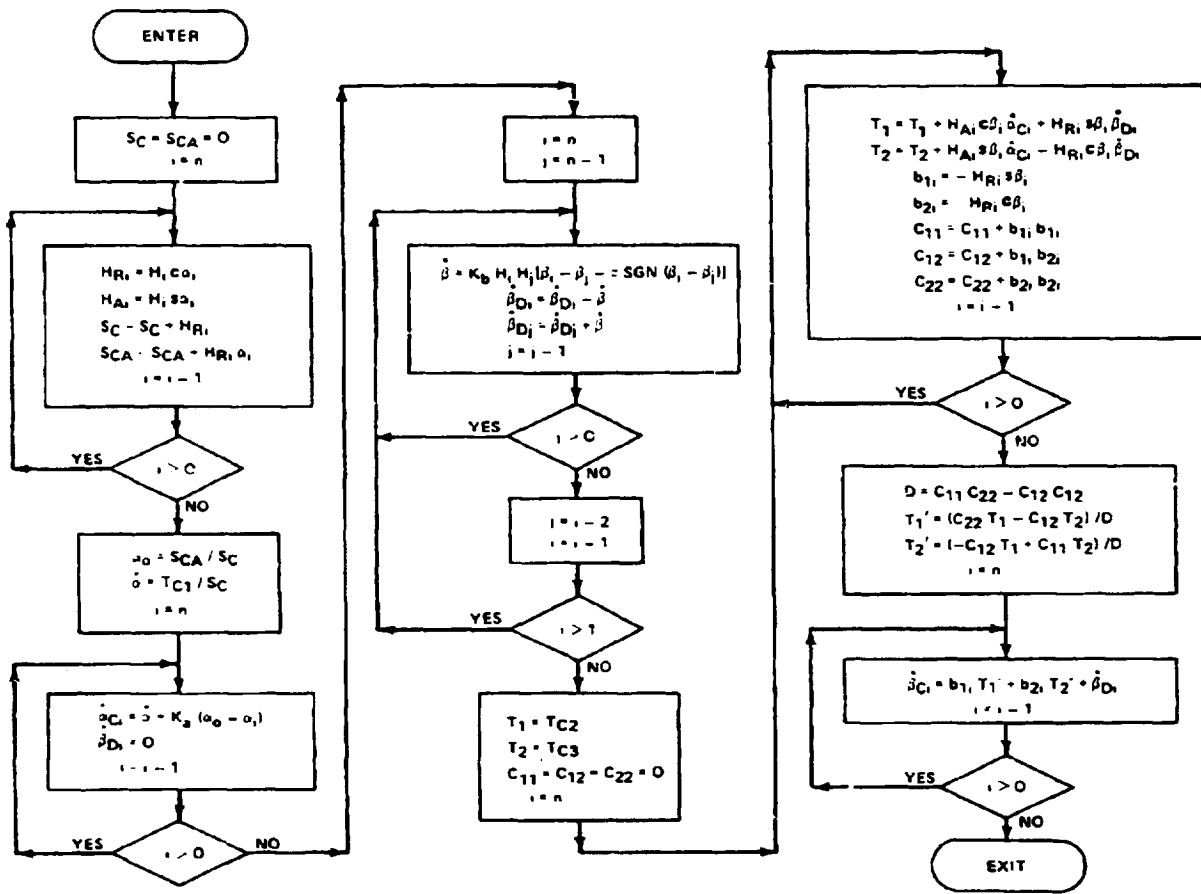


Figure 4.-Detailed logic flow.

## DEFINITION OF SYMBOLS

Symbol	Definition
[B]	$2 \times n$ torque matrix (for outer rates); Nms
$b_{ij}$	components of [B]; $i = 1, 2; j = 1, 2, \dots, n$ ; Nms
c	cos (before Greek symbol)
DIV	divisor for rate limiting
$H_i$	angular momentum magnitude of the $i$ -th CMG; $i = 1, 2, \dots, n$ ; Nms
$\underline{H}_G$	total angular momentum of the CMG system; Nms
$H_{G1}, H_{G2}, H_{G3}$	components of $\underline{H}_G$ ; Nms
$\dot{H}_p$	angular momentum change for power generation; Nm
i	index
j	index
$K_a$	inner distribution gain; 1/s
$K_b$	outer distribution gain; 1/s
$K_i$	$T_{LIMi}/H_i$ ; CMG torque constant; 1/s
n	number of double-gimbaled CMGs
s	sin (before Greek symbol)
$\underline{T}_C$	control torque command; Nm
$T_{C1}, T_{C2}, T_{C3}$	components of $\underline{T}_C$ ; Nm
$T_{CM2}, T_{CM3}$	modified torque commands; Nm
$\underline{T}_G$	total CMG torque on the vehicle; Nm
$T_{G1}, T_{G2}, T_{G3}$	components of $\underline{T}_G$ ; Nm
$T_{LIM}$	maximum CMG gimbal torquer torque; Nm
$T_{1i}, T_{2i}, T_{3i}$	torque components in the W-coordinate system (with $\beta_i = 0$ ); $i = 1, 2, 3 \dots n$ ; Nm

DEFINITION OF SYMBOLS (Concluded)

Symbol	Definition
$T_2', T_3'$	torque components due to $\dot{\alpha}_i$ 's and $\dot{\beta}_{Di}$ 's; Nm
$W_1, W_2, W_3$	CMG coordinate system axes
$\alpha_0$	inner gimbal reference angle; rad
$\alpha_i, \beta_i$	inner and outer gimbal angle; $i = 1, 2, \dots, n$ ; rad
$\alpha_R$	ideal inner gimbal reference angle; rad
$\dot{\alpha}_i, \dot{\beta}_i$	total inner and outer rates; $i = 1, 2, \dots, n$ ; rad/s
$\dot{\alpha}_{Di}, \dot{\beta}_{Di}$	inner and outer distribution rate; $i = 1, 2, \dots, n$ ; rad/s
$\dot{\alpha}_L, \dot{\beta}_L$	inner and outer rate limit; rad/s
$\dot{\alpha}_{LIM}, \dot{\beta}_{LIM}$	inner and outer rate limit due to hardware; rad/s
$\dot{\alpha}_{TLIM}, \dot{\beta}_{TLIM}$	inner and outer rate limit due to $T_{LIM}$ ; rad/s
$\dot{\beta}_C$	outer rate command vector (due to $T_{CM2}, T_{CM3}$ ); rad/s
$\dot{\beta}_{Ci}$	components of $\dot{\beta}_C$ ; $i = 1, 2, \dots, n$ ; rad/s
$\dot{\beta}_{DMAX}$	maximum possible outer distribution rate; rad/s
$\delta_{ij}$	$\left. \begin{array}{l} = 0 \text{ for } i \neq j \\ = 1 \text{ for } i = j \end{array} \right\} \text{ Kronecker delta}$
$\bar{\quad}$	a bar under a quantity denotes a vector
$[ \ ]^T$	a superscript T denotes a transpose on a vector or a matrix
$\{ \}^{-1}$	a superscript -1 denotes the matrix inverse
$\dot{\quad}$	a dot over a quantity indicates time derivative

REFERENCE

1. Kennel, Hans F.: Steering Law for Parallel Mounted Double-Gimbaled Control Moment Gyros - Revision A. NASA TM-82390, January 1981.

APPENDIX  
SYMBOLS AND ABBREVIATIONS

AC	alternating current; attitude control
ACS	attitude control system
A/D	analog to digital converter
ADV-FW	advanced flywheel
AFML	Air Force Materials Laboratory
AMCD	annular momentum control device
APL	Applied Physics Laboratory
B	flux density
BOL	beginning of life
BRG	bearing
CDR	critical design review
CM	command
CMG	control moment gyro
CNTL	control
CSDL	Charles Stark Draper Laboratory
D/A	digital to analog converter
DC,dc	direct current
DOD	Department of Defense
DOE	Department of Energy
DSP	Defense Support Program
emf	electromotive force
EPS	electrical power system
ERDA	Energy Research and Development Administration
ES	energy storage
ESA	European Space Agency
E.S.W.	energy storage wheel
FET	field effect transistor

FH	flight hardware
FY	fiscal year
GATT	gate-assisted turn-off thyristor
GSFC	Goddard Space Flight Center
H	momentum
H/M	ratio of momentum to mass
I	current
IA	input axis
I.D.	inner diameter
I/O	input/output
IPACS	Integrated Power/Attitude Control System
$I^2R$	resistive loss
IR&D	independent research and development
IRU	inertial reference unit
$K_v$	voltage constant
KVAR	kilovolt ampere reactance
LED	light-emitting diode
LeRC	Lewis Research Center
LLNL	Lawrence Livermore National Laboratory
LTP	liter
LVLH	local vertical local horizontal
MAG	magnetic
MAU	million accounting units
MEST	mechanical energy storage technology
M/G, M-G	motor/generator, motor-generator
MJS	Mars Jupiter Saturn
NDI	nondestructive inspection

NDT        nondestructive testing  
NRL        Naval Research Laboratory  
NSF        National Science Foundation  
OA        output axis  
OAST      Office of Aeronautics and Space Technology  
O.D.      outer diameter  
 $P_o$       load  
PDR      preliminary design review  
PSS      power storage system  
PV        photovoltaic  
PVF<sub>2</sub>     polyvinyl fluoride  
PWM      pulse width modulation  
R        resistance  
 $R_L$       load resistance  
RF        radio frequency  
RFP      request for proposals  
R.L.      running losses  
ROM      read-only memory  
RPC      remote power controller  
RPM      revolutions per minute  
RWMS     reaction wheel momentum subsystem  
S/A      solar array  
S/C      spacecraft  
SCR      silicon-controlled rectifier  
SDF      single degree of freedom  
SMC      sheet molding compound  
SOA-FW   state-of-the-art flywheel  
SRA      single rotation axis

t time  
TACH tachometer  
TDRS tracking data relay satellite  
TTL transistor-transistor logic  
UMTA Urban Mass Transit Authority  
VAC vacuum  
VLF very low frequency  
VOC voltage command  
VSCF variable speed constant frequency  
W.R.T. with respect to  
Y-12 facility at Oak Ridge National Laboratory

